Universität Bremen

MAX-PLANCK-INSTITUT FÜR MARINE MIKROBIOLOGIE

Using fluorescence *in situ* hybridization to study intracellular properties

Dissertation
zur Erlangung des Doktorgrades
der Naturwissenschaften
- Dr. rer. nat. -

dem Fachbereich 2 Biologie/Chemie
der Universität Bremen
vorgelegt von

Jan David Brüwer

Bremen, März 2024

Die vorliegende Doktorarbeit wurde im Rahmen des Programms *International Max Planck Research School of Marine Microbiology* (MarMic) in der Zeit von Juni 2019 bis März 2024 am Max-Planck-Institut für Marine Mikrobiologie, Bremen (Deutschland), angefertigt.

This thesis was prepared under the framework of the *International Max Planck Research School of Marine Microbiology* (MarMic) at the Max Planck Institute for Marine Microbiology, Bremen (Germany, from June 2019 to March 2024.

Gutachter: **PD Dr. Bernhard M Fuchs**
Gutachter: **Prof. Dr. Stephen Giovannoni**
Gutachterin: **Dr. Cristina Moraru**

Prüfer: **Prof. Dr. Michael W Friedrich**
Prüfer: **PD Dr. Bernhard M Fuchs**
Prüfer: **Prof. Dr. Stephen Giovannoni**
Prüferin: **Dr. Cristina Moraru**
Datum des Promotionskolloquiums: 03. Mai 2024

How long will it last, this peace I found at sea?

Bernard Moitessier

ABSTRACT

Microorganisms dominate the surface ocean and significantly shape biogeochemical cycles, particularly the carbon cycle. Through photosynthesis, primary producers fix inorganic carbon and produce organic matter. The phytoplankton-derived organic matter fuels differently specialized heterotrophic bacteria that remineralize large proportions of it. At the same time, phages, which are viruses that infect bacteria, shape the bacterial community composition through top-down controls. Environmental microbial ecology often uses microscopically derived changes in cell abundance or incubation experiments with labeled substrates to derive bacterial growth or activity. However, the former does not account for mortality, while the latter is prone to biases by bottle effects and substrate preferences. Nevertheless, marine microbial ecology requires a thorough understanding of bacterial growth and mortality to understand the effects on, e.g., the carbon cycle. Additionally, microbial ecologists have little understanding of the effect of phages on the heterotrophic community. For example, no studies have quantified the amount of phage-infected heterotrophs in complex marine samples to date.

For this thesis, I studied the bacterial life cycle, from cell division to cell death, in environmental samples. To do so, I used fluorescence *in situ* hybridization (FISH) techniques and high-throughput image cytometry, complemented with metagenomic analyses. A significant focus was on bacteria of the SAR11 clade. SAR11 are specialized to grow in oligotrophic habitats that are nutrient and substrate-depleted. They are assumed to be outcompeted by specialized bacteria during high-substrate conditions, such as phytoplankton blooms. Additionally, there is an ongoing debate on whether phage infection has a considerable effect on SAR11 communities. In this thesis, I demonstrate rapidly dividing SAR11 communities during phytoplankton blooms with a concomitantly high phage infection rate.

In Chapter 2, I used FISH in combination with a fluorescent DNA stain to study the frequency of dividing cells by visualizing the intracellular DNA distribution. During a cell replication cycle, the dublicated genomes need to be separated into the future daughter cells. The correlation with experimentally derived *in situ* cell division rates allowed the calculation of cell division across an entire phytoplankton bloom. Measurements revealed faster SAR11 cell division rates than anticipated by cell counts. Hence, calculated mortality rates were high during these times. As the

mortality was taxon-specific, I hypothesized phage-induced lysis as a cause.

In Chapter 3, I designed direct-geneFISH probes to visualize phage-infected SAR11 cells in the environment. I could thereby provide the missing link between cell division and mortality rates, as revealed in Chapter 2. The highest amounts of phage-infected SAR11 cells (up to 19% of the SAR11 cells) were detected when taxon-specific mortality and cell division rates were highest. Additionally, I found a phenomenon of phage-infected, ribosome-depleted cells, which I dubbed 'zombie cells'. I thoroughly discuss possible explanations for their emergence and propose that nucleotides from ribosomal RNA are used as substrates for phage genome synthesis. Additionally, I show that both phage-infected and zombie cells occur globally.

In Chapter 4, I assessed the influences of future ocean scenarios and a marine heatwave on the microbial community, including cell division and grazing rates. Anthropogenic influences shape the ocean as a habitat with unknown consequences for the microbial community. I found no significant influences of the mild marine heatwave, while the future ocean scenarios caused differences in bacterial abundances. Overall, the results indicate a stable and adaptable marine microbial community in the face of a changing ocean.

In the general discussion (Chapter 5), I discuss the methodological approaches used in this thesis to study bacterial cell division rate and the viral community. I further summarize and discuss the insights into SAR11 ecology gained through this thesis, as well as the importance and emergence of zombie cells. The discussion is rounded off with an outlook, proposing directions for future research projects to understand further the interplay of bacterial hosts and their phages, as well as zombie cells.

Enjoy the read!

ZUSAMMENFASSUNG

Mikroorganismen dominieren das Oberflächenwasser der Ozeane und bestimmen maßgeblich biogeochemische Kreisläufe, insbesondere den Kohlenstoffkreislauf. Durch Photosynthese binden sie als Primärproduzenten anorganischen Kohlenstoff und erzeugen organische Materie. Das vom Phytoplankton produzierte Material dient als Nährstoff für unterschiedlich spezialisierte heterotrophe Bakterien, welche einen großen Teil davon remineralisieren. Gleichzeitig beeinflussen Phagen, Viren von Bakterien, die Zusammensetzung der bakteriellen Gemeinschaft durch sogenannte Top-Down-Kontrolle. In der mikrobiellen Umweltökologie werden häufig durch die Mikroskopie ermittelte Veränderungen der Zellzahlen oder Inkubationsexperimente mit markierten Substraten verwendet, um das Wachstum oder die Aktivität von Bakterien zu erfassen. Erstere berücksichtigen jedoch nicht die Mortalität, während letztere anfällig für Verzerrungen durch Bottle Effects und Substratpräferenzen sind. Allerdings ist ein tiefgründiges Verständnis von Bakterienwachstum und Mortalität in der mikrobiellen Ökologie unabdingbar, um zum Beispiel die Auswirkungen auf den Kohlenstoffkreislauf zu verstehen. Zusätzlich wissen wir zu wenig über den Einfluss von Phagen auf die heterotrophe Gemeinschaft. So gibt es zum Beispiel bisher keine Studien, die die Menge von phageninfizierten heterotrophen Bakterien in komplexen Meeresproben quantitativ bestimmt haben.

In dieser Arbeit habe ich den bakteriellen Lebenszyklus von der Zellteilung bis zur Mortalität in Umweltproben untersucht. Dazu habe ich Fluoreszenz-in-situ-Hybridisierungen (FISH) mit der Hochdurchsatz Bildzytometrie kombiniert und mit metagenomischen Analysen ergänzt. Ein wesentlicher Schwerpunkt dieser Arbeit lag auf Bakterien der SAR11 Gruppe. SAR11 Bakterien sind auf oligotrophe, das heißt nährstoff- und substratarme Lebensräume spezialisiert. Man geht davon aus, dass sie unter substratreichen Bedingungen, wie zum Beispiel bei Phytoplanktonblüten, von spezialisierten Bakterien verdrängt werden. Darüber hinaus gibt es eine anhaltende Debatte darüber, welchen Einfluss die Phageninfektionen auf die SAR11-Gemeinschaten hat. Im Rahmen dieser Arbeit zeige ich, dass SAR11-Bakterien sich während einer Phytoplanktonblüte sehr schnell teilen und gleichzeitig viele Zellen von Phagen infiziert werden.

In Kapitel 2 habe ich FISH in Kombination mit einem fluoreszierenden DNA-Farbstoff verwendet, um die intrazelluläre DNA-Verteilung sichtbar zu machen und die Häufigkeit von sich

teilenden Zellen zu untersuchen. Im Zuge eines Zellzyklus muss das replizierte Genom in die zukünftigen Tochterzellen aufgeteilt werden. Korrelationen mit experimentell bestimmten Zellteilungsraten in den Umweltproben ermöglichten die Berechnung von Zellteilungsraten während der gesamten Phytoplanktonblüte. Die Messungen ergaben schnellere SAR11-Zellteilungsraten als durch Zellzählungen erwartet, wodurch sich ebenfalls hohe Mortalitätsraten in dieser Zeit berechnen ließen. Da diese Mortalität für SAR11 spezifisch war, stellte ich die Hypothese auf, dass eine durch Phagen ausgelöste Lyse die Ursache sein könnte.

In Kapitel 3 habe ich direct-geneFISH-Sonden entwickelt, um von Phagen infizierte SAR11-Zellen in der Umwelt sichtbar zu machen. Damit konnte ich das fehlende Bindeglied zwischen Zellteilung und Mortalität aus Kapitel 2 herstellen. Ich habe die meisten von Phagen infizierten SAR11 Zellen detektiert (bis zu 19% der SAR11 Zellen), wenn die taxonspezifische Mortalität und die Zellteilungsraten am höchsten waren. Darüber hinaus habe ich ein Phänomen von phageninfizierten Zellen entdeckt, die keine oder sehr wenige Ribosomen enthalten und habe diese als Zombiezellen benannt. Ich diskutiere die Möglichkeiten ihrer Entstehung als Folge einer Phageninfizierung und vermute, dass Nukleotide aus der ribosomalen RNA als Bausteine für die Synthese neuer Phagengenome verwendet werden. Ebenfalls kann ich zeigen, dass sowohl phageninfizierte als auch Zombiezellen weltweit vorkommen.

In Kapitel 4 untersuche ich die Effekte von Zukunftsszenarien der Ozeane und einer marinen Hitzewelle auf die mikrobielle Gemeinschaft mit besonderem Fokus auf Zellteilungs- und Fraßraten. Menschliche Einflüsse formen die Meere als Lebensraum mit unbekannten Folgen für die mikrobiellen Gemeinschaften. In der Untersuchung konnte ich keinen Einfluss einer milden Hitzewelle auf die Mikroben feststellen, jedoch haben die Zukunftsszenarien einen Einfluss auf die Zellzahlen. Im Großen und Ganzen deuten die Ergebnisse auf eine gefestigte und anpassungsfähige mikrobielle Gemeinschaft angesichts eines sich verändernden Ozeans hin.

In der allgemeinen Diskussion (Kapitel 5) erörtere ich die in dieser Arbeit verwendeten methodischen Ansätze zur Untersuchung der bakteriellen Zellteilungsrate und der viralen Gemeinschaft. Außerdem fasse ich die in dieser Arbeit gewonnenen Erkenntnisse über die SAR11-Ökologie sowie die Bedeutung und das Auftreten von Zombiezellen zusammen und diskutiere sie. Die Diskussion wird mit einem Ausblick abgerundet, in dem Richtungen für zukünftige Forschungsprojekte vorgeschlagen werden, um das Zusammenspiel von bakteriellen Wirten und ihren Phagen sowie Zombiezellen besser zu verstehen.

Viel Spaß beim Lesen!

CONTENTS

Abstract I

Zusammenfassung III

Contents V

List of Abbreviations VIII

List of Figures X

1 General Introduction 1

1.1 The microbial loop and the role of viruses . . . 1
1.2 Phytoplankton blooms . . . 2
1.2.1 Heterotrophic bacteria during phytoplankton blooms . . . 4
1.3 Seeing is believing . . . 5
1.3.1 Automated microscopy . . . 6
1.3.2 Studying bacterial growth and activity . . . 6
1.3.3 Direct-geneFISH . . . 7
1.4 Aims . . . 8
1.5 Contributions . . . 10

2 *In situ* cell division and mortality rates 13

2.1 Abstract . . . 15
2.1.1 Importance . . . 15
2.2 Introduction . . . 16
2.3 Results . . . 17
2.3.1 Frequency of dividing cells as a robust parameter to investigate cell division 18
2.3.2 Growth activity changes of SAR11, SAR86, *Bacteroidetes* and *Aurantivirga* in 2018 . . . 18
2.3.3 2020 spring bloom cell division rates for SAR11, SAR86, *Bacteroidetes*, and *Aurantivirga* . . . 20

2.3.4 Cell division rates versus net growth rates during 2020 spring bloom . . . 22
2.3.5 Bioinformatic assessment of taxon diversity and growth measures during the 2018 bloom . . . 23
2.4 Discussion . . . 24
2.4.1 The microbes constant struggle against mortality . . . 28
2.5 Conclusion . . . 28
2.6 Material and Methods . . . 28
2.6.1 Sampling . . . 28
2.6.2 Cell division rates based on dilution grazing experiments . . . 29
2.6.3 Cell counts and FISH . . . 30
2.6.4 Automated image recording . . . 30
2.6.5 Image cytometry . . . 30
2.6.6 DNA extraction, metagenome sequencing, and diversity and growth estimation . . . 31
2.6.7 Determining growth, modelling, and statistical analyses . . . 32
2.6.8 Visualisations . . . 32
2.7 Acknowledgements . . . 33
2.8 Supplements . . . 33
2.8.1 Supplementary Material and Methods . . . 33
2.8.2 Supplementary results . . . 37
2.8.3 Supplementary Figures . . . 38
References . . . 47

3 Pelagiphage infections and zombie cells 57
3.1 Abstract . . . 59
3.2 Main Text . . . 59
3.3 Results . . . 60
3.3.1 Quantifying phage-infected SAR11 cells and discovery of zombie cells . 60
3.3.2 Phage-infection regulates SAR11 abundance during phytoplankton bloom 61
3.3.3 Global distribution of phage-infected and zombie cells . . . 64
3.4 Discussion . . . 65
3.4.1 Zombie cells: Clever persisters or ‘phage puppets’? . . . 66
3.5 Conclusion . . . 67
3.6 Material and Methods . . . 68
3.6.1 Cultivation of *Ca.* P. ubique infected with HTVC031P, HTVC027P, and HTVC023P . . . 68
3.6.2 Environmental sampling . . . 68
3.6.3 Pelagiphage FISH probe design and synthesis . . . 69

3.6.4 Fluorescence *in situ* hybridization . . . 69
3.6.5 Microscopy . . . 70
3.6.6 Image cytometry . . . 70
3.6.7 Metagenomic abundance estimates for SAR11 MAGs, 16S rRNA gene, and Pelagiphages . . . 70
3.6.8 Identification of defence systems within SAR11 genomes . . . 71
3.6.9 Statistics and modelling . . . 71
3.7 Supplements . . . 72
3.7.1 Supplementary material and methods . . . 72
3.7.2 Supplementary Figures . . . 74
3.7.3 Supplementary Tables . . . 81
References . . . 81

4 The future Ocean **87**
4.1 Abstract . . . 89
4.2 Introduction . . . 89
4.3 Material and Methods . . . 91
4.3.1 Mesocosm set-up . . . 91
4.3.2 Measurements throughout the experiment . . . 92
4.3.3 DAPI, SYBR-gold, and fluorescence *in situ* hybridization (FISH) staining to count microbes and virus-like particles . . . 92
4.3.4 Microscopy and image analysis . . . 93
4.3.5 DNA isolation and 16S sequencing . . . 93
4.3.6 Dilution grazing experiments . . . 94
4.3.7 Statistical analysis and visualizations . . . 94
4.4 Results . . . 95
4.4.1 Phytoplankton responds to future ocean scenario with little effect of heatwave treatments . . . 95
4.4.2 Future ocean scenarios shape total cell counts, while the marine heatwave has no effect . . . 95
4.4.3 No taxon-specific effects in response to future ocean scenarios and heatwave exposure . . . 97
4.4.4 16S data reveals stable community over heatwave, small effect of future ocean scenario . . . 97
4.4.5 No indications of heatwave impact on virus-like particle counts . . . 99
4.4.6 Dilution experiments indicate no treatment-specific influence on cell division or grazing rates . . . 100
4.4.7 High abundance of filaments during the sampling campaign . . . 101

4.5 Discussion . . . 102
4.5.1 Effect of future ocean scenario due to altered bottom-up processes . . . 103
4.5.2 Microbial community resistant to heatwave treatments . . . 104
4.6 Supplements . . . 106
4.6.1 Supplementary Tables . . . 106
References . . . 106

5 General Discussion **113**
5.1 Methods . . . 113
5.1.1 The power of frequency of dividing cells . . . 114
5.1.2 Quantitative virus ecology . . . 117
5.1.3 Species-specific grazing by eukaryotes . . . 120
5.2 SAR11 ecology . . . 122
5.2.1 What enables the early start of high cell division of SAR11? . . . 122
5.2.2 Are SAR11 defense specialists? . . . 125
5.3 Zombie cells . . . 126
5.3.1 The emergence of zombie cells . . . 127
5.3.2 Zombie cells in microbial ecology . . . 127
5.4 Concluding remarks . . . 129
5.5 Outlook . . . 129
5.6 Supplements . . . 131
5.6.1 Supplementary Text . . . 131
5.6.2 Supplementary Tables . . . 132
5.6.3 Supplementary Figures . . . 136

References **XIX**

Acknowledgements **XXXIV**

Eidesstattliche Erklärung **XXXVI**

List of Abbreviations

ACME	Automatic cell measuring and enumeration tool
AHW	AMB plus heatwave in the mesocosms
AIC	Akaike information criterion
AMB	Ambient treatment in the mesocosms
ANOVA	Analysis of variance
ASV	Amplicon sequence variant
bp	Base pairs
CARD	Catalyzed reporter deposition
CCD	Charged-coupled device
DAPI	4',6-diamidino-2-phenylindole ($C_{16}H_{15}N_5$)
DOM	Dissolved organic matter
FA	Formaldehyde
FDC	Frequency of dividing cells
FISH	Fluorescence *in situ* hybridization
FOV	Field of view
GAM	Generalized additive model
GRiD	Growth rate index
LTER	Long Term Ecological Research Station
MAG	Metagenome-assembled genomes
mbp	Mega base pairs
NA	Numerical aperture
PAR	Photosynthetically active radiation
PBS	Phosphate-buffered saline
PC	Polycarbonate
POM	Particulate organic matter
RCP	Representative Concentrations Pathway
RHW	RCP treatment plus heatwave in mesocosms
SAG	Single amplified genomes

TEM	Transmission electron microscopy
UNK	Gene of unknown function
VLP	Virus like particle

LIST OF FIGURES

1.1 **The marine carbon cycle with a focus on the microbial loop, viral shunt, and viral shuttle.** CO_2 is fixed by primary producers. Virus-induced lysis and sloppy feeding by grazers create dissolved (DOM) and particulate organic matter (POM), which feeds the microbial loop. Protistan grazing of bacterioplankton transfers organic matter to higher trophic levels. Microbial and other respiration releases CO_2 back into the environment. Part of the POM sinks and is exported into deeper water layers. For references, please see the main text. The top right corner represents the "Lange Anna", an iconic rock of Helgoland, where most of the samples of this thesis were taken. Figure generated with BioRender.com. 3

1.2 **Thesis abstract: Visualizing the bacterial life cycle.** Microbial cells replicate their genome before cell division and grow in volume, which was assessed in Chapter 2 to study cell division rates. Bacteria can be grazed by protists, which was addressed in Chapters 2 and 4. Mortality through phage-induced lysis was studied in Chapter 3. The subsequent release of organic matter (OM) fuels the growth of new cells. Figure created with BioRender.com. 7

2.1 **Cellular parameters of SAR11 during the spring bloom in 2020.** (A) Cell abundances in blue and chlorophyll a concentration as grey background. (B) Cell volumes and (C) ribosome contents were calculated from CARD-FISH signals and plotted as means per day (black points) ±sd (black lines). A *loess* smoothing of all data is depicted in blue. (D) The FDC, as a measure of cell division, was determined from cells with two internal local DAPI maxima. An FDC per sampling day are shown as black points and *loess* smoothing as blue line. 19

2.2 **Correlation of cellular parameters and cell division rates.** (A) Box and whiskers plot of cell volume in relation to FDC with regression in blue. (B) Box and whiskers plot of ribosome content (fluorescence per cell) in relation to FDC with regression in blue. Box in (A) and (B) represent 25th and 75th percentile, the mean is drawn as solid line within the box. The whiskers are 1.5x interquartile percentile. Outliers are not visualized. (C) Ribosome content plotted over measured cell volume as black points with linear regression depicted in blue. (D) Cell division rates were assessed in dilution experiments and correlated to FDC. Standard error is shown as grey shading. 20

2.3 **Cell abundances and FDC in 2018 and 2020.** Cell abundances of SAR11, SAR86, *Bacteroidetes*, and *Aurantivirga* during the spring bloom 2018 (upper row) and 2020 (lower row) in coloured points with *loess* smoothing as coloured lines. Taxon-specific FDC are shown by black dots and *loess* smoothing as lines. Chlorophyll a concentration is shown as grey shading in the background in all plots. 21

2.4 **Taxon-specific net growth, cell division, and mortality rates during 2020 spring bloom.** Taxon-specific cell division rates were calculated based on FDC throughout the spring bloom (black points with *loess* smoothing as black line). Net growth was calculated based on FISH abundance data (magenta points with *loess* smoothing as magenta line). Mortality is the cell division rate minus net growth (green points with *loess* smoothing as green line). Measured cell division rates by dilution experiments are depicted with a red asterisk. 22

2.5 **gRodon-predicted minimal doubling times.** Box and whisker plots of genomic potential for minimal doubling times predicted by gRodon for SAR11, SAR86, *Bacteroidetes*, and *Aurantivirga* MAGs, retrieved from 2018 spring phytoplankton bloom. Boxes indicate 25th and 75th percentile, the mean is drawn as solid line. Whiskers represent 1.5x IQR, outliers are not visualized. Points indicate results of individual MAGs. Dotted line indicates threshold between oligotrophs (minimal doubling time >5 h) and copiotrophs (minimal doubling time <5 h), according to the authors of gRodon. 24

S2.1 Total DAPI-stained cell counts with chlorophyll a concentration (grey, background), temperature, and photosynthetically active radiation (PAR) during the spring phytoplankton bloom (A) 2018 and (B) 2020. 38

S2.2 Taxon and year-specific correlation of cellular parameters measured with FISH. (A) Ribosome content to cell volume. (B) Ribosome content over FDC. (C) Cell volume over FDC. Box-whisker plots in (B) and (C) range from 25th to 75th percentile and the whiskers represent 1.5x interquartile range. Outliers are visualized by dots. Mean is drawn as a solid line inside the boxes. Statistic results of regressions are reported supplementary results. 39

S2.3 (A) Linear correlations of microscopically-derived FDC and cell division rates determined by dilution experiments. Information about the linear regression can be found in table S2 (at doi.org/10.6084/m9.figshare.22290166). (B) Taxon-specific grazing rates over mortality rates in 2020. Taxon-specific grazing rates were determined with dilution experiments on 5 time-points during the 2020 phytoplankton bloom. Mortality rates were calculated from cell division rates and on net growth. Net growth rates could not be retrieved for SAR11 and SAR86 on one sampling day, as local regressions of abundance values were computed to calculate net growth and the regressions were partly negative. Black line is an ideal line of 1:1 correlation of grazing and mortality rates. 40

S2.4 Phylogenetic tree with SAR11 MAGs that have >50% completeness and <5% contamination described in this study with previously published SAR11 single amplified genomes (SAGs; Haro-Moreno et al. 2020) and SAR11 isolates (Delmont et al. 2019). Colours according to clade assignment (indicated in outer ring) according to the literature (see above). 41

S2.5 Metagenome-based assessment of microbial growth in 2018. Relative abundances of metagenome assembled genomes (MAGs; A-D), as well as GRiD values (E–H), of all four taxa were calculated across the spring bloom 2018. For SAR11, SAR86, and *Aurantivirga* results of individual MAGs are visualized. For *Bacteroidetes*, results are summarized on the genus level (C, G with standard deviation). (I-L) MAG-derived GRiD values plotted versus FDC for phytoplankton spring bloom 2018. 42

S2.6 Comparison of GRiD values and abundance estimates from the 2018 phytoplankton spring bloom with different mappings for (A) SAR11, (B) SAR86, and (C) *Aurantivirga*. From left to right: GRiD values from customized alignment, retrieved with BBmap; GRiD software in default mode (minimum coverage: 5); GRiD software in default mode (minimum coverage: 5) and re-alignment of ambiguous reads with Pathoscope2 within the GRiD software. 43

S2.7 Relationship of SAR11 FDC to PAR for 2018 and 2020. Left: FDC over Photosynthetically active radiation (PAR) on the left. A *loess* moving average is plotted. Right: PAR (ochre) and FDC (black) are plotted over the spring blooms with chlorophyll a plotted in the background. Scale is the same as Fig. 2.1 and 2.2. Red dashed line indicate potential threshold of 25 Einstein $m^{-2}d^{-1}$ for SAR11 activity in the beginning of the bloom. 44

S2.8 Correlation of CARD-FISH and tetra-labelled FISH cell volumes and signal intensities for *Bacteroidetes* and SAR11 cells from selected 2020 spring bloom dates. Displayed are means of each sampling day and linear regression of the means. The displayed statistics are for the linear regression model on the means. 45

S2.9 Screenshots of the ACME tool. (A) is the image in the DAPI channel, (B) FISH channel, and (C) the autofluorescence channel. DAPI positive objects have a light-blue, FISH positive a green, and auto-fluorescent particles a red outline. Red box is a zoom-in on an example of a FISH positive cell with two local DAPI maxima (i.e., a dividing cell). Yellow circle is around an algae cell, yellow arrow points towards debris. Images are an example of 20th April and the samples were hybridized with the SAR11 mix. Each field of view is 1388x1040 pixel and each pixel has a height and width of 0.106 µm. 46

3.1 **Infections of *Ca.* P. ubique HTCC1062 with HTVC027P and HTVC031P and example epifluorescence microscopy images.** Bargraphs show triplicate samples during the infection cycle. "p.i." stands for post infection. The negative control was uninfected. Abundance of 100% corresponds to total cell counts of DAPI-stained cells. Example microscopy images on the right display DAPI (DNA; cyan), FISH for 16S rRNA (yellow) and phage genes via direct-geneFISH (magenta). Outlines were drawn manually. Images were recorded using SR-SIM on a ZEISS LSM780 equipped with ELYRA PS.1 and analysed using the ZEN software. Scale bar: 0.5 µm. 61

3.2 **SAR11 and phage population dynamics during 2020 phytoplankton spring blooms at Helgoland Roads.** (A) Chlorophyll a concentration, as a proxy for phytoplankton bloom development, (B) SAR11 cell division rate, and (C) SAR11 cell count data has previously been presented in Brüwer et al.(2023). (D) Proportion of phage-infected SAR11 cells (purple; relative to SAR11 cell counts) and zombie cells (yellow; relative to total DAPI-stained cell counts) are plotted as raw values per day. *Loess* smoothing is displayed as line plots. The amount of infected and zombie cells is proportional to only SAR11 and total cell counts, respectively. The average negative control over all samples is shown as a red-dashed line. . . . 62

3.3 **Bioinformatic abundance estimates of SAR11 during phytoplankton spring bloom.** (A) metagenome assembled genomes (MAG) and (B) 16S rRNA gene sequences classified as *Pelagibacterales*. All data originated from PacBio Sequel II metagenomes from the 0.2 to 3 µm fraction (Sidhu et al. 2023). RPKM is Reads per Kilobase per Million Mapped reads. 63

3.4 **Global distribution of SAR11, phage-infected SAR11, and zombie cells.** Map with sampling locations during different cruises and long-term ecological research station Helgoland Roads. Relative abundance of SAR11 (left y-axis), phage-infected SAR11(right y-axis), and zombie cells (right y-axis) from the Atlantic, Southern Ocean, and Pacific with respective cruises in brackets. Raw data is displayed as individual points and areas represent *loess* smoothing for the Atlantic and Pacific. Subset (boxes) of data from Southern Ocean without smoothing is displayed. Complete data of the Southern Ocean is available in Fig. S3.4. 64

S3.1 Examples of high-throughput images to determine phage-infected SAR11 cells in control cultures. *Ca.* P. ubique HTCC1062 were infected with HTVC027P, HTVC031P, and HTVC023P. DNA was stained with DAPI, 16S ribosomal RNA with CARD-FISH (SAR11-mix), and phage genes were stained with direct-geneFISH (phage mix for HTVC027P, HTVC031P, and *Greip*). HTVC023P served as negative control. Images were cropped to a quarter of original size for visualization purposes and scale bars were inserted using ImageJ/Fiji. 74

S3.2 Microscopy-based vs. bioinformatic estimates of phage-infected cells during the 2020 spring phytoplankton bloom at Helgoland Roads. Upper panel: Abundance of phage-infected SAR11 cells per individual phage, based on microscopy estimates. Lower panel: Relative abundances of respective phages were normalized by the total number of reads mapped to all SAR11 MAGs in the same sample. . . 75

S3.3 Amount of zombie cells in all bacteria vs. SAR11. All bacteria were targeted with the EUB338 I-III FISH probe, while SAR11 was targeted with the SAR11-mix (Table S7). 76

S3.4 Distribution of SAR11, phage-infected SAR11, and zombie cells in the Southern Ocean. Complete results for Fig. 3.4. 77

S3.5 Statistical modelling applying Bayesian beta regression between SAR11 abundance, phage-infected SAR11 cells, and zombie cells. (A) relative abundance of phage-infected SAR11 cells and Zombie cells, (B) relative abundance of Zombie and SAR11 cells, and (C) phage-infected SAR11 cells and frequency of dividing cells (FDC), which is a proxy for cell division activity. Points represent raw data from different sampling campaigns. Line represent data modelled with Bayesian beta regression (back transformed from logit scale). 78

S3.6 Direct-geneFISH ("phage") signal content from pure cultures. (A) SAR11 infected with HTVC027P. (B) SAR11 infected with HTVC031P. "Infected cells" corresponds to 16S FISH-positive and direct-geneFISH-positive cells, whereas "Zombie cells" do not contain a 16S FISH signal. Boxplots show median and upper and lower quartile. Whiskers show maximum data points within upper/lower quartile range plus 1.5 times the interquartile range. Outliers not shown. 79

S3.7 16S FISH fluorescence intensity of phage-infected SAR11 cells from infection experiments. Boxplots show median and upper and lower quartile. Whiskers show maximum data points within upper/lower quartile range plus 1.5 times the interquartile range. Outliers not shown. Violin plot show data distribution on y-Axis. Red-dashed line represents defined threshold from image analysis. 80

4.1 **Temperature, chlorophyll a concentrations, and total cell counts during the sampling period.** Dashed lines indicate beginning and end of heatwave treatment. Shown are mean and standard deviation across four replicates as dots and error bars, respectively. Colored curves are GAM models with 95% confidence intervals as ribbons. Temperature and total cell counts are based on Meunier et al. (in prep). 96

4.2 **Relative abundance of all bacteria, SAR11, *Bacteroidota*, and *Gammaproteobacteria*, assessed by FISH quantifications.** Dashed lines indicate beginning and end of the heatwave treatment. Shown is one replicate per treatment. Colors represent treatment. 98

4.3 **Microbial community composition assessed by 16S rRNA sequencing.** Top: 14 most abundant genera. Mean of 4 replicates is shown. Bottom: Individual taxa over the sampling campaign. Dots represent mean, with standard deviation (4 replicates). Colours represent experimental condition. Dotted vertical line is beginning and end of heatwave. Asterisk indicate taxonomic groups identified on the family level only. 99

4.4 **Virus-like particle (VLP) concentrations during the mesocosm experiment.** Shown are mean and standard deviation across four replicates as dots and error bars, respectively. Colored curves are GAM models with 95% confidence intervals as ribbons. Dashed lines indicate beginning and end of heatwave treatment. . . . 100

4.5 **Cell division and grazing rates, determined by dilution experiments.** Dashed lines indicate beginning and end of the heatwave treatment. Shown are mean and standard deviation across four replicates as dots and error bars, respectively. In case of *Bacteroidota* and *Gammaproteobacteria*, only one replicate was assessed. Colored lines are GAM models with 95% confidence intervals as ribbons, where statistically significant differences between AMB and AHW treatments could be detected. 101

4.6 **Number of filamentous bacteria during sampling period.** Dashed lines indicate beginning and end of the heatwave treatment. Shown are mean and standard deviation across four replicates as dots and error bars, respectively. Colored curves are GAM models with 95% confidence intervals as ribbons. 102

5.1 **Conceptual overview of the frequency of dividing cells.** Representative microscopy images of a non-dividing (left) and a dividing (right) SAR11 cell from the phytoplankton bloom in Chapter 2 (April 2, 2020). Histograms represent fluorescence intensity along drawn arrows. Images were recorded on a ZEISS LSM780 and analysed using the ZEN software. 114

5.2 **Microscopy images of free phages.** Automatically recorded microscopy images of phage Baltilda (Bartlau 2020). Phages from a 0.2 µm filtrate were immobilized on 0.02 µm AnoDisc filters. DNA of phages was stained with SYBR gold and hybridized using direct-geneFISH (Alexa594). Top: Hybridization with Baltilda-specific probes. Bottom: Hybridization with UNK probes (Barrero-Canosa et al. 2017) that served as a negative control. Images were recorded on a Zeiss AxioImager.Z2m (further specifications see Chapter 3). 119

5.3 **The full virus cycle**, following the example of the full ribosomal approach. The aim is to identify viruses from sequencing information and quantify and visualize them by molecular techniques. Created with BioRender.com. 121

5.4 **The 2022 Helgoland phytoplankton spring bloom.** Chlorophyll a concentrations (upper panel), SAR11 cell counts (blue), and SAR11-specific frequency of dividing cells (FDC, red) were determined as described in Chapter 2. Raw values and *loess* smoothing are visualized. Red dashed line represents the start of increased SAR11 FDC, green dotted line represents increased chlorophyll a values. Data courtesy of Fuchs et al. (*unpublished*). 123

5.5 **Conceptual overview of what fuels the increased SAR11 cell division before the phytoplankton bloom.** Y-axis represents time over a phytoplankton spring bloom. The sun pictogram indicates the threshold of increased light availability enabling phytoplankton growth. Top: Phytoplankton abundance. Thick and thin arrows from the phytoplankton cells visualize amount of organic matter produced by phytoplankton. Middle: SAR11 cell division rate. Bottom: SAR11 cell abundance. Dashed lines indicate the beginning of increased SAR11 cell division and increasing phytoplankton abundances, respectively. Created with BioRender.com. 124

5.6 **Conceptual phage infection in SAR11, which leads to the formation of a zombie cell.** The figure should be read as a timeline from left to right. Between middle and late genes, RNA nucleotides are processed to be available for phage genome synthesis. Created with BioRender.com. 128

S5.1 High-molecular weight compound concentration during the Helgoland phytoplankton spring bloom 2020. Grey box is the time of high interest between the increase of cell division increase of SAR11 and the beginning of phytoplankton bloom. Samples were taken in triplicates (dots). Loess smoothing was applied over the entire spring bloom. Colors indicate the extraction method. The graph is divided into different epitopes. The full names of epitopes are provided in Table 5.2. Data was published in Sidhu et al. (2023) 136

S5.2 Monosaccharide analysis after acid hydrolysis during the Helgoland phytoplankton spring bloom 2020. Grey box is the time of high interest between the increase of cell division increase of SAR11 and the beginning of phytoplankton bloom. Loess smoothing was applied over the entire spring bloom. The graph is divided for different monosacchardides. Data was published in Sidhu et al (2023). 137

1

General Introduction

The oceans cover more than 70% of the planet and comprise the largest habitats on earth. Every corner of it is inhabited by microorganisms, which can be found from shallow coastal waters to the deep sea. With an estimated global abundance of 10^{29} cells (Whitman et al. 1998), microorganisms constitute up to 70% of the biomass in the ocean (Ciais et al. 2014; Whitman et al. 1998). Microorganisms have considerably shaped the ocean and all major chemical cycles, including the carbon cycle. For example, primary producers in the oceans are dominated by unicellular organisms, which are responsible for about half of the global oxygen production (Field et al. 1998; Friedlingstein et al. 2022). The primary producers fix inorganic carbon in form of CO_2 and build organic matter through photosynthesis. An estimated 0.4 to 2.4% of the photosynthesis-derived products are sequestered into the deep sea by a process called the biological carbon pump (Legendre et al. 2015; Polimene et al. 2017). However, the majority of the fixed organic carbon is remineralized in shallow water, mainly by microorganisms.

1.1 The microbial loop and the role of viruses

Phytoplankton and the produced organic matter form the foundational elements of a complex food web. Sloppy feeding by zooplankton, virus-induced lysis, and exudation of photosynthesis products into the environment creates a pool of dissolved and particulate organic matter (DOM and POM, respectively; Fig. 1.1). This pool of organic matter sustains a heterogeneous consortium of heterotrophic microorganisms, constituting a significant component of the microbial loop (Azam et al. 2022). Microorganisms metabolize parts of the organic matter and thereby release CO_2 back into the environment. An important aspect of the microbial loop is that grazing by protozoans transfers fixed organic carbon to higher trophic levels (Azam et al. 2022; Buchan et al. 2014).

Besides grazing, virus-induced lysis is a main mortality factor for microorganisms. Viruses are the most abundant biological entity in the ocean and influence all biogeochemical cycles. Virus-induced lysis of eukaryotic or prokaryotic hosts may produce sticky lysates, which sink to

the deep sea and increase the carbon export - a process called viral shuttle (Sullivan et al. 2017).

Viruses infecting bacteria are called phages and outnumber their bacterial host by ca. 10-fold in the surface ocean (Suttle 2005), with reports varying from 3 to over 100-fold (Wigington et al. 2016). In global approximations, it is estimated that ca. 30% of microorganisms are infected by a phage at any given time (Breitbart et al. 2018), which demonstrates their importance in microbial ecology. Phage-induced lysis adds to the pool of organic matter, which in turn fuels other microorganisms within the microbial loop (Fig. 1.1). This so-called viral shunt reduces the amount of organic matter, which is transferred into higher trophic levels via the predation of bacteria by protozoans (Wilhelm and Suttle 1999).

Phages often contain auxiliary metabolic genes (AMGs), which are homologous to genes of their bacterial hosts. A well-studied example are AMGs of phages infecting cyanobacteria. These phages contain parts of the photosystem I machinery, enhancing their hosts' photosynthetic activity. However, instead of increasing the carbon fixation, the Calvin cycle is inhibited and the pentose phosphate pathway is upregulated. Consequently, the additional energy is funneled to increase the production of nucleotides, which are used for phage genome synthesis (Lindell et al. 2004; Puxty et al. 2015; Thompson et al. 2011). Other examples include the alteration of the phosphate metabolism, methylation, and cellular regulation by phage-encoded AMGs (Wang et al. 2023). In summary, phages and viruses in general are important mortality factors in the ocean, which significantly influence biogeochemical cycles in the ocean.

1.2 Phytoplankton blooms: A hotspot of bacterial turnover

Phytoplankton blooms are characterized by rapidly growing and accumulating phytoplankton, which only last a few days to weeks (Buchan et al. 2014). In some regions, phytoplankton blooms are recurring events, following an annual cycle. Spring phytoplankton blooms depend on high nutrient concentrations, that become available during winter months, rising temperatures, and light availability (Gerdts et al. 2004). The bursts of phytoplankton productivity release great amounts of organic matter into the environment, which in turn fuel a distinct succession of bacterial groups (Bunse and Pinhassi 2017; Fuhrman et al. 2015; Sison-Mangus et al. 2016; Teeling et al. 2016).

Phytoplankton-derived carbohydrates may include a diverse array of monosaccharides, including glucose, mannose, fucose, and others, and might contain additional side-chains such as sulfate groups (Bligh et al. 2022; Mühlenbruch et al. 2018; Sperling et al. 2017). The composition of phytoplankton-derived carbohydrates is not static but changes with the progression of the bloom (Francis et al. 2021; Kappelmann et al. 2019; Vidal-Melgosa et al. 2021). While some of the produced carbohydrates are more accessible to be digested by the microbial community, others require highly specialized enzymes (Kappelmann et al. 2019; Orellana et al. 2021). For example, laminarin is a common storage compound of macroalgae (Becker et al. 2020) and

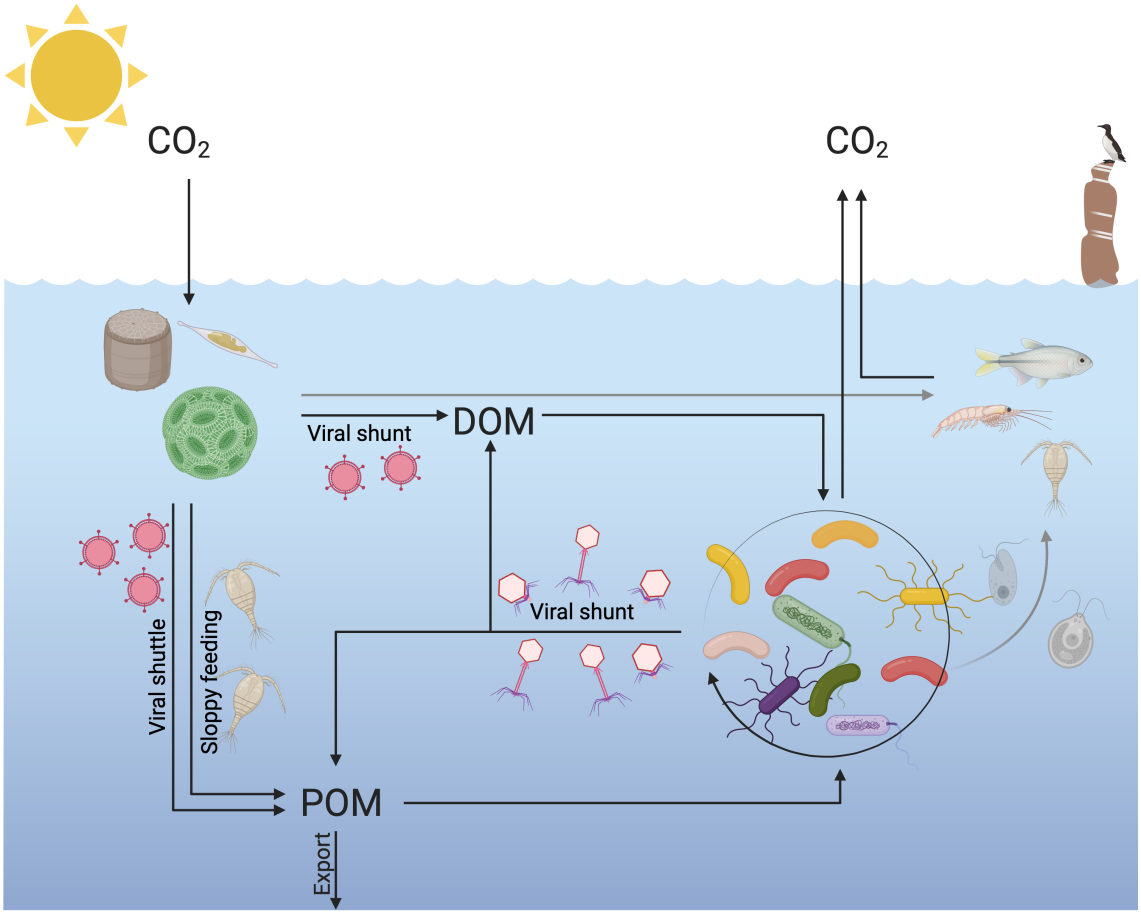

Figure 1.1: The marine carbon cycle with a focus on the microbial loop, viral shunt, and viral shuttle. CO_2 is fixed by primary producers. Virus-induced lysis and sloppy feeding by grazers create dissolved (DOM) and particulate organic matter (POM), which feeds the microbial loop. Protistan grazing of bacterioplankton transfers organic matter to higher trophic levels. Microbial and other respiration releases CO_2 back into the environment. Part of the POM sinks and is exported into deeper water layers. For references, please see the main text. The top right corner represents the "Lange Anna", an iconic rock of Helgoland, where most of the samples of this thesis were taken. Figure generated with BioRender.com.

available to many heterotrophic bacteria (e.g., Reintjes et al. 2020). In contrast, fucoidan requires many specialized enzymes and in some cases microcompartments to be metabolized (Orellana et al. 2021; Sichert et al. 2020). The capability of microorganisms to digest the different complex carbohydrates results in specific competitive advantages at discrete stages throughout the bloom. As a consequence, the distinct succession of bacterial groups is a result of their genomic capability and driven by bottom-up (substrate) pulses during phytoplankton blooms (Sperling et al. 2017; Teeling et al. 2012).

In addition to bottom-up processes, top-down factors shape the microbial community through taxon-specific or non-specific mortality. Top-down factors include mortality due to grazing by flagellates, phage-induced lysis (Fuhrman et al. 2015), and predatory bacteria feeding on other bacteria (Tang et al. 2020; Williams et al. 2016). Heterotrophic flagellates are a polyphyletic group of eukaryotes that are the main consumers of bacteria in the sea (Kiørboe 2024). Their

grazing is thought to be size-dependent (Pernthaler 2005; Weinbauer et al. 2019), while some studies suggest a preference for specific species by some flagellate grazers (further discussed in Chapter 5; Ballen-Segura et al. 2017; Dopheide et al. 2011; Hirakata et al. 2020). As discussed above, viruses and phages are important mortality factors in the marine realm. Phages usually have a narrow host range, implying species-specific effects on the microbial community (Bartlau et al. 2022; Breitbart et al. 2018; Fuhrman et al. 2015). During phytoplankton blooms, abundance patterns and succession of viruses and phages are similar to those of their hosts (Chow and Fuhrman 2012; Fuhrman et al. 2015).

1.2.1 Heterotrophic bacteria during phytoplankton blooms

Heterotrophic bacteria dominating during phytoplankton blooms characteristically have a copiotrophic lifestyle. Their abundance patterns follow 'boom and bust' cycles, with short-term high cellular abundances. Copiotrophic taxa dominate nutrient-rich habitats and typically have fast growth rates (Kirchman 2016). They are specialized in the degradation of more complex carbohydrates, which are available throughout phytoplankton blooms. Many marine members of the phylum *Bacteroidota* are known to benefit from phytoplankton blooms and are characterized as copiotrophs. Previous studies often reported fast growth rates (2.2 to 5.1 d^{-1}), and high cell abundances of *Bacteroidota* during phytoplankton blooms (Díez-Vives et al. 2014; Yokokawa et al. 2004). *Bacteroidota* contain a variety of so-called carbohydrate-active enzymes (CAZymes), a group of enzymes involved in the assembly, modification, and breakdown of carbohydrates (Lombard et al. 2013). More specifically, CAZymes include glycoside hydrolases, polysaccharide lyases, glycosyltransferases, and others. Often, the corresponding genes are encoded in polysaccharide utilization loci (PULs), which frequently include the genes for Ton-B dependent SusCD transporters for the intracellular uptake of the substrates (Glenwright et al. 2017; Gray et al. 2021) and may also encompass genes encoding for sulfatases (Kappelmann et al. 2019; Krüger et al. 2019). During phytoplankton blooms, *Bacteroidota* convert high-molecular-weight substrates into low-molecular-weight compounds, which in turn fuel the growth of other specialized species (Teeling et al. 2012).

Oligotrophic taxa are the opposite of copiotrophs. They dominate substrate-depleted habitats and characteristically have slow growth rates (Kirchman 2016). They often dominate the microbial community during winter and decrease in (relative) abundance during phytoplankton blooms. They have a lower "Monod constant" than copiotrophs, meaning they have a higher substrate affinity but lower maximum growth rates at substrate saturation (Kirchman 2016). Here, the Monod constant is to be understood like the Michaelis Menten constant but for bacterial growth instead of enzymatic activity (Liu 2007). Hence, copiotrophs have a competitiv advantage over oligotrophs, due to their maximum growth rates. For example, SAR11 (*Pelagibacterales*, class *Alphaproteobacteria*) dominate nutrient-depleted waters (Giovannoni 2017) and have been

observed to be outcompeted by fast growing copiotrophs during phytoplankton blooms (Teeling et al. 2012; Teeling et al. 2016). As a consequence, they are often characterized (ultra-)oligotrophs (Giovannoni 2017).

Nevertheless, SAR11 are the most abundant bacterial group in the surface ocean across all ocean basins. Members of the SAR11 account for about a third of all microbial cells in surface seawater (Giovannoni 2017). Their streamlined genomes (1.3 Mbp) are well adapted for low-substrate environments, and they are specialized for low-molecular-weight compounds instead of complex carbohydrates. SAR11 are photoheterotrophs, as they are capable of proteorhodopsin-dependent ATP synthesis (Giovannoni 2017). Additionally, they can oxidize a wide variety of methylated compounds and one-carbon compounds, amino acids, and osmolytes to meet their energy demands (Giovannoni 2017; Sun et al. 2011; Tripp 2013). SAR11 have a high density of ABC transporters (Noell and Giovannoni 2019; Sowell et al. 2008). ABC transporters use substrate-binding proteins that diffuse freely in the periplasm and bind the substrate before it is transported across the membrane into the cytoplasm (Bosdriesz et al. 2015). The high density of ABC transporters enable SAR11 sufficient substrate uptake at low substrate concentrations (Noell and Giovannoni 2019; Norris et al. 2021). At the same time, this process is partly diffusion-limited and constrains growth, resulting in low growth rates (Norris et al. 2021). In fact, SAR11 cell division rates are generally believed to be low, with the cultured representative *Candidatus* Pelagibacter ubique growing <0.5 divisions d^{-1} in the laboratory (Carini et al. 2013; Rappé et al. 2002). It is a conundrum how a slow-growing microorganism can dominate the surface ocean. The notion that SAR11 could be immune to destruction by viruses (Suttle 2007) has continuously influenced and defined the discussion within scientific literature, despite the first isolation of phages infecting SAR11 over a decade ago. This thesis will address both the taxon-specific cell division rates of SAR11 and other taxa and the number of phage-infected cells in environmental samples.

1.3 Seeing is believing – studying microbes using fluorescence microscopy

The invention of the microscope was essential for the emergence of the research field of microbiology. The first visual observation of tiny single-celled organisms in a water droplet by Antonie van Leeuwenhoek in the 17th century is often understood as the beginning of microbiology (Gest 2004). The small size of the microbes leaves little room for distinct morphological features. Microorganisms were described as cocci (spherical), bacilli (rod-shaped), vibrio (crescent-shaped), or as a spirochete, with additional smaller variations such as streptococci (chains of spheres) or staphylococcus (aggregation of spheres). However, this does not do justice to the taxonomic (and functional) diversity. A taxonomic identification of environmental microorganisms is simply not possible with a microscope.

The discovery of the highly conserved 16S rRNA as a molecular clock, first introduced by Carl Woese (Woese and Fox 1977), has drastically advanced the research on taxonomic diversity and microbial community compositions. For example, it enabled the development of techniques to quantify individual taxonomic groups in environmental samples via fluorescence *in situ* hybridization (FISH; Amann et al. 1990). FISH is a culture-independent method that allows the identification and quantification of bacteria with fluorescence microscopy in environmental samples. It is based on short nucleotide sequences, which are complementary to the 16S rRNA of target taxonomic groups. The nucleotide sequences are either labeled with a fluorescent dye (Amann et al. 1995) or a peroxidase, allowing for a subsequent signal amplification (Amann and Fuchs 2008). For example, over two decades ago, 16S rRNA cloning studies discovered bacteria of the SAR11 clade and hypothesized that they are dominating surface seawater communities (Giovannoni et al. 1990). FISH confirmed the hypothesis (Morris et al. 2002; Rappé et al. 2002) and found that SAR11 constitute about a third of surface seawater microbial communities.

1.3.1 Automated microscopy

The quantification of cells with 16S FISH is not limited to manual counting by a researcher but can be used with high-throughput methods for reliable and reproducible quantifications. For example, 16S FISH may be combined with flow cytometry or automated microscopy. Flow cytometry is a precise and efficient tool for analyzing samples based on optical properties, such as the fluorescent 16S FISH signal (Czechowska et al. 2008; Sekar et al. 2004). As an alternative, microbes from environmental samples can be immobilized on polycarbonate filters, to be analyzed with automated microscopy and image cytometry (Bennke et al. 2016; Zeder et al. 2011). Advantages include that recorded images may be re-analyzed and additional information extracted. More specifically, cell volumes (Schattenhofer et al. 2009; Tada et al. 2011) or their fluorescence intensity (Poulsen et al. 1993; Yang et al. 2008) may be retrieved, which allows for assessing the growth of microbial cells. Additionally, the intracellular DNA localization might hint toward actively dividing cells (Affronti and Marshall 1994). The replicated genome needs to be separated into the future daughter cells (Fig. 1.2), which can be used to determine the frequency of dividing cells (Hagström et al. 1979). These parameters are frequently assessed in eukaryotes (Lyons 2000), but few studies have explored their potential to study taxon-specific growth in microbial communities (Hagström et al. 2017).

1.3.2 Studying bacterial growth and activity

Growth is a key ecological trait. It indicates the success of a microbe in each environment. Microbial growth scales with metabolic processes (Kirchman 2018), hence studying growth directly enhances our understanding of the role of a microbe in cycling carbon and the microbial food web in general. Often, growth is determined via changes in abundance over time (micro-

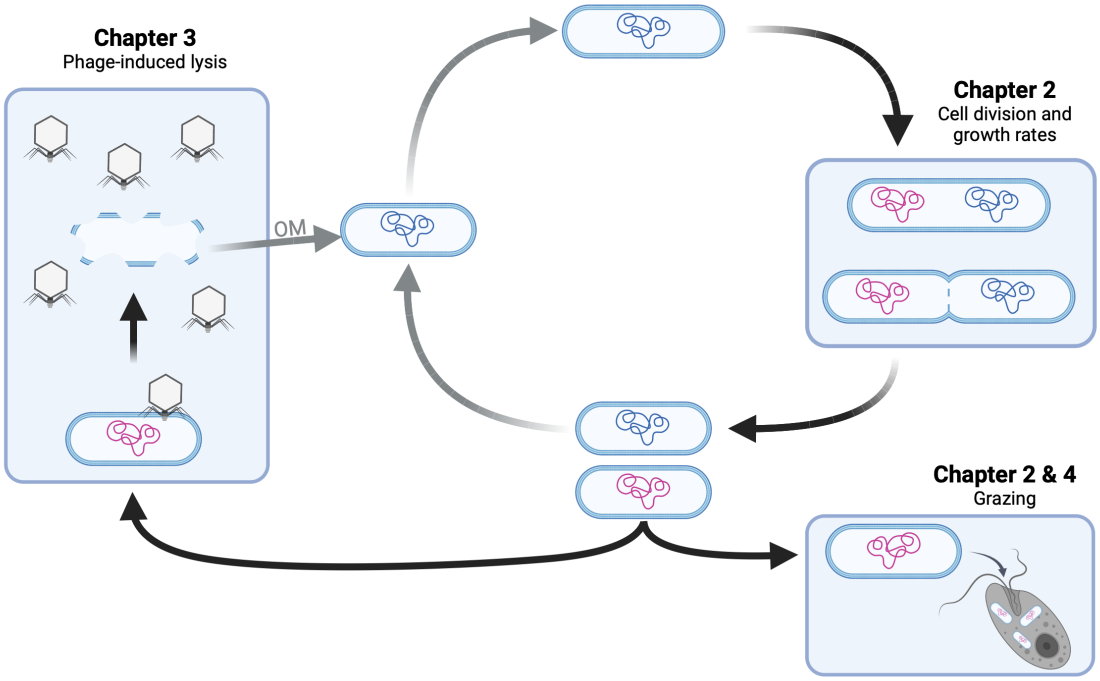

Figure 1.2: Thesis abstract: Visualizing the bacterial life cycle. Microbial cells replicate their genome before cell division and grow in volume, which was assessed in Chapter 2 to study cell division rates. Bacteria can be grazed by protists, which was addressed in Chapters 2 and 4. Mortality through phage-induced lysis was studied in Chapter 3. The subsequent release of organic matter (OM) fuels the growth of new cells. Figure created with BioRender.com.

scopically or bioinformatically). This approach only assesses the *net growth*, as it neglects the effect of mortality on a given microbial population ($net\ growth = cell\ division - mortality$). In more sophisticated approaches, metabolic activity and cellular growth are commonly assessed by uptake rates of (radio-)labeled substrates during incubation experiments (Brock 1967; Fuhrman and Azam 1980; Kirchman 2018). These experiments are labor intensive and prone to biases, as substrate uptake rates are not necessarily distributed equally between microbes. Additionally, bottle effects influence the reliability of incubation experiments. In this thesis (Chapter 2), I show how to exploit FISH data of individual microbial taxa to assess *in situ* cell division and growth without the need for incubation experiments. Additionally, mortality can be calculated when combined with *net growth* from time-series data.

1.3.3 Direct-geneFISH

For more detailed information, the development of geneFISH and direct-geneFISH enables to mark individual genes in double-stranded DNA fluorescently (Barrero-Canosa et al. 2017; Moraru et al. 2010). In combination with 16S FISH, direct-geneFISH allows to visualize a gene of interest within a targeted taxonomic group (Barrero-Canosa et al. 2017). Since the invention of direct-geneFISH, the method has been used to answer various scientific questions

on multiple environmental samples. For example, it was used to test a metagenomic hypothesis of hydrogenase-containing and -lacking symbiont strains in mussels (Ansorge et al. 2019). Next, the visualization of the glycoside hydrolase family 92 unraveled two distinct ecological niches of closely related marine *Polaribacter* (phylum *Bacteroidota*) strains (Zeugner et al. 2021). In addition, the visualization approach identified a preference for a particle-attached lifestyle of the two strains.

Gene-FISH and direct-geneFISH enable the visualization and quantification of viral genes in environmental samples (Allers et al. 2013). Rahlff et al. (2021) visualized a virus infection from absorption via advanced infections to viral lysis in *Candidatus* Altiarchaeum from samples with low taxonomic diversity (Rahlff et al. 2021). Using a combination of direct-geneFISH with scanning electron microscopy, the same laboratory identified a spatial separation between the host and viral DNA in the infected host cell (Banas et al. 2023). Direct-geneFISH is a powerful tool to quantify phage-infected cells and phages as a well-acknowledged mortality factor of bacteria. Nevertheless, little is known about the number of phage-infected cells in complex environmental samples (Coclet and Roux 2021).

1.4 Aims of the thesis

This thesis aimed to study the bacterial life cycle (Fig. 1.2) of individual bacterial taxa in the environment. With the bacterial life cycle, I refer to the beginning via cell division all the way to the death of a cell. Central to my thesis was the use of high-throughput image cytometry, integrating various FISH methods. More specifically, the objectives of my thesis were:

1. **Analyze taxon-specific cell division and mortality rates**
   Assessing microbial cell division rates is an essential ecological parameter, as it reflects the success and activity of a microorganism. Here, I aimed to use 16S FISH and image cytometry to study microbial cell division. More precisely, cell volumes, ribosome densities, and the frequency of dividing cells were assessed for individual taxonomic groups from time-series data. Subsequently, I evaluated all three parameters in light of experimentally determined *in situ* cell division rates. Combined with net growth rates from 16S FISH abundance data, I additionally aimed to calculate taxon-specific mortality rates.

2. **Quantify the number of phage-infected host cells in environmental samples**
   While it is generally acknowledged that phages are a main mortality factor of microorganisms, we know little about the number of phage-infected cells in environmental samples. By answering the objective above, I found that during a phytoplankton bloom, SAR11 cell counts decreased, although their cell division rates increased. As the mortality was SAR11-specific, I designed direct-geneFISH probes for three abundant SAR11 phages.

I aimed to quantify phage-infected SAR11 cells in environmental samples. I thereby provided an explanation for the discrepancy of cell division rates and cell abundances. Next, it enabled the discovery of a novel phenomenon: ribosome-deprived but phage-infected cells, which I dubbed 'Zombie' cells.

3. **Assess taxon-specific influences of the future Ocean**
   Anthropogenic influences change the ocean as a habitat. The influences of increasing CO_2 concentrations and sea-surface temperatures on the microbial loop are poorly understood. To assess taxon-specific impacts of future ocean conditions, the microbial community was studied in multiple driver mesocosms. Specifically, I analyzed the bacterial community for taxon-specific effects on cell division and grazing rates, as well as cell abundances by the future ocean and heatwave treatments.

Lastly, I discuss the main findings of the three original scientific articles considering current and future microbial ecology research. I critically evaluate the advantages of microscopy and sequencing methods. I further aim to discuss my findings about SAR11 ecology and the discovery of zombie (phage-infected but ribosome-deprived) cells. My thesis contributes to delineating the differences between *in situ* abundance and activity estimates, which will further advance our understanding of the microbial loop. Additionally, the quantification of phage-infected cells in complex environmental samples is part of the beginning of quantitative phage ecology and helps us assess the impact of individual phages on their hosts.

1.5 Further contributions

Niche differentiation within bacterial key-taxa in stratified surface waters of the Southern Pacific Gyre. In review at *ISME Journal*.
Monike Oggerin, Tomeu Viver, ***Jan D. Brüwer****, Daniela Voß, Marina García-Llorca, Oliver Zielinski, Luis H. Orellana, Bernhard M. Fuchs*
Contribution: Determining frequency of dividing cells

Probing the open ocean with the research sailing yacht Eugen Seibold for climate geochemistry. In review *JGR Atmospheres*.
Ralf Schiebel, Hedy M. Aardema, . . . , ***Jan D. Brüwer****, . . . Ulrich Pöschl, Gerald H. Haug*
The author list has been shortened, as >50 authors are listed.
Contribution: Sampling, on-board analysis and interpretation of results, writing of cruise reports (will be deposited)

Influence of marine heatwaves today and tomorrow on the structure of coastal planktonic food webs, a mesocosm experiment. In preparation for submission to *Global Change Biology*.
Cédric L. Meunier, Josefin Schmidt, Antonia Ahme, Areti Balkoni, Katharina Berg, Maarten Boersma, ***Jan D. Brüwer****, Bernhard M. Fuchs, Luis Gimenez, Maite Guignard, Ruben Schulte-Hillen, Herwig Stilbor, Maria Stockenreiter, Felix Weber, Karen Helen Wiltshire, Sylke Wohlrab, Inga V. Kirstein*
Contribution: Assistance during sampling, automatic cell counts for total cell counts

Microbial latitudinal diversity gradients and lineage-specific exchange between the Atlantic surface ocean and the lower atmosphere. In preparation for submission to *PNAS*.
Isabella Hrabe de Angelis, S. Emil Ruff, Hedy M. Aardema, Sanja Basic, ***Jan D. Brüwer****, Hans A. Slagter, Jens Weber, Maria Ll. Calleja, Zoe Cardon, Antonis Dragoneas, Anna Lena Leifke, Björn Nillius, Subha S. Raj, David Walter, Bettina Weber, Bernhard M. Fuchs, Gerald H. Haug, Ulrich Pöschl, Ralf Schiebel, Christopher Pöhlker*
Contribution: Sampling of water and air samples during S/Y Eugen Seibold cruises, automatic data acquisition, and determining cell counts

Size-resolved fluorescent particle distribution, composition, exchange, and origin over the Nort Atlantic Ocean. In preparation.
Isabella Hrabe de Angelis, Hedy M. Aardema, Thomas Klimach, S. Emil Ruff, Hans A. Slagter, ***Jan D. Brüwer****, Maria Ll. Calleja, Antonis Dragoneas, Tobias Könemann, Björn Nillius, Subhja Raj, Jens Weber, David Walter, Gerald Haus, Ulrich Pöschl, Ralf Schiebel, Christopher Pöhlker*
Contribution: On-board sampling, data acquisition via automated microscope, and data analysis

Bimodal bioaerosol population in the Amazon observed by automated fluorescence microscopy. In preparation.
Maria Prass, ***Jan D. Brüwer****, Thomas Klimach, Leslia A. Kremper, Isabella Hrabe de Angelis, Meinrat O. Andreae, Paulo Artaxo, Sebastian Brill, Florian Ditas, Jan-David Förster, Daniel Pickersgrill, David Walter, Ulrich Pöschl, Bernhard M. Fuchs, Christopher Pöhlker*
Contribution: Automatic cell counts and data interpretation

Microbial realms in surface sediments: microbial communities in porewater, loosely attached, and firmly attached cell fractions are distinct and have different metabolic activities. In preparation.
Chyrene Moncada, Carol Arnosti, ***Jan D. Brüwer****, Dirk de Beer, Rudolf Amann, Katrin Knittel*
Contribution: Field-work in the Arctic, determining the frequency of dividing cells

Taxonomic and metabolic responses of microbes in Arctic sediment fractions to extreme seasonal changes. In preparation.
Chyrene Moncada, Carol Arnosti, ***Jan D. Brüwer****, ...*[1]*, Rudolf Amann, Katrin Knittel*
Contribution: Field-work in the Arctic, determining the frequency of dividing cells

Ice nucleation activity over the North Atlantic Ocean. In preparation.
Isabella Hrabe de Angelis, Sanja Basic, Hedy M. Aardema, Hans A. Slagter, Anna Backes, ***Jan D. Brüwer****, Maria Ll. Calleja, Björn Nillius, Jens Weber, Antonis Dragoneas, David Walter, Janine Fröhlich-Nowoisky, Bernhard Fuchs, Gerald Haug, Ulrich Pöschl, Ralf Schiebel, Christopher Pöhlker*
Contribution: On-board sampling, data analysis

[1] To be announced

2

In situ CELL DIVISION AND MORTALITY RATES OF SAR11, SAR86, *Bacteroidetes*, AND *Aurantivirga* DURING PHYTOPLANKTON BLOOMS REVEAL DIFFERENCES IN POPULATION CONTROLS

Jan D. Brüwer[1], Luis H. Orellana[1], Chandni Sidhu[1], Helena C. L. Klip[2], Cedric L. Meunier [2], Maarten Boersma [2,3], Karen H. Wiltshire[2,4], Rudolf Amann[1], Bernhard M. Fuchs[1]

[1]Max Planck Institute for Marine Microbiology, Bremen, Germany
[2]Alfred-Wegener-Institut, Helmholtz-Zentrum für Polar- und Meeresforschung, Biologische Anstalt Helgoland, Helgoland, Germany
[3]University of Bremen, Bremen, Germany
[4]Alfred-Wegener-Institut, Helmholtz-Zentrum für Polar- und Meeresforschung, Wattenmeerstation, List auf Sylt, Germany

Published in *mSystems* (DOI: 10.1128/msystems.01287-22),
©2023 Brüwer et al.

Contributions

Experimental concept and design: 50%
Acquisition of experimental data: 60%
Preparation of figures and tables: 100%
Drafting of the manuscript: 80%

2.1 Abstract

Net growth of microbial populations, that is, changes in abundances over time, can be studied using 16S rRNA fluorescence *in situ* hybridization (FISH). However, this approach does not differentiate between mortality and cell division rates. We used FISH-based image cytometry in combination with dilution culture experiments to study net growth, cell division, and mortality rates of four bacterial taxa over two distinct phytoplankton blooms: the oligotrophs SAR11 and SAR86, and the copiotrophic phylum *Bacteroidetes*, and its genus *Aurantivirga*. Cell volumes, ribosome content, and frequency of dividing cells (FDC) co-varied over time. Among the three, FDC was the most suitable predictor to calculate cell division rates for the selected taxa. The FDC-derived cell division rates for SAR86 of up to $0.8\,d^{-1}$ and *Aurantivirga* of up to $1.9\,d^{-1}$ differed, as expected for oligotrophs and copiotrophs. Surprisingly, SAR11 also reached high cell division rates of up to $1.9\,d^{-1}$, even before the onset of phytoplankton blooms. For all four taxonomic groups, the abundance-derived net growth (-0.6 to $0.5\,d^{-1}$) was about an order of magnitude lower than the cell division rates. Consequently, mortality rates were comparably high to cell division rates, indicating that about 90% of bacterial production is recycled without apparent time lag within 1 d. Our study shows that determining taxon-specific cell division rates complements omics-based tools and provides unprecedented clues on individual bacterial growth strategies including bottom–up and top–down controls.

2.1.1 Importance

The growth of a microbial population is often calculated from their numerical abundance over time. However, this does not take cell division and mortality rates into account, which are important for deriving ecological processes like bottom–up and top–down control. In this study, we determined growth by numerical abundance and calibrated microscopy-based methods to determine the frequency of dividing cells and subsequently calculate taxon-specific cell division rates *in situ*. The cell division and mortality rates of two oligotrophic (SAR11 and SAR86) and two copiotrophic (*Bacteroidetes* and *Aurantivirga*) taxa during two spring phytoplankton blooms showed a tight coupling for all four taxa throughout the blooms without any temporal offset. Unexpectedly, SAR11 showed high cell division rates days before the bloom while cell abundances remained constant, which is indicative of strong top–down control. Microscopy remains the method of choice to understand ecological processes like top–down and bottom–up control on a cellular level.

2.2 Introduction

Growth is an important ecological trait that reflects the success and activity of microbes in a given environment. Often, changes in cell numbers are referred to as apparent or net growth. But this does not take into account that net growth is the sum of cell division and mortality rates. While the net growth of microbial taxa is often reported, little is known about the associated cell division and mortality rates and the temporal coupling of the latter two. We studied two spring phytoplankton blooms, when a de-coupling of cell division and mortality rates can be expected. The initial phase of phytoplankton blooms is often characterized by a dynamic substrate-driven succession of bacterial taxa that is fuelled by the release of carbon-rich algal polysaccharides and other organic matter (Teeling et al. 2012; Teeling et al. 2016). They promote high abundances of copiotrophic clades, which characteristically react quickly to substrate pulses, in a context with initially low mortality. It has been argued that copiotrophic taxa thereby outcompete the slow-growing oligotrophs (Giovannoni et al. 2014). For example, many taxa of the phylum *Bacteroidetes* are stereotypic copiotrophs with sizable genomes of up to 6 million base pairs (Kappelmann et al. 2019; Krüger et al. 2019). Owing to their fast growth rates (2.2 to 5.1 d^{-1}; Arandia-Gorostidi et al. 2017; Yokokawa et al. 2004), they can rapidly grow to high abundances during phytoplankton blooms (Díez-Vives et al. 2014; Teeling et al. 2016). *Aurantivirga* is such a representative genus of *Bacteroidetes*, which recur and is highly abundant during and after phytoplankton blooms in the North Sea (Krüger et al. 2019; Sidhu et al. 2022).

Oligotrophic taxa commonly have small genomes, which provide a more limited capability to react to environmental changes (Kirchman 2016). They have little plasticity in their cell division rates and cell volumes, and generally show slow cell division rates (<0.5 d^{-1}; Ho et al. 2017; Westoby et al. 2021). The well-studied oligotrophic SAR11 clade (Carini et al. 2013; Rappé et al. 2002), which thrives in nutrient-depleted waters, accounts for about a third of all the bacteria in surface ocean waters (Giovannoni 2017; Giovannoni et al. 2005; Malmstrom et al. 2004). Its ∼1.3 Mbp genome is amongst the smallest of all known free-living bacteria (Giovannoni 2017) and its cultured representative *Pelagibacter ubique* is characterized by slow cell division rates in the laboratory (<0.5 d^{-1}; Carini et al. 2013; Rappé et al. 2002). Similarly, the gammaproteobacterial SAR86 clade also represents another group of ubiquitous and abundant oligotrophs in the surface ocean water (Dupont et al. 2012; Schattenhofer et al. 2009), which has thus far evaded cultivation. Members of this clade have small genomes ranging from ∼1.2 to 1.7 Mbp (Dupont et al. 2012) and have been reported to be slow growing (∼0.5 d^{-1}; Teira et al. 2009).

Here, we determine and compare the *in situ* cell division, net growth, and mortality rates of four well-characterized oligotrophic and copiotrophic taxonomic groups over the course of two spring phytoplankton blooms. While net growth rates can be calculated from changes in the number of individuals over time, determining the net growth of a particular microbial population

in a complex sample is inherently difficult due to the lack of unique morphological features of the unicellular organisms. Fluorescence *in situ* hybridization (FISH) allows the identification and detection of individual taxonomic groups through targeting of the 16S ribosomal RNA with oligonucleotide probes (Amann and Fuchs 2008). It enables tracing of taxonomically-defined populations across environments and through time (Amann and Fuchs 2008). In addition to abundance data, FISH allows conclusions to be drawn about microbial growth activity. Hybridized cells from highly active microbial populations appear, on average, larger compared to less active cells (Nikrad et al. 2014). Cell volumes may be derived from the FISH signal area, which is a two-dimensional representation of the cell volume (or more precisely the cytosol; Zeder et al. 2011a). At the same time, FISH signal intensities correspond to cellular ribosome content, reflecting the potential for protein synthesis and thus growth. Previous studies have determined a linear correlation between ribosome contents and the growth rates for individual taxa (Elser et al. 2003; Poulsen et al. 1993; Yang et al. 2008). Prior to cell division, cells segregate their replicated genomes into the maturing daughter cells. Combining FISH with a DNA stain shows the intracellular DNA distribution, allowing the study of the frequency of dividing cells (FDC; Bloem et al. 1995; Hagström et al. 1979). The FDC has a linear correlation with the uptake of radio-labelled substrates (Affronti and Marshall 1994) but has rarely been used in microbial ecology (Hagström et al. 2017). Metagenomics has also been suggested for studying growth activities, as it would allow for a higher taxonomic resolution down to the species level. Most circular bacterial genomes are bidirectionally replicated. In short-read metagenomes, actively dividing cells are expected to have higher coverage of the origin of replication than their termini (Emiola and Oh 2018).

We sampled spring phytoplankton blooms at the long-term ecological research station (LTER) Helgoland Roads in the German Bight in 2018 and 2020. We used 16S rRNA-FISH and taxon-specific image-cytometry to study cell volumes, ribosome content, and the FDC for *Bacteroidetes*, *Aurantivirga*, SAR86 and SAR11. Using taxon-specific cell division rates from dilution experiments, we calibrated FDC values to calculate cell division rates across a spring bloom. We also determined FISH-derived net growth rates and calculated mortality based on net growth and cell division rates. Our microscopy results were contextualized with data derived from the analyses of corresponding metagenomes.

2.3 Results

The 2018 and 2020 spring phytoplankton blooms at the LTER station Helgoland Roads were diatom dominated (Giljan et al. 2022; Sidhu et al. 2022), as in previous years (Teeling et al. 2016). In both years, microbial cell counts increased after increases in the chlorophyll a concentration, which marked the onset of the spring phytoplankton blooms. In 2018, the chlorophyll a concentration increased from 0 - 2 $\mu g\, L^{-1}$ (March till mid-April) to 6.7 $\mu g\, L^{-1}$ on

April 27. The total DAPI cell counts increased 4-fold from 0.8×10^6 cells mL^{-1} (April 30) to 3.2×10^6 cells mL^{-1} on May 24 (Fig. S2.1A). In 2020, chlorophyll a concentration increased from below 1 µg L^{-1} at the end of March to 7 µg L^{-1} (April 26) and 9.4 µg L^{-1} (April 28). The total microbial cell counts increased approximately 3-fold from 0.6×10^6 cells mL^{-1} (mid-April) to 1.6×10^6 cells mL^{-1} (April 20), then collapsed to below pre-bloom conditions, and finally increased to 1.8×10^6 cells mL^{-1} on May 26 (Fig. S2.1B).

2.3.1 Frequency of dividing cells as a robust parameter to investigate cell division

In 2020, SAR11 cell counts followed the general patterns of the total microbial counts (Fig. 2.1A, S2.1). Their abundance decreased towards the end of March from 1.9×10^5 cells mL^{-1} to 0.7×10^5 cells mL^{-1} (Fig. 2.1A, 2.2E). Thereafter, cell counts increased and peaked on April 20 (3.9×10^5 cells mL^{-1}), decreased until May 4 (0.7×10^5 cells mL^{-1}), and increased again until the end of the sampling campaign. During the same period of time the average cell volume, based on FISH signals, increased by a factor ∼1.5 and showed opposing trends to the cell counts (Fig. 2.1B). Average cell volumes increased from 0.10 ± 0.05 µm^3 (mean ±standard deviation) on March 2 to 0.15 ±0.06 µm^3 on April 1. Thereafter, the volumes decreased until April 20 (0.11 ± 0.04 µm^3), when cell counts were maximal, but subsequently increased during the first week of May (0.18 ±0.07 µm^3 on May 4). The amount of ribosomes per cell, determined using FISH fluorescence, showed a similar pattern to the cell volumes. They increased by a factor of ∼2 from beginning March to April from 2.0 ±1.3 to 4.1 ±2.2 arbitrary units (AU), then decreased until April 20 (2.1 ±1.1 AU), and again increased in the first week of May (5.0 ±2.5 AU; Fig. 2.1C). The trends in the FDC concur with cell volume and ribosome content data (Fig. 2.1D). The FDC increased approximately three-fold from around 4% in early March to a maximum of 12.6% on March 27, dropped to pre-bloom conditions until mid-April and peaked a second time on May 8 (12.5%).

The three cellular characteristics (cell volume, ribosome content, and FDC) were not only positively correlated to each other for SAR11 (Fig. 2.2), but also for the three other taxonomic groups *Bacteroidetes*, *Aurantivirga* and SAR86 (Fig. S2.2). The multiple linear regressions between the three characteristics among themselves, each with the additional interaction terms of the sampled year and the respective FISH probes, were statistically significant ($p < 0.0001$, further info in supplementary information SI). Due to reasons discussed below, we proceeded with FDC as a suitable proxy of cell division rates, though all three characteristics would be suitable.

2.3.2 Growth activity changes of SAR11, SAR86, *Bacteroidetes* and *Aurantivirga* in 2018

We could only assess relative growth activity changes by studying FDC in 2018, as calibrations of FDC with dilution experiments were only done in 2020. The FDC values ranged be-

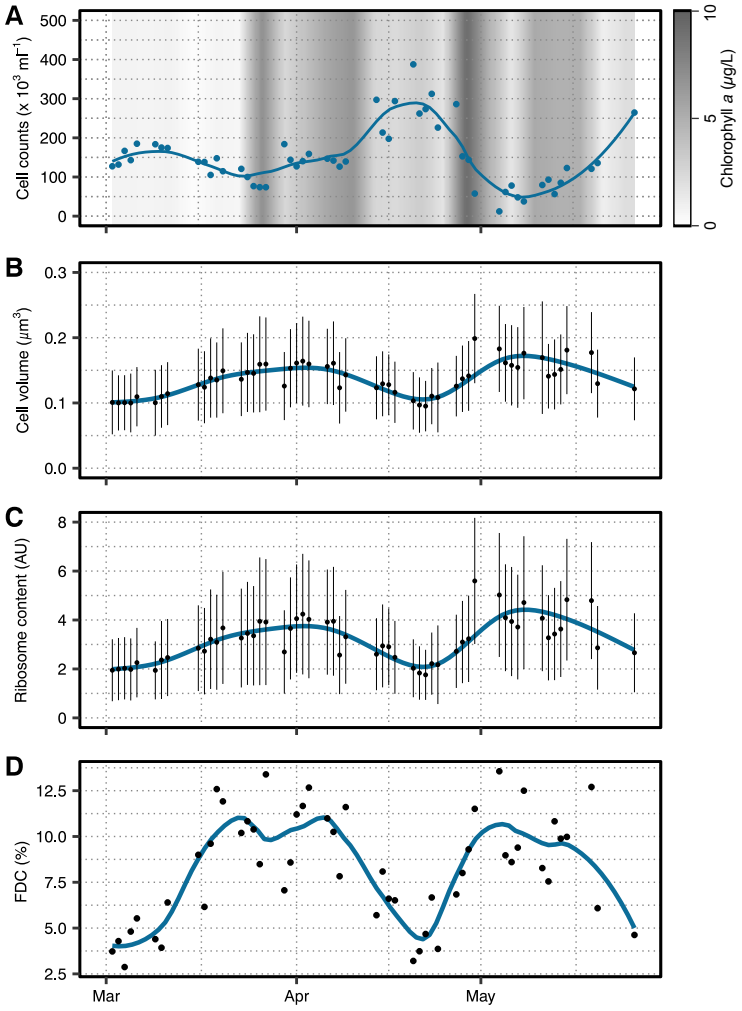

Figure 2.1: Cellular parameters of SAR11 during the spring bloom in 2020. (A) Cell abundances in blue and chlorophyll a concentration as grey background. (B) Cell volumes and (C) ribosome contents were calculated from CARD-FISH signals and plotted as means per day (black points) ±sd (black lines). A *loess* smoothing of all data is depicted in blue. (D) The FDC, as a measure of cell division, was determined from cells with two internal local DAPI maxima. An FDC per sampling day are shown as black points and *loess* smoothing as blue line.

tween 5 and 15% with a few exceptions, mainly within the genus *Aurantivirga*. For SAR11, the FDC was initially between 8 and 10% from March 1 to April 11 but increased thereafter to 15% by April 13. This increase occurred notably before chlorophyll a concentration started to increase by the end of April. The SAR11 FDC started to decrease after May 4 to pre-bloom conditions. SAR11 cell counts exceeded 2.5×10^5 cells mL^{-1} by April 3 and steadily increased to 1.1×10^6 cells $mL^{-1}$by May 24 (Fig. 2.3A). SAR86 FDC increased from 4 to 8% until April 3, doubled to 16.5% by April 30, and decreased thereafter to around 10%. SAR86 cell counts were between 1×10^4 cells mL^{-1} to 3×10^4 cells mL^{-1} until May 8, then abundances increased >10-fold, peaking at 3.5×10^5 cells mL^{-1} on May 24 (Fig. 2.3B). *Bacteroidetes* FDC was initially low (4.7 to 6.6%) until April 9, increased thereafter to reach 16.3% on April 26, and decreased after-

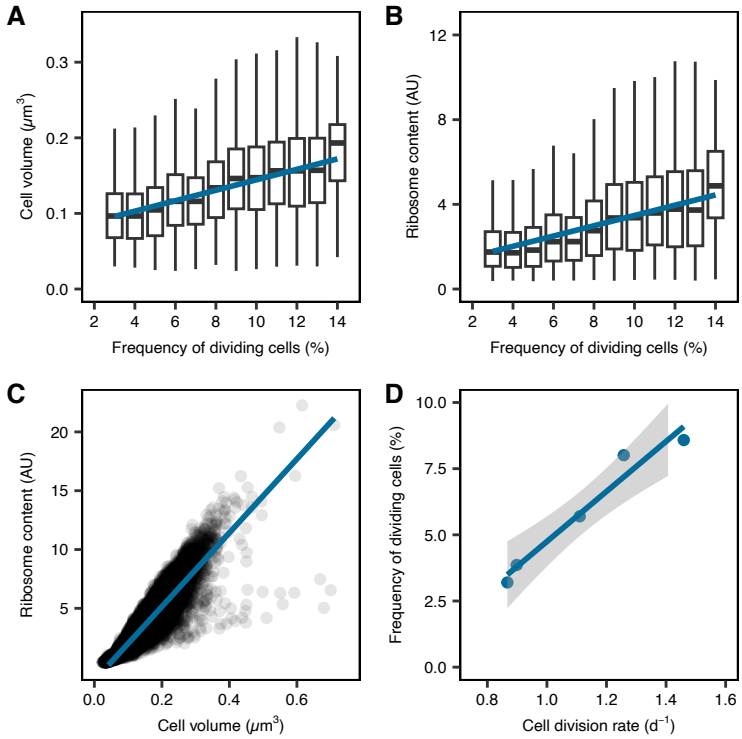

Figure 2.2: Correlation of cellular parameters and cell division rates. (A) Box and whiskers plot of cell volume in relation to FDC with regression in blue. (B) Box and whiskers plot of ribosome content (fluorescence per cell) in relation to FDC with regression in blue. Box in (A) and (B) represent 25th and 75th percentile, the mean is drawn as solid line within the box. The whiskers are 1.5x interquartile percentile. Outliers are not visualized. (C) Ribosome content plotted over measured cell volume as black points with linear regression depicted in blue. (D) Cell division rates were assessed in dilution experiments and correlated to FDC. Standard error is shown as grey shading.

wards to pre-bloom conditions. *Bacteroidetes* cell counts varied between 0.6×10^5 cells mL^{-1} to 1.7×10^5 cells mL^{-1} until May 3, peaked at 2.7×10^5 cells mL^{-1} on May 9 and peaked a second time with 6.2×10^5 cells mL^{-1} on May 24 (Fig. 2.3C). *Aurantivirga* FDC was low in March (2 to 6%, Fig. 2.3D) and increased to a maximum of 20% on April 27. In early May, FDC was around 2.5% but increased to 13% by May 28. *Aurantivirga* cell counts ranged between 0.1×10^4 cells mL^{-1} to 0.9×10^4 cells mL^{-1} until mid-April, when they started to increase to peak first on May 7 (3.4×10^3 cells mL^{-1}) and again on May 24 (9.3×10^3 cells mL^{-1}, Fig. 2.3D).

2.3.3 2020 spring bloom cell division rates for SAR11, SAR86, *Bacteroidetes*, and *Aurantivirga*

We conducted dilution experiments on five days across the 2020 spring bloom to experimentally determine taxon-specific cell division rates (Table S1 at doi.org/10.6084/m9.figshare.22290166). We used multiple linear regressions with the null hypothesis that a) FDC (FDC) is independent of experimentally-derived cell division rates (μ) and b) this relationship is independent of the assessed taxon ($taxon$; formula: $FDC \sim \mu * taxon$). We rejected both null hypotheses ($R^2 = 0.86$; $p < 0.0001$) and could calculate taxon-specific

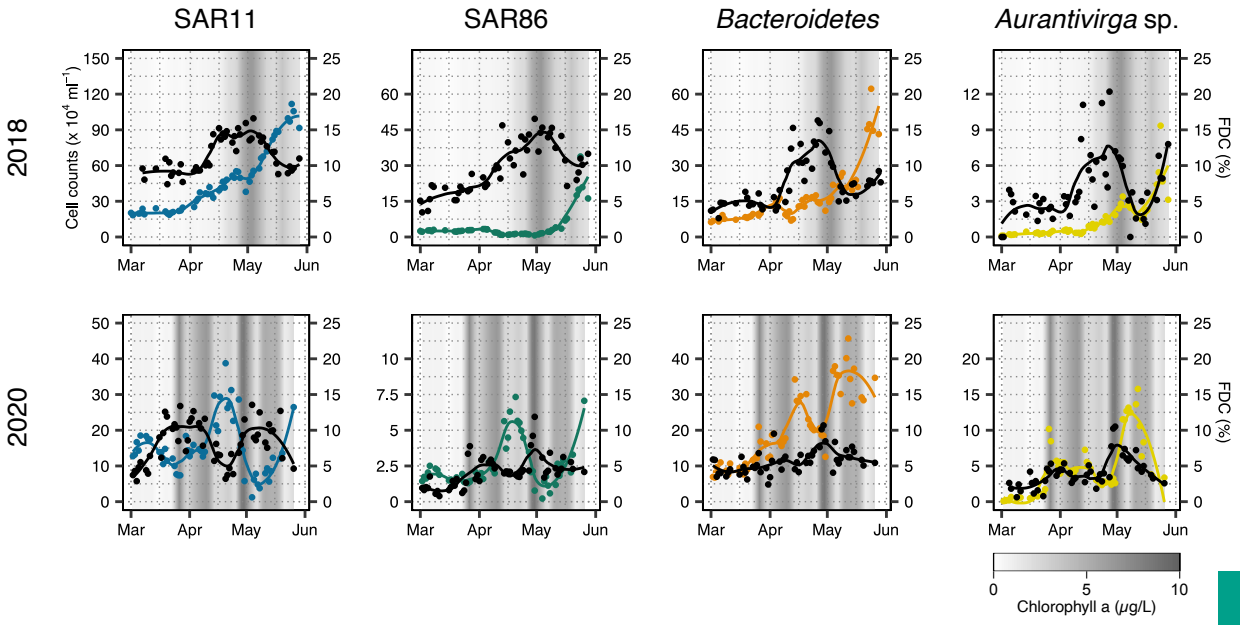

Figure 2.3: Cell abundances and FDC in 2018 and 2020. Cell abundances of SAR11, SAR86, *Bacteroidetes*, and *Aurantivirga* during the spring bloom 2018 (upper row) and 2020 (lower row) in coloured points with *loess* smoothing as coloured lines. Taxon-specific FDC are shown by black dots and *loess* smoothing as lines. Chlorophyll a concentration is shown as grey shading in the background in all plots.

cell division rates from the FDC across the 2020 spring bloom (Fig. S2.3A, Table S2 at doi.org/10.6084/m9.figshare.22290166).

Cell division rates varied noticeably over the course of the bloom of 2020. Generally, SAR11 and *Bacteroidetes* grew at rates of 0.5 to 2 d^{-1}. SAR86, on the other hand, exceeded 0.5 d^{-1} only once in late April. Please note that calculated cell division rates for SAR86 might be underestimated due to a single data point (Fig. S2.3A). However, they did not exceed rates of 0.6 d^{-1} in the dilution experiments. *Aurantivirga* cell division rates were highly variable, ranging from no cell division to 1.9 d^{-1}. In detail, SAR11 cell division rates increased ~3-fold in March, even before the phytoplankton bloom started. Cell division rates reached their first maximum of 1.9 d^{-1} on March 27, one week prior to the maximum in chlorophyll a concentration. It is remarkable that cell counts decreased to about half during the same time. Subsequently, cell division rates decreased to pre-bloom levels in mid-to-end of April (0.8 to 1.2 d^{-1}), when cell counts increased to reach a maximum. Furthermore, SAR11 cell division rates were >1 d^{-1} on 43 of 53 sampling days in 2020 (Fig. 2.4). By contrast, SAR86 divided <0.5 d^{-1} on 52 sampling days (Fig. 2.4). The average *Bacteroidetes* cell divided ~1 d^{-1} in pre-phytoplankton bloom conditions. Their cell division rate reached a maximum of 2.1 d^{-1} on April 29, shortly before cell counts reached a maximum of 4.6×10^5 cells mL^{-1} (Fig. 2.4). *Aurantivirga* cell division rates covered the greatest range. While calculated rates were between 0 to 0.5 d^{-1}) pre-bloom, they peaked at 0.9 d^{-1} on March 27 and 1.9 d^{-1} on April 30, coinciding with an overall increased cell abundances *in situ* (Fig. 2.4H).

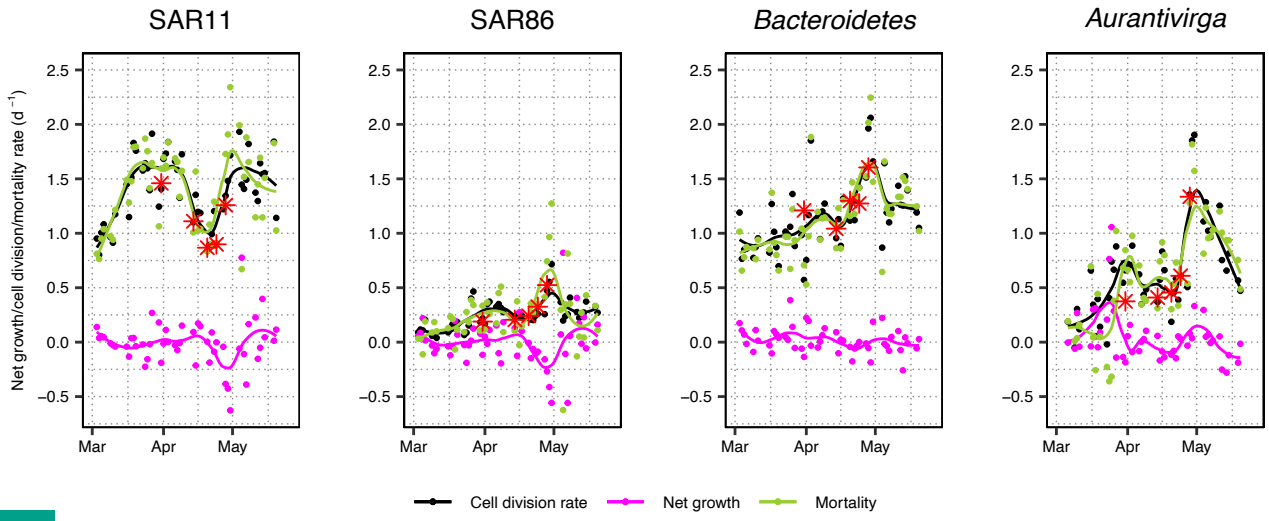

Figure 2.4: Taxon-specific net growth, cell division, and mortality rates during 2020 spring bloom. Taxon-specific cell division rates were calculated based on FDC throughout the spring bloom (black points with *loess* smoothing as black line). Net growth was calculated based on FISH abundance data (magenta points with *loess* smoothing as magenta line). Mortality is the cell division rate minus net growth (green points with *loess* smoothing as green line). Measured cell division rates by dilution experiments are depicted with a red asterisk.

2.3.4 Cell division rates versus net growth rates during 2020 spring bloom

Besides cell division rates (calculated from the FDC), we also determined the net growth rate, based on the FISH abundance data. Net growth rates for all taxa ranged between -0.6 and $0.5\,\mathrm{d}^{-1}$, with two exception for *Aurantivirga*, and one for SAR11 and SAR86, each (Fig. 2.4). These net growth rates were corresponding to doublings in cell abundances spanning multiple days. For example, the approximate doubling in SAR11 cell counts from 1.4×10^5 cells mL^{-1} (April 9) to 3.0×10^5 cells mL^{-1} (April 14) occurred within 5 days, which corresponds to a net growth rate of $0.15\,\mathrm{d}^{-1}$. The net growth (r) of for example SAR11 was almost an order of magnitude lower (minimum/maximum: -0.6 to $0.39\,\mathrm{d}^{-1}$, with one exception) than the cell division rates (μ, 0 – $2\,\mathrm{d}^{-1}$). It follows that the calculated mortality rates (d=μ-r) were high and close to the cell division rates (Fig. 2.4). We compared these calculated mortality rates to grazing rates, which were determined in the dilution experiments. Both were significantly correlated in a multiple regression model of $grazing \sim mortality * taxon$ ($R2$ = 0.86; p = 0.002; Fig. S2.3B). The regression for SAR86 and *Bacteroidetes* were negative, due to the spread of the data. Nevertheless, data from all taxa combined followed the 1:1 ratio or calculated mortality was larger than grazing. This indicates that our calculated mortality rates can to a large extend be explained by grazing, with few cases where, for example, viral lysis might play an important role. Similarly, Sanchez et al. (2020) found in a recent study that mortality due to grazers was larger than viral lysis, across multiple seasons and bacterial taxa.

2.3.5 Bioinformatic assessment of taxon diversity and growth measures during the 2018 bloom

Two metagenomes were sequenced per week during the 2018 sampling campaign. We compared our cytometric results to metrics derived from these metagenomes. First, we assessed the diversity of retrieved representative metagenome assembled genomes (MAGs) from the four studied taxa across the spring bloom. We checked whether community shifts within one taxon could be responsible for the observed changes in abundances, FDC, and growth rates. SAR11 was represented by 5 MAGs, of which 4 belong to the open ocean clade 1a.1 and MAG r31 to clade 3 (Fig. S2.4; Delmont et al. 2019; Haro-Moreno et al. 2020). Both, SAR11 and SAR86 were dominated by a single MAG towards the end of the bloom (Fig. S2.5). For *Bacteroidetes*, different species of the family *Flavobacteriaceae* succeeded each other. First, MAGs belonging to the GTDB-Tk genus-level clade MAG-121220-bin8 were most abundant until mid-April, and was followed by the genus-level clade Hel1-33-131 (Fig. S2.5, Table S3 at doi.org/10.6084/m9.figshare.22290166). Within the genus *Aurantivirga*, MAG r29 initially dominated, until mid-April, then MAG r261 took over until end of April (Fig. S2.5).

Next, we aimed to assess microbial growth parameters during the 2018 spring bloom using Growth Rate index (GRiD) values. We tested different mapping algorithms, which resulted in substantially different GRiD values, while the estimates of sequencing depth for individual MAGs was comparable between methods (Fig. S2.6). Here we focus on GRiD values obtained using default settings. GRiD values fluctuated between 1.1 and 2.8 for all the assessed MAGs. However, no SAR86 MAG exceeded a GRiD value of 2, in contrast to the three other groups. GRiD values of the most abundant MAGs exhibited little variability over the spring bloom (Fig. S2.5). For example, SAR11 MAG r27 was the most abundant, especially towards the end of the spring bloom, but had low GRiD values compared to other SAR11 MAGs (Fig. S2.5). The determined GRiD values correlated positively to FDC, with a taxon-specific interaction term, though with high variance ($p < 0.0001$, $R2 = 0.12$; Fig. S2.5).

Finally, we used the codon usage bias method gRodon to predict possible maximum cell division rates (Fig. 2.4). Four out of five assessed SAR11 MAGs were identified as oligotrophs. SAR11 MAG r116 had a predicted maximum growth rate of $10\,d^{-1}$ (Table S4 at doi.org/10.6084/m9.figshare.22290166) but had amongst the lowest relative abundances ($\leq$1% and absent in mid to end May) throughout the 2018 phytoplankton bloom. All SAR86 MAGs were identified as oligotrophs and the *Aurantivirga* MAGs as copiotrophs. The phylum of *Bacteroidetes* was rather heterogeneous, with 48 MAGs classified as copiotrophs and 38 MAGs as oligotrophs (Fig. 2.5, Table S4 at doi.org/10.6084/m9.figshare.22290166). Interestingly, the *Bacteroidetes* GTDB-tk genus MAG-121220-bin 8, the first dominating *Bacteroidetes* genus, was classified as an oligotroph (maximum growth rate $<4\,d^{-1}$), while Hel1-33-131, the most abundant MAG

towards the end of the sampling, is classified as a copiotroph (maximum growth rate 6.9 d^{-1}).

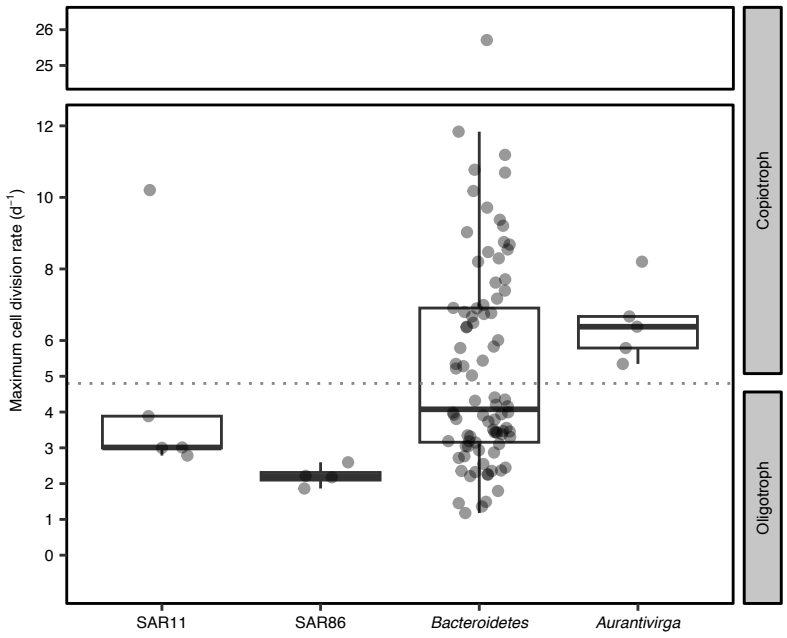

Figure 2.5: gRodon-predicted minimal doubling times. Box and whisker plots of genomic potential for minimal doubling times predicted by gRodon for SAR11, SAR86, *Bacteroidetes*, and *Aurantivirga* MAGs, retrieved from 2018 spring phytoplankton bloom. Boxes indicate 25th and 75th percentile, the mean is drawn as solid line. Whiskers represent 1.5x IQR, outliers are not visualized. Points indicate results of individual MAGs. Dotted line indicates threshold between oligotrophs (minimal doubling time >5 h) and copiotrophs (minimal doubling time <5 h), according to the authors of gRodon.

2.4 Discussion

We studied taxon-specific growth changes using *in situ* image cytometry during the course of two spring diatom blooms. FDC is the method of choice to assess cell division activity, though all FISH-derived parameters, namely cell volume and ribosome content, and FDC, co-varied over time (Fig. 2.1, S2.2). First, FDC quantifies the proportion of actively dividing cells, whereas cell volume and ribosome content are indirect measures of cellular growth spreading over a continuum of values with no defined threshold of cell division. Secondly, FDC is methodologically advantageous over the former two, as it combines two separate stains. Hence, the object identification (i.e., FISH-positive cell) and the measured property (i.e., DAPI distribution) are effectively independent from each other (Miura and Nørrelykke 2021). Next, relative differences were most pronounced for FDC, allowing the detection also of small changes in microbial growth. Furthermore, FDC correlated linearly with taxon-specific cell division rates determined in dilution experiments (Fig. S2.3), corroborating earlier findings from pure cultures and environmental samples (Matsuyama 1993; Møller et al. 1995).

Our image cytometry approach had some limitations regarding cell volume measurements

and dilution experiments. First, cells are filtered onto polycarbonate filter and might lose some of their height due to fixation. Therefore, our 3D models of cells volumes most likely somewhat overestimate in the third dimension. Second, cell volume measurements are derived from a CARD amplification signal, which often seem to overshadow the cell boundaries and hence overestimate the cell dimensions. Additionally, object identification and volume measurement were both done on the same signal. The thresholds to identify a cell, immediately influence the cell size and volume estimates (Miura and Nørrelykke 2021). Taken together, this could contribute to an overestimation of cell volume measurements. Nevertheless, this should not affect comparisons of cell volumes within this study. Finally, our dilution experiments did not exclude phage-free cell division rates, as other studies have done (Sánchez et al. 2020). The dilutions were prepared with 0.2 µm filtered water, which is larger than most phages.

We challenged the FDC-derived cell division rates using bioinformatic predictions from metagenomes and MAGs for the 2018 spring bloom. We computed GRiD (Emiola and Oh 2018), which were highly susceptible to the mapping tools that were used, not yielding any reproducible results. Therefore, we cannot support using the GRiD algorithm at this developmental stage. GRiD values generated under default mode were generally correlated with the taxon-specific FDC, though with little predictive power ($R^2 = 0.12$). Although GRiD could in theory be useful to assess individual species or strains to a higher taxonomic resolution than FISH-based microscopy, microscopically derived growth measures remain more direct and precise. In addition, we computed gRodon values to predict the genomic potential for maximum cell division rates. They can be used to categorize the retrieved MAGs as copiotrophic and oligotrophic, according to the authors of gRodon (Weissman et al. 2021). The gRodon results were in line with our assumptions that SAR11 and SAR86 can be considered oligotrophs and *Aurantivirga* a copiotroph. *Bacteroidetes* being heterogeneous, with the majority of clades putatively slow growing, confirms previous findings of few actively growing *Bacteroidetes* clades during phytoplankton blooms (Krüger et al. 2019). All experimental cell division rates were slower than gRodon-predicted genomic potentials for maximum cell division rates, which indicates that – on a community level – none of the assessed groups divides to their full capacity.

Under constant substrate and nutrient conditions, cell division and mortality rates are both temperature dependent (Ratkowsky et al. 1982; Vaqué et al. 1994). This is also known for bacteria in environmental samples (López-Urrutia and Morán 2007; White et al. 1991) but only partly visible in our case (Fig. S2.1, Table S5 at doi.org/10.6084/m9.figshare.22290166). For example, though the temperature increased between April and May 2020 from 9.9 °C to 11.4 °C (Fig. S2.1B), the cell division rates of *Bacteroidetes* and *Aurantivirga* decreased in May and SAR11 cell division rates fell to pre-bloom levels in mid-April and end of May. Other than temperature, the bacterial communities are shaped by phytoplankton-derived organic matter (Teeling et al. 2012; Teeling et al. 2016). Inorganic nutrients such as nitrate, ammonium, phosphate, and silicate, which are tightly monitored at the LTER Helgoland, are negatively correlated with FDC (Table

S5 at doi.org/10.6084/m9.figshare.22290166; 2018: Giljan et al. 2022, 2020: Sidhu et al. 2022). However, these nutrients are directly taken up and depleted by phytoplankton and are, thus, only indirectly correlated with FDC without causation (Giljan et al. 2022; Teeling et al. 2016).

The diverse phylum *Bacteroidetes* comprised fast and slow growing bacteria. The observed cell division rates for *Bacteroidetes* (minimum to maximum: 0.6 to 2.1 d^{-1}) agree with previous reports, ranging from 0.5 to 5.1 d^{-1}; Arandia-Gorostidi et al. 2017; Eilers et al. 2001; Teira et al. 2009; Yokokawa et al. 2004). Metagenome analyses confirmed that the *Bacteroidetes* constituted a highly diverse phylum with a large variety in minimal doubling times, predicted from MAGs using gRodon, and large variations in growth as reconstructed by GRiD. Thus, division rates of individual *Bacteroidetes* species might be considerably higher than those for the remainder of the community.

The genus *Aurantivirga* is known as one of the first responders to phytoplankton blooms, not only in the North Sea (Francis et al. 2021), but also in polar waters (Kieft et al. 2020; Liu et al. 2020). In this study, *Aurantivirga* showed the greatest plasticity in cell volume and cell division rates (0 to 1.9 d^{-1}) over the course of the 2020 spring bloom, with a pronounced peak during the later bloom stages. *Aurantivirga* have previously been found to outcompete other taxa by their capability to digest algae-derived polysaccharides (Francis et al. 2021; Krüger et al. 2019; Sidhu et al. 2022). This fits with the general observation that *Aurantivirga* net growth and cell division rates increased with the peaks in chlorophyll a in both years, although the net growth and cell division rates were statistically not correlated. Our metagenome-derived gRodon results indicate that all *Aurantivirga* MAGs have minimal doubling times typical for copiotrophs. We conclude that the *Aurantivirga* populations had a copiotrophic lifestyle with rapid boom and bust cycles.

SAR86 cell division rates increased at the beginning of the 2020 bloom, which indicates the dependence of SAR86 on organic matter exudated by live phytoplankton (Mayerhofer et al. 2021). At the end of April, SAR86 cells were apparently exposed to changes in top-down control factors, as its net growth bottomed (-0.1 to -0.2 d^{-1}) while the cell division rates peaked (>0.5 d^{-1}). SAR86 cell volumes were comparable (0.16 to 0.40 μm^3) to *Bacteroidetes* (0.22 to 0.53 μm^3) and therefore much larger than previously reported (0.06 to 0.08 μm^3; Nikrad et al. 2014), but this might be an overestimation (please see the critical evaluation of our cell volume measures above). SAR86 was the only taxonomic group for which the MAGs never exceeded GRiD values of 2 throughout the spring bloom. Likewise, the gRodon values characterized all SAR86 MAGs as oligotrophic. SAR86 cell division were amongst the lowest in our study, not only from the dilution experiments (max. 0.6 d^{-1}), but also the calculated rates throughout the spring bloom (<0.75 d^{-1}).

SAR11 comprised the smallest cells of all four groups in our study with the least variability in cell volume. Due to the assumed slower cell division rates of SAR11, we hypothesized less variation in ribosomal content compared to putatively faster growing *Bacteroidetes* and *Aurantivirga* (Campbell et al. 2011). While generally lower, the ribosomal content of SAR11 cells fluctuated

comparable to the three other taxa. They divided faster (max. 1.9 d^{-1}) than cultivated SAR11 in optimized media (<0.5 d^{-1}; Becker et al. 2019; Carini et al. 2013; Rappé et al. 2002). However, our findings are in line with previous SAR11 cell division rates from dilution experiments (1.2 to 1.8 d^{-1}) from coastal Mediterranean waters (Ferrera et al. 2011; Sánchez et al. 2020; Sánchez et al. 2017). The here-assessed coastal SAR11 were dominated by members of the clade 1a.1, which is commonly attributed to the open-ocean, in 2018 (Fig. S2.5) and 2020 (Sidhu et al. 2022).

To our surprise, SAR11 increased their cell division rates days to weeks before the main phytoplankton bloom started in both studied years. SAR11, like SAR86, *Aurantivirga*, and other *Bacteroidetes*, are potential photoheterotrophs capable of proteorhodopsin-dependent ATP synthesis (Dupont et al. 2012; Giovannoni et al. 2005; Song et al. 2015). Hence, increasing light intensities during the spring blooms could support growth by fuelling energy-dependent transport albeit only SAR11 cells seemed to have benefitted from this. Above ~25 Einstein $m^{-2}d^{-1}$, SAR11 cell division was increased gradually (Fig. S2.1, S2.7), which could potentially be considered as a threshold in our case to obtain enough energy for increased activity. Previous incubations detected increased proteorhodopsin-derived activity in SAR11 after incubations with 36 Einstein $m^{-2}d^{-1}$ (Lami et al. 2009).

Despite high cell division rates (>1 d^{-1}) before the phytoplankton bloom 2020, SAR11 cell abundances did not increase and even decreased. Net growth was almost an order of magnitude lower than the cell division rate, indicating tight top-down controls. Since SAR11 exhibited the highest mortality rates before the phytoplankton bloom, we assume a SAR11-specific top-down control factor. Non-specific grazing is rather unlikely due to the small cell size (Pernthaler 2005) and taxon-specific grazing (Gerea et al. 2013; Thurman et al. 2010) has to yet be shown for SAR11. Besides grazing, viruses are known to shape the SAR11 community (Ferrera et al. 2011; Morris et al. 2020; Zhao et al. 2013). Previous dilution experiments in the Mediterranean Sea accounted for viral lysis. The authors found an increased influence of viruses on the SAR11 community especially during autumn but less in spring (Sánchez et al. 2020). Considering the overall dynamics in our data, the timing of sampling is crucial and could explain, why similar earlier experiments did not detect an effect of viruses on the SAR11 community (Ferrera et al. 2011).

All in all, it is not only their high cellular abundance (Mayerhofer et al. 2021) but mainly the high cell division and mortality rates that impact on our perception of the microbial loop and thereby the entire marine carbon cycle. Based on our data, we propose that the clade SAR11 not only consists of clear-cut oligotrophs, but that coastal strains (including clade 1a.1) exhibit fast cell division rates typical of copiotrophs.

2.4.1 The microbes constant struggle against mortality

In addition to cell division rates, we also estimated net growth rates based on FISH abundance data. The difference between these two rates yields corresponding mortality rates. For all studied taxonomic groups, the cell division and mortality rates were generally close to each other. We validated our derived mortality rates against the grazing rates obtained from the dilution experiments, which largely followed a 1:1 ratio. A 1:1 ratio would mean that all mortality is due to grazing. Our results reveal that despite several cell divisions per day, mortality diminishes the increase in cell abundance. In other words, cell division rates in the environment are higher than anticipated, however mortality removes >90% of newly produced bacterial biomass each day. Similar tight couplings have been reported earlier (Sánchez et al. 2020), though with great variation throughout an entire year but not resolved on a temporal scale as our data. In this context it is also interesting to note that mortality sets in almost instantaneously with no detectable delay. This means that grazers and / or phages are present and ready to control the growing community effectively at all times. This scenario also seems to be the rule rather than the exception, as we could demonstrate such a tight trophic coupling in four taxonomic groups for two spring blooms with high primary production covering a period of 3 month each.

2.5 Conclusion

In our study we have shown that FDC values enable the measurement of cell division rates *in situ*, after taxon-specific calibrations. This is rather straightforward to implement in future studies. Based on changes in FDC over time, we showed evidence for an interplay between bottom-up and top-down controls in the early phase of spring phytoplankton blooms. These results raise many questions. For example, what fuels SAR11 to grow at high cell division rates of 1.9 d^{-1} before the phytoplankton bloom? Similarly, what are the top-down controls that balance these fast division rates? In the past, much research has focused on bottom-up control factors. With the tools presented here, future research may include top-down control factors, which equally shape the bacterial world.

2.6 Material and Methods

2.6.1 Sampling

Marine surface water (∼1 m depth) was sampled at the LTER Helgoland Roads (54° 11.3' N, 7° 54.0' E; Wiltshire and Dürselen 2004 in a well-mixed pelagic water column during spring phytoplankton blooms in 2018 and 2020. Microscopy samples were collected every working day between March to June by the research vessel Aade. We fixed samples of 10 mL (SAR11 and *Bacteroidetes*) or 100 mL (SAR86 and *Aurantivirga*) with 0.2 µm-filtered formaldehyde (1% final

concentration, 1 hour at room temperature). These different volumes were necessary to account for variation in abundance. Subsequently, fixed cells were filtered onto 0.2 µm polycarbonate filters (47 mm diameter, Sigma Aldrich, Taufkirchen, Germany) and placed on 0.45 µm cellulose nitrate support filters (Sigma Aldrich). The filters were stored at −20 °C until further processing. Chlorophyll a concentration was measured twice a week via HPLC using the method of Zapata et al. (2000) and Wiltshire et al. (2008). Photosynthetically active radiation (PAR) remote sensing data was retrieved for the sampling period from the NASA Goddard Space Flight Center (NASA Goddard Space Flight Center Ocean Biology Processing Group 2022). Data was analyzed with the R package raster (Hijmans et al. 2015) cropped to cover the German Bight (53° 41' 17.8794" to 54° 41' 17.8794" N and 7° 24.0' to 8° 24.0' E). A *loess* average of the cropped data was visualized (Fig. S2.1).

For metagenomic sequencing, seawater was sampled at 1 m depth twice a week over a period of three months. One litre of unfixed seawater was sequentially filtered through 10, 3, and 0.2 µm pore-size polycarbonate filters. Filters were flash frozen in liquid nitrogen and stored at −20 °C until further use.

2.6.2 Cell division rates based on dilution grazing experiments

We conducted five dilution grazing experiments before, during, and after the phytoplankton bloom of 2020 (March 31 and April 14, 20, 24 and 28) in order to determine the cell division rates of individual bacterial clades. Sea water was sampled at Helgoland Roads and sieved (200 µm) to exclude mesozooplankton such that the only consumers were microzooplankton and heterotrophic nanoflagellates. This water was subsequently diluted with 0.2 µm sterile-filtered seawater to create a dilution series of 100% (undiluted), 50% (1:1), 25% (1:3), and 10% (1:9) in 1 L cell culture flasks (Greiner, Kremsmünster, Austria). No further nutrients were added. One aliquot of the undiluted samples was taken as a reference at the beginning of sampling (t0). All dilutions and 24 h incubations were prepared in duplicate.

The flasks were placed on a plankton-wheel (∼3.2 rpm) to prevent sedimentation of the planktonic organisms and incubated with a day-to-night regime of 14 h to 10 h (20 to 30 photons $m^{-2}s^{-1}$) for 24 h in a temperature-controlled room set at the *in situ* sea surface temperature of the corresponding day. After 24 h, samples were taken from all the duplicated dilutions, and fixed and filtered as described for the microscopy samples.

Total and taxon-specific cell concentrations were determined through DAPI staining and FISH experiments similar to those for the environmental samples, as described below and in detail in the SI. Cellular concentrations from the dilution experiments are provided in Table S1 (at doi.org/10.6084/m9.figshare.22290166). Cell division rates were calculated following Landry and Hassett (1982), as described in the SI.

2.6.3 Cell counts and FISH

Samples were stained with the DNA stain 4',6-diamidino-2-phenylindole (DAPI; 1 µg mL^{-1}, 7 min at room temperature) and subsequently washed with deionized water and ethanol. CARD-FISH was performed with probes targeting SAR11 (SAR11-mix), SAR86, *Bacteroidetes* (CF319a), and *Aurantivirga* (AUR452; Table S6 at doi.org/10.6084/m9.figshare.22290166) following the protocol described in Fuchs et al. (2007) and in more detail in the SI. The nonsense-probe NON338 was included as a negative control. All probes were purchased from Biomers (Biomers, Ulm, Germany).

We excluded a potential impact of the CARD signal amplification on the linearity of the fluorescence measurements and cell volume determinations by a comparison between CARD-FISH to tetra-labelled FISH on selected samples on the 2020 dataset (Fig. S2.8). All samples were embedded in antifading media Citifluor:Vectashield (1:3; Citifluor Ltd, London, UK; Vector Laboratories, Burlingame, CA, USA) for microscopy.

2.6.4 Automated image recording

Images were recorded on a Zeiss AxioImager.Z2m microscope with a cooled charged-coupled device (CCD) camera (Zeiss AxioCam MRm, Zeiss Oberkochen, Germany). The microscope was equipped with a Zeiss Colibri 7 LED (385 nm for DAPI, 469 nm for Alexa 488 dye, and 590 nm for autofluorescence) and a Multi Zeiss 62 HE filter cube (Beam splitter FT 395+495+610). The Zeiss AxioVision software (Zeiss, Germany) was used for automated image acquisition with a custom-built macro (Bennke et al. 2016; Zeder et al. 2011a; Zeder et al. 2011b). The focal planes of 120 fields of view (FOV) per sample were identified with 1x magnification. Subsequent fine tuning and image recording was done with a 63x Plan Apochromat objective (1.4 NA, oil immersion).

2.6.5 Image cytometry

The obtained 8-bit greyscale images were loaded into our Automated Cell Measuring and Enumeration tool (ACME, available from https://www.mpi-bremen.de/automated-microscopy.html) for manual curation and image analysis (Fig. S2.9) as described previously (Bennke et al. 2016; Zeder et al. 2011b). FISH signal-derived cell size and signal intensity measurements were exported from the ACME tool. To calculate cell volumes V from the FISH signal-derived cell sizes (two-dimensional projection), we used the basic geometric approximation of cylinders with hemispherical caps (Fry 1990; Khachikyan et al. 2019; La Ferla et al. 2014), with the cylinder radius r and length l (i.e., total length $l_{tot} - 2r$): $V = \frac{4}{3}\pi r^3 + \pi r^2 l$. Previous research has shown differences as low as $\sim$1% to more sophisticated models (Zeder et al. 2011a).

We measured the total fluorescence (i.e., the sum of grey values of all pixels within one cell), based on the FISH signal. Additionally, the image processing software ImageJ/Fiji (v2.1.0/1.53e;

Schindelin et al. 2012) with the plug-in MicrobeJ (v5.13l; Ducret et al. 2016) was used to calculate the FDC. A FISH-positive cell was defined as dividing if it contained two local DAPI maxima (compared to one local maximum for non-dividing cells). FDC was calculated for each taxon individually as $FDC = \frac{\sum dividing\ cells}{\sum all\ cells}$. A more thorough description for the ACME tool and MicrobeJ image processing are provided in the SI.

2.6.6 DNA extraction, metagenome sequencing, and diversity and growth estimation

DNA from free-living bacteria from the 0.2 to 3 µm fraction was extracted following Zhou et al. (1996) and quantified on a NanoDrop 2000c spectrophotometer (Thermo Scientific, Waltham, Massachusetts, USA). The DNA concentrations ranged from 3 to 45 ng DNA μL^{-1}. Extracted DNA was sequenced at the Max Planck Genome Centre, Cologne. The sequencing was performed with PCR-free DNA library type on an Illumina HiSeq 2500 platform (rapid mode) with 2x 250 base pair chemistry (San Diego, California, USA). Raw reads (accession numbers in Table S7 at doi.org/10.6084/m9.figshare.22290166) were quality trimmed and filtered using the bbduk.sh script of the BBMap suite (v35.14; Bushnell 2014) and assembled into contigs using SPAdes (v3.11.1; Bankevich et al. 2012). Contigs were further binned within anvi'o (v6.2; Eren et al. 2015) using sequencing depth from at least three other samples. Retrieved bins were manually refined by invoking the anvi-refine command within anvi'o. The quality of bin in terms of completeness and contamination was assessed by checkM (v1.0.18; Parks et al. 2015). In total, 1,222 MAGs were retrieved, 852 of which were >50% complete and had <5% contamination (Bowers et al. 2017). As assembly and binning was performed on individual samples, redundant MAGs were obtained. Dereplication of MAGs was performed using dRep (v3.0.0; Olm et al. 2017) applying an average nucleotide identity (ANI) of 99%. Taxonomic classification of representative MAGs was performed with GTDB-tk (v1.7.0) using GTDB r202 (Chaumeil et al. 2020). MAGs belonging to SAR11 (g_Pelagibacter, n = 5), SAR86 (o_SAR86, n = 4), *Aurantivirga* (g_SCGC-AAA160-P02, n = 10), and *Bacteroidetes* (p_Bacteroidota, n = 86) were chosen based on their phylogenetic assignments. SAR11 MAGs were included in a reference tree for more detailed phylogenetic identification (SI). MAG abundances were calculated as described in the SI. MAGs were renamed with a consecutive number for this study. The original names, checkM quality scores, and gRodon results (see below) are in Table S4 (at doi.org/10.6084/m9.figshare.22290166).

We determined the GRiD (Emiola and Oh 2018) for all MAGs during the spring bloom. We compared GRiD results using different settings for SAR11, SAR86, and *Aurantivirga*: default settings, default settings with re-assignment of ambiguous reads, and our own mappings using bowtie2 (SI). The main figures of this manuscript show GRiD values obtained from default settings.

Maximum growth rate estimations were calculated using the R package gRodon (Weissman

et al. 2021), which is based on codon usage bias. Taxa with higher growth rates are adapted to use DNA codons with the highest abundance of corresponding tRNAs in their cells (Long et al. 2021; Vieira-Silva and Rocha 2010). The authors of gRodon identified a threshold of 5 h minimal doubling time ($\hat{=}$ growth rate <4.8 h^{-1}). Below 5 h predicted minimal doubling times the respective microbe is considered as copiotroph, while microbes with doubling times above this threshold are classified as oligotroph. We followed all the suggestions in the gRodon manual under default settings, including prokka genome annotation (Seemann 2014) and Biostrings R package usage (Pagès et al. 2020).

2.6.7 Determining growth, modelling, and statistical analyses

All modelling and statistical analyses were executed in R (v1.2.5042; Core Team et al. 2013). Calculated cell volumes, cellular fluorescence intensities, and FDC were modelled with local estimated scatterplot smoothing (*loess* (span = 0.4)).
We statistically tested the relationship of the modelled FDC over the experimentally derived cell division rates μ with an interaction term of the used $FISHprobe$ ($FDC \sim \mu * FISHprobe$). The estimated regression model, including the interaction term, was significant ($p < 0.0001$, $R2 = 0.85$; see SI for results of post hoc test). We proceeded with the model and used its coefficients to calculate cell division rates μ, based on the FDC (Table S2 at doi.org/10.6084/m9.figshare.22290166).

We calculated net growth (r) using FISH-derived abundance data with a sliding window of five timepoints from: $r = \frac{\ln(N_{End}/N_{Start})}{(t_{End}-t_{Start})}$ with N_{Start} and N_{End} respectively being the modelled abundance at timepoint t_{Start} and t_{End}. For each timepoint, two preceding and two succeeding datapoints were included, as part of the sliding window. In cases where the linear regression resulted in negative values, net growth could not be calculated, as the natural logarithm is only defined for x > 0. Using net growth r and cell division rate μ, we also calculated mortality or death rates from: $r = \mu - d$.

2.6.8 Visualisations

Data was organized and visualized using the R packages ggplot2 (v3.3.3, Wickham 2011a), plyr (v1.8.6, Wickham 2011b), lubridate (v1.7.10, Grolemund and Wickham 2011), reshape2 (v1.4.4, Wickham 2007), cowplot (v1.1.1, Wilke 2020), ggpubr (v0.4.0, Kassambara and Kassambara 2020), gghalves (v0.1.3, Tiedemann 2022), emmeans (v1.7.5, Lenth 2023), and car (v3.1.0, Fox and Weisberg 2019). The colour schemes were inspired by the Wes Anderson palette (v0.3.6, Ram and Wickham 2018). All R scripts were uploaded to GitLab and are freely available (https://gitlab.mpi-bremen.de/jbruewer/bacterial-activity-manuscript-figures).

2.7 Acknowledgements

We would like to thank the captain and crew of RV Aade, Lilly Franzmeyer, Karl-Peter Rücknagel, Fengqing Wang, and Mikkel Schultz Johansen for collecting and processing samples during the 2018 and 2020 spring bloom on Helgoland. Karl-Peter Rücknagel, Jörg W. Wulf, and Kathrin Büttner assisted with CARD-FISH experiments and automated microscopy for the dilution experiments. We would like to thank Lisa Bauer for the CARD-FISH versus Tetra-FISH experiments. We are grateful to Nikolaus Leisch, Jakob Pernthaler, and Benedikt Geier for their valuable suggestions regarding data analysis. We thank Ben Francis and Fengqing Wang for MAG sequence submission and Hanno Teeling for critical reading and suggestions. Victor Kelly is acknowledged for language editing. Funding was provided by the German Research Foundation (DFG) project FOR 2406/2 "Proteogenomics of Marine Polysaccharide Utilization (POMPU)" by grants of B.M.F. (FU 627/2-2) and R.A. (AM 73/9-2) and by the Max Planck Society to J.D.B., L.H.O., C.S., R.A., and B.M.F.

The authors declare no competing interests.

2.8 Supplemental Material

2.8.1 Supplementary Material and Methods

Catalyzed Reporter Deposition (CARD)-FISH

All mentioned chemicals were acquired by Carl Roth, Karlsruhe, Germany, if not stated otherwise. Microscopy filters were embedded in 0.1% LE agarose (w/v, Biozym, Hessisch Oldendorf, Germany) to reduce cell losses during sample handling. Cell walls were partly digested with 10 mg mL^{-1} lysozyme (Sigma Aldrich, Darmstadt, Germany) in lysozyme buffer (0.05 M EDTA, 0.1 M Tris-HCl pH 8.0) for 1 h at 37 °C. Endogenous peroxidases were inactivated with 0.15% H_2O_2 in methanol for 20 min at room temperature. Subsequently, samples were washed thoroughly in deionized water, air dried, and stored at −20 °C until further processing.

CARD-FISH probes contained a horseradish peroxidase on their 5' end for the signal amplification. FISH probes were diluted to a final concentration of 0.84 pmol mL^{-1} into the hybridization mixture (900 mM NaCl, 20 mM Tris-HCl pH 8.0, formamide (concentration depending on probe; see Table S2 at doi.org/10.6084/m9.figshare.22290166), 1% blocking reagent, 0.1 g mL-1 dextran sulfate, and 0.02% SDS). Humidity chambers were prepared by adding a tissue, soaked with a formamide-water mixture (concentration depending on probe), into an airtight household container. Sample filters were hybridized on petri dishes in the humidity chambers for 3 h at 46 °C. Thereafter, samples were washed first in washing buffer (20 mM Tris-HCl pH 8.0, 5 mM EDTA pH 8.0, 0.01% SDS, and NaCl (0.225 M, 0.159 M, or 0.08 M for 20%, 25%, or 35% formamide in hybridization mixture, respectively) for 15 min at 48 °C and afterwards in 1x PBS for 15 min at room temperature. For signal amplification, 1 µg mL^{-1} A488 tyramids (synthesized

according to Pernthaler and Pernthaler (2007) with Alexa 488 dyes (Thermo Fisher, Waltham, Massachusetts, USA) were mixed with 0.0015% H_2O_2 in an amplification buffer (1x PBS, 2 M NaCl, 0.1% blocking reagent and 1 g mL^{-1} dextran sulfate). Filters were incubated in the amplification mixture in a humidity chamber (only water) for 45 min at 46 °C. Subsequently, samples were thoroughly washed in deionized water and 96% ethanol, before DAPI staining and embedding in Citifluor:Vectashield (1:3).

Tetra-labelled (or 4-times labelled) FISH

Tetra-labelled FISH probes were ordered from Biomers (Biomers, Ulm, Germnay) with Alexa 488 fluorophores conjugated to modified bases. The FISH hybridization protocol was shortened. No lysozyme digestion, deactivation of endogeneous peroxidases and CARD-amplification was applied. Experiments with tetra-labelled FISH probes were conducted on samples from 3rd, 10th, 17th, and 26th March, 8th, 15th, 20th, 24th, 28th, and 29th April, 11th and 20th May and done with probes targeting SAR11 and *Bacteroidetes*, as well as the negative control probe NON338 (results not shown).

ACME tool settings

Images were imported into the ACME tool. Field of views (FOVs) were manually approved based on images recorded in the DAPI channel. Unsuitable FOVs (e.g., out of focus, overexposure, off grid, etc.) were removed from the downstream analysis. High-quality images were first segmented within the ACME tool (kernel size = 19 pixel, offset = 11 pixel, removal of objects <21). Subsequently, objects were identified based on the area of objects (DAPI channel: >24 pixel; FISH channel: >14.95 pixel), signal-to-background-ratio (DAPI channel: >2.7; FISH channel: >3.2), and circularity (DAPI channel: >0.55). Identified objects (DAPI positive) with a signal in the autofluorescence channel were neglected. Identified objects (DAPI positive) with a signal in the FISH channel were considered FISH-positive. In both cases, a threshold of a minimum overlap of 40% in signal area was chosen.

Cell concentrations were calculated in two different approaches. Cells stained with the SAR11-mix and CF319a FISH probe, relative amounts of DAPI-stained cells were calculated and extrapolated to total cell counts. We, thus, account for potential cell losses during the sample handling of the FISH protocol. Due to overall lower cell abundances, the SAR86 and AUR452 probes were hybridized on 10x filters (total volume: 100 mL). As these filters are more densly loaded, segmentation of individual DAPI-stained cells was not always possible. Hence, we directly calculated the concentrations based on the total number of FISH-stained cell per FOV.

MicrobeJ settings for frequency of dividing cell calculations

High quality images (see above) were additionally loaded in to the image processing software imageJ/Fiji (v2.1.0/1.53e, Schindelin et al. 2012) and were processed with the plug-in microbeJ (v5.13l, Ducret et al. 2016). Object identification was done on the FISH channel in dark mode and an offset on the threshold value of -50. Objects had to be 7-250 pixel^2, have a circularity of 0.55-max and a Z-score 2.8-max. Maxima were identified with the association "inside" (corresponding box was ticked), in dark and 'Point' mode with a tolerance of 25. Similar to the ACME tool, FISH-positive cells required to have a minimum of one DAPI signal and no autofluorescence signal.

Calculation of cell volume based on signal area

Volumes were calculated based on the geometrical approximation of a cylinder with hemispherical capping. In a two-dimensional projection, this results in a rectangle with two half-circles. The area A of the two-dimensional projections can be calculated with the radius r and the length l of the rectangle:

(1) $A = \pi r^2 + 2lr$ which can be reordered to

(2) $l = \frac{A-\pi r^2}{2r}$

and the perimeter P (3) $P = 2\pi r + 2l$.

The area A, perimeter P, and circularity C of the two-dimensional microscopy images were exported from the ACME tool. Inserting (2) in (3) allows us to calculate r and l.

(4) $P = 2\pi r + 2(\frac{A-\pi r^2}{2r})$

(5) $r_{1,2} = \frac{P \pm \sqrt{P^2 - 4\pi A}}{2\pi}$

The Volume V can be calculated with the approximation of a cylinder with hemispherical caping $V = \frac{4}{3}\pi r^3 + \pi r^2 l$.

Metagenomic abundance estimates

The abundance of MAGs was determined as the quotient between the calculated truncated average sequencing depth (TAD80, Orellana et al. 2021) and the total sequencing depth of the microbial genomes (i.e., genome equivalence, Nayfach and Pollard 2015). To determine TAD80 values for individual MAGs of each of the four groups analysed in this study, we performed competitive read mapping. First, we created a bowtie2 (Langmead and Salzberg 2012) database containing all contigs from the MAGs of each group. The mapping of reads to the concatenated file was performed using bowtie2 (v2.4.2, –no-discordant –no-mixed –reorder –no-unal). To obtain the individual mapping of each MAG, we filtered matching reads to each individual MAG and selected for at least 97% identity between the read and the MAG using the script 'sam.filter.rb' of the enveomics collection (Rodriguez-R and Konstantinidis

2016). Then, from the filtered mapping to each MAG, we determined the TAD80 value using the "BedGraph.tad.rb" script (-r 0.8) from the same script collection. Genome equivalents were determined using MicrobeCensus (Nayfach and Pollard 2015) for each metagenomic sample.

Taxonomic characterization of SAR11 MAGs

SAR11 single amplified genomes (SAGs), described in Haro-Moreno et al. (2020), were retrieved from NCBI. Additionally, SAR11 isolate genomes described in Delmont et al. (2019) were downloaded from doi:10.6084/m9.figshare.5248945. All genomes were aligned using GTDB-TK with <identify> and <align> (Chaumeil et al. 2020). An approximately-maximum-likelihood phylogenetic tree was calculated using FastTree (Price et al. 2010). The calculated tree was visualized with iTol (Letunic and Bork 2021), exported, and colourized with Affinity Designer (Serif, Nottingham, UK). Clade and sub-clade assignment are based on Haro-Moreno et al. (2020) and Delmont et al. (2019).

Growth Rate Index (GRiD)

GRiD values reported in the main text were retrieved using default settings of the GRiD software with a minimum coverage of 5. We expected some ambiguous read-mapping, especially for SAR11, due to genomic diversity and the difficulty to retrieve MAGs. We wanted to account for ambiguous read-mapping and to compare our results with different read-mappings. Besides running GRiD under default mode, we activated the -p flag, which enables the "reassignment of ambiguous reads using Pathoscope2", according to the GRiD manual. Additionally, we used the mappings (sam files) generated from Bowtie2 (Langmead and Salzberg 2012) using the same settings described above for TAD80 determination.

Cell division rate calculations from Dilution experiments

Cell division rate estimates follow the first description of Landry and Hasset (1982). Net growth rates can be calculated with time t, abundance at the start N_0, abundance at the end point N_t, and the respective dilution factor d:

$Net\ growth = \frac{1}{t} ln \frac{N_t}{N_0 d}$

The linear model of the apparent growth over the dilution factor can be used to estimate the grazing rate k (d^{-1}; slope of the linear model) and cell division rate μ (d^{-1}; y-axis intercept). The linear regressions were manually curated: In case of strong non-linear relation of cell abundances in dilution experiment (SAR11 and *Aurantivirga* 31st March), undiluted samples were neglected. A non-linear dilution experiment indicates a saturation in predation and is a known bias to dilution experiments (Li et al. 2017). More sophisticated models to deal with non-linear outcomes are discussed in Li et al. (2017).

2.8.2 Supplementary results

Statistical evaluation of image cytometric data and cell division rates

The taxon-specific ribosome content was positively correlated to the respective cell volume (R^2=0.94, $p<2.2 \times 10^{-16}$) and to the FDC (R^2=0.29, $p<2.2 \times 10^{-16}$). The taxon-specific cell volume was positively correlated to the FDC (R^2=0.27, $p<2.2 \times 10^{-16}$). The linear relation between FDC and the interaction term of cell division rate μ and used $FISH probe$ ($FDC \sim \mu * FISH probe$) was significant ($\mu$: $p < 0.0001$; $FISH probe$: $p = 0.005$; $\mu : FISH probe$ $p = 0.019$). A post hoc test with p value adjustment, following the tukey method, revealed that the y-axis (FDC) intercept is insignificantly different for all taxa (Table S8 at doi.org/10.6084/m9.figshare.22290166). The differences in the slopes for SAR86 and AUR452 were significant ($p = 0.023$) but insignificant in all other relations (but see CF319a – SAR86: $p = 0.059$; Table S9 at doi.org/10.6084/m9.figshare.22290166).

Metagenomic assessment of taxon-diversity

Four out of five assessed SAR11 MAGs were classified as SAR11 Cluster Ia.1. They were dominated by MAG r27, which contributed between 2.2% (19th March 2020) up to 21.6 (11th and 17th May) to the entire microbial community. MAGs r30 (2.2 to 5.7%), r119 (2.1 to 5.0%), and r116 ($\leq$1%) remained relatively stable throughout the spring bloom. Lower abundances (0.1 to 0.2%) were determined for MAG r31 belonging to the SAR11 cluster III. The SAR86 community was dominated by MAG r157, which was least abundant on 26th April (0.1%) and most abundant on 24th May (3.5%). Additionally, MAG r159 contributed 0.6 to 0.7% between 19th March and 5th April, but contributed less for the rest of the sampling period. MAG r29 (0.2 to 0.5%) dominated the *Aurantivirga* community for most of the spring bloom, though r261 (max. 0.6%) and r179 (max. 0.4%) were most abundant beginning and mid of May, respectively (Fig. S2.5).

For *Bacteroidetes*, first, MAGs belonging to GTDB-Tk genus-level clade MAG-121220-bin8 were most abundant until mid-April (Fig. S2.5, red bar) with MAGs r79, r45, and r152 contributing 2.0 to 4.0% until 10th April (Fig. S2.8). In May, MAGs of the genus-level clade Ulvibacter_B dominated the *Bacteroidetes* community (Fig. S2.5, yellow bar). The clade was highly diverse with individual MAGs r111, r126, r136, r154, r187, r216, r255, r276, and r78 accounting <1% each to the entire bacterial community (Fig. S2.5).

2.8.3 Supplementary Figures

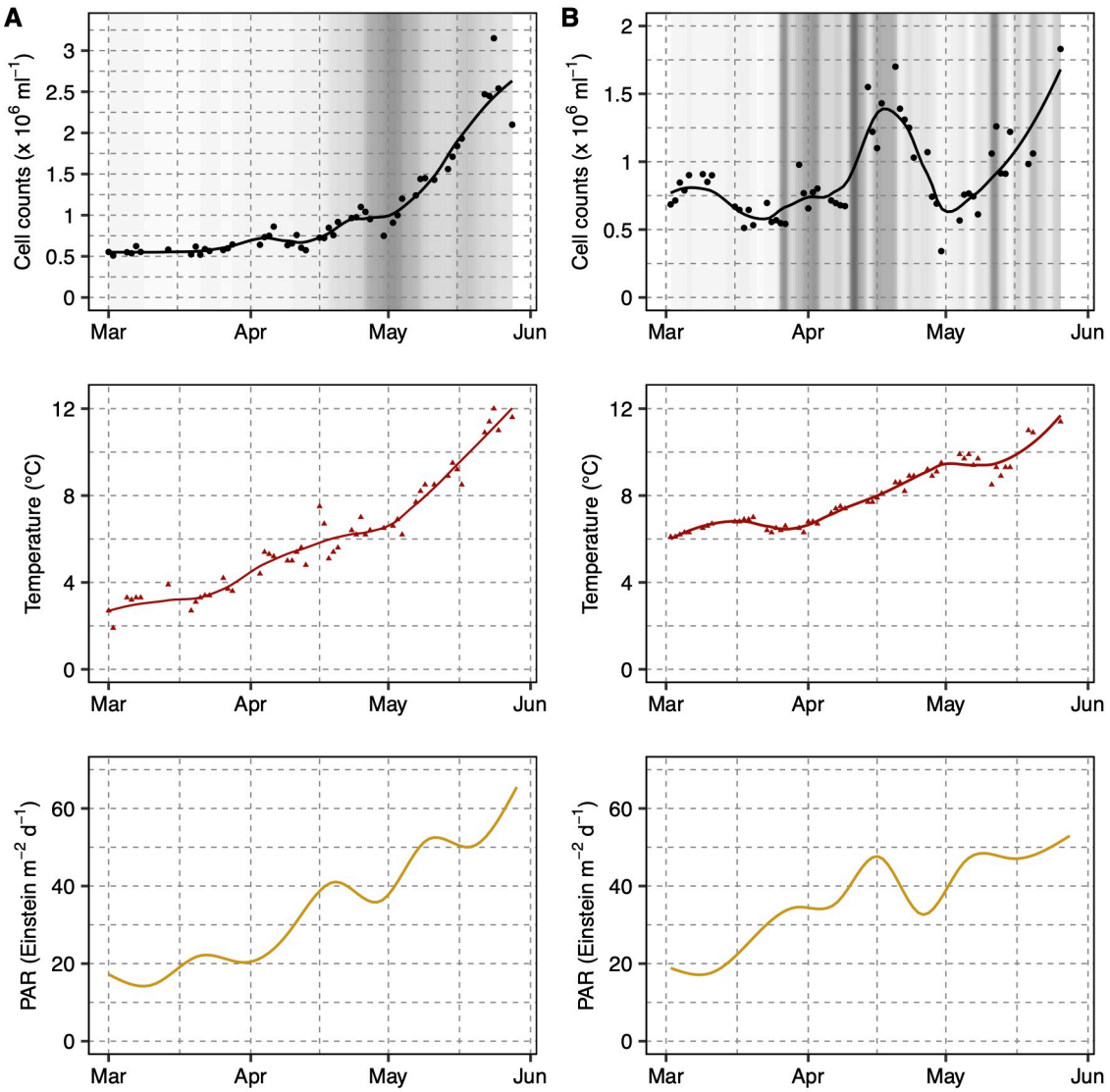

Figure S2.1: Total DAPI-stained cell counts with chlorophyll a concentration (grey, background), temperature, and photosynthetically active radiation (PAR) during the spring phytoplankton bloom (A) 2018 and (B) 2020.

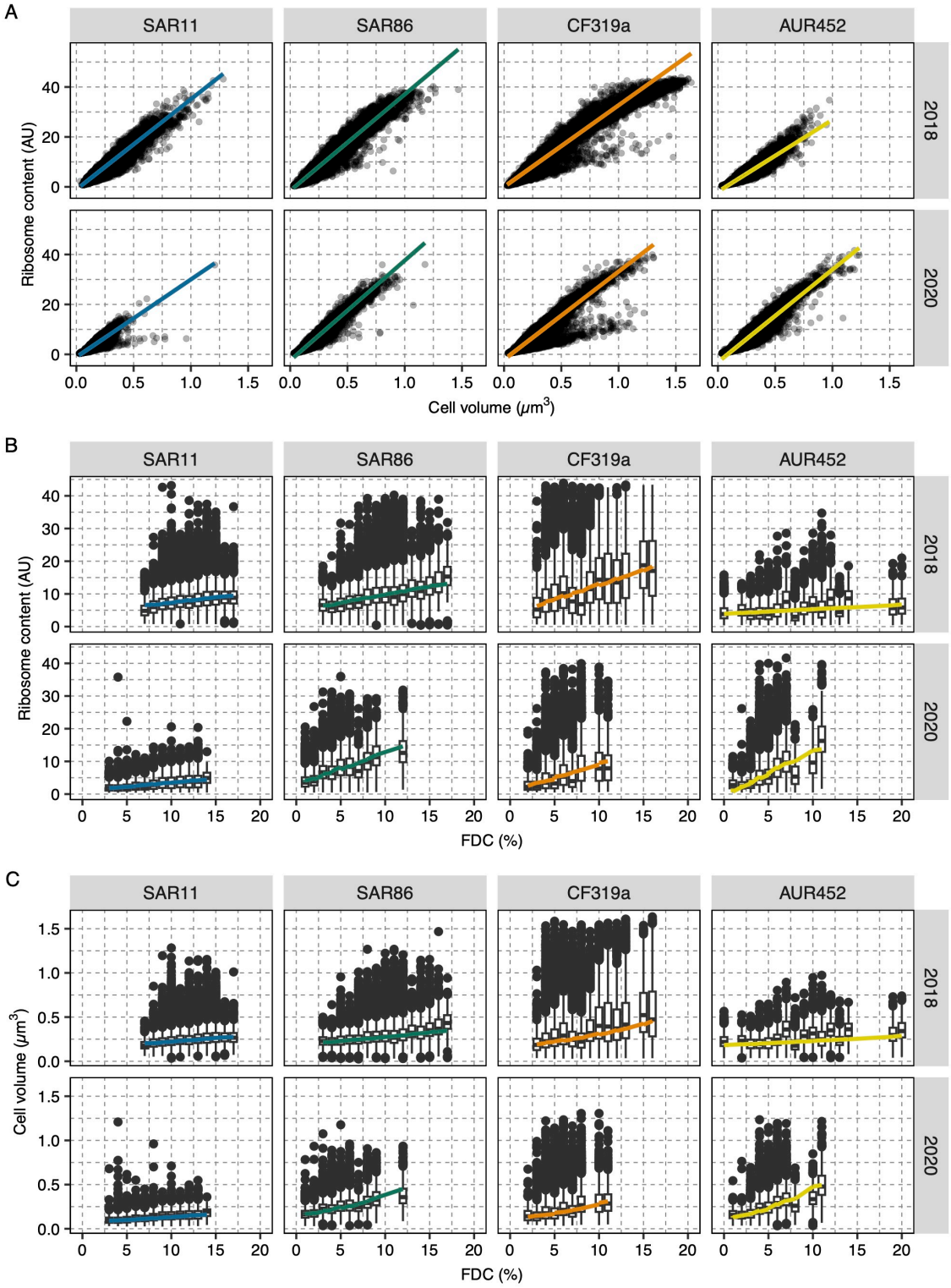

Supplementary Figure S2.2: Taxon and year-specific correlation of cellular parameters measured with FISH. (A) Ribosome content to cell volume. (B) Ribosome content over FDC. (C) Cell volume over FDC. Box-whisker plots in (B) and (C) range from 25th to 75th percentile and the whiskers represent 1.5x interquartile range. Outliers are visualized by dots. Mean is drawn as a solid line inside the boxes. Statistic results of regressions are reported supplementary results.

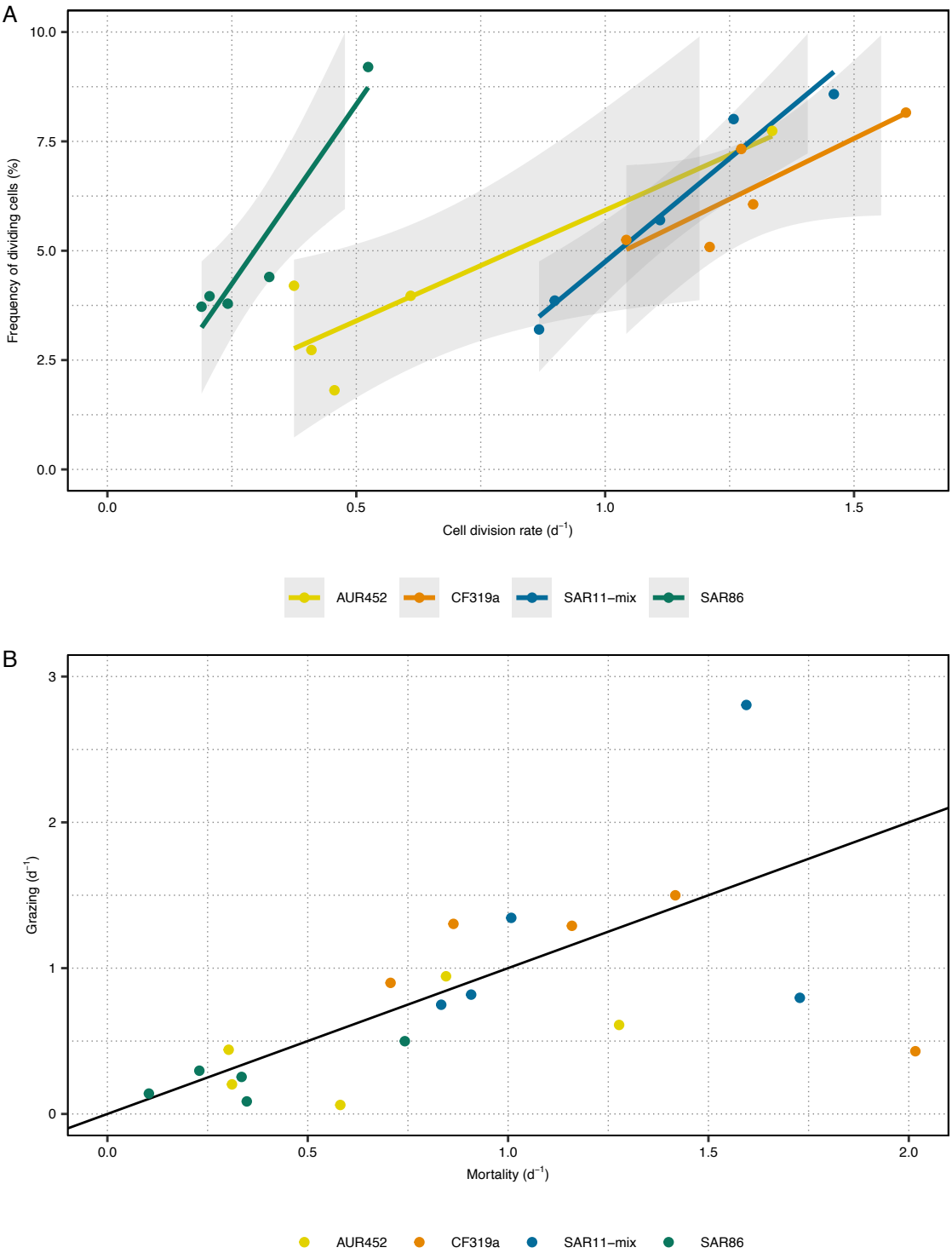

Supplementary Figure S2.3: (A) Linear correlations of microscopically-derived FDC and cell division rates determined by dilution experiments. Information about the linear regression can be found in table S2 (at doi.org/10.6084/m9.figshare.22290166). (B) Taxon-specific grazing rates over mortality rates in 2020. Taxon-specific grazing rates were determined with dilution experiments on 5 time-points during the 2020 phytoplankton bloom. Mortality rates were calculated from cell division rates and on net growth. Net growth rates could not be retrieved for SAR11 and SAR86 on one sampling day, as local regressions of abundance values were computed to calculate net growth and the regressions were partly negative. Black line is an ideal line of 1:1 correlation of grazing and mortality rates.

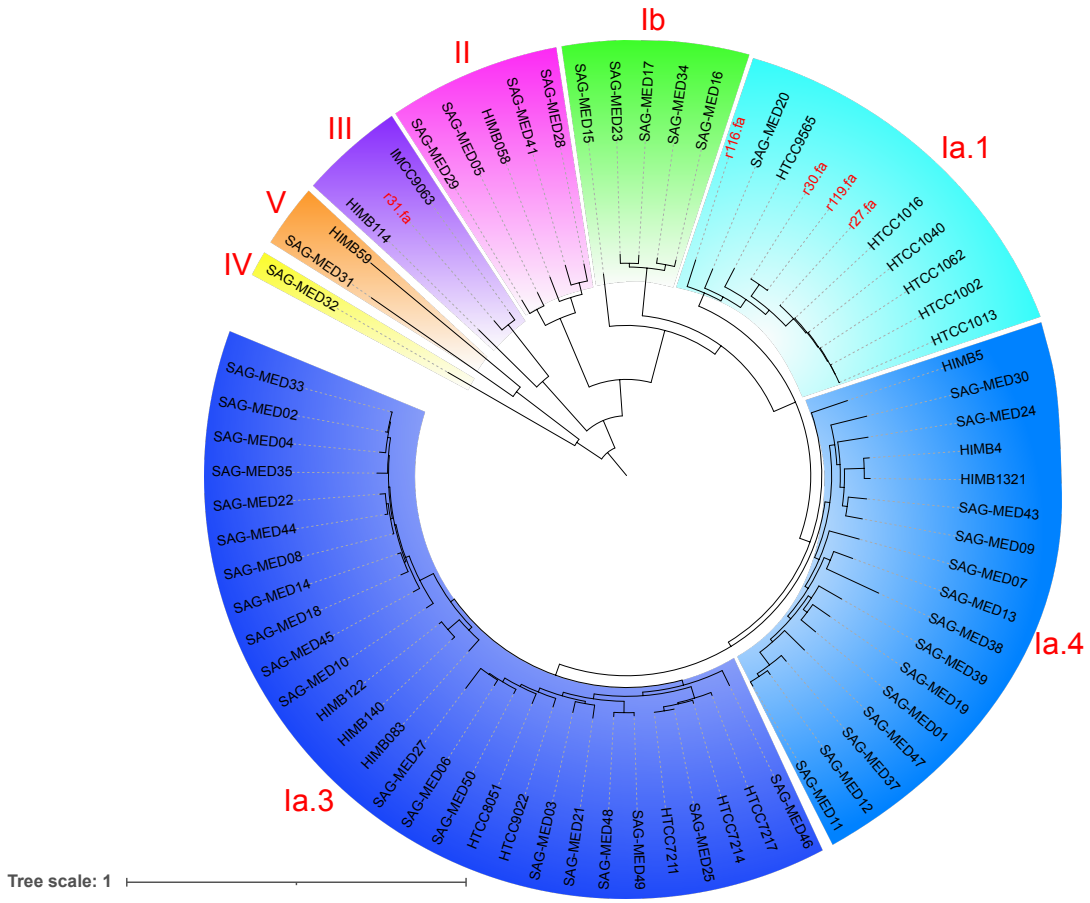

Supplementary Figure S2.4: Phylogenetic tree with SAR11 MAGs that have >50% completeness and <5% contamination described in this study with previously published SAR11 single amplified genomes (SAGs; Haro-Moreno et al. 2020) and SAR11 isolates (Delmont et al. 2019). Colours according to clade assignment (indicated in outer ring) according to the literature (see above).

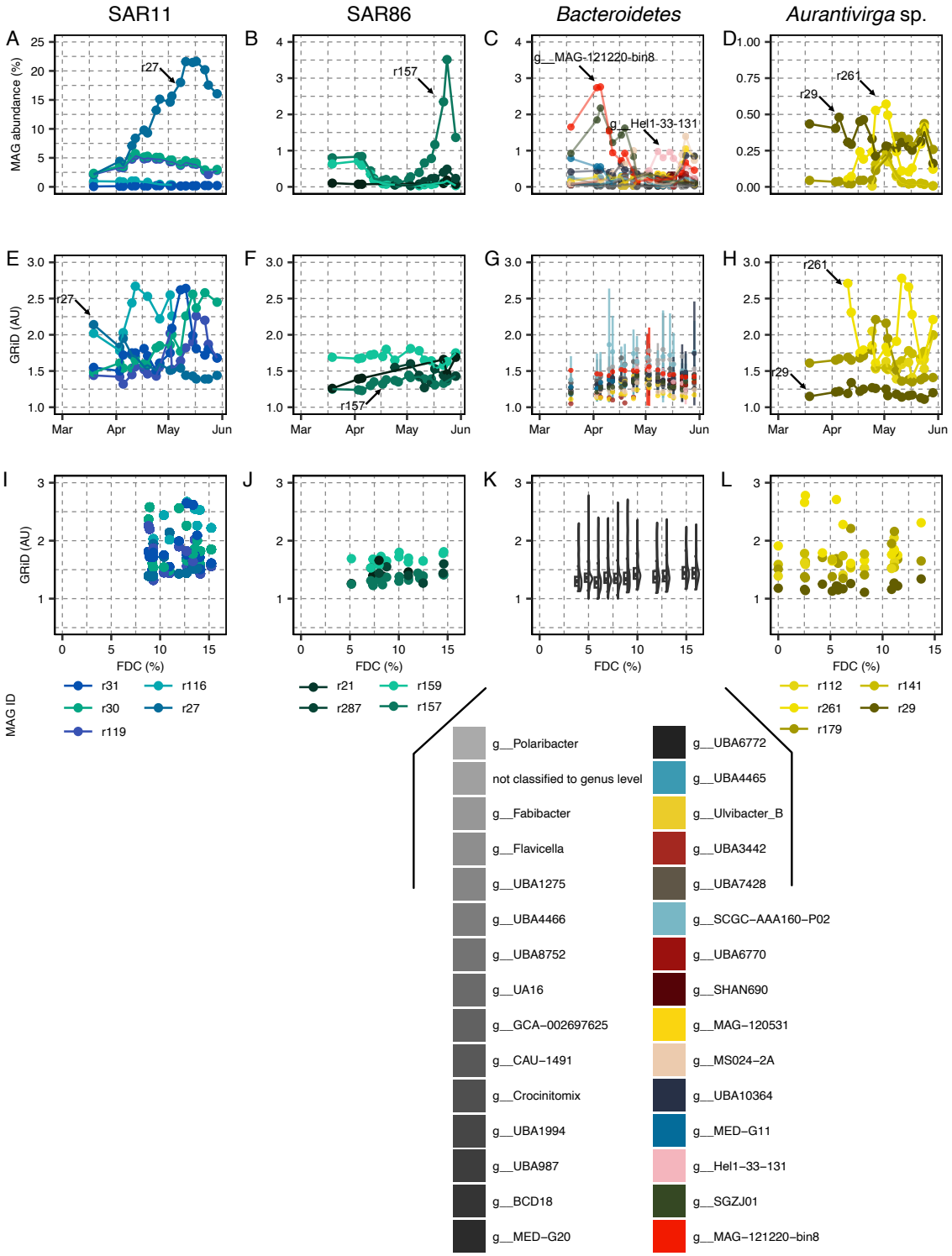

Supplementary Figure S2.5: Metagenome-based assessment of microbial growth in 2018. Relative abundances of metagenome assembled genomes (MAGs; A-D), as well as GRiD values (E–H), of all four taxa were calculated across the spring bloom 2018. For SAR11, SAR86, and *Aurantivirga* results of individual MAGs are visualized. For *Bacteroidetes*, results are summarized on the genus level (C, G with standard deviation). (I-L) MAG-derived GRiD values plotted versus FDC for phytoplankton spring bloom 2018.

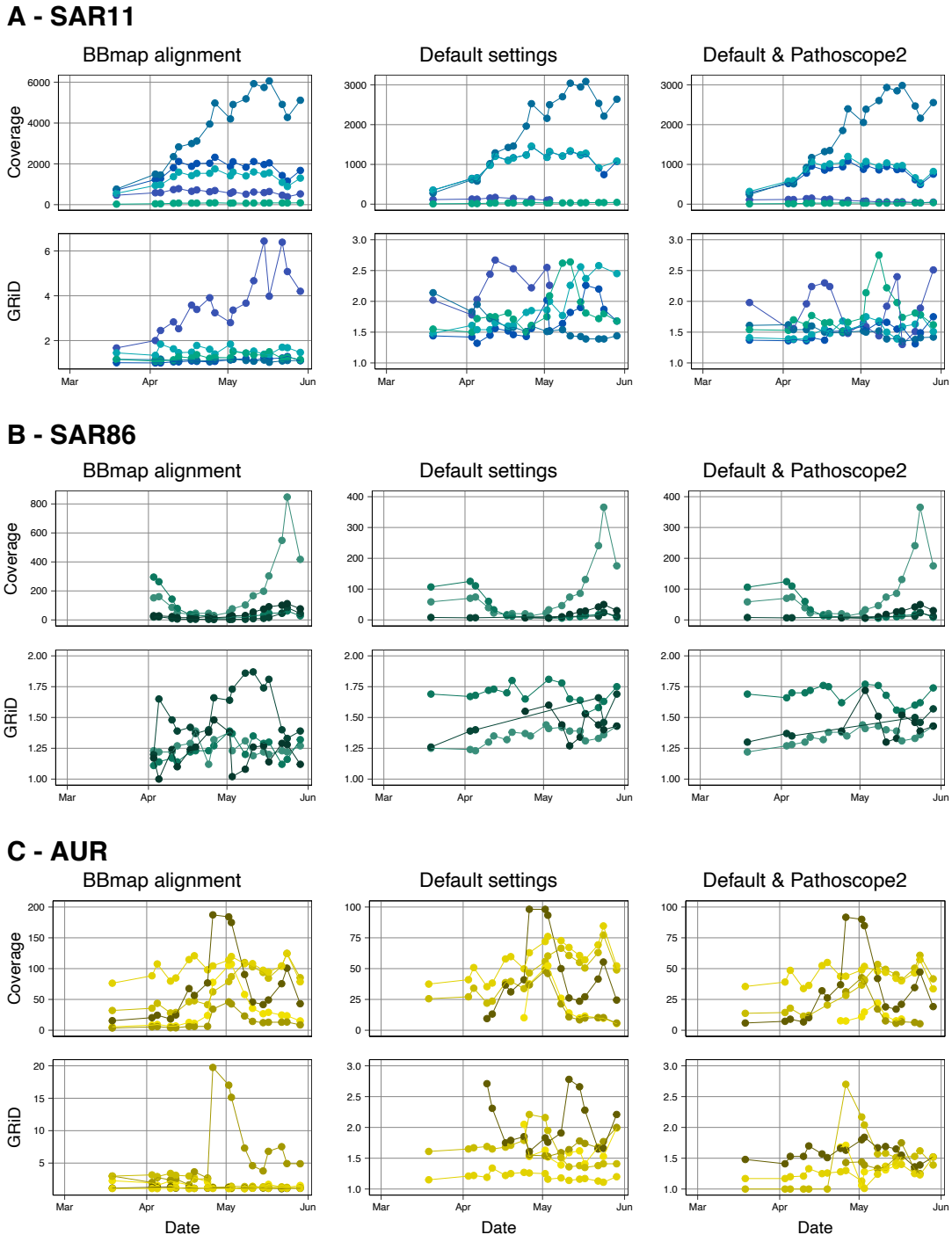

Supplementary Figure S2.6: Comparison of GRiD values and abundance estimates from the 2018 phytoplankton spring bloom with different mappings for (A) SAR11, (B) SAR86, and (C) *Aurantivirga*. From left to right: GRiD values from customized alignment, retrieved with BBmap; GRiD software in default mode (minimum coverage: 5); GRiD software in default mode (minimum coverage: 5) and re-alignment of ambiguous reads with Pathoscope2 within the GRiD software.

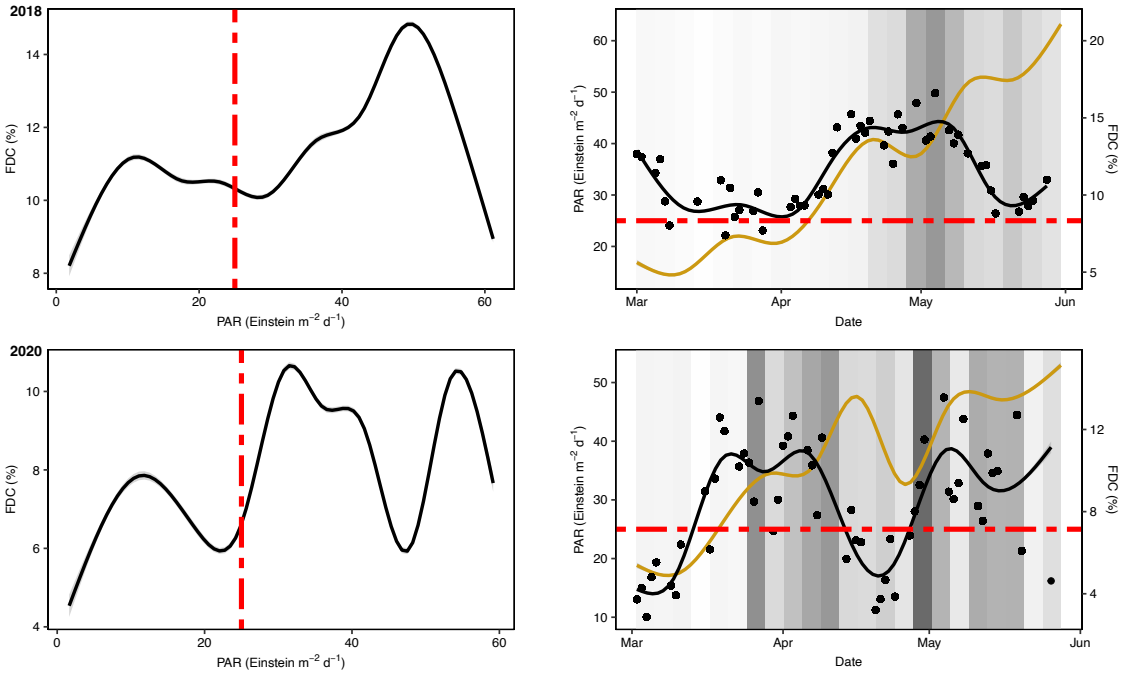

Supplementary Figure S2.7: Relationship of SAR11 FDC to PAR for 2018 and 2020. Left: FDC over Photosynthetically active radiation (PAR) on the left. A *loess* moving average is plotted. Right: PAR (ochre) and FDC (black) are plotted over the spring blooms with chlorophyll a plotted in the background. Scale is the same as Fig. 2.1 and 2.2. Red dashed line indicate potential threshold of 25 Einstein $m^{-2}d^{-1}$ for SAR11 activity in the beginning of the bloom.

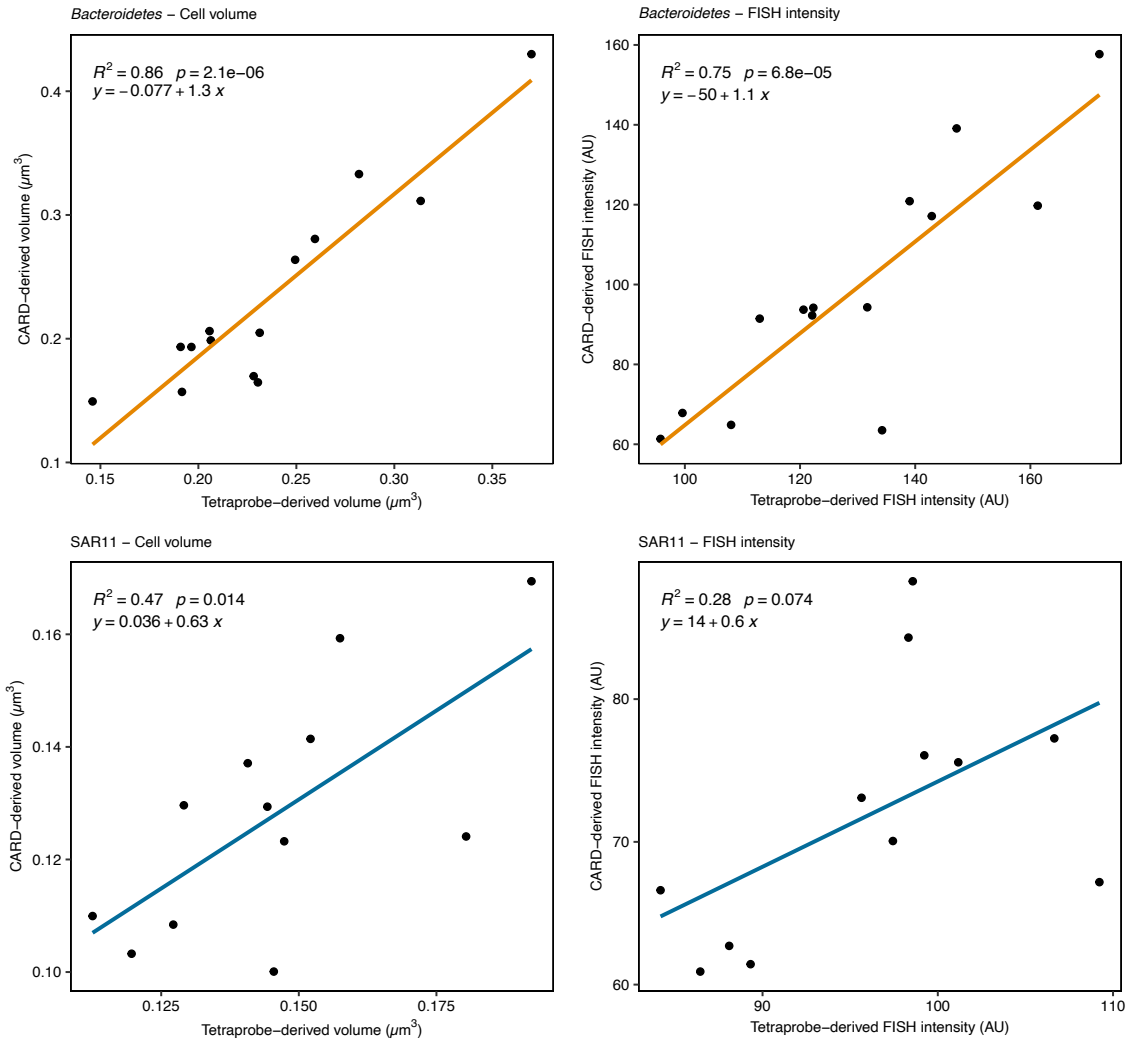

Supplementary Figure S2.8: Correlation of CARD-FISH and tetra-labelled FISH cell volumes and signal intensities for *Bacteroidetes* and SAR11 cells from selected 2020 spring bloom dates. Displayed are means of each sampling day and linear regression of the means. The displayed statistics are for the linear regression model on the means.

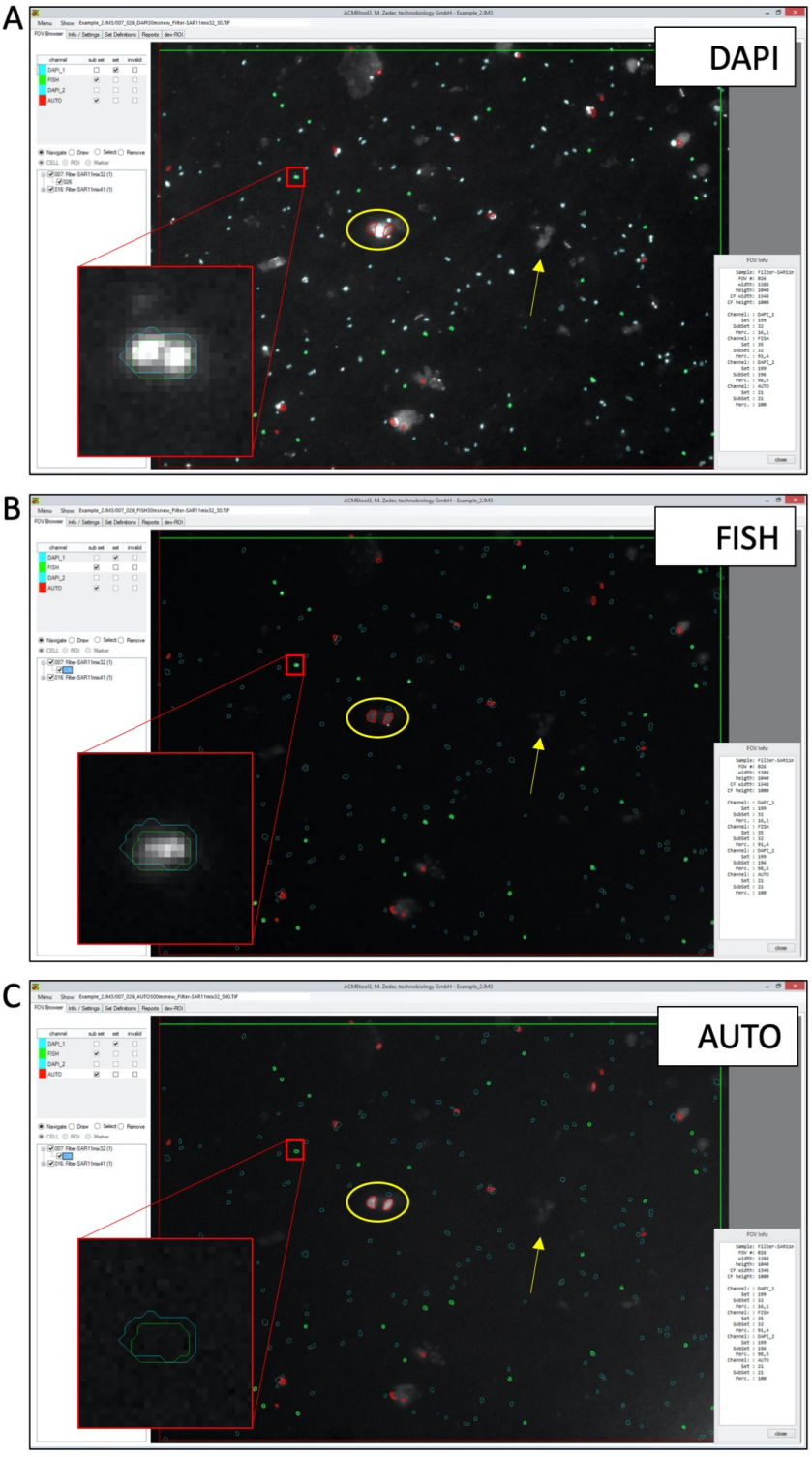

Supplementary Figure S2.9: Screenshots of the ACME tool. (A) is the image in the DAPI channel, (B) FISH channel, and (C) the autofluorescence channel. DAPI positive objects have a light-blue, FISH positive a green, and auto-fluorescent particles a red outline. Red box is a zoom-in on an example of a FISH positive cell with two local DAPI maxima (i.e., a dividing cell). Yellow circle is around an algae cell, yellow arrow points towards debris. Images are an example of 20th April and the samples were hybridized with the SAR11 mix. Each field of view is 1388x1040 pixel and each pixel has a height and width of 0.106 µm.

References

Affronti, L. F. and H. G. Marshall (1994). "Using frequency of dividing cells in estimating autotrophic picoplankton growth and productivity in the Chesapeake Bay". *Hydrobiologia* 284.3, pages 193–203 (cited on page 17).

Amann, R. and B. M. Fuchs (2008). "Single-cell identification in microbial communities by improved fluorescence *in situ* hybridization techniques". *Nature Reviews Microbiology* 6.5, pages 339–348 (cited on page 17).

Arandia-Gorostidi, N., T. M. Huete-Stauffer, L. Alonso-Sáez, and X. A. G. Morán (2017). "Testing the metabolic theory of ecology with marine bacteria: different temperature sensitivity of major phylogenetic groups during the spring phytoplankton bloom". *Environmental Microbiology* 19.11, pages 4493–4505 (cited on pages 16, 26).

Bankevich, A., S. Nurk, D. Antipov, A. A. Gurevich, M. Dvorkin, A. S. Kulikov, V. M. Lesin, S. I. Nikolenko, S. Pham, and A. D. Prjibelski (2012). "SPAdes: a new genome assembly algorithm and its applications to single-cell sequencing". *Journal of Computational Biology* 19.5, pages 455–477 (cited on page 31).

Becker, J. W., S. L. Hogle, K. Rosendo, and S. W. Chisholm (2019). "Co-culture and biogeography of *Prochlorococcus* and SAR11". *ISME Journal* 13.6, pages 1506–1519 (cited on page 27).

Bennke, C. M., G. Reintjes, M. Schattenhofer, A. Ellrott, J. Wulf, M. Zeder, and B. M. Fuchs (2016). "Modification of a high-throughput automatic microbial cell enumeration system for shipboard analyses". *Applied and Environmental Microbiology* 82.11, pages 3289–3296 (cited on page 30).

Bloem, J., M. Veninga, and J. Shepherd (1995). "Fully automatic determination of soil bacterium numbers, cell volumes, and frequencies of dividing cells by confocal laser scanning microscopy and image analysis". *Applied and Environmental Microbiology* 61.3, pages 926–936 (cited on page 17).

Bowers, R. M., N. C. Kyrpides, R. Stepanauskas, M. Harmon-Smith, D. Doud, T. Reddy, F. Schulz, J. Jarett, A. R. Rivers, and E. A. Eloe-Fadrosh (2017). "Minimum information about a single amplified genome (MISAG) and a metagenome-assembled genome (MIMAG) of bacteria and archaea". *Nature Biotechnology* 35.8, pages 725–731 (cited on page 31).

Bushnell, B. (2014). *BBMap: a fast, accurate, splice-aware aligner*. Report. Lawrence Berkeley National Lab.(LBNL), Berkeley, CA (United States) (cited on page 31).

Campbell, B. J., L. Yu, J. F. Heidelberg, and D. L. Kirchman (2011). "Activity of abundant and rare bacteria in a coastal ocean". *Proceedings of the National Academy of Sciences* 108.31, pages 12776–12781 (cited on page 26).

Carini, P., L. Steindler, S. Beszteri, and S. J. Giovannoni (2013). "Nutrient requirements for growth of the extreme oligotroph '*Candidatus* Pelagibacter ubique' HTCC1062 on a defined medium". *ISME Journal* 7.3, pages 592–602 (cited on pages 16, 27).

Chaumeil, P.-A., A. J. Mussig, P. Hugenholtz, and D. H. Parks (2020). "GTDB-Tk: a toolkit to classify genomes with the Genome Taxonomy Database". *Bioinformatics* 36.6, pages 1925–1927 (cited on pages 31, 36).

Core Team, R. et al. (2013). "R: A language and environment for statistical computing". *R Foundation for statistical computing, Vienna* (cited on page 32).

Delmont, T. O., E. Kiefl, O. Kilinc, O. C. Esen, I. Uysal, M. S. Rappé, S. Giovannoni, and A. M. Eren (2019). "Single-amino acid variants reveal evolutionary processes that shape the biogeography of a global SAR11 subclade". *eLife* 8, e46497 (cited on pages 23, 36, 41).

Díez-Vives, C., J. M. Gasol, and S. G. Acinas (2014). "Spatial and temporal variability among marine *Bacteroidetes* populations in the NW Mediterranean Sea". *Systematic and Applied Microbiology* 37.1, pages 68–78 (cited on page 16).

Ducret, A., E. M. Quardokus, and Y. V. Brun (2016). "MicrobeJ, a tool for high throughput bacterial cell detection and quantitative analysis". *Nature Microbiology* 1.7, pages 1–7 (cited on pages 31, 35).

Dupont, C. L., D. B. Rusch, S. Yooseph, M.-J. Lombardo, R. A. Richter, R. Valas, M. Novotny, J. Yee-Greenbaum, J. D. Selengut, and D. H. Haft (2012). "Genomic insights to SAR86, an abundant and uncultivated marine bacterial lineage". *ISME Journal* 6.6, pages 1186–1199 (cited on pages 16, 27).

Eilers, H., J. Pernthaler, J. Peplies, F. O. Glöckner, G. Gerdts, and R. Amann (2001). "Isolation of novel pelagic bacteria from the German Bight and their seasonal contributions to surface picoplankton". *Applied and Environmental Microbiology* 67.11, pages 5134–5142 (cited on page 26).

Elser, J., K. Acharya, M. Kyle, J. Cotner, W. Makino, T. Markow, T. Watts, S. Hobbie, W. Fagan, and J. Schade (2003). "Growth rate–stoichiometry couplings in diverse biota". *Ecology Letters* 6, pages 936–943 (cited on page 17).

Emiola, A. and J. Oh (2018). "High throughput in situ metagenomic measurement of bacterial replication at ultra-low sequencing coverage". *Nature Communications* 9.1, pages 1–8 (cited on pages 17, 25, 31).

Eren, A. M., Ö. C. Esen, C. Quince, J. H. Vineis, H. G. Morrison, M. L. Sogin, and T. O. Delmont (2015). "Anvi'o: an advanced analysis and visualization platform for 'omics data". *PeerJ* 3, e1319 (cited on page 31).

Ferrera, I., J. M. Gasol, M. Sebastián, E. Hojerová, and M. Koblížek (2011). "Comparison of growth rates of aerobic anoxygenic phototrophic bacteria and other bacterioplankton groups in coastal Mediterranean waters". *Applied and Environmental Microbiology* 77.21, pages 7451–7458 (cited on page 27).

Fox, J. and S. Weisberg (2019). *An R companion to applied regression; Third edition*. Sage publications (cited on page 32).

Francis, T. B., D. Bartosik, T. Sura, A. Sichert, J.-H. Hehemann, S. Markert, T. Schweder, B. M. Fuchs, H. Teeling, and R. I. Amann (2021). "Changing expression patterns of TonB-dependent transporters suggest shifts in polysaccharide consumption over the course of a spring phytoplankton bloom". *ISME Journal* 15.8, pages 1–15 (cited on page 26).

Fry, J. C. (1990). "2 Direct methods and biomass estimation". *Methods in Microbiology* 22, pages 41–85 (cited on page 30).

Fuchs, B. M., J. Pernthaler, and R. Amann (2007). "Single cell identification by fluorescence *in situ* hybridization". *Methods for general and molecular microbiology*. Edited by C. Reddy, T. Beveridge, J. Breznak, G. Marzluf, T. Schmidt, and L. R. Snyder. Wiley Online Library, pages 886–896 (cited on page 30).

Gerea, M., C. Queimaliños, M. R. Schiaffino, I. Izaguirre, I. Forn, R. Massana, and F. Unrein (2013). "*In situ* prey selection of mixotrophic and heterotrophic flagellates in Antarctic oligotrophic lakes: an analysis of the digestive vacuole content". *Journal of Plankton Research* 35.1, pages 201–212 (cited on page 27).

Giljan, G., C. ARNosti, I. V. Kirstein, R. Amann, and B. M. Fuchs (2022). "Strong seasonal differences of bacterial polysaccharide utilization in the North Sea over an annual cycle". *Environmental Microbiology* 24.5, pages 2333–2347 (cited on pages 17, 26).

Giovannoni, S. J. (2017). "SAR11 bacteria: the most abundant plankton in the oceans". *Annual review of marine science* 9, pages 231–255 (cited on page 16).

Giovannoni, S. J., L. Bibbs, J.-C. Cho, M. D. Stapels, R. Desiderio, K. L. Vergin, M. S. Rappé, S. Laney, L. J. Wilhelm, and H. J. Tripp (2005). "Proteorhodopsin in the ubiquitous marine bacterium SAR11". *Nature* 438.7064, pages 82–85 (cited on pages 16, 27).

Giovannoni, S. J., J. C. Thrash, and B. Temperton (2014). "Implications of streamlining theory for microbial ecology". *ISME Journal* 8.8, pages 1553–1565 (cited on page 16).

Grolemund, G. and H. Wickham (2011). "Dates and times made easy with lubridate". *Journal of Statistical Software* 40.3, pages 1–25 (cited on page 32).

Hagström, Å., F. Azam, C. Berg, and U. L. Zweifel (2017). "Isolates as models to study bacterial ecophysiology and biogeochemistry". *Aquatic Microbial Ecology* 80.1, pages 15–27 (cited on page 17).

Hagström, Å., U. Larsson, P. Hörstedt, and S. Normark (1979). "Frequency of dividing cells, a new approach to the determination of bacterial growth rates in aquatic environments". *Applied and Environmental Microbiology* 37.5, pages 805–812 (cited on page 17).

Haro-Moreno, J. M., F. Rodriguez-Valera, R. Rosselli, F. Martinez-HeRNandez, J. J. Roda-Garcia, M. L. Gomez, O. FoRNas, M. Martinez-Garcia, and M. López-Pérez (2020). "Ecogenomics of the SAR11 clade". *Environmental Microbiology* 22.5, pages 1748–1763 (cited on pages 23, 36, 41).

Hijmans, R. J., J. Van Etten, J. Cheng, M. Mattiuzzi, M. Sumner, J. A. Greenberg, O. P. Lamigueiro, A. Bevan, E. B. Racine, A. Shortridge, et al. (2015). "Package 'raster'". *R package* 734, page 473 (cited on page 29).

Ho, A., D. P. Di Lonardo, and P. L. Bodelier (2017). "Revisiting life strategy concepts in environmental microbial ecology". *FEMS Microbiology Ecology* 93.3, fix006 (cited on page 16).

Kappelmann, L., K. Krüger, J.-H. Hehemann, J. Harder, S. Markert, F. Unfried, D. Becher, N. Shapiro, T. Schweder, and R. I. Amann (2019). "Polysaccharide utilization loci of North Sea *Flavobacteriia* as basis for using SusC/D-protein expression for predicting major phytoplankton glycans". *ISME Journal* 13.1, pages 76–91 (cited on page 16).

Kassambara, A. and M. A. Kassambara (2020). "Package 'ggpubr'". *R package version 0.1* 6.0 (cited on page 32).

Khachikyan, A., J. Milucka, S. Littmann, S. Ahmerkamp, T. Meador, M. Könneke, T. Burg, and M. M. Kuypers (2019). "Direct cell mass measurements expand the role of small microorganisms in nature". *Applied and Environmental Microbiology* 85.14, e00493–19 (cited on page 30).

Kieft, K., Z. Zhou, and K. Anantharaman (2020). "VIBRANT: automated recovery, annotation and curation of microbial viruses, and evaluation of viral community function from genomic sequences". *Microbiome* 8.1, pages 1–23 (cited on page 26).

Kirchman, D. L. (2016). "Growth rates of microbes in the oceans". *Annual review of Marine Science* 8, pages 285–309 (cited on page 16).

Krüger, K., M. Chafee, T. B. Francis, T. G. Del Rio, D. Becher, T. Schweder, R. I. Amann, and H. Teeling (2019). "In marine *Bacteroidetes* the bulk of glycan degradation during algae blooms is mediated by few clades using a restricted set of genes". *ISME Journal* 13.11, pages 2800–2816 (cited on pages 16, 25, 26).

La Ferla, R., G. Maimone, G. Caruso, F. Azzaro, M. Azzaro, F. Decembrini, A. Cosenza, M. Leonardi, and R. Paranhos (2014). "Are prokaryotic cell shape and size suitable to ecosystem characterization?" *Hydrobiologia* 726.1, pages 65–80 (cited on page 30).

Lami, R., M. T. Cottrell, B. J. Campbell, and D. L. Kirchman (2009). "Light-dependent growth and proteorhodopsin expression by *Flavobacteria* and SAR11 in experiments with Delaware coastal waters". *Environmental Microbiology* 11.12, pages 3201–3209 (cited on page 27).

Landry, M. and R. Hassett (1982). "Estimating the grazing impact of marine micro-zooplankton". *Marine Biology* 67.3, pages 283–288 (cited on pages 29, 36).

Langmead, B. and S. L. Salzberg (2012). "Fast gapped-read alignment with Bowtie 2". *Nature Methods* 9.4, pages 357–359 (cited on pages 35, 36).

Lenth, R. V. (2023). *emmeans: Estimated Marginal Means, aka Least-Squares Means*. R package version 1.8.5 (cited on page 32).

Letunic, I. and P. Bork (2021). "Interactive Tree Of Life (iTOL) v5: an online tool for phylogenetic tree display and annotation". *Nucleic Acids Research* 49.W1, W293–W296 (cited on page 36).

Li, Q. P., P. J. Franks, and M. R. Landry (2017). "Recovering growth and grazing rates from nonlinear dilution experiments". *Limnology and Oceanography* 62.5, pages 1825–1835 (cited on page 36).

Liu, Y., S. Blain, O. Crispi, M. Rembauville, and I. ObeRNosterer (2020). "Seasonal dynamics of prokaryotes and their associations with diatoms in the Southern Ocean as revealed by an autonomous sampler". *Environmental Microbiology* 22.9, pages 3968–3984 (cited on page 26).

Long, A. M., S. Hou, J. C. Ignacio-Espinoza, and J. A. Fuhrman (2021). "Benchmarking microbial growth rate predictions from metagenomes". *ISME Journal* 15.1, pages 183–195 (cited on page 32).

López-Urrutia, Á. and X. A. G. Morán (2007). "Resource limitation of bacterial production distorts the temperature dependence of oceanic carbon cycling". *Ecology* 88.4, pages 817–822 (cited on page 25).

Malmstrom, R. R., R. P. Kiene, M. T. Cottrell, and D. L. Kirchman (2004). "Contribution of SAR11 bacteria to dissolved dimethylsulfoniopropionate and amino acid uptake in the North Atlantic Ocean". *Applied and Environmental Microbiology* 70.7, pages 4129–4135 (cited on page 16).

Matsuyama, M. (1993). "Frequency of Dividing Cells of *Chromatium* sp. Blooming in Lake Kaiike as an Estimate of Growth Rate". *Japanese Journal of Limnology* 54.2, pages 137–140 (cited on page 24).

Mayerhofer, M. M., F. Eigemann, C. Lackner, J. Hoffmann, and F. L. Hellweger (2021). "Dynamic carbon flux network of a diverse marine microbial community". *ISME Communications* 1.1, pages 1–10 (cited on pages 26, 27).

Miura, K. and S. F. Nørrelykke (2021). "Reproducible image handling and analysis". *EMBO Journal* 40.3, e105889 (cited on pages 24, 25).

Møller, S., C. S. Kristensen, L. K. Poulsen, J. M. Carstensen, and S. Molin (1995). "Bacterial growth on surfaces: automated image analysis for quantification of growth rate-related parameters". *Applied and Environmental Microbiology* 61.2, pages 741–748 (cited on page 24).

Morris, R. M., K. R. Cain, K. L. Hvorecny, and J. M. Kollman (2020). "Lysogenic host–virus interactions in SAR11 marine bacteria". *Nature Microbiology* 5.8, pages 1011–1015 (cited on page 27).

NASA Goddard Space Flight Center Ocean Biology Processing Group, . (2022). "Moderate-resolution imaging spectroradiometer (MODIS) aqua photosynthetically available radiation data". *NASA OB DAAC* (cited on page 29).

Nayfach, S. and K. S. Pollard (2015). "Average genome size estimation improves comparative metagenomics and sheds light on the functional ecology of the human microbiome". *Genome Biology* 16.1, pages 1–18 (cited on pages 35, 36).

Nikrad, M. P., M. T. Cottrell, and D. L. Kirchman (2014). "Growth activity of gammaproteobacterial subgroups in waters off the west Antarctic Peninsula in summer and fall". *Environmental Microbiology* 16.6, pages 1513–23 (cited on pages 17, 26).

Olm, M. R., C. T. Brown, B. Brooks, and J. F. Banfield (2017). "dRep: a tool for fast and accurate genomic comparisons that enables improved genome recovery from metagenomes through de-replication". *ISME Journal* 11.12, pages 2864–2868 (cited on page 31).

Orellana, L. H., T. B. Francis, M. Ferraro, J.-H. Hehemann, B. M. Fuchs, and R. I. Amann (2021). "*Verrucomicrobiota* are specialist consumers of sulfated methyl pentoses during diatom blooms". *The ISME Journal*, pages 1–12 (cited on page 35).

Pagès, H., P. Aboyoun, R. Gentleman, and S. DebRoy (2020). *Biostrings: Efficient manipulation of biological strings. R package version 2.48. 0* (cited on page 32).

Parks, D. H., M. Imelfort, C. T. Skennerton, P. Hugenholtz, and G. W. Tyson (2015). "CheckM: assessing the quality of microbial genomes recovered from isolates, single cells, and metagenomes". *Genome Research* 25.7, pages 1043–1055 (cited on page 31).

Pernthaler, A. and J. Pernthaler (2007). "Fluorescence *in situ* hybridization for the identification of environmental microbes". *Protocols for nucleic acid analysis by nonradioactive probes*. Springer, pages 153–164 (cited on page 34).

Pernthaler, J. (2005). "Predation on prokaryotes in the water column and its ecological implications". *Nature Reviews Microbiology* 3.7, pages 537–546 (cited on page 27).

Poulsen, L. K., G. Ballard, and D. A. Stahl (1993). "Use of rRNA fluorescence *in situ* hybridization for measuring the activity of single cells in young and established biofilms". *Applied and Environmental Microbiology* 59.5, pages 1354–1360 (cited on page 17).

Price, M. N., P. S. Dehal, and A. P. Arkin (2010). "FastTree 2–approximately maximum-likelihood trees for large alignments". *PloS One* 5.3, e9490 (cited on page 36).

Ram, K. and H. Wickham (2018). "wesanderson: A Wes Anderson palette generator". *R package version 0.3* 6, page 2018 (cited on page 32).

Rappé, M. S., S. A. Connon, K. L. Vergin, and S. J. Giovannoni (2002). "Cultivation of the ubiquitous SAR11 marine bacterioplankton clade". *Nature* 418.6898, pages 630–633 (cited on pages 16, 27).

Ratkowsky, D. A., J. Olley, T. McMeekin, and A. Ball (1982). "Relationship between temperature and growth rate of bacterial cultures". *Journal of Bacteriology* 149.1, pages 1–5 (cited on page 25).

Rodriguez-R, L. M. and K. T. Konstantinidis (2016). *The enveomics collection: a toolbox for specialized analyses of microbial genomes and metagenomes*. Report 2167-9843. PeerJ Preprints (cited on page 35).

Sánchez, O., I. Ferrera, I. Mabrito, C. R. Gazulla, M. Sebastián, A. Auladell, C. Marín-Vindas, C. Cardelós, I. Sanz-Sáez, and M. C. Pernice (2020). "Seasonal impact of grazing, viral mortality,

resource availability and light on the group-specific growth rates of coastal Mediterranean bacterioplankton". *Scientific Reports* 10.1, page 19773 (cited on pages 22, 25, 27, 28).

Sánchez, O., M. Koblížek, J. M. Gasol, and I. Ferrera (2017). "Effects of grazing, phosphorus and light on the growth rates of major bacterioplankton taxa in the coastal NW Mediterranean". *Environmental Microbiology Reports* 9.3, pages 300–309 (cited on page 27).

Schattenhofer, M., B. M. Fuchs, R. Amann, M. V. Zubkov, G. A. Tarran, and J. Pernthaler (2009). "Latitudinal distribution of prokaryotic picoplankton populations in the Atlantic Ocean". *Environmental Microbiology* 11.8, pages 2078–2093 (cited on page 16).

Schindelin, J., I. Arganda-Carreras, E. Frise, V. Kaynig, M. Longair, T. Pietzsch, S. Preibisch, C. Rueden, S. Saalfeld, and B. Schmid (2012). "Fiji: an open-source platform for biological-image analysis". *Nature Methods* 9.7, pages 676–682 (cited on pages 31, 35).

Seemann, T. (2014). "Prokka: rapid prokaryotic genome annotation". *Bioinformatics* 30.14, pages 2068–2069 (cited on page 32).

Sidhu, C., I. V. Kirstein, C. L. Meunier, J. Rick, K. H. Wiltshire, N. Steinke, S. Vidal-Melgosa, J.-H. Hehemann, B. Huettel, and T. Schweder (2022). "Grazers affect the composition of dissolved storage glycans and thereby bacterioplankton composition during a biphasic North Sea spring algae bloom". *bioRxiv* (cited on pages 16, 17, 26, 27).

Song, J., A. Choi, M. Im, Y. Joung, S. Yoshizawa, J.-C. Cho, and K. Kogure (2015). "*Aurantivirga profunda* gen. nov., sp. nov., isolated from deep-seawater, a novel member of the family *Flavobacteriaceae*". *International Journal of Systematic and Evolutionary Microbiology* 65.12, pages 4850–4856 (cited on page 27).

Teeling, H., B. M. Fuchs, D. Becher, C. Klockow, A. Gardebrecht, C. M. Bennke, M. Kassabgy, S. Huang, A. J. Mann, and J. Waldmann (2012). "Substrate-controlled succession of marine bacterioplankton populations induced by a phytoplankton bloom". *Science* 336.6081, pages 608–611 (cited on pages 16, 25).

Teeling, H., B. M. Fuchs, C. M. Bennke, K. Krüger, M. Chafee, L. Kappelmann, G. Reintjes, J. Waldmann, C. Quast, and F. O. Gloeckner (2016). "Recurring patterns in bacterioplankton dynamics during coastal spring algae blooms". *eLife* 5, e11888 (cited on pages 16, 17, 25, 26).

Teira, E., S. Martínez-García, C. Lønborg, and X. A. álvarez-Salgado (2009). "Growth rates of different phylogenetic bacterioplankton groups in a coastal upwelling system". *Environmental Microbiology Reports* 1.6, pages 545–554 (cited on pages 16, 26).

Thurman, J., J. D. Parry, P. J. Hill, and J. LaybouRN-Parry (2010). "The filter-feeding ciliates *Colpidium striatum* and *Tetrahymena pyriformis* display selective feeding behaviours in the presence of mixed, equally-sized, bacterial prey". *Protist* 161.4, pages 577–588 (cited on page 27).

Tiedemann, F. (2022). *gghalves: Compose Half-Half Plots Using Your Favourite Geoms*. R package version 0.1.4 (cited on page 32).

Vaqué, D., J. M. Gasol, and C. Marrasé (1994). “Grazing rates on bacteria: the significance of methodology and ecological factors”. *Marine Ecology Progress Series*, pages 263–274 (cited on page 25).

Vieira-Silva, S. and E. P. Rocha (2010). “The systemic imprint of growth and its uses in ecological (meta) genomics”. *PLoS Genetics* 6.1, e1000808 (cited on page 32).

Weissman, J. L., S. Hou, and J. A. Fuhrman (2021). “Estimating maximal microbial growth rates from cultures, metagenomes, and single cells via codon usage patteRNs”. *Proceedings of the National Academy of Sciences* 118.12, e2016810118 (cited on pages 25, 31).

Westoby, M., D. A. Nielsen, M. R. Gillings, E. Litchman, J. S. Madin, I. T. Paulsen, and S. G. Tetu (2021). “Cell size, genome size, and maximum growth rate are near-independent dimensions of ecological variation across bacteria and archaea”. *Ecology and Evolution* 11.9, pages 3956–3976 (cited on page 16).

White, P. A., J. Kalff, J. B. Rasmussen, and J. M. Gasol (1991). “The effect of temperature and algal biomass on bacterial production and specific growth rate in freshwater and marine habitats”. *Microbial Ecology*, pages 99–118 (cited on page 25).

Wickham, H. (2007). “Reshaping data with the reshape package”. *Journal of Statistical Software* 21.12, pages 1–20 (cited on page 32).

Wickham, H. (2011a). *ggplot2*. Volume 3. Wiley Interdisciplinary Reviews: Computational Statistics. Springer-Verlag New York, pages 180–185 (cited on page 32).

Wickham, H. (2011b). “The split-apply-combine strategy for data analysis”. *Journal of Statistical Software* 40, pages 1–29 (cited on page 32).

Wilke, C. O. (2020). “Cowplot: streamlined plot theme and plot annotations for “ggplot2.”” *Streamlined plot theme and plot annotations for ggplot2* 1 (cited on page 32).

Wiltshire, K. H. and C.-D. Dürselen (2004). “Revision and quality analyses of the Helgoland Reede long-term phytoplankton data archive”. *Helgoland Marine Research* 58.4, pages 252–268 (cited on page 28).

Wiltshire, K. H., A. M. Malzahn, K. Wirtz, W. Greve, S. Janisch, P. Mangelsdorf, B. F. Manly, and M. Boersma (2008). “Resilience of North Sea phytoplankton spring bloom dynamics: An analysis of long-term data at Helgoland Roads”. *Limnology and Oceanography* 53.4, pages 1294–1302 (cited on page 29).

Yang, L., J. A. Haagensen, L. Jelsbak, H. K. Johansen, C. SteRNberg, N. Høiby, and S. Molin (2008). “*In situ* growth rates and biofilm development of *Pseudomonas aeruginosa* populations in chronic lung infections”. *Journal of Bacteriology* 190.8, pages 2767–2776 (cited on page 17).

Yokokawa, T., T. Nagata, M. T. Cottrell, and D. L. Kirchman (2004). “Growth rate of the major phylogenetic bacterial groups in the Delaware estuary”. *Limnology and Oceanography* 49.5, pages 1620–1629 (cited on pages 16, 26).

Zapata, M., F. Rodríguez, and J. L. Garrido (2000). “Separation of chlorophylls and carotenoids from marine phytoplankton: a new HPLC method using a reversed phase C8 column and pyridine-containing mobile phases”. *Marine Ecology Progress Series* 195, pages 29–45 (cited on page 29).

Zeder, M., E. Kohler, L. Zeder, and J. Pernthaler (2011a). “A novel algorithm for the determination of bacterial cell volumes that is unbiased by cell morphology”. *Microscopy and Microanalysis* 17.5, pages 799–809 (cited on pages 17, 30).

Zeder, M., A. Ellrott, and R. Amann (2011b). “Automated sample area definition for high-throughput microscopy”. *Cytometry Part A* 79.4, pages 306–310 (cited on page 30).

Zhao, Y., B. Temperton, J. C. Thrash, M. S. Schwalbach, K. L. Vergin, Z. C. Landry, M. Ellisman, T. Deerinck, M. B. Sullivan, and S. J. Giovannoni (2013). “Abundant SAR11 viruses in the ocean”. *Nature* 494.7437, pages 357–360 (cited on page 27).

Zhou, J., M. A. Bruns, and J. M. Tiedje (1996). “DNA recovery from soils of diverse composition”. *Applied and Environmental Microbiology* 62.2, pages 316–322 (cited on page 31).

3

GLOBALLY OCCURRING PELAGIPHAGE INFECTIONS CREATE RIBOSOME-DEPRIVED CELLS

Jan D. Brüwer[1*], Chandni Sidhu[1], Yanlin Zhao[2], Andreas Eich[3], Leonard Rößler[1], Luis H. Orellana[1], Bernhard M. Fuchs[1*]

[1]Max Planck Institute for Marine Microbiology, Bremen, Germany
[2]College of Juncao Science and Ecology, Fujian Agriculture and Forestry University, Fuzhou, China
[3]PSL Research University, EPHE-UPVD-CNRS, UAR 3278 CRIOBE; Moorea, French Polynesia
[*]Corresponding author.

In review at *Nature Communications*.

Contributions

Experimental concept and design: 95%
Acquisition of experimental data: 80%
Preparation of figures and tables: 100%
Drafting of the manuscript: 95%

3.1 Abstract

Phages play an essential role in controlling bacterial populations. Those infecting *Pelagibacterales* (SAR11), the dominant bacteria in surface oceans, have been studied *in silico* and by cultivation attempts. However, little is known about the quantity of phage-infected cells in the environment. Using fluorescence *in situ* hybridization techniques, we here show pelagiphage-infected SAR11 cells across multiple global ecosystems and present evidence for tight community control of pelagiphages on the SAR11 hosts in a case study. Up to 19% of SAR11 cells were phage-infected during a phytoplankton bloom, coinciding with a ∼90% reduction in SAR11 cell abundance within five days. Frequently, a fraction of the infected SAR11 cells were devoid of detectable ribosomes, which appear to be a yet undescribed possible stage during pelagiphage infection. We dubbed those cells 'zombies' and propose, among other possible explanations, a mechanism in which ribosomal RNA is used as a resource for the synthesis of new phage genomes. On a global scale, we detected phage-infected SAR11 and zombie cells in the Atlantic, Pacific, and Southern Oceans. Our findings illuminate the important impact of pelagiphages on SAR11 populations and unveil the presence of ribosome-deprived zombie cells as part of the infection cycle.

3.2 Main Text

Pelagibacterales, known as the SAR11 clade, are small free-living marine bacteria that account for 20-50% of planktonic cells in the oceans and are crucial components of marine biogeochemical cycles (Giovannoni 2017). The reasons for their ecological success in the pelagic ocean are still being elucidated (Giovannoni 2017). One proposed explanation was that SAR11 are slow-growing defense specialists, minimally affected by phage predation (Suttle 2007). However, several phages infecting SAR11 (pelagiphages) have been described and discussed (Giovannoni et al. 2013; Martinez-Hernandez et al. 2019; Våge et al. 2013; Zhao et al. 2019; Zhao et al. 2013) and studied through cultivation and sequencing efforts with increasing attention in recent years. Metagenomic and -viromic studies not only explored the functional abilities of their genomes (Wittmers et al. 2022) but also suggest that pelagiphages, including uncultivated representatives, are the most abundant phages in the ocean (Buchholz et al. 2021; Eggleston and Hewson 2016; Martinez-Hernandez et al. 2017; Martinez-Hernandez et al. 2019; Zhang et al. 2021). Despite the ubiquity of pelagiphages, they appear to have low lytic activity within the host population (Alonso-Sáez et al. 2018; Zhong et al. 2023). However, direct quantifications of pelagiphage infected cells, and thus investigations of their role in controlling SAR11 abundance, have not been done so far.

In a recent study, we identified a contrary trend of cell division rates and cell abundances of SAR11 during the 2020 phytoplankton spring bloom at Helgoland Roads, German Bight (Brüwer

et al. 2023). Phytoplankton spring blooms are characterized by high phytoplankton-derived organic matter availability and a recurring succession of fast-growing specialized bacterial taxa (Teeling et al. 2012). Due to low abundances during phytoplankton blooms, SAR11 was generally considered to be outcompeted by specialized taxa. However, when growth rates of SAR11 were measured during the 2020 phytoplankton bloom, SAR11 grew at ∼1.9 divisions d^{-1}, while cell abundances decreased by ∼90% over five days (Brüwer et al. 2023). As this decrease was taxon-specific, we hypothesized viral-induced mortality to cause the discrepancy (Brüwer et al. 2023). Here, we quantified the number of pelagiphage-infected cells using advanced microscopy techniques. We first established the protocol on pure cultures of the pelagiphages and their hosts and subsequently assessed infection dynamics throughout the phytoplankton spring bloom described above. For a global perspective, we analyzed the distribution of pelagiphage-infected SAR11 cells in cruise samples across the Pacific, Atlantic, and Southern Ocean. Our investigation of the pure cultures and environmental samples has led us to discover ribosome-deprived but phage-infected cells, a new phenomenon during phage infection.

3.3 Results

3.3.1 Quantifying phage-infected SAR11 cells and discovery of zombie cells

To characterize pelagiphage:SAR11 interactions, we designed fluorescence *in situ* hybridization (FISH) probes for the three pelagiphages HTVC027P (Zhang et al. 2021), HTVC031P (Zhao et al. 2019), and *Greip* (*Iscarvirus greipi*; EXVC021P; closely related to HTVC010P; Buchholz et al. 2023; Buchholz et al. 2021), that were isolated on the SAR11 strain *Candidatus* Pelagibacter ubique HTCC1062. We targeted those pelagiphages, as they are amongst the most abundant phages globally (Martinez-Hernandez et al. 2019; Zhang et al. 2021) and could be detected in metagenomes originating from the same phytoplankton bloom as described above (this study, Sidhu et al. 2023). These phages are lytic, and a temperate infection can be excluded. We tested hybridization conditions and stringency of the newly designed probes on cultures of *Ca.* P. ubique HTCC1062 infected with either HTVC027P or HTVC031P (Fig. 3.1). Positive controls with *Greip* were not available to us. As negative controls, we included samples of pelagiphage HTVC023P, which is phylogenetically closely related to HTVC027P (Zhang et al. 2021) but is not targeted by the designed probes (Fig. S3.1). In a first experiment, we found through FISH and high-throughput image cytometry that 70.0 ±7.0% (mean ±sd; HTVC027P, n=3) and 17.4 ±10.1% (HTVC031P, n=3) of the cells were infected in non-synchronized cultures. The negative control of HTVC023P (n=3) contained <0.1% of false positive signals (Fig. S3.1, Table S1). In an independent second experiment, 36.3 ±2.7% (mean ±sd) and 32.4 ±5.0% of cells were infected with HTVC027P (n=3) 18 and 26 h after infection, respectively (Fig. 3.1). Additionally, 14.3 ±6.6% and 17.2 ±6.8% of cells were infected with HTVC031P (n=3) 20 and 28 h post-infection, respectively (Fig. 3.1).

In all positive controls, we consistently noticed phage-infected cells with no detectable ribosomal RNA signal (22.7 ±3.1% (t18) and 23.1 ±3.6% (t26) of total cell counts for HTVC027P; 25.8 ±17.4% (t20) and 30.4 ±24.6% (t28) for HTVC031P; Fig. 3.1, Table S1). We named these "zombie" cells as they are probably in a transitional state between living and dead cells. Zombies are different from 'ghost cells,' which were defined as non-living cell envelopes lacking nucleoids (Zweifel and Hagstrom 1995) or any cytoplasmic content including DNA (Hajam et al. 2017). In contrast, all zombie cells contained DNA. We excluded the possibility that zombie cells are free phages, since they were too large to be individual phages or vesicles according to our image analysis criteria (Table S2).

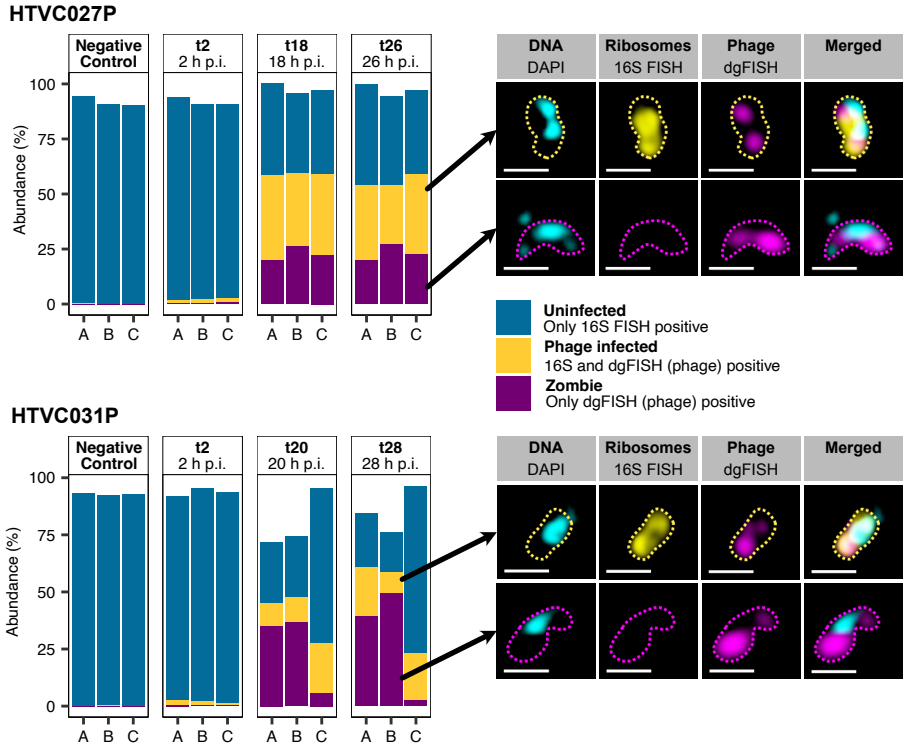

Figure 3.1: Infections of *Ca.* P. ubique HTCC1062 with HTVC027P and HTVC031P and example epifluorescence microscopy images. Bargraphs show triplicate samples during the infection cycle. "p.i." stands for post infection. The negative control was uninfected. Abundance of 100% corresponds to total cell counts of DAPI-stained cells. Example microscopy images on the right display DAPI (DNA; cyan), FISH for 16S rRNA (yellow) and phage genes via direct-geneFISH (magenta). Outlines were drawn manually. Images were recorded using SR-SIM on a ZEISS LSM780 equipped with ELYRA PS.1 and analysed using the ZEN software. Scale bar: 0.5 µm.

3.3.2 Phage-infection regulates SAR11 abundance during phytoplankton bloom

To investigate the impact of pelagiphages on the SAR11 host population in the environment, we analyzed 67 samples collected over 133 days in spring 2020 at Helgoland Roads, German Bight. Previously, we showed that fast cell division rates in SAR11 coincided with a rapid decrease in cell abundances (at the end of March and in May; Fig. 3.2; Brüwer et al. 2023).

We could identify phages as a plausible cause for this unintuitive decrease in cell abundances by quantifying the amount of pelagiphage-infected SAR11 cells in our samples. We found two peaks of phage-infected SAR11 cells, in late March and in early May, accounting for up to 9% and 19% of SAR11 cells, respectively (Fig. 3.2C). During the remaining sampling period, the abundances of phage-infected cells were close to the detection limit (Fig. 3.2C) and cell division rates were low (Fig. 3.2B). These findings highlight the importance of the timing of sampling, potentially explaining why SAR11 phage infection was considered low in earlier studies (Alonso-Sáez et al. 2018; Sánchez et al. 2020; Zhong et al. 2023). We next assessed the SAR11 community composition in metagenomes from the same phytoplankton bloom sampling campaign in 2020 (Sidhu et al. 2023). We determined relative abundances of 16S rRNA gene sequences and metagenome-assembled genomes (MAGs), classified as *Pelagibacterales*, by read mapping. The outcomes from both abundance estimates indicate that the SAR11 community is dominated by the same species or strains throughout the bloom situation (Fig. 3.3).

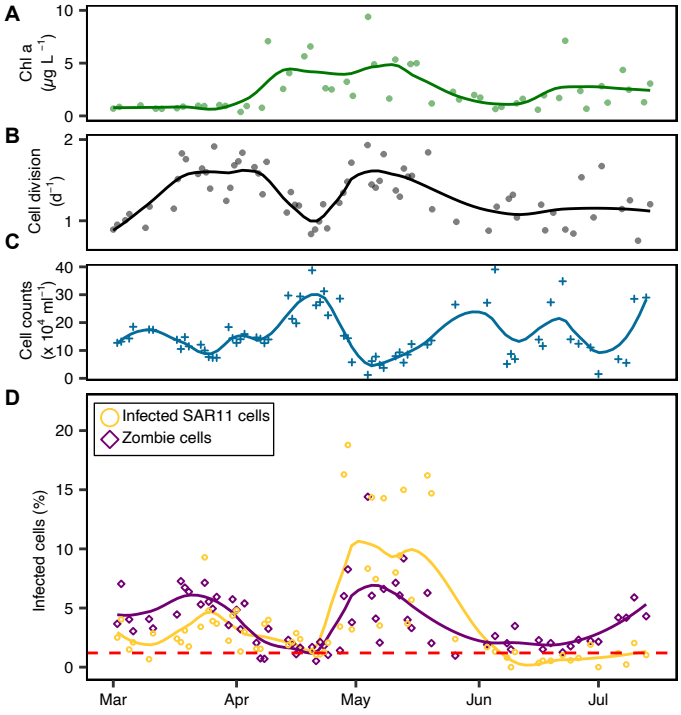

Figure 3.2: SAR11 and phage population dynamics during 2020 phytoplankton spring blooms at Helgoland Roads. (A) Chlorophyll a concentration, as a proxy for phytoplankton bloom development, (B) SAR11 cell division rate, and (C) SAR11 cell count data has previously been presented in Brüwer et al. (2023). (D) Proportion of phage-infected SAR11 cells (purple; relative to SAR11 cell counts) and zombie cells (yellow; relative to total DAPI-stained cell counts) are plotted as raw values per day. *Loess* smoothing is displayed as line plots. The amount of infected and zombie cells is proportional to only SAR11 and total cell counts, respectively. The average negative control over all samples is shown as a red-dashed line.

Individual assessments of the three pelagiphages HTVC027P, HTVC031P, and *Greip*, revealed that HTVC031P infected more SAR11 cells than the other two phages during high-infection periods. However, differences between the three phages were minor (Fig. S3.2A), highlighting

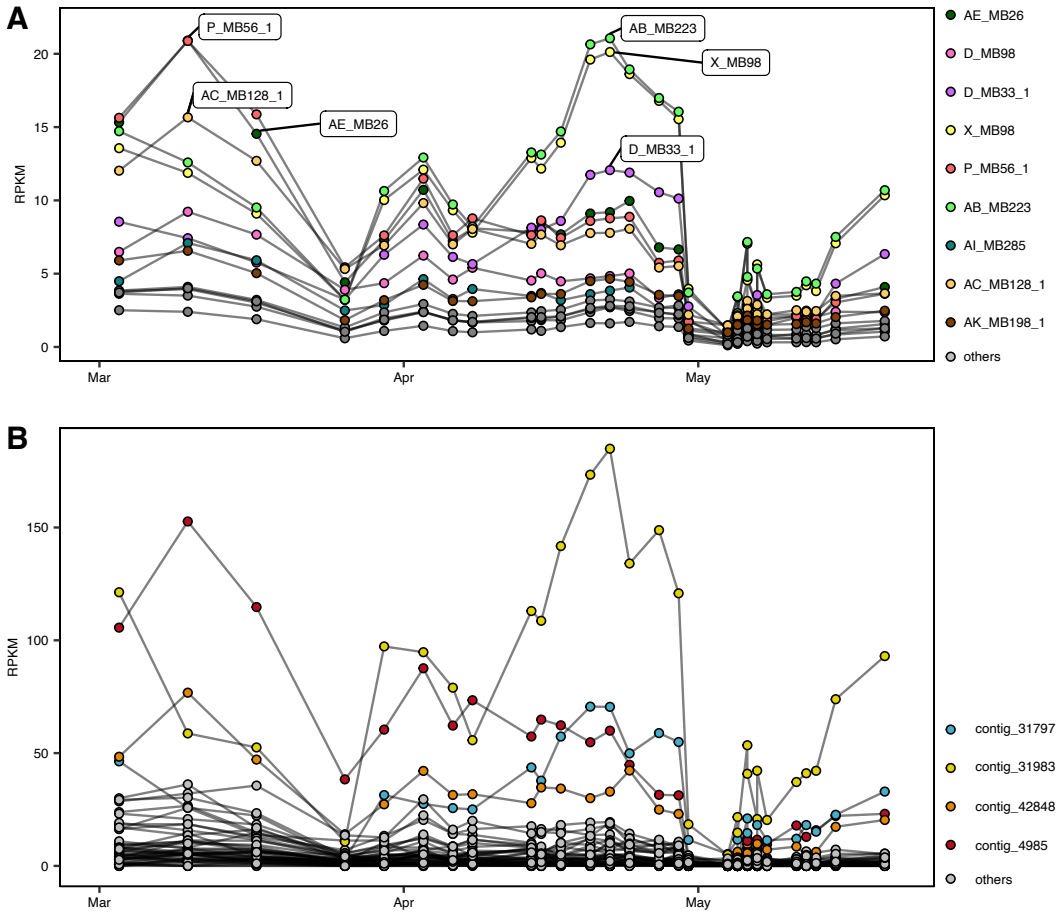

Figure 3.3: Bioinformatic abundance estimates of SAR11 during phytoplankton spring bloom. (A) metagenome assembled genomes (MAG) and (B) 16S rRNA gene sequences classified as *Pelagibacterales*. All data originated from PacBio Sequel II metagenomes from the 0.2 to 3 µm fraction (Sidhu et al. 2023). RPKM is Reads per Kilobase per Million Mapped reads.

that infections with each of the three pelagiphages are important *in situ*. As bioinformatic analyses revealed that the dominating SAR11 strains fluctuate simultaneously (Fig. 3.3) and there are little differences in abundance between the three phages, we believe all strains are susceptible to the three assessed phages. Additionally, our findings are in contrast to bioinformatic analyses, that predict HTVC027P to be more abundant than the other two phages both globally (Buchholz et al. 2021; Zhang et al. 2021) and during our sampling period (Fig. 3.3B; this study). This stresses the importance of experimental evidence for quantification approaches in phage ecology. Differences in abundance estimates between metagenomic and microscopy-based approaches are well-known for bacteria and similar causes may apply for phage abundances. Primer and assembly biases might skew bioinformatic approaches, while low signal intensities might underestimate microscopy-based abundances.

Zombie cell abundances coincided with the number of phage-infected SAR11 cells during the phytoplankton bloom. They were increased at the end of March (max. 7.1% of total cell counts) and early May (max. 14.4%), when SAR11 infection rates were highest (Fig. 3.2). To exclude

that the phages cross-infected other bacteria besides SAR11, we visualized all bacteria with the EUB338 I-III probe (Amann et al. 1990; Daims et al. 1999). We conclude that the assessed phages are SAR11-specific, as no significant differences were observed between zombie cell abundances in all bacteria (mean ±sd: $3.4 \times 10^4 \pm 1.6 \times 10^4$ cells mL^{-1}) and SAR11 ($4.2 \times 10^4 \pm 2.9 \times 10^4$ cells mL^{-1}) over five time-points from 27th April to 4th May (Fig. S3.3; $F(1,1)=0.61$, $p=0.578$, repeated measures ANOVA; Table S3).

3.3.3 Global distribution of phage-infected and zombie cells

To assess the broader relevance of our findings, we next examined the global distribution of phage-infected SAR11 and zombie cells in samples collected from surface and deep-chlorophyll maximum water in the Atlantic (cruise PS132 Wiltshire and Dummermuth 2023; 21 samples from 11 stations; Aug to Sept 2022), Southern (cruise PS133 Klaas 2023; 22 samples from 11 stations; Oct to Nov 2022), and Pacific Ocean (cruise SO245 Zielinski et al. 2018; 38 samples from 15 stations; Dec 2015 to Jan 2016; Fig. 3.4;S3.4). We detected phage-infected SAR11 and zombie cells across all three transects (Fig. 3.4), indicating their global abundance and importance. Phage infection exhibited the lowest prevalence in the Pacific (mean ±sd: 1.3 ±1.2% of SAR11 cell counts), while the Atlantic (2.9 ±1.6%) and Southern Ocean (3.3 ±1.4%) showed higher infection rates. In contrast to phage-infected SAR11 cells, zombie cell abundances were highest in the Pacific (mean ±sd: 5.1 ±5.1% of total cell counts), followed by lower abundances in the Southern (4.3 ±1.8%) and Atlantic (2.5 ±1.2%) Oceans.

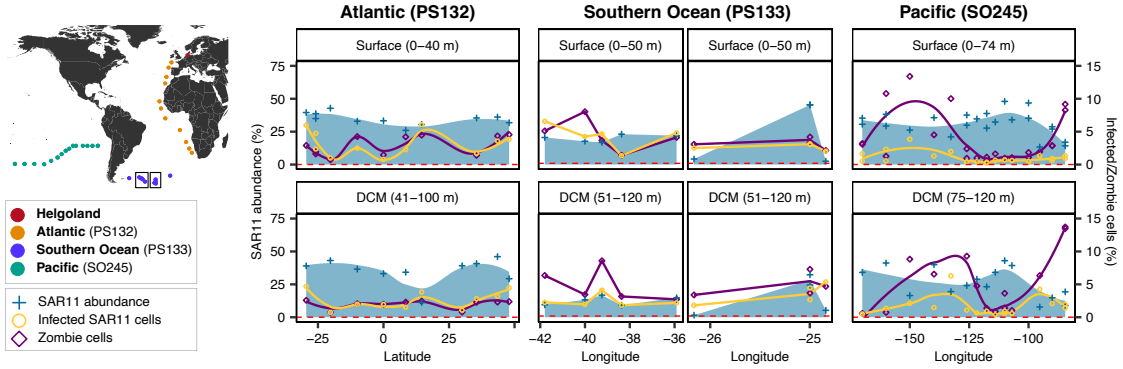

Figure 3.4: Global distribution of SAR11, phage-infected SAR11, and zombie cells. Map with sampling locations during different cruises and long-term ecological research station Helgoland Roads. Relative abundance of SAR11 (left y-axis), phage-infected SAR11(right y-axis), and zombie cells (right y-axis) from the Atlantic, Southern Ocean, and Pacific with respective cruises in brackets. Raw data is displayed as individual points and areas represent *loess* smoothing for the Atlantic and Pacific. Subset (boxes) of data from Southern Ocean without smoothing is displayed. Complete data of the Southern Ocean is available in Fig. S3.4.

SAR11 phage infection and zombie cell abundances were less prominent in the assessed transects compared to the relatively high infection stages observed in the Helgoland Roads

phytoplankton bloom data. This suggests that our cruise samples might not have coincided with periods of intense infection by the assessed phages. Nevertheless, across all samples (transects and time-series data), we found a positive correlation between the relative abundance of phage-infected and zombie cells (Fig. S3.5A; 0% of posterior distribution ≤ 0), a negative correlation between the relative abundance of zombie and SAR11 cells (Fig. S3.5B; 0% of posterior distribution ≥ 0), and a positive correlation between the relative abundance of phage-infected SAR11 cells and the frequency of dividing cells, which is a proxy for cell division activity (Fig. S3.5C; 0.000125% of posterior distribution ≤ 0; Brüwer et al. 2023). This indicates higher infection rates in faster-growing hosts. Our microscopic evidence of phage-infected and zombie cells indicates that they are globally distributed and suggests that zombie cells are an integral part of pelagiphage infections.

3.4 Discussion

In this study, we used direct-geneFISH to visualize and quantify the abundance of phage-infected SAR11 cells. We assessed the impact of phage infection on the SAR11 community during a phytoplankton bloom and showed the global distribution of phage infections by the assessed phages. We additionally discovered ribosome-deprived but phage-infected cells, whose abundance is correlated to the amount of phage-infected SAR11 cells.

During the phytoplankton bloom, up to 19% of SAR11 cells were phage-infected, which cooccurred with a ∼90% decrease in SAR11 abundances. Assuming *in situ* phage lysis within 24 h or faster (Zhao et al. 2013), our results are in line with global estimates of up to 30% phage-mediated cell lysis within one day (Breitbart et al. 2018; Eggleston and Hewson 2016). We interpret this as part of a 'boom and bust' cycle, where SAR11 cell abundances reached a critical population density that was subsequently reduced by phage infection. The "kill-the-winner" hypothesis describes the disproportionally higher phage-induced lysis rates of faster-growing bacteria. Further, different bacterial strains from the same species may succeed each other, especially in bloom situations, as the majority of phages are believed to be strain-specific (Thingstad and Lignell 1997; Thingstad et al. 2014). As metagenomic data suggest that the SAR11 community was dominated by the same species and potential strains (Fig. 3.3; Sidhu et al. 2023), our findings of fast-growing SAR11 and high infection rates suggest a 'kill-the-winner' behavior (Thingstad et al. 2014). In addition, the almost equal contribution of phage infection by the three assessed phages suggests that all the abundant strains are susceptible to the assessed phages. The dominance of individual strains succeeding each other would be in accordance with previously reported Red Queen dynamics, describing constantly changing host and viral communities on the fine strain level (Ignacio-Espinoza et al. 2020).

3.4.1 Zombie cells: Clever persisters or 'phage puppets'?

Pelagiphage-infection of SAR11 cells results in the formation of zombie cells – cells devoid of any detectable 16S ribosomal RNA. Such a major cell transformation may be caused by a yet-unknown anti-phage defense system. Infected cells may digest their ribosomes to prevent phage proteins from being synthesized and reduce their metabolism – they may become 'persisters' as recently proposed (Fernández-García et al. 2023). In fact, we have previously shown the ability of SAR11 to regulate their ribosome content according to growth rates (Brüwer et al. 2023). However, no anti-phage defense system targeting rRNA or an abortive infection has yet been described for SAR11 or any other bacterium yet (Fernández-García and Wood 2023). Nevertheless, we screened all SAR11 MAGs (n=14), which could be recovered from the phytoplankton bloom in 2020, none of which contained any anti-phage system (Table S4). We further analyzed 172 publicly available *Ca.* P. ubique genomes, of which 19 contained putative anti-phage systems. These were all classified as restriction-modification (RM) systems and are involved in epigenetic modifications (i.e., methylation or phosphorothiolation of the ribophosphate) of the host DNA and restrictions of unmodified phage-DNA (Georjon and Bernheim 2023) (Table S4). However, a close monitoring of HTVC027P and HTVC031P infections of batch-cultured HTCC1062 over time speak against an anti-phage system.

Firstly, if an anti-phage system existed, zombie cells would enrich over time, while the phage would eventually lyse 16S rRNA-containing infected cells. We could not detect abundance differences 18 and 26 h (HTVC027P) or 20 and 28 h (HTVC031P) post-infection for both cell types ($t(3.9) = -0.166$, $p=0.88$ for HTVC027P, $t(3.6)=-0.26$, $p=0.81$ for HTVC031P, Welch's two sample t-test, Fig. 3.1). Additionally, we assessed the phage DNA content by measuring the phage FISH fluorescence intensity. The fluorescence intensity in cells infected with HTVC027P increased over time ($F(1)=0.31$, $p<0.001$) indicative for ongoing phage DNA synthesis, but we could not detect differences between zombie and phage-infected 16S positive cells ($F(1)=0.303$, $p=0.582$, ANOVA, Fig. S3.6). For cells infected with HTVC031P, the fluorescence not only increased over time, but was also increased in the zombie cells, compared to the phage-infected 16S positive cells ($F(1)=100.18$, $p<0.001$). This indicates a continuous production of phage DNA in both, the zombie and the infected 16S rRNA containing cells and speaks against a defense mechanism. Lastly, the host's DNA content, and consequently their abundance in metagenomes across the 2020 spring bloom, would remain unchanged, if zombies were a result of an anti-phage system. However, SAR11 cell abundances from FISH and metagenomic (MAG and 16S rRNA-based) data do fluctuate synchronously (Fig. 3.2 & 3.3), rendering the hypothesis of an anti-phage defense in SAR11 unlikely.

Alternatively, phage infection may result in phage-induced RNA degradation to recycle ribonucleotides for phage genome synthesis. In this case, the phages become the 'puppet masters' of the SAR11 host (Breitbart et al. 2018). The use of host RNA to build new phage genomes has previously been suggested for *Prochlorococcus* cyanophages (Sullivan et al. 2005) and is

not limited to rRNA but may also include mRNA, tRNA, or other RNAs. In fact, we detected all intermediate stages between phage-infected with and without a ribosomal signal, suggesting the general use of RNAs (Fig. S3.7). In the pure cultures of HTVC027P, we assessed the 16S FISH signal areas, which were truncated at the lower detection limit, indicating a continuum of decreasing ribosomal content (Fig. S3.7). Hence, there is no switch (i.e., "yes" or "no") whether ribosomal RNA is used during phage infection but rather suggests a continuous use of all available RNA to complement the nucleotide pool.

The annotation of HTVC031P revealed the presence of ribonucleases and deoxyribonucleotide dehydrogenase subunits alpha and beta (Table S5), which are essential for the breakdown of RNA and the subsequent conversion to DNA nucleotides. On the genome, the ribonucleases and dehydrogenases were middle genes, located and transcribed between DNA replication (early) and structural (late) phage proteins encoding genes (Yang et al. 2014). Timing is essential, as nucleotides must be available early in the infection cycle, while phages rely on host ribosomes, which should not be digested too early. In the case of HTVC027P and *Greip*, the dehydrogenase genes were not found in their genomes. Either host proteins or one of the many uncharacterized proteins (Table S5) may be used. RNA nucleotides are a valuable resource, especially when DNA nucleotides are scarce. Nucleotides are frequently a limiting factor. For example, cyanophages not only enhance their host's photosynthesis activity but also modify the host's metabolism to increase nucleotide production (Thompson et al. 2011), although the host genomes are much larger than SAR11. SAR11 have amongst the smallest genomes (∼1.3 million base pairs) of free-living bacteria (Giovannoni 2017), and they might have epigenetic modifications in their DNA (discussed above), reducing the availability of DNA nucleotides (Loenen and Raleigh 2014). At the same time, SAR11 have an estimated 150-700 ribosomes per cell (Zhao et al. 2017), which equates to 0.6–3.0 million bases of single-stranded RNA. This could be a valuable resource, almost doubling the number of nucleotides available for double-stranded DNA phage genomes. To summarize, while we cannot entirely exclude an anti-phage system as a cause for zombie cells, we believe phage-induced ribosome digestion is more likely.

3.5 Conclusion

We present the first microscopic quantification of phage-infected SAR11 cells *in situ*, advancing our understanding of SAR11 clade dynamics, and present zombie cells as a new phenomenon. We demonstrate that pelagiphage infections play a critical role in regulating SAR11 populations, especially during phytoplankton spring blooms. The global prevalence, evident by our data from various oceans, highlights their significance in marine microbial ecology. The discovery of the globally occurring zombie cell phenomenon underscored the complexity of phage-host interactions. We provide possible explanations for the formation of zombie cells, which are phage-infected cells without detectable rRNA. We suggest a phage-induced recycling of ribosomal RNA,

though this requires further exploration in future studies. As zombie cells are likely not restricted to SAR11 hosts, but widely distributed among other phage-host pairs, our discovery of zombies has implications beyond marine microbial ecology. This research not only sheds new light on the intricate dynamics of SAR11 and their viruses, as well as their turnover rates, but also opens new possibilities for exploring microbial and viral strategies in the ocean's biogeochemical cycles.

3.6 Material and Methods

3.6.1 Cultivation of *Ca.* P. ubique infected with HTVC031P, HTVC027P, and HTVC023P

The SAR11 strain *Ca.* P. ubique HTCC1062 was kindly provided by Professor Stephen Giovannoni, Oregon State University, USA. HTCC1062 was cultured in artificial seawater-based ASM1 medium supplemented with 1 mM NH_4Cl, 100 µM KH_2PO_4, 1 µM $FeCl_3$, 100 µM pyruvate, 50 µM glycine, and 50 µM methionine (Carini et al. 2013). HTCC1062 cultures were incubated at 17 °C without shaking and light. Exponentially growing HTCC1062 cultures were infected with HTVC023P, HTVC027P, and HTVC031P independently at a phage-bacteria ratio of approximately 10:1 in triplicates. Cell mortality was monitored using the Guava EasyCyte flow cytometer (Millipore, USA). When cell mortality was detected, samples were fixed with formaldehyde (1% final concentration) for 1 h at room temperature and filtered on 0.2 µm polycarbonate filters (Merck Millipore, Burlington Massachusetts, US). In a repeated experiment, *Ca.* P. ubique HTCC1062 were infected with HTVC027P and HTVC031P, as described above. Samples were taken from three time-points (2 h after infection; approximately 2 h before cell lysis; approximately 6 h after cell lysis) and fixed and filtered as described above.

3.6.2 Environmental sampling

Samples were collected during the 2020 phytoplankton spring bloom from ∼1 m depth at the long-term ecological research station Helgoland Roads (54° 11.3' N, 7° 54.0' E), German Bight (Table S6; Brüwer et al. 2023). Samples from the Atlantic and Southern Ocean were collected using a Seabird SBE 911+ CTD in 2022 during the R/V Polarstern cruises PS132 (Wiltshire and Dummermuth 2023) and PS133/1 (Klaas 2023), respectively. Samples from the Pacific Ocean were collected with a Seabird SBE 911+ CTD during the R/V Sonne cruise SO245 (Zielinski et al. 2018). SAR11 cell counts from SO245 were retrieved from Reintjes et al. (2019). During the cruises, samples were collected from surface water and deep-chlorophyll maximum (DCM; Table S6). Samples were fixed with formaldehyde (1% final concentration) for 1 h at room temperature. Cells were immobilized on 0.2 µm polycarbonate filters (Merck Millipore, Burlington Massachusetts, US), which were stored at −20 °C until further processing. The final sampling volume varied depending on total cell counts in the samples (Table S6).

3.6.3 Pelagiphage FISH probe design and synthesis

We designed direct-geneFISH probes (Barrero-Canosa et al. 2017) based on alignments between each of the three isolates, namely HTVC027P, HTVC031P, and *Greip*, and PacBio Sequel II metagenomes from the 2020 spring phytoplankton bloom at Helgoland, North Sea (ENA project: PRJEB52999, Sidhu et al. 2023). Targeted probe-regions were identified from assembled contigs (Supplementary material and methods). Subsequently, probes were designed manually within Geneious (v2022.1.1; Kearse et al. 2012). We aimed for 10-13 probes per phage of 156-318 bp length and a GC content similar to the host and phages (22.0 – 43.2%, mean ±sd: 32.9 ±4.9%). Further, reference genomes and metagenome data from Helgoland Roads needed to share a minimum of 90% nucleotide identity for usability during direct-geneFISH (Zeugner et al. 2021). We aimed to target genes encoding terminases, polymerases, or structural proteins, as we expect higher conservancy in these genes. Ambiguous alignment with any other sequence was excluded, against the nr database using the NCBI BLAST webservice (14th February 2023).
Probes (Table S7) were ordered as "oPools" from integrated DNA Technologies (IDT, Coralville, Iowa, USA) and resuspended in water as directed by the manufacturer. Probes were labelled with the ULYSIS Alexa 594 conjugation kit (Invitrogen, Waltham, Massachusetts, USA) with minor modifications as described in Zeugner et al. (2021) and subsequently purified using Micro Bio-Spin chromatography columns P-30 (Bio-Rad, Hercules, California, USA). Labelling efficiencies were calculated as described by the manufacturer's instructions for the ULYSIS kit, using a NanoDrop (Thermo Fisher Scientific, Waltham, Massachusetts, USA).

3.6.4 Fluorescence *in situ* hybridization

First, CARD-FISH targeting the 16S rRNA of SAR11 (SAR11-mix, Table S7) was conducted (Fuchs et al. 2007). Secondly, samples were hybridized with equimolar amounts of the probes targeting HTVC027P, HTVC031P, and *Greip*, using direct-geneFISH as described earlier (Barrero-Canosa et al. 2017; Zeugner et al. 2021) with minor modifications. Hybridization buffer with 25% formamide was used and no ethanol washing was conducted after direct-geneFISH to prevent any loss of fluorescence signal. Hybridized filters were counter-stained with the DNA stain 4',6-diamidino-2-phenylindole (DAPI; 1 µg mL^{-1}). Samples were embedded in ProLong Glass Antifade (Invitrogen, Waltham, Massachusetts, USA) for microscopy. As negative controls, samples of HTVC023P were hybridized with the probe mix, targeting all three phages. Additionally, environmental negative controls included samples which were not exposed to the phage-probe mix to account for any autofluorescence within cells.

3.6.5 Microscopy

Samples were imaged on a Zeiss AxioImager.Z2m, equipped with a charged-coupled device (CCD) camera (Zeiss AxioCam MRm, Zeiss, Oberkochen, Germany), and illuminated with a Zeiss Colibri 7 LED (excitation: 385 nm for DNA, 469 nm for 16S rRNA CARD-FISH, and 590 nm for direct-geneFISH signals). The microscope was equipped with a Multi-Zeiss 62 HE filter cube (Beam splitter FT 395+495+610). Images were recorded with a custom-built macro (Bennke et al. 2016; Zeder et al. 2011) within the Zeiss AxioVision software (Zeiss, Germany). A total of 120 fields of view per sample were recorded with a 63x Plan Apochromat objective (1.4 NA, oil immersion). For high-resolution imaging, we used a Zeiss LSM 780 (Zeiss, Oberkochen, Germany), with an ELYRA PS.1 detector upgrade. The microscope was equipped with a 63x plan apochromatic oil immersion objective and the excitation lasers 405 nm (DAPI), 488 nm (16S rRNA CARD-FISH), and 591 nm (direct-geneFISH).

3.6.6 Image cytometry

Quality control and automated cell counting of 8-bit greyscale images was done within the Automated Cell Measuring and Enumeration tool (ACME, available from https://www.mpi-bremen.de/automated-microscopy.html; Bennke et al. 2016; Zeder et al. 2011) with channel-specific settings (Table S2). Cells for total cell counts were defined by a DNA (DAPI)-specific signal. SAR11 cells were defined with an overlapping DNA and 16S rRNA (CARD-FISH) signal and phage-infected cells needed an additional phage (direct-geneFISH) signal. Zombies were cells with a phage signal but no 16S rRNA signal. We calculated the frequency of dividing cells – a proxy for cell-division rate – as previously described (Brüwer et al. 2023) using the MicrobeJ plugin (Ducret et al. 2016) within ImageJ/Fiji (Schindelin et al. 2012). In principle, a cell containing two local DNA maxima was counted as a dividing cell.

3.6.7 Metagenomic abundance estimates for SAR11 MAGs, 16S rRNA gene, and Pelagiphages

To determine the relative abundance of SAR11 metagenome-assembled genomes (MAGs) during the 2020 phytoplankton spring bloom, we performed a mapping analysis utilizing PacBio metagenomic reads obtained from the prokaryotic fraction (0.2 µm to 3 µm) across all 30 samples. The reference MAGs, classified under the order *Pelagibacterales* by gtdbk-tk (v1.3.0, release 202; Chaumeil et al. 2020), were initially derived from the same phytoplankton bloom metagenomes, described above (Sidhu et al. 2023). Raw reads were mapped using the minimap2-pb (Li 2018) algorithm, executed within the SqueezeMeta pipeline (v1.3.1; Tamames and Puente-Sánchez 2019). The mapping outcomes were normalized using the reads per kilobase per million mapped reads (RPKM) metric, which considers both the length of the

MAG and the library size of each sample. The RPKM value was determined using the formula $RPKM = \frac{Reads\ mapped\ to\ SAR11\ MAG * 10^6}{total\ read\ in\ a\ sample * length\ of\ MAG\ in\ kilobase\ pairs}$.

For quantifying the abundance of the 16S rRNA gene, we extracted the full-length 16S rRNA sequences from metagenome assemblies using Barrnap (v0.9; https://github.com/tseemann/barrnap). Similar to the SAR11 MAGs, these sequences underwent mapping, and their relative abundance was computed using the RPKM method as described earlier.

To assess the relative abundance of the phages HTVC027P, HTVC031P, and *Greip*, mapping of metagenomic reads to the reference genomes were performed in a similar fashion. To facilitate a comprehensive comparison with our microscopy data, and considering the specificity of these phages to SAR11, we calculated the abundance of these pelagiphages relative to SAR11 community present during spring phytoplankton bloom in 2020. Therefore, phage relative abundance was determined as $\frac{Reads\ mapped\ to\ phage\ genome * 10^6}{\sum(read\ mapped\ to\ all\ SAR11\ MAGs) * (length\ of\ phage\ in\ kilobase\ pairs)}$.

3.6.8 Identification of defence systems within SAR11 genomes

All available *Ca.* P. ubique genomes (n=172) available in the RefSeq database (from October 22nd 2023; O'Leary et al. 2016) and MAGs from the 2020 phytoplankton spring bloom (n=14; Sidhu et al. 2023) were screened for anti-phage defence mechanisms. DefenceFinder (Tesson et al. 2022) was used with the default database from October 22nd 2023.

3.6.9 Statistics and modelling

Statistical analyses and corresponding visualizations were done in R (v4.2.2; R Core Team 2022; for used packages see supplementary material and methods). Repeated measures ANOVA was used to test for the specificity of pelagiphages to SAR11. Zombies were detected in all bacteria, using the 16S FISH probe EUB338 I-III and compared to zombies in SAR11 (SAR11-mix, Table S7). Samples originated from the time-series and were not independent from each other. Thus, repeated measures ANOVA was chosen.

Bayesian beta regressions were applied to assess the relationship between (a) the abundance of phage-infected and zombie cells, with the model formula $rel_inf_T \sim Zombie_cells$ and (b) abundance of zombie and SAR11 cells, using the model formula $Zombie_cells \sim rel_SAR11_abundance$. rel_inf_T is the relative infection rate, transformed by adding 0.001 because two values of the data (148 data points) originally contained 0 for which the beta distribution is not defined; *Zombie_cells* is the relative abundance of Zombie cells; *rel_SAR11_abundance* is the relative SAR11 abundance; and *FDC_percent* is the frequency of dividing cells. The model predictions were back-transformed from the logit-scale for the plots in Fig. S3.5.

a) We assumed a positive relationship between phage-infected cells and Zombie cells, as the

95% credible interval [4.083, 9.554] of the slope (on logit-scale) excluded 0 and all values of the posterior distribution for the slope were ≥ 0. The model predicts an intercept of -3.72 ± 0.1 and a slope of 6.92 ± 1.41 (on logit-scale; means $\pm$SD).

b) A negative relationship was assumed between the relative abundances of zombie and SAR11 cells, as all values of the posterior distribution for the slope were < 0. The 95% credible interval was $[-2.800, -0.953]$ (on logit-scale). The model predicted an intercept of -2.74 ± 0.1 and a slope of -1.87 ± 0.5 (on logit-scale; mean $\pm$SD).

c) We assumed a positive relationship between phage-infected cells and Zombie cells, as the 95% credible interval [0.02, 0.05] of the slope (on logit-scale) excluded 0 and only 1 of the 8,000 values of the posterior distribution for the slope was ≤ 0. The model predicts an intercept of -3.72 ± 0.1 and a slope of 0.04 ± 0.01 (on logit-scale, mean $\pm$SD).

In the model, flat priors (brms default) were used and 2000 iterations for 4 chains after a warmup period of 2000 iterations per chain.

3.7 Supplementary Information

3.7.1 Supplementary material and methods

Pelagiphage FISH probe design and synthesis

During the Helgoland 2020 spring phytoplankton bloom, 30 PacBio Sequel II metagenomes were sampled between March 3 and May 20 (European Nucleotide Archive (ENA) project PRJEB52999). Sampling, DNA extraction, sequencing, and assembly are described in detail in Sidhu et al. (2023). Briefly, 10 L of unfixed seawater was sampled at the long-term ecological research station Helgoland Roads (54° 11.3' N, 7° 54.0' E), filtered sequentially through 10, 3, and 0.2 µm polycarbonate filters (47 mm diameter, Sigma Aldrich, Taufkirchen, Germany) and stored at $-80\,^{\circ}$C until further processing. DNA was extracted from 0.2 µm filters, following Zhou et al. (1996). Samples were sequenced on a PacBio Sequel II (Pacific Biosciences, Menlo Park, CA, USA) using one SMRT cell per sample in long-read HiFi mode at the Max Planck Genome Centre, Cologne, Germany. Raw reads were assembled using Flye (v2.8.3; Kolmogorov et al. 2019) in *-meta* and *-pacbiohifi* mode.

Potential viruses were identified from assembled contigs using VIBRANT (v1.2.0; Kieft et al. 2020). Retrieved sequences were aligned against a database composed of the viral NCBI RefSeq (r203; O'Leary et al. 2016), as well as additional pelagiphage sequences from isolated phages (Buchholz et al. 2021; Zhang et al. 2021; Zhao et al. 2019) using BLASTn (v2.5.0; Camacho et al. 2009). Sequences with an alignment to a known phage were further validated by identifying the closest neighbor in a proteomic tree, using VipTree in 2D mode (v1.1.2; Nishimura et al. 2017) with the same database as described above. Retrieved sequences were annotated using DRAM-v.py annotate (Shaffer et al. 2020) (with *–use_uniref*) and subsequently aligned with their

closest reference using MAFFT (v7.450; algorithm “auto”, scoring matrix “200PAM/k=2”, gap open penalty: 1.53, offset value:0.123; Katoh and Standley 2013) within Geneious (v2022.1.1; Kearse et al. 2012).

Probes were designed on these alignments with the guideline of ca. 150-300 bp length and minimum 90% nucleotide identity between reference genome and metagenome sequences. A minimum of 10 probes was designed to target a single phage genome. We aimed to target genes encoding terminases, polymerases, or structural proteins, based on the DRAM-v annotation, where possible. Ambiguous alignment with any other sequence was excluded, using BLASTn against the NCBI webservice (14th February 2023).

Statistical modelling and visualizations

All statistical analyses done in R (v4.2.2, R Core Team 2022) with the packages brms (v2.19.0, Bürkner 2017), tidyr (v1.3.0, Wickham et al. 2023), tidybayes (v3.0.4, Kay 2023), cmdstanr (v0.5.3, Gabry and Češnovar 2022), and ez (v4.4-0, Lawrence and Lawrence 2016). For visualizations we used the packages ggplot (v3.4.2, Wickham 2011a), plyr (v1.8.8, Wickham 2011b), ggpubr (v0.6.0, Kassambara and Kassambara 2020), cowplot (v1.1.1, Wilke 2020), and lubridate (v1.9.2, Grolemund and Wickham 2011. Color schemes were inspired by the WesAnderson package (v0.3.6, Ram and Wickham 2018).

3.7.2 Supplementary Figures

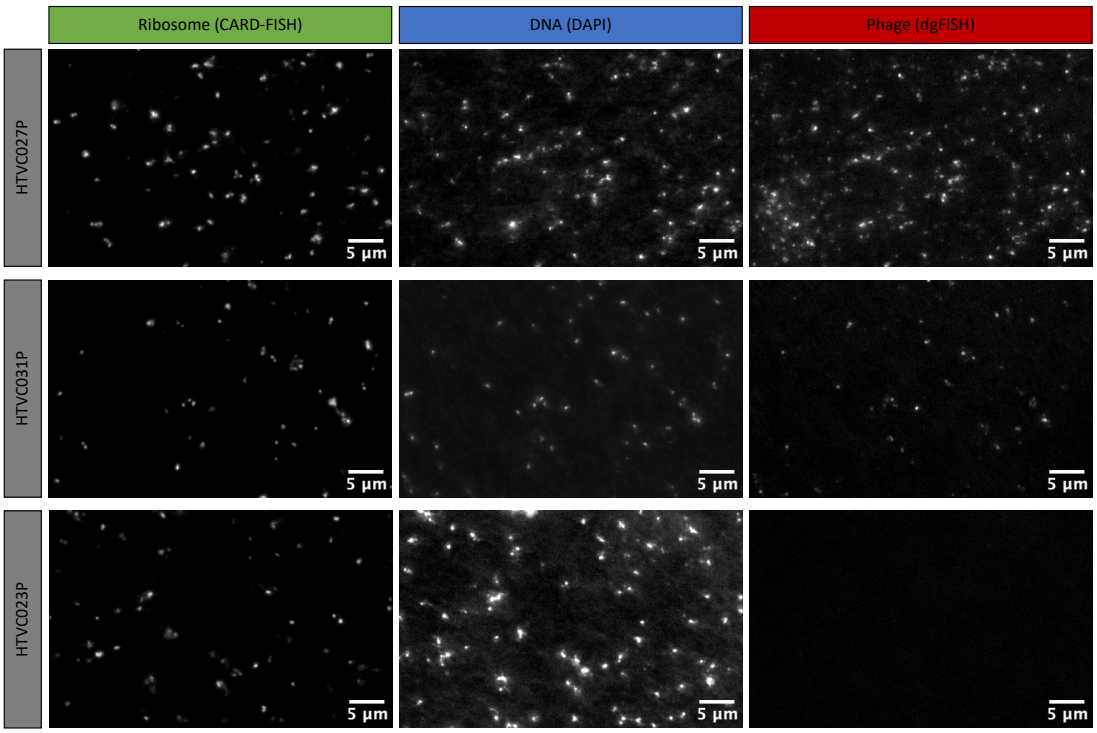

Figure S3.1: Examples of high-throughput images to determine phage-infected SAR11 cells in control cultures. *Ca.* P. ubique HTCC1062 were infected with HTVC027P, HTVC031P, and HTVC023P. DNA was stained with DAPI, 16S ribosomal RNA with CARD-FISH (SAR11-mix), and phage genes were stained with direct-geneFISH (phage mix for HTVC027P, HTVC031P, and *Greip*). HTVC023P served as negative control. Images were cropped to a quarter of original size for visualization purposes and scale bars were inserted using ImageJ/Fiji.

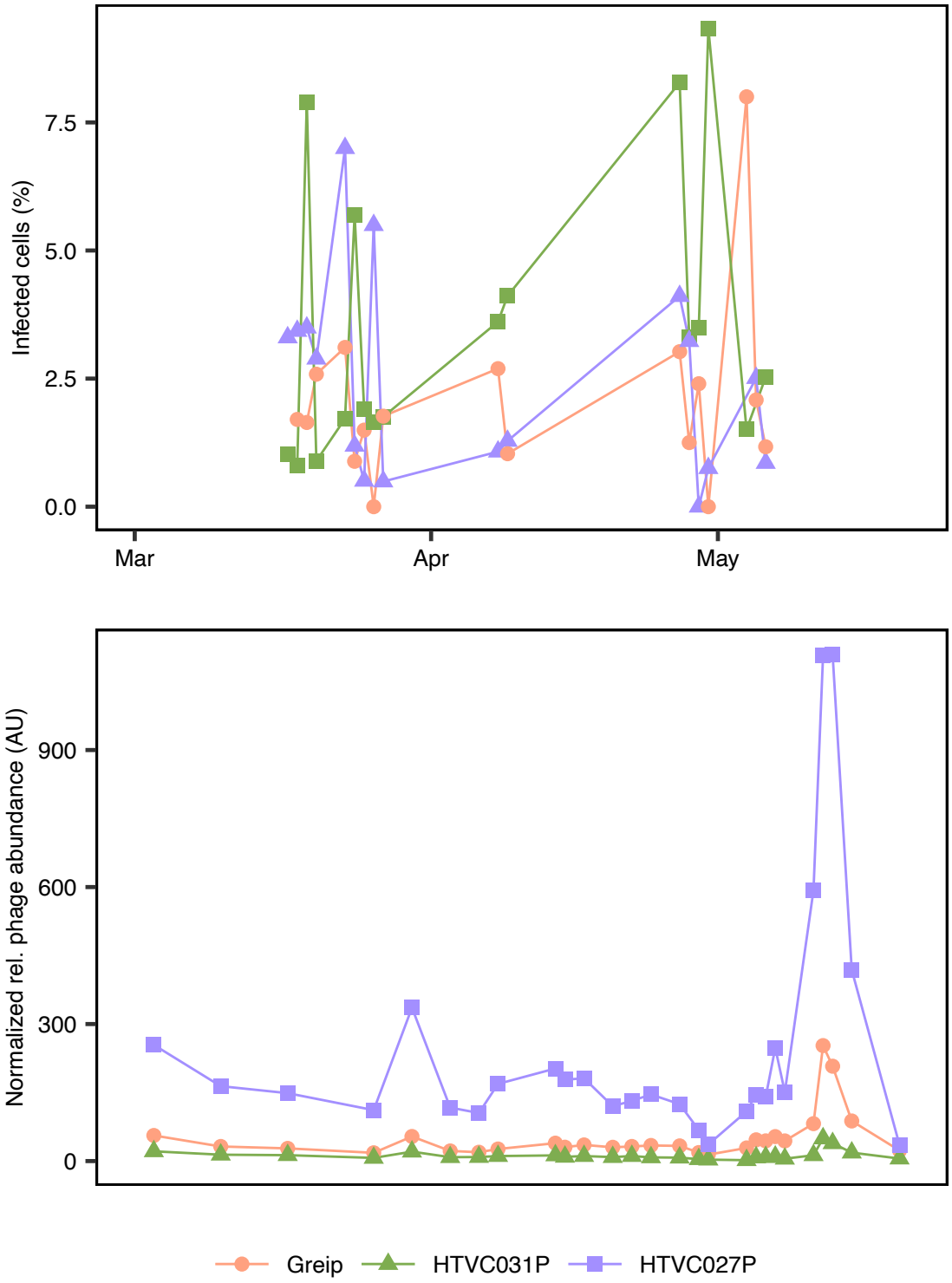

Supplementary Figure S3.2: Microscopy-based vs. bioinformatic estimates of phage-infected cells during the 2020 spring phytoplankton bloom at Helgoland Roads. Upper panel: Abundance of phage-infected SAR11 cells per individual phage, based on microscopy estimates. Lower panel: Relative abundances of respective phages were normalized by the total number of reads mapped to all SAR11 MAGs in the same sample.

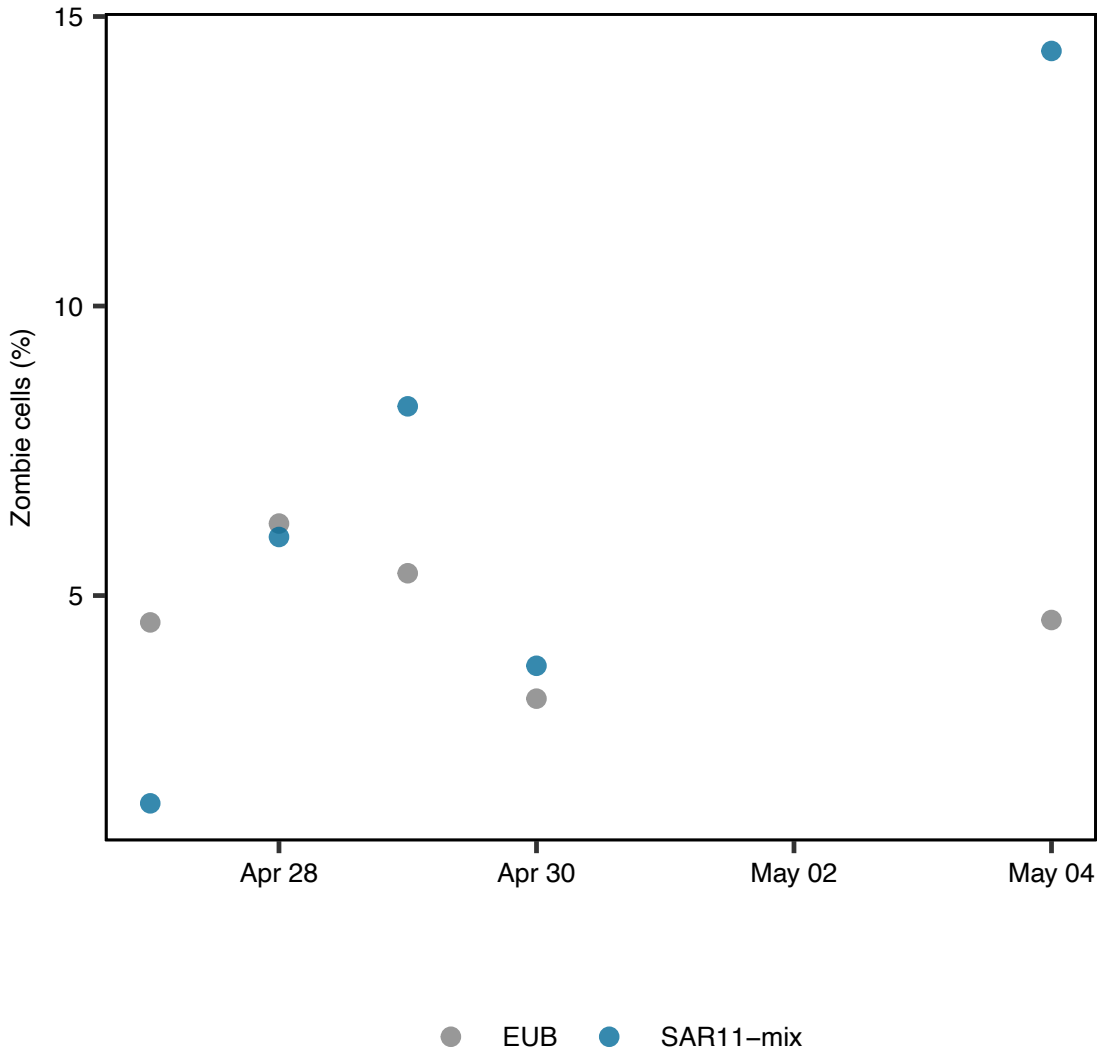

Supplementary Figure S3.3: Amount of zombie cells in all bacteria vs. SAR11. All bacteria were targeted with the EUB338 I-III FISH probe, while SAR11 was targeted with the SAR11-mix (Table S7).

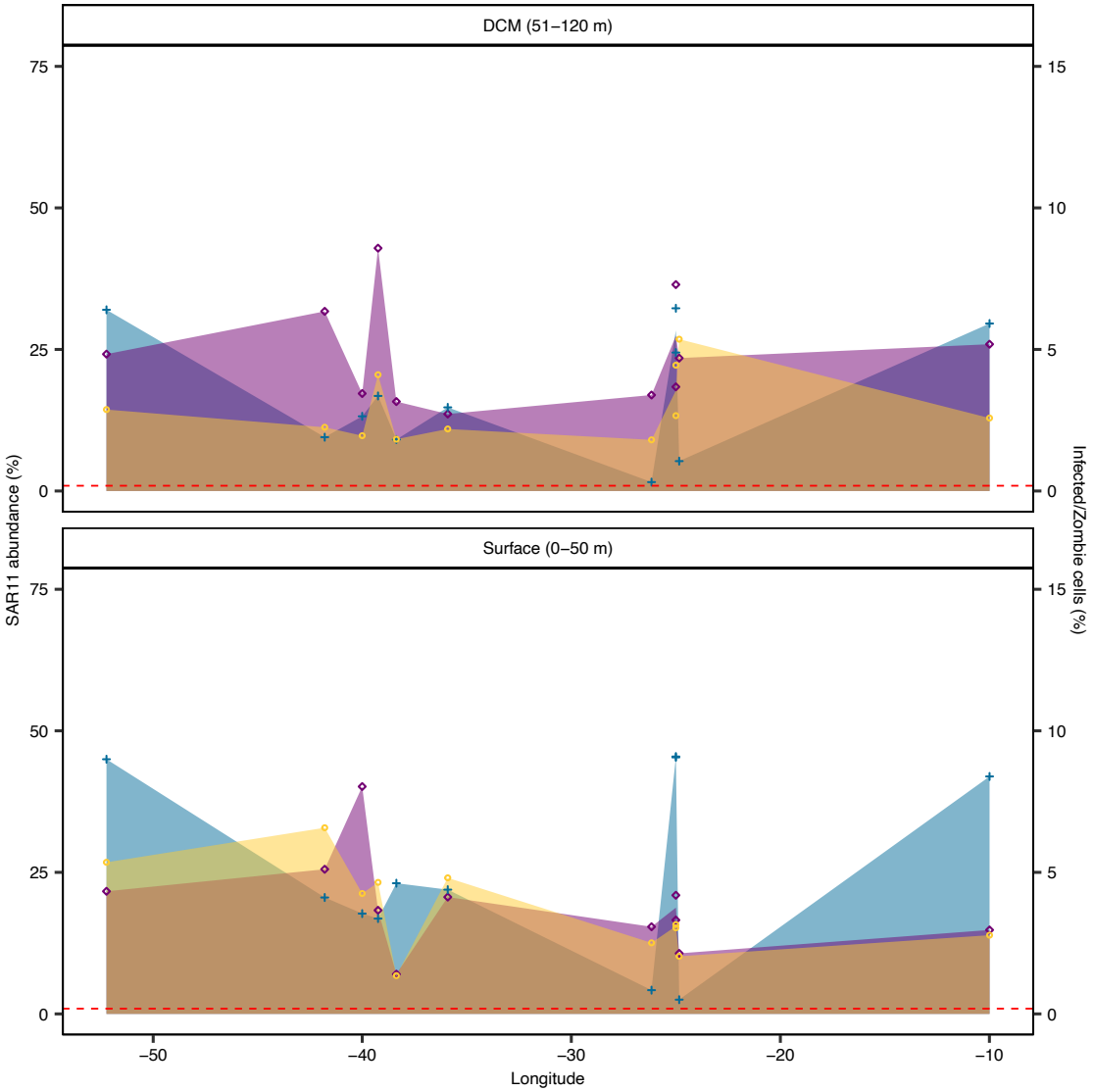

Supplementary Figure S3.4: Distribution of SAR11, phage-infected SAR11, and zombie cells in the Southern Ocean. Complete results for Fig. 3.4.

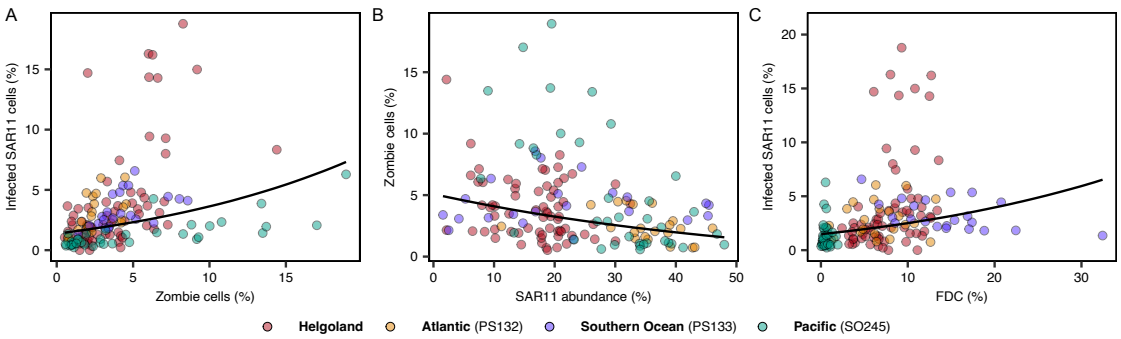

Supplementary Figure S3.5: Statistical modelling applying Bayesian beta regression between SAR11 abundance, phage-infected SAR11 cells, and zombie cells. (A) relative abundance of phage-infected SAR11 cells and Zombie cells, (B) relative abundance of Zombie and SAR11 cells, and (C) phage-infected SAR11 cells and frequency of dividing cells (FDC), which is a proxy for cell division activity. Points represent raw data from different sampling campaigns. Line represent data modelled with Bayesian beta regression (back transformed from logit scale).

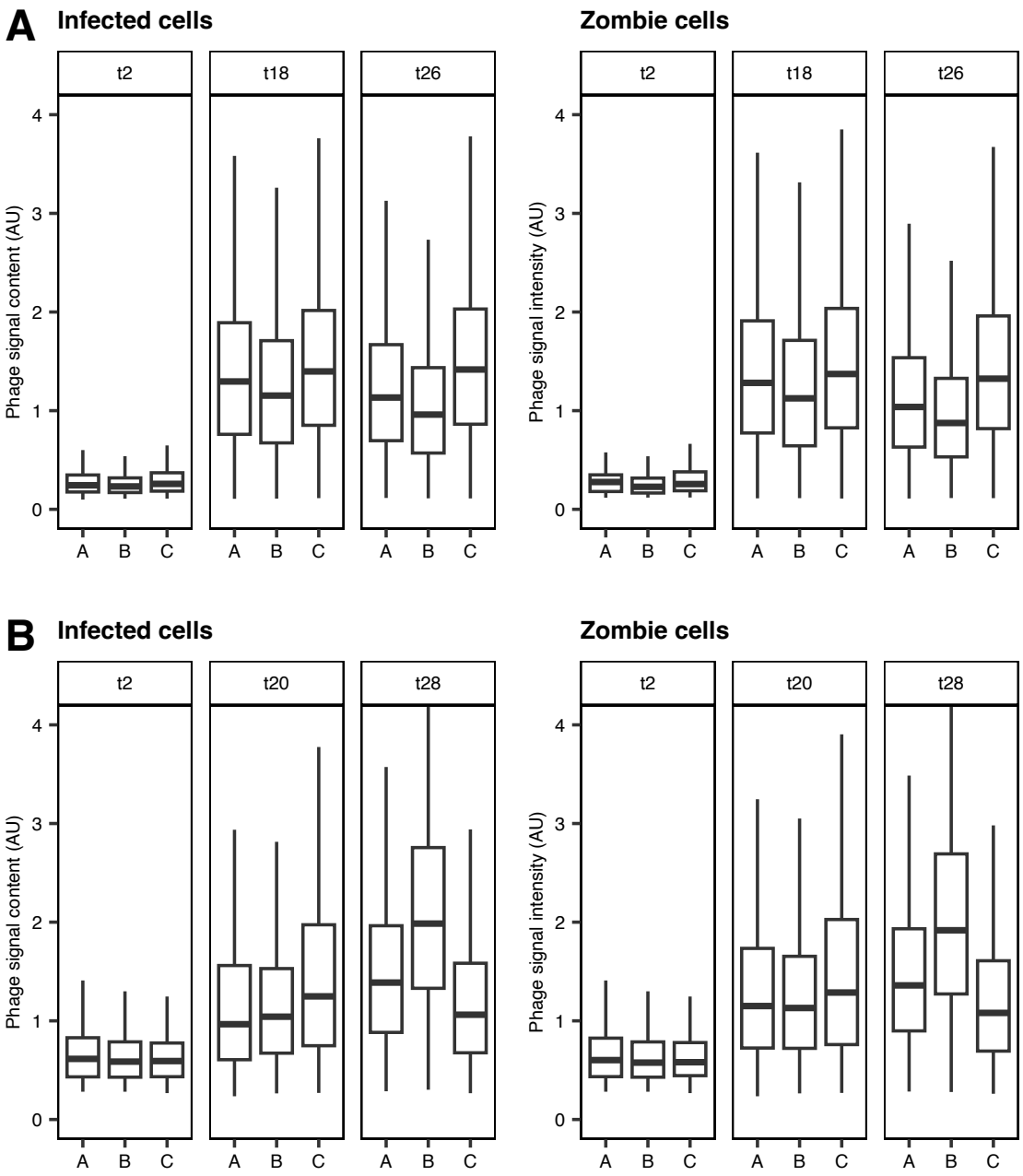

Supplementary Figure S3.6: Direct-geneFISH ("phage") signal content from pure cultures. (A) SAR11 infected with HTVC027P. (B) SAR11 infected with HTVC031P. "Infected cells" corresponds to 16S FISH-positive and direct-geneFISH-positive cells, whereas "Zombie cells" do not contain a 16S FISH signal. Boxplots show median and upper and lower quartile. Whiskers show maximum data points within upper/lower quartile range plus 1.5 times the interquartile range. Outliers not shown.

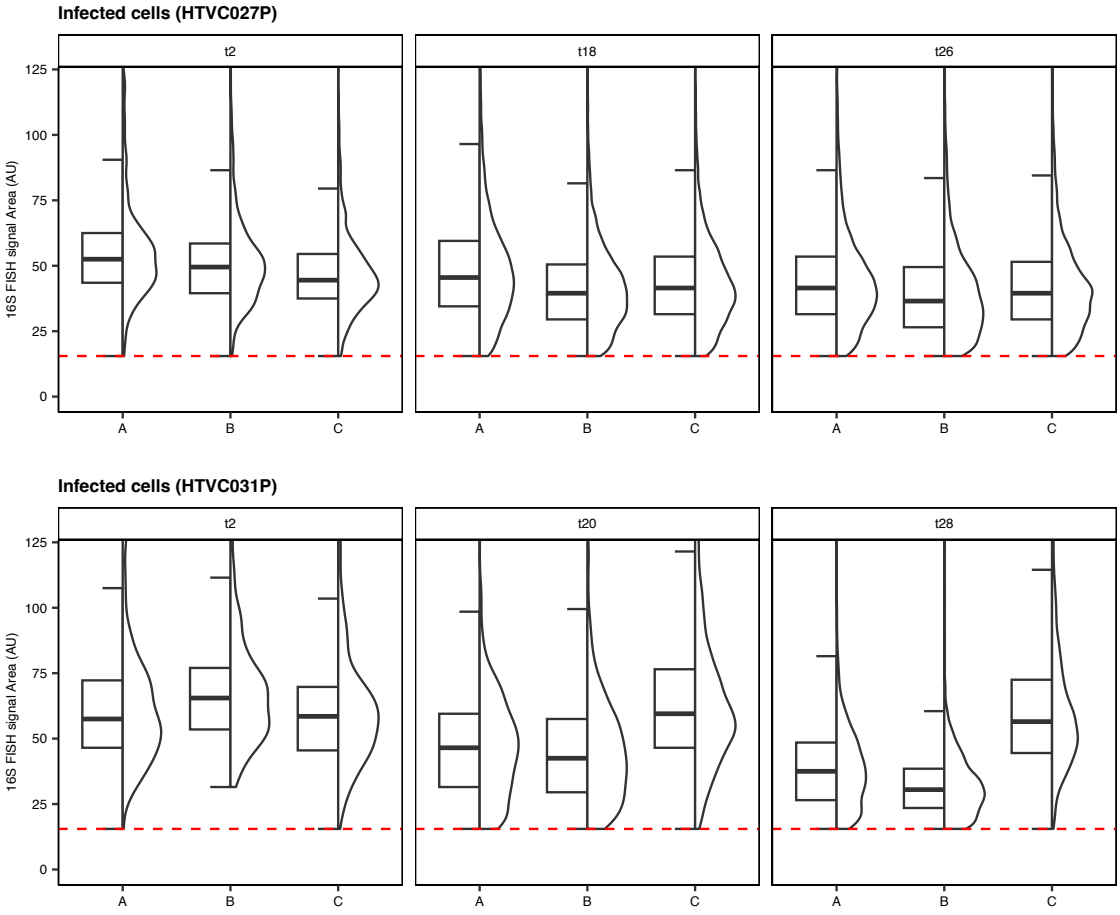

Supplementary Figure S3.7: 16S FISH fluorescence intensity of phage-infected SAR11 cells from infection experiments. Boxplots show median and upper and lower quartile. Whiskers show maximum data points within upper/lower quartile range plus 1.5 times the interquartile range. Outliers not shown. Violin plot show data distribution on y-Axis. Red-dashed line represents defined threshold from image analysis.

3.7.3 Supplementary Tables

Supplementary tables are available from Edmond: https://doi.org/10.17617/3.Q3HWX6.

References

Alonso-Sáez, L., X. A. G. Morán, and M. R. Clokie (2018). "Low activity of lytic pelagiphages in coastal marine waters". *The ISME Journal* 12.8, pages 2100–2102 (cited on pages 59, 62).

Amann, R. I., B. J. Binder, R. J. Olson, S. W. Chisholm, R. Devereux, and D. Stahl (1990). "Combination of 16S rRNA-targeted oligonucleotide probes with flow cytometry for analyzing mixed microbial populations". *Applied and Environmental Microbiology* 56.6, pages 1919–1925 (cited on page 64).

Barrero-Canosa, J., C. Moraru, L. Zeugner, B. M. Fuchs, and R. Amann (2017). "Direct-geneFISH: a simplified protocol for the simultaneous detection and quantification of genes and rRNA in microorganisms". *Environmental Microbiology* 19.1, pages 70–82 (cited on page 69).

Bennke, C. M., G. Reintjes, M. Schattenhofer, A. Ellrott, J. Wulf, M. Zeder, and B. M. Fuchs (2016). "Modification of a high-throughput automatic microbial cell enumeration system for shipboard analyses". *Applied and Environmental Microbiology* 82.11, pages 3289–3296 (cited on page 70).

Breitbart, M., C. Bonnain, K. Malki, and N. A. Sawaya (2018). "Phage puppet masters of the marine microbial realm". *Nature Microbiology* 3.7, pages 754–766 (cited on pages 65, 66).

Brüwer, J. D., L. H. Orellana, C. Sidhu, H. C. Klip, C. L. Meunier, M. Boersma, K. H. Wiltshire, R. Amann, and B. M. Fuchs (2023). "*In situ* cell division and mortality rates of SAR11, SAR86, *Bacteroidetes*, and *Aurantivirga* during phytoplankton blooms reveal differences in population controls". *mSystems*, e01287–22 (cited on pages 59–62, 65, 66, 68, 70).

Buchholz, H. H., L. M. Bolaños, A. G. Bell, M. L. Michelsen, M. J. Allen, and B. Temperton (2023). "Novel pelagiphage isolate *Polarivirus skadi* is a polar specialist that dominates SAR11-associated bacteriophage communities at high latitudes". *The ISME Journal*, pages 1–11 (cited on page 60).

Buchholz, H. H., M. L. Michelsen, L. M. Bolaños, E. Browne, M. J. Allen, and B. Temperton (2021). "Efficient dilution-to-extinction isolation of novel virus–host model systems for fastidious heterotrophic bacteria". *The ISME Journal* 15.6, pages 1585–1598 (cited on pages 59, 60, 63, 72).

Bürkner, P.-C. (2017). "Advanced Bayesian multilevel modeling with the R package brms". *arXiv preprint arXiv:1705.11123* (cited on page 73).

Camacho, C., G. Coulouris, V. Avagyan, N. Ma, J. Papadopoulos, K. Bealer, and T. L. Madden (2009). "BLAST+: architecture and applications". *BMC Bioinformatics* 10, pages 1–9 (cited on page 72).

Carini, P., L. Steindler, S. Beszteri, and S. J. Giovannoni (2013). "Nutrient requirements for growth of the extreme oligotroph '*Candidatus* Pelagibacter ubique' HTCC1062 on a defined medium". *The ISME Journal* 7.3, pages 592–602 (cited on page 68).

Chaumeil, P.-A., A. J. Mussig, P. Hugenholtz, and D. H. Parks (2020). "GTDB-Tk: a toolkit to classify genomes with the Genome Taxonomy Database". *Bioinformatics* 36.6, pages 1925–1927 (cited on page 70).

Daims, H., A. Brühl, R. Amann, K.-H. Schleifer, and M. Wagner (1999). "The domain-specific probe EUB338 is insufficient for the detection of all Bacteria: development and evaluation of a more comprehensive probe set". *Systematic and Applied Microbiology* 22.3, pages 434–444 (cited on page 64).

Ducret, A., E. M. Quardokus, and Y. V. Brun (2016). "MicrobeJ, a tool for high throughput bacterial cell detection and quantitative analysis". *Nature Microbiology* 1.7, pages 1–7 (cited on page 70).

Eggleston, E. M. and I. Hewson (2016). "Abundance of two *Pelagibacter ubique* bacteriophage genotypes along a latitudinal transect in the North and South Atlantic Oceans". *Frontiers in Microbiology* 7, page 1534 (cited on pages 59, 65).

Fernández-García, L., J. Kirigo, D. Huelgas-Mendez, M. Tomas, R. Garcia-Contreras, and T. K. Wood (2023). "Phages Produce Persisters". *bioRxiv*, page 2023.10. 17.562728 (cited on page 66).

Fernández-García, L. and T. K. Wood (2023). "Phage-Defense Systems Are Unlikely to Cause Cell Suicide". *Viruses* 15.9, page 1795 (cited on page 66).

Fuchs, B. M., J. Pernthaler, and R. Amann (2007). "Single cell identification by fluorescence *in situ* hybridization". *Methods for General and Molecular Microbiology*, pages 886–896 (cited on page 69).

Gabry, J. and R. Češnovar (2022). "cmdstanr: R Interface to'CmdStan'". *URL: https://mc-stan.org/cmdstanr, https://discourse. mc-stan. org* (cited on page 73).

Georjon, H. and A. Bernheim (2023). "The highly diverse antiphage defence systems of bacteria". *Nature Reviews Microbiology* 21.10, pages 686–700 (cited on page 66).

Giovannoni, S., B. Temperton, and Y. Zhao (2013). "Giovannoni et al. reply". *Nature* 499.7459, E4–E5 (cited on page 59).

Giovannoni, S. J. (2017). "SAR11 bacteria: the most abundant plankton in the oceans". *Annual Review of Marine Science* 9, pages 231–255 (cited on pages 59, 67).

Grolemund, G. and H. Wickham (2011). "Dates and times made easy with lubridate". *Journal of Statistical Software* 40.3, pages 1–25 (cited on page 73).

Hajam, I. A., P. A. Dar, G. Won, and J. H. Lee (2017). "Bacterial ghosts as adjuvants: mechanisms and potential". *Veterinary Research* 48.1, pages 1–13 (cited on page 61).

Ignacio-Espinoza, J. C., N. A. Ahlgren, and J. A. Fuhrman (2020). “Long-term stability and Red Queen-like strain dynamics in marine viruses”. *Nature Microbiology* 5.2, pages 265–271 (cited on page 65).

Kassambara, A. and M. A. Kassambara (2020). *ggpubr: 'ggplot2' Based Publication Ready Plots*. Journal Article (cited on page 73).

Katoh, K. and D. M. Standley (2013). “MAFFT multiple sequence alignment software version 7: improvements in performance and usability”. *Molecular Biology and Evolution* 30.4, pages 772–780 (cited on page 73).

Kay, M. (2023). “tidybayes: Tidy data and geoms for Bayesian models”. *R package version* 2.1, page 1 (cited on page 73).

Kearse, M., R. Moir, A. Wilson, S. Stones-Havas, M. Cheung, S. Sturrock, S. Buxton, A. Cooper, S. Markowitz, and C. Duran (2012). “Geneious Basic: an integrated and extendable desktop software platform for the organization and analysis of sequence data”. *Bioinformatics* 28.12, pages 1647–1649 (cited on pages 69, 73).

Kieft, K., Z. Zhou, and K. Anantharaman (2020). “VIBRANT: automated recovery, annotation and curation of microbial viruses, and evaluation of viral community function from genomic sequences”. *Microbiome* 8.1, pages 1–23 (cited on page 72).

Klaas, C. (2023). “The Expedition PS133/1 of the Research Vessel Polarstern to the Atlantic Ocean in 2022”. *Berichte zur Polar-und Meeresforschung: Reports on polar and marine research* 774 (cited on pages 64, 68).

Kolmogorov, M., J. Yuan, Y. Lin, and P. A. Pevzner (2019). “Assembly of long, error-prone reads using repeat graphs”. *Nature Biotechnology* 37.5, pages 540–546 (cited on page 72).

Lawrence, M. A. and M. M. A. Lawrence (2016). “Package ‘ez’”. *R package version* 4.0 (cited on page 73).

Li, H. (2018). “Minimap2: pairwise alignment for nucleotide sequences”. *Bioinformatics* 34.18, pages 3094–3100 (cited on page 70).

Loenen, W. A. and E. A. Raleigh (2014). “The other face of restriction: modification-dependent enzymes”. *Nucleic Acids Research* 42.1, pages 56–69 (cited on page 67).

Martinez-Hernandez, F., O. Fornas, M. Lluesma Gomez, B. Bolduc, M. J. De la Cruz Peña, J. M. Martínez, J. Anton, J. M. Gasol, R. Rosselli, and F. Rodriguez-Valera (2017). “Single-virus genomics reveals hidden cosmopolitan and abundant viruses”. *Nature Communications* 8.1, page 15892 (cited on page 59).

Martinez-Hernandez, F., O. Fornas, M. Lluesma Gomez, I. Garcia-Heredia, L. Maestre-Carballa, M. López-Pérez, J. M. Haro-Moreno, F. Rodriguez-Valera, and M. Martinez-Garcia (2019). “Single-cell genomics uncover Pelagibacter as the putative host of the extremely abundant uncultured 37-F6 viral population in the ocean”. *The ISME Journal* 13.1, pages 232–236 (cited on pages 59, 60).

Nishimura, Y., T. Yoshida, M. Kuronishi, H. Uehara, H. Ogata, and S. Goto (2017). "ViPTree: the viral proteomic tree server". *Bioinformatics* 33.15, pages 2379–2380 (cited on page 72).

O'Leary, N. A., M. W. Wright, J. R. Brister, S. Ciufo, D. Haddad, R. McVeigh, B. Rajput, B. Robbertse, B. Smith-White, and D. Ako-Adjei (2016). "Reference sequence (RefSeq) database at NCBI: current status, taxonomic expansion, and functional annotation". *Nucleic Acids Research* 44.D1, pages D733–D745 (cited on pages 71, 72).

R Core Team, R. (2022). *R: A language and environment for statistical computing*. Journal Article. R Foundation for Statistical Computing. Vienna, Austria (cited on pages 71, 73).

Ram, K. and H. Wickham (2018). "wesanderson: A Wes Anderson palette generator". *R package version 0.3* 6 (cited on page 73).

Reintjes, G., H. E. Tegetmeyer, M. Bürgisser, S. Orlić, I. Tews, M. Zubkov, D. Voß, O. Zielinski, C. Quast, and F. O. Glöckner (2019). "On-site analysis of bacterial communities of the ultra-oligotrophic South Pacific Gyre". *Applied and Environmental Microbiology* 85.14, e00184–19 (cited on page 68).

Sánchez, O., I. Ferrera, I. Mabrito, C. R. Gazulla, M. Sebastián, A. Auladell, C. Marín-Vindas, C. Cardelós, I. Sanz-Sáez, and M. C. Pernice (2020). "Seasonal impact of grazing, viral mortality, resource availability and light on the group-specific growth rates of coastal Mediterranean bacterioplankton". *Scientific Reports* 10.1, page 19773 (cited on page 62).

Schindelin, J., I. Arganda-Carreras, E. Frise, V. Kaynig, M. Longair, T. Pietzsch, S. Preibisch, C. Rueden, S. Saalfeld, and B. Schmid (2012). "Fiji: an open-source platform for biological-image analysis". *Nature Methods* 9.7, pages 676–682 (cited on page 70).

Shaffer, M., M. A. Borton, B. B. McGivern, A. A. Zayed, S. L. La Rosa, L. M. Solden, P. Liu, A. B. Narrowe, J. Rodríguez-Ramos, and B. Bolduc (2020). "DRAM for distilling microbial metabolism to automate the curation of microbiome function". *Nucleic Acids Research* 48.16, pages 8883–8900 (cited on page 72).

Sidhu, C., I. V. Kirstein, C. L. Meunier, J. Rick, V. Fofonova, K. H. Wiltshire, N. Steinke, S. Vidal-Melgosa, J.-H. Hehemann, and B. Huettel (2023). "Dissolved storage glycans shaped the community composition of abundant bacterioplankton clades during a North Sea spring phytoplankton bloom". *Microbiome* 11.1, pages 1–18 (cited on pages 60, 62, 63, 65, 69–72).

Sullivan, M. B., M. L. Coleman, P. Weigele, F. Rohwer, and S. W. Chisholm (2005). "Three *Prochlorococcus* cyanophage genomes: signature features and ecological interpretations". *PLoS Biology* 3.5, e144 (cited on page 66).

Suttle, C. A. (2007). "Marine viruses—major players in the global ecosystem". *Nature Reviews Microbiology* 5.10, pages 801–812 (cited on page 59).

Tamames, J. and F. Puente-Sánchez (2019). "SqueezeMeta, a highly portable, fully automatic metagenomic analysis pipeline". *Frontiers in Microbiology* 9, page 3349 (cited on page 70).

Teeling, H., B. M. Fuchs, D. Becher, C. Klockow, A. Gardebrecht, C. M. Bennke, M. Kassabgy, S. Huang, A. J. Mann, and J. Waldmann (2012). "Substrate-controlled succession of marine bac-

terioplankton populations induced by a phytoplankton bloom". *Science* 336.6081, pages 608–611 (cited on page 60).

Tesson, F., A. Hervé, E. Mordret, M. Touchon, C. d'Humières, J. Cury, and A. Bernheim (2022). "Systematic and quantitative view of the antiviral arsenal of prokaryotes". *Nature Communications* 13.1, page 2561 (cited on page 71).

Thingstad, T. F. and R. Lignell (1997). "Theoretical models for the control of bacterial growth rate, abundance, diversity and carbon demand". *Aquatic Microbial Ecology* 13.1, pages 19–27 (cited on page 65).

Thingstad, T. F., S. Våge, J. E. Storesund, R.-A. Sandaa, and J. Giske (2014). "A theoretical analysis of how strain-specific viruses can control microbial species diversity". *Proceedings of the National Academy of Sciences* 111.21, pages 7813–7818 (cited on page 65).

Thompson, L. R., Q. Zeng, L. Kelly, K. H. Huang, A. U. Singer, J. Stubbe, and S. W. Chisholm (2011). "Phage auxiliary metabolic genes and the redirection of cyanobacterial host carbon metabolism". *Proceedings of the National Academy of Sciences* 108.39, E757–E764 (cited on page 67).

Våge, S., J. E. Storesund, and T. F. Thingstad (2013). "SAR11 viruses and defensive host strains". *Nature* 499.7459, E3–E4 (cited on page 59).

Wickham, H., D. Vaughan, and M. Girlich (2023). "tidyr: Tidy Messy Data". *tidyr: Tidy Messy Data* (cited on page 73).

Wickham, H. (2011a). *ggplot2*. Volume 3. Wiley Interdisciplinary Reviews: Computational Statistics. Springer-Verlag New York, pages 180–185 (cited on page 73).

Wickham, H. (2011b). "The split-apply-combine strategy for data analysis". *Journal of Statistical Software* 40.1, pages 1–29 (cited on page 73).

Wilke, C. (2020). *cowplot: streamlined plot theme and plot annotations for 'ggplot2'. R package version 1.1. 1*. Journal Article (cited on page 73).

Wiltshire, K. H. and A. Dummermuth (2023). "The Expedition PS132 of the Research Vessel POLARSTERN to the Atlantic Ocean in 2022". *Berichte zur Polar- und Meeresforschung = Reports on polar and marine research*, page 46 (cited on pages 64, 68).

Wittmers, F., D. M. Needham, E. Hehenberger, S. J. Giovannoni, and A. Z. Worden (2022). "Genomes from uncultivated pelagiphages reveal multiple phylogenetic clades exhibiting extensive auxiliary metabolic genes and cross-family multigene transfers". *mSystems* 7.5, e01522–21 (cited on page 59).

Yang, H., Y. Ma, Y. Wang, H. Yang, W. Shen, and X. Chen (2014). "Transcription regulation mechanisms of bacteriophages: recent advances and future prospects". *Bioengineered* 5.5, pages 300–304 (cited on page 67).

Zeder, M., A. Ellrott, and R. Amann (2011). "Automated sample area definition for high-throughput microscopy". *Cytometry Part A* 79.4, pages 306–310 (cited on page 70).

Zeugner, L. E., K. Krüger, J. Barrero-Canosa, R. I. Amann, and B. M. Fuchs (2021). "In situ visualization of glycoside hydrolase family 92 genes in marine flavobacteria". *ISME Communications* 1.1, page 81 (cited on page 69).

Zhang, Z., F. Qin, F. Chen, X. Chu, H. Luo, R. Zhang, S. Du, Z. Tian, and Y. Zhao (2021). "Culturing novel and abundant pelagiphages in the ocean". *Environmental Microbiology* 23.2, pages 1145–1161 (cited on pages 59, 60, 63, 72).

Zhao, X., C. L. Schwartz, J. Pierson, S. J. Giovannoni, J. R. McIntosh, and D. Nicastro (2017). "Three-dimensional structure of the ultraoligotrophic marine bacterium "*Candidatus* Pelagibacter ubique"". *Applied and Environmental Microbiology* 83.3, e02807–16 (cited on page 67).

Zhao, Y., F. Qin, R. Zhang, S. J. Giovannoni, Z. Zhang, J. Sun, S. Du, and C. Rensing (2019). "Pelagiphages in the *Podoviridae* family integrate into host genomes". *Environmental Microbiology* 21.6, pages 1989–2001 (cited on pages 59, 60, 72).

Zhao, Y., B. Temperton, J. C. Thrash, M. S. Schwalbach, K. L. Vergin, Z. C. Landry, M. Ellisman, T. Deerinck, M. B. Sullivan, and S. J. Giovannoni (2013). "Abundant SAR11 viruses in the ocean". *Nature* 494.7437, pages 357–360 (cited on pages 59, 65).

Zhong, K. X., J. F. Wirth, A. M. Chan, and C. A. Suttle (2023). "Mortality by ribosomal sequencing (MoRS) provides a window into taxon-specific cell lysis". *The ISME Journal* 17.1, pages 105–116 (cited on pages 59, 62).

Zhou, J., M. A. Bruns, and J. M. Tiedje (1996). "DNA recovery from soils of diverse composition". *Applied and Environmental Microbiology* 62.2, pages 316–322 (cited on page 72).

Zielinski, O., R. Henkel, D. Voß, and T. Ferdelman (2018). *Physical oceanography during SONNE cruise SO245 (UltraPac)*. data set. Institute for Chemistry and Biology of the Marine Environment, Carl-von-Ossietzky University of Oldenburg, Germany (cited on pages 64, 68).

Zweifel, U. L. and A. Hagstrom (1995). "Total counts of marine bacteria include a large fraction of non-nucleoid-containing bacteria (ghosts)". *Applied and Environmental Microbiology* 61.6, pages 2180–2185 (cited on page 61).

4

RESILIENCE AND RESPONSE OF MARINE MICROBES TO A SHORT-TERM MARINE HEATWAVE AND THE FUTURE OCEAN – INSIGHTS FROM MESOCOSM EXPERIMENTS

Jan D. Brüwer[1], Micah Reismann[1], Antje Wichels[2], Uwe John[2], Josefin Schmidt[2], Cédric L. Meunier[2], Inga Kirstein[2], Bernhard M. Fuchs[1*]

[1]Max Planck Institute for Marine Microbiology, Bremen, Germany

[2]Alfred-Wegener-Institut, Helmholtz-Zentrum für Polar- und Meeresforschung, Biologische Anstalt Helgoland, Helgoland, Germany

[*]Corresponding author.

In preparation.

Contributions

Experimental concept and design: 20%
Acquisition of experimental data: 20%
Preparation of figures and tables: 100%
Drafting of the manuscript: 100%

4.1 Abstract

Anthropogenic influences shape the future ocean. Sea surface temperature and CO_2 concentrations will increase alongside more frequent extreme weather events. Previous research suggests a shift within the phytoplankton community in future ocean scenarios. However, the effects on the microbial community and the combined influence of marine heatwaves are less well-studied. Here, we simulated future ocean scenarios (1000 ppm CO_2, +3 °C, Nitrogen:Phosphate ratio of 25) in combination with a mild marine heatwave (+2 °C for 5 d) in mesocosms, and studied the effect on the microbial food web. A control (ambient conditions), which was also exposed to the heatwave conditions, was included. We used fluorescence *in situ* hybridization and high-throughput microscopy to analyze the responses of key microbial taxa (SAR11, *Bacteroidota*, and *Gammaproteobacteria*). With a focus on the ambient mesocosms, we studied the effect of the heatwave on cell division and grazing rates, as well as virus-like particle abundances. Our results suggest a bottom-up driven effect of the future ocean scenarios on total cell counts, while taxon-specific responses were negligible. The marine heatwave had no noticeable effect on the microbial community. Overall, our findings underscore the stability and adaptability of marine microbial communities in the face of anthropogenic-driven ocean changes.

4.2 Introduction

Anthropogenic activities and the resultant global climate change are shaping the future ocean. The Representative Concentration Pathways (RCP) 8.5 scenario projects CO_2 concentrations to reach 1000 ppm by 2100, with a resultant pH decrease of 0.3 units (Pörtner et al. 2022). The ocean has already absorbed about a quarter of total anthropogenic CO_2 emissions (DeVries et al. 2017) and approximately 90% of heat associated with climate change (Cheng et al. 2017; Gattuso et al. 2015), which leads to increased sea-surface temperatures. Furthermore, the frequency and severity of extreme weather events, such as marine heatwaves, are anticipated to increase globally (Lee et al. 2023a). Especially in coastal regions, heatwaves will occur more often, as these regions warm faster than the global average (Amorim et al. 2023). Marine heatwaves are defined as events lasting five days or longer with elevated sea surface temperature exceeding the 90^{th} percentile of a 30-year average seasonal climatology (Hobday et al. 2016). Despite their increasing impact and importance, the effects of marine heatwaves on microbial communities remain largely unknown.

Phytoplankton are the basis of the marine food web, as they fix inorganic CO_2 into organic matter. They are impacted by the projected anthropogenic influences. For example, warming leads to a community shift within the phytoplankton community, favoring smaller species like picophytoplankton and nanophytoplankton (Gao et al. 2018; Moreno et al. 2022). Additionally, ocean acidification may enhance photosynthesis and biomass production (Gattuso et al. 2013; Moreno et al. 2022), including carbon-rich biomass such as transparent exopolymer particles

(Gao et al. 2018). When phytoplankton-derived organic matter is released into the environment, it fuels heterotrophic bacteria (Buchan et al. 2014).

In contrast to the phytoplankton community, the microbial community appears resilient to ocean acidification or altered CO_2 concentrations. Mesocosm studies in the Baltic-Sea (Bergen et al. 2016), the coast of Portugal (Barbosa et al. 2023), and New Zealand (Deans 2022) indicate that increased CO_2 concentrations have no significant impact on microbial cell abundances or community composition, while Endres et al. (2014) observed higher microbial abundances with higher CO_2 concentrations. On the other hand, increased temperatures should induce faster growth rates in the microbial community (Barbosa et al. 2023; Berner et al. 2018; Hutchins and Fu 2017). In general, the thermal optimum of heterotrophic bacteria is usually higher than the average *in situ* temperatures, though this difference varies between seasons (Joint and Smale 2017). Joint and Smale (2017) studied the differences between the thermal optimum of microbes and *in situ* temperatures in the English Channel. They found ca. 3 °C difference in summer and ca. 20 °C. Thus, the effect of a heatwave, as described above, depends on the affected season. Taxon-specific effects of temperature vary, with distinct influences reported in different regions. Generally speaking, higher temperatures are suggested to favor smaller cells, such as SAR11 (*Alphaproteobacteria*; Hutchins and Fu 2017). Correspondingly, a mesocosm study from the Mediterranean Sea reported higher abundances of SAR11 in warmer waters (Tsiola et al. 2023). In contrast, in the Baltic Sea, *Bacteroidota* benefit from warmer temperatures, whereas *Alphaproteobacteria* (mainly SAR11) and *Gammaproteobacteria* benefit from colder conditions (Bergen et al. 2016).

In general, SAR11 bacteria are considered slow-growing oligotrophs (Giovannoni 2017), although their fast growth rates during phytoplankton blooms have recently been shown (Brüwer et al. 2023). *Bacteroidota* are known to comprise many fast-growing copiotrophic bacteria, which are known to increase quickly in cell abundances during substrate pulses, such as phytoplankton blooms (Arandia-Gorostidi et al. 2017; Buchan et al. 2014; Kappelmann et al. 2019). The phylum of *Gammaproteobacteria* comprises a mixture of different growth strategies. For example, SAR86 are considered oligotrophs (Dupont et al. 2012), while many species of the genus *Vibrio* have a copiotrophic lifestyle (Lauro et al. 2009).

Viruses that infect bacteria are termed phages and are a main mortality factor of bacteria. It is estimated that ∼25% of phytoplankton-fixed carbon is cycled through phages (Breitbart et al. 2018). Nevertheless, the effects of anthropogenic influences on the viral community are less well explored. It is anticipated that grazing and virus-induced lysis will respond similarly to bacteria under altered environmental conditions (Hutchins and Fu 2017; Sarmento et al. 2010), with increased temperatures potentially leading to elevated rates of viral lysis and grazing (Hutchins and Fu 2017; Lara et al. 2013). Besides phage-induced lysis, grazing by flagellates is the second main mortality factor of bacteria in the sea. Similarly, little is known about the effects of anthropogenic influences or a marine heatwave on grazing of the microbial community.

Here, we conducted integrated multiple driver mesocosm experiments to understand the effect of a future ocean scenario in combination with a marine heatwave on the microbial community and their mortality factors. Our four treatment conditions included a future ocean scenario according to RCP 8.5, extended with an altered N:P ratio (1000 ppm pCO_2, +3 °C, N:P ratio 25) and a control, as well as both scenarios with an additional +2 °C marine heatwave lasting for five days. Employing fluorescence *in situ* hybridization (FISH) and high-throughput microscopy, we examined taxon-specific responses of the microbial community, focusing on SAR11, *Bacteroidota*, and *Gammaproteobacteria*. Additionally, we investigated the effects of a marine heatwave in the ambient conditions on taxon-specific cell division and grazing rates, as well as the abundances of virus-like particles as a major factor influencing bacterial mortality. Our study aims to contribute a more comprehensive understanding of the multifaceted impacts of climate change and extreme weather events on the marine microbial community.

4.3 Material and Methods

4.3.1 Mesocosm set-up

To assess the impact of heatwaves on ambient and future ocean scenarios, a multiple-driver experiment was conducted using a total of 16 mesocosms. The mesocosm design and set-up are described in Meunier et al. (in prep). Briefly, mesocosms were exposed to four scenarios with four replicates each. The scenarios contained ambient "AMB" conditions (ambient temperature, pH, pCO_2, N:P ratio 16) or a future ocean scenario "ERCP" based on the RCP 8.5 scenario developed by the IPCC for the year 2100, extended with an additional adjusted nitrogen to phosphorous (N:P) ratio (+3.0 °C, −0.3 pH, pCO_2=1000 ppm, N:P ratio 25). Additionally, each treatment was exposed to a moderate heatwave of +2 °C for 5 days ("AHW", "ERHW") or not ("AMB", "ERCP") starting on day 11. Before and after the heatwaves, the temperatures were adjusted stepwise by +1 °C d^{-1} for 2 days to reach the heatwave or ambient temperatures, respectively.

The mesocosms were located at the Wadden Sea Station, Alfred-Wegener Institute for Polar and Marine Research, Germany. They were filled with 100 µm-filtered seawater from the Sylt Roads Station 1 (55°1'48" N, 8°27'36" E) and were incubated between September 1 and September 27, 2021. Each mesocosm (1800 L) contained an LDPE transparent bag (520 L) comprising the experimental water mass. The surrounding water was used for temperature regulation. The mesocosms were covered with an HDPE translucent lid, allowing 90% of photosynthetically active radiation to pass through. Additionally, it allowed to change the atmospheric pCO_2 above the mesocosm to adjust the pCO_2 in the future ocean scenarios. Mesocosms were mixed with a custom-build propeller attached to a mortar mixer (TC-MX 1400-2 E, Einhell Germany AG, Landau/Isar, Germany) with a 1-minute-mixing/30-minutes-pause interval.

4.3.2 Measurements throughout the experiment

Abiotic parameters, including temperature, pH, total alkalinity, dissolved nitrogen, and particulate carbon, nitrogen, and phosphate, were measured daily and are reported elsewhere (Meunier et al. in prep). To assess phytoplankton abundances, we determined chlorophyll a concentrations daily using spectral fluorometry at a fluorescence of 685 nm (AlgaeLabAnalyser, bbe Moldaenke GmbH, Schwentinental, Germany).

To study the microbial community of the mesocosm, 10 mL samples were fixed with 0.2 µm-filtered formaldehyde (1% final concentration) and immobilized on 0.2 µm polycarbonate filters (Merck Millipore, Burlington Massachusetts, US). Filters were stored at −20 °C until further processing. An aliquot of 1 mL of the 0.2 µm fixed filtrate was immobilized on a 0.02 µm aluminum oxide filter (Whatman, Maidstone, United Kingdom) to study the viral community by quantifying virus-like particle concentrations.

4.3.3 DAPI, SYBR-gold, and fluorescence *in situ* hybridization (FISH) staining to count microbes and virus-like particles

To determine total cell counts, a sample of the 0.2 µm polycarbonate filters was embedded in the anti-bleaching agent Citifluor:Vectashield (Citifluor Ltd, London, UK; Vector Laboratories, Burlingame, CA, USA), containing 1 µg mL^{-1} 4',6-diamidino-2-phenylindole (DAPI). To determine virus-like particle counts, 0.02 µm aluminum oxide filters were cut into quarters. Each quarter was embedded in 0.2 µm-filtered 1:1 (vol:vol) PBS:glycerol, containing 0.01% (wt/vol; final concentration) p-phenylendiamine and 10x SYBR-gold (final concentration, Invitrogen, Waltham, Massachusetts, United Kingdom).

We used catalyzed reporter deposition-fluorescence *in situ* hybridization (CARD-FISH) to visualize and count individual taxonomic groups (Fuchs et al. 2007). Briefly, a subsample of the 0.2 µm polycarbonate filters was first embedded in 0.1% LE agarose to prevent cell loss during sample handling. Cell walls were permeabilized using 10 mg mL^{-1} lysozyme in buffer (0.05 M EDTA, 0.1 M Tris-HCl) for 1 h at 37 °C and 60 U mL^{-1} achromopeptidase in buffer (0.01 M NaCl, 0.01 M Tris-HCl). Endogenous peroxidases were inactivated using 0.15% H_2O_2 in methanol for 15-20 min. Hybridizations were conducted in humidity chambers, containing probe-specific formamide and NaCl concentrations (see Fuchs et al. 2007 and Table 4.1). Samples were incubated in hybridization buffer (900 mM NaCl, 20 mM 20 mM Tris-HCl, 1% blocking reagent, 0.1 g L^{-1} dextran sulfate, 0.02% SDS, and varying formamide; Table 4.1) for 3 h at 47 °C and subsequently washed in washing buffer (20 mM Tris-HCl, 5 mM EDTA, 0.01% SDS, NaCl concentration depending on FA concentration) for 15 min at 48 °C. CARD signal amplification was done with 0.00015% H_2O_2 and Alexa488 labeled tyramide (Invitrogen, Waltham, Massachusetts, United Kingdom) in an amplification buffer (1x PBS, 2 M NaCl, 0.1% blocking reagent, 0.1 g mL^{-1} dextran sulfate). We used probes to target all bacteria, SAR11,

Bacteroidota, and *Gammaproteobacteria* (Table 4.1). After FISH, filters were embedded in Citifluor:Vectashield with DAPI, as described above.

4.3.4 Microscopy and image analysis

Automated microscopy images were generated on a Zeiss AxioImager.Z2m (Zeiss, Oberkochen, Germany) with a charged-coupled device (CCD) camera (Zeiss, Oberkochen, Germany) and a custom-built macro within the Zeiss AxioVision software (Bennke et al. 2016; Zeder et al. 2011). The microscope was equipped with a 63x Plan Apochromat objective (1.4 NA, oil immersion). Samples were illuminated using a Zeiss Colibri 7 LED (excitation: 385 nm for DNA and 469 nm for 16S CARD-FISH) and a Multi-Zeiss 62 HE filter cube (Beam splitter FT 395+495+610). Recorded 8-bit greyscale images were manually quality controlled and analyzed in the automated cell measuring and enumeration tool (ACME, available from https://www.mpi-bremen.de/automated-microscopy.html, Bennke et al. 2016; Zeder et al. 2011) with channel-specific settings (Table 4.3).

During the image analysis, we observed an unusual number of filamentous microbes. As automatic quantification of filaments is not trivial, they were counted manually on a Zeiss AxioImager.D2, equipped with a Zeiss Colibri 7 LED. Filaments were quantified on a subset of samples (days 1, 2, 3, 7, 9, 11, 13, 15, 19, 23, and 27).

4.3.5 DNA isolation and 16S sequencing

The prokaryotic community composition was assessed using 16S rRNA metabarcoding. Every Monday, Wednesday, and Friday throughout the sampling campaign, 500 mL sample from each mesocosm was sieved over a 150 µm nylon mesh, subsequently filtered through 3 µm and 0.2 µm polycarbonate filters (47 mm diameter, Millipore, USA), and stored at −20 °C until further processing. DNA was extracted using the NucleoSpin Soil extraction kit (Macherey-Nagel, Düren, Germany), according to the manufacturer's instructions. For the lysis of the cells, an additional bead beating step was included (MagNA Lyser, Roche, Switzerland). After DNA extraction, 5 ng μL^{-1} (final concentration) DNA was used for PCR amplification and library construction, according to Illumina's 16S rRNA gene metabarcoding sequencing library preparation guide[1], with modifications for 16S rRNA gene amplicons preparation. The V4 region of the 16S rRNA gene was amplified using the forward MS_V4_515F_N (Parada et al. 2016) and reverse MS_V4_806R_1 (Apprill et al. 2015) primer (each 0.2 µM final concentration) and the 2x KAPA HiFi HotStart ReadyMix (KAPABiosystems, Boston, USA). The PCR program included an initial denaturation at 95 °C for 3 min, followed by 25 cycles of denaturation at 95 °C for 30 s, annealing at 55 °C for 30 s, extension at 72 °C for 30 s, and a final extension at 72 °C for 5 min. PCR

[1] https://support.illumina.com/downloads/16s_metagenomic_sequencing_library_preparation.html, doc.no 15044223B

products were cleaned with AMPure XP beads (BeckmanCoulter Life Sciences, Indianapolis, US), validated using the 2100 Bioanalyzer (Agilent), and pooled in equimolar concentrations. Amplicon libraries were sequenced on a MiSeq sequencer at the Alfred-Wegener-Institute, Bremerhaven, Germany, using the MiSeq Reagent Kit v3 (600-cycle) MS-102-3003. Retained sequences were trimmed with CUTADAPT 2.8 (Martin 2011). The DADA2 pipeline (Callahan et al. 2016) was used for quality control and defining amplicon sequence variants (ASVs). The taxonomical assignation was done against the SILVA Reference Database.

4.3.6 Dilution grazing experiments

We conducted four dilution experiments (day 6, 13, 20, and 27) in the AMB and AHW treatments to determine cell division and grazing rates of the prokaryotic community after Landry and Hasset (1982). To exclude mesozooplankton and larger grazers, samples were sieved (200 µm) before dilution with 0.2 µm sterile-filtered seawater. Dilution series of 100% (undiluted), 50%, 30%, and 15% were prepared in 1 L cell culture flasks (Greiner, Kremsmünster, Austria). No nutrients were added. Samples from the general sampling scheme served as a reference (t_0) for the experiments. We prepared one dilution series per mesocosm replicate (in total 8, for 2 treatments with 4 replicate each).

The flasks were placed on a plankton wheel (∼1.2 rpm) to prevent sedimentation of the planktonic organisms and incubated with a day-to-night regime of 16-to-18 h (20–30 µmol photons m^{-2} s^{-1}) for 24 h in a temperature-controlled room set at the *in situ* sea surface temperature of the corresponding day. After the incubation, samples were fixed and filtered as described above.

4.3.7 Statistical analysis and visualizations

Statistical analysis and visualizations were conducted in R (v4.2.2) with the packages ggplot2 (v3.4.2; Wickham 2011), mgcv (v1.8.42, 2011), cowplot (v1.1.1, Wilke 2020), and dplyr (v1.1.2, 2023). We tested the influence of the heatwave and future ocean scenarios using generalized additive models (GAM) on the following parameters: chlorophyll a concentration, total cell counts, relative FISH abundances (for each FISH probe individually), virus-like particle counts, cell division and grazing rates, and the amount of counted filaments (*response variable* below). In each case, the GAM was tested with the formula $response\ variable \sim s(Day\ of\ experiment,\ by = ERCP) + s(Day\ of\ experiment,\ by = Heatwave) + Heatwave + ERCP$, where $Heatwave$ and $ERCP$ were categorical ("yes" or "no") and the smoothing term $Day\ of\ experiment$ was provided in days. Simpler models with only one explanatory variable were computed and models were compared using the Akaike information criterion (AIC). Models with the lowest AIC were chosen. The effect of a particular treatment was tested using analysis of variance (ANOVA). Test results of the parametric terms are reported in this manuscript. In all cases, the smoothing terms

were $p<0.05$, indicating a significant contribution of explaining the variability in the response variable.

4.4 Results

4.4.1 Phytoplankton responds to future ocean scenario with little effect of heatwave treatments

Chlorophyll a concentrations, as a proxy for phytoplankton abundance, increased across all treatments from 3.4 $\pm$0.4 µg L^{-1} (mean $\pm$sd) to 21.3 $\pm$4.3 µg L^{-1} within the first five days of the experiment (Fig. 4.1). Subsequently, concentrations decreased more or less gradually to starting concentrations until day 18 and 15 for the ambient (AMB + AHW) and future ocean (ERCP + ERHW) scenarios, respectively. Notably, the ambient treatments (AMB + AHW) showed another fluctuation in chlorophyll a concentrations between days 7 and 9, just preceding the onset of the heatwave. A second minor phytoplankton bloom was observed in the future ocean (ERCP + ERHW) treatments after 2 weeks and in the ambient treatments after 3 weeks. The ERCP treatment exerted a pronounced and statistically significant impact on chlorophyll a concentrations (GAM, $F(1)=73.863$, $p<0.001$). The additional heatwave treatments (AHW and ERHW) also had a significant impact on chlorophyll a concentrations (GAM, $F(1)=6.041$, $p=0.014$), with the primary influence observed during the final two days of the experiment. Collectively, the applied GAM models explained 80.4% of the deviance.

4.4.2 Future ocean scenarios shape total cell counts, while the marine heatwave has no effect

We measured total DAPI-stained cell counts, using fluorescence microscopy. Total cell counts of the ambient (AMB + AHW) and future ocean (ERCP + ERHW) treatments developed very differently from each other throughout the mesocosm experiments, necessitating separate descriptions. In fact, statistical analysis revealed significant differences in total cell counts between ambient and future ocean treatments (GAM, $F(1)=21.11$, $p<0.001$), underscoring an impact of the experimental conditions on the microbial population. Conversely, the application of a heatwave treatment did not yield any discernible effect (GAM, $F(1)=$, 0.53, $p=0.467$), suggesting a resilience of microbial abundance to the short-term moderate heatwave. The GAM model explained 79.8% of the deviance between predicted and observed values. Notably, as the experiments progressed, discrepancies between replicates of the same treatments became more pronounced after approximately three weeks, evident in the larger error bars depicted in Fig. 4.1C. These variations signify uncontrolled differences, diminishing the informative value of the microbial community within the mesocosms.

In the ambient treatments (AMB + AHW), total cell counts initially decreased from 3.6

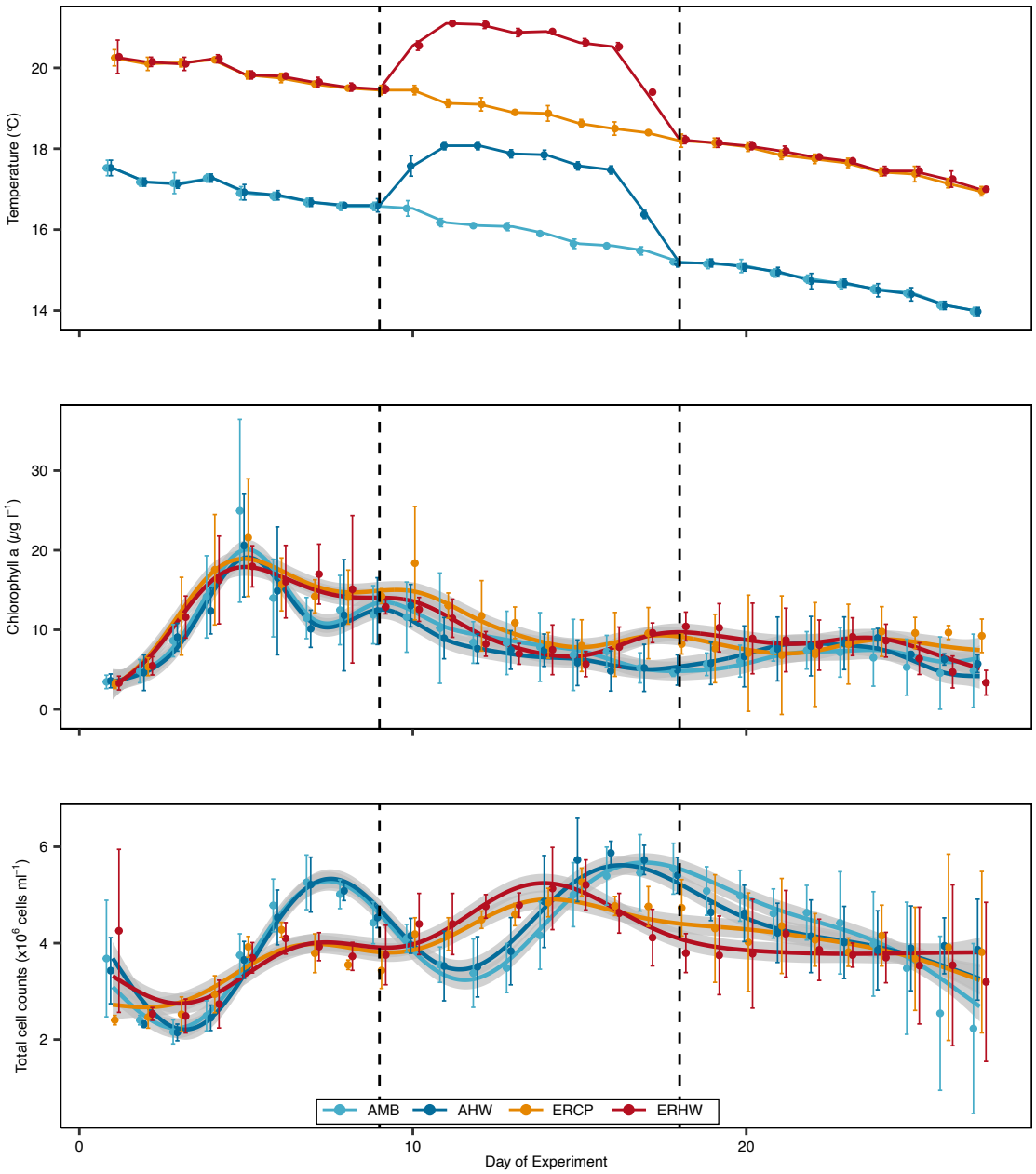

Figure 4.1: Temperature, chlorophyll a concentrations, and total cell counts during the sampling period. Dashed lines indicate beginning and end of heatwave treatment. Shown are mean and standard deviation across four replicates as dots and error bars, respectively. Colored curves are GAM models with 95% confidence intervals as ribbons. Temperature and total cell counts are based on Meunier et al. (in prep).

$\pm 0.5 \times 10^6$ cells mL^{-1} (mean $\pm$sd) to 2.1 $\pm 0.1 \times 10^6$ cells mL^{-1} within the first three days. Subsequently, the population increased to 5.2 $\pm 0.3 \times 10^6$ cells mL^{-1} (day seven), decreased to initial concentrations on day 12, increased a second time to reach 5.6 $\pm 0.3 \times 10^6$ cells mL^{-1} on day 16, and decreased thereafter. In contrast, total cell counts in the future ocean treatments (ERCP + ERHW) were more stable and fluctuated less. They increased to 4.2 $\pm 0.2 \times 10^6$ cells mL^{-1} within the first six days, declined to 3.6 $\pm 0.3 \times 10^6$ cells mL^{-1} in the following three days and increased to 5.2 $\pm 0.2 \times 10^6$ cells mL^{-1} on day 15. Subsequently, total cell counts in these

treatments declined slowly to reach starting concentrations by the end of the experiment.

4.4.3 No taxon-specific effects in response to future ocean scenarios and heatwave exposure

To further assess the influences of the future ocean scenario in combination with the applied heatwave, we estimated taxon-specific cell counts by FISH for all bacteria, SAR11, *Bacteroidota*, and *Gammaproteobacteria* (Fig. 4.2). Due to logistical constraints, a single replicate was analyzed of each treatment. In case of *Bacteroidota*, variations could be observed between AMB and AHW, within the first 9 days. It is crucial to note that the heatwave commenced on day 9, rendering AMB and AHW as replicates during this period. Consequently, caution is warranted in interpreting taxon-specific data during this timeframe. On a different note, relative abundances of SAR11 remained generally comparable between treatments but began to deviate after the third week, reinforcing the cautionary note highlighted above.

Based on the relative abundances, no differences in taxon-specific influences of the future ocean scenario, nor the heatwave treatment could be observed. Utilizing GAMs to elucidate the effects of the four treatments on the microbial community, we selected the best-fitting models based on AIC (see Methods). This led to the exclusion of the factor "heatwave" for all assessed taxa. The future ocean scenario did not exert a significant effect on all bacteria (GAM, $F(1)=2.52$, $p=0.116$) or SAR11 (GAM, $F(1)$, 0.239, $p=0.626$). Additionally, based on the AIC, we excluded the factor “future ocean scenario” for *Bacteroidota* and *Gammproteobacteria*. The GAMs explained 21.3% (all bacteria), 46.7% (SAR11), 36.8% (*Bacteroidota*), and 44.8% (*Gammaproteobacteria*) of deviance.

4.4.4 16S data reveals stable community over heatwave, small effect of future ocean scenario

We used 16S sequencing to gain a better understanding of the microbial community and its changes during the experimental setup. We here provide a brief overview, while a more detailed analysis will be included elsewhere. Over all samples and replicates, SAR11 contributed <2% of ASVs, which is in contrast to FISH-derived abundances (>20% of total cell counts). We used primers, which were optimized to detect bacteria of the SAR11 clade (Apprill et al. 2015; Parada et al. 2016). Nevertheless, the phenomenon of the under representation of SAR11 has previously been observed (Fadeev et al. 2021; Lee et al. 2023b).

Based on the 14 most abundant microbial genera (mitochondrial sequences were excluded from the top 15 genera), we could not observe any major effects of the applied heatwaves (Fig. 4.3, no statistics applied). Additionally, the microbial communities changed over time and the future ocean scenarios had little effect on the community composition (Fig. 4.3). When

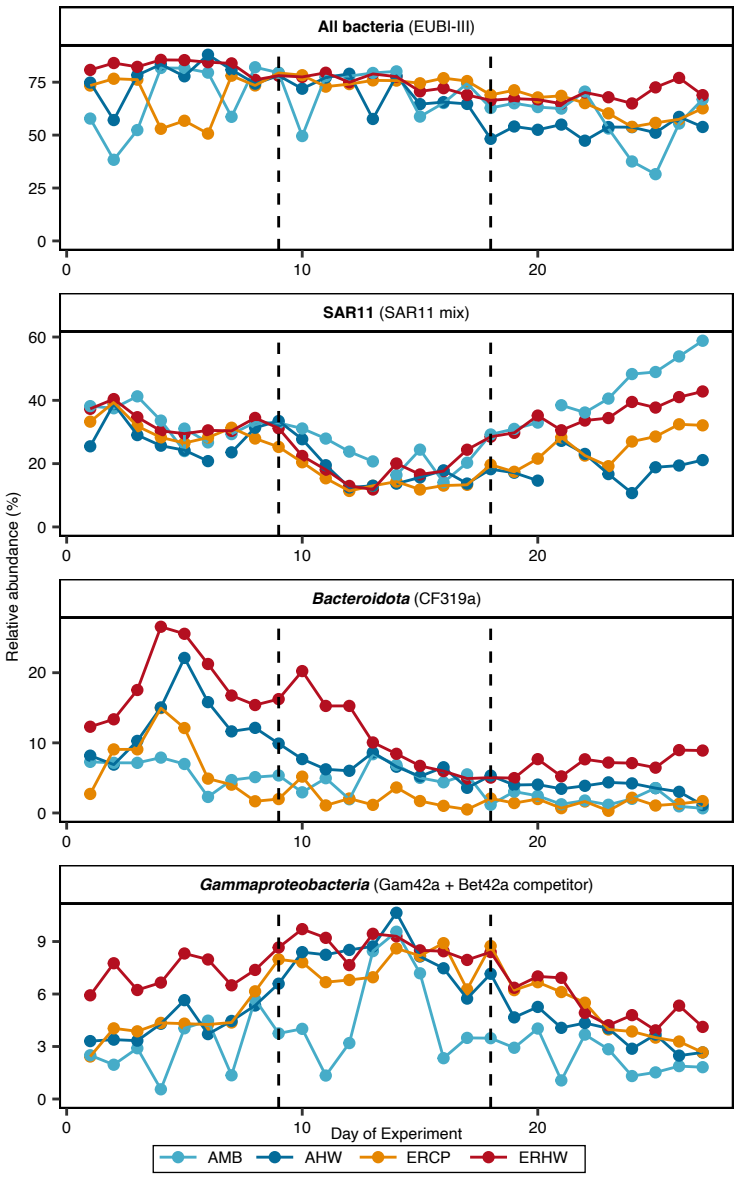

Figure 4.2: Relative abundance of all bacteria, SAR11, *Bacteroidota*, and *Gammaproteobacteria*, assessed by FISH quantifications. Dashed lines indicate beginning and end of the heatwave treatment. Shown is one replicate per treatment. Colors represent treatment.

looking in more detail, less abundant taxa differed in relative abundance between the samples. To mention four examples, *Persicirhabdus* (*Verrucomicrobiota*) increased in relative abundance after 20 days in the ambient treatments (GAM, $F(1)=82.17$, $p<0.001$) and were slightly more abundant in the heatwave treatments (GAM, $F(1)=10.77$, $p=0.001$, Fig. 4.3). *Lentimonas*, another *Verrucomicrobiota* genus, increased in relative abundance after ca. 10 to 15 days in the ambient treatments, and after ca. 20 days in the future ocean scenarios, though these changes were insignificant (GAM, RCP: $F(1)=0.304$, $p=0.582$, Heatwave: $F(1)=0.088$, $p=0.298$). On the other hand, the *Bacteroidota* NS11 – 12 marine group (GAM, $F(1)=167.055$, $p<0.001$) and NS4 marine group (GAM, $F(1)=58.27$, $p<0.001$) appeared to benefit from the future ocean scenarios, but

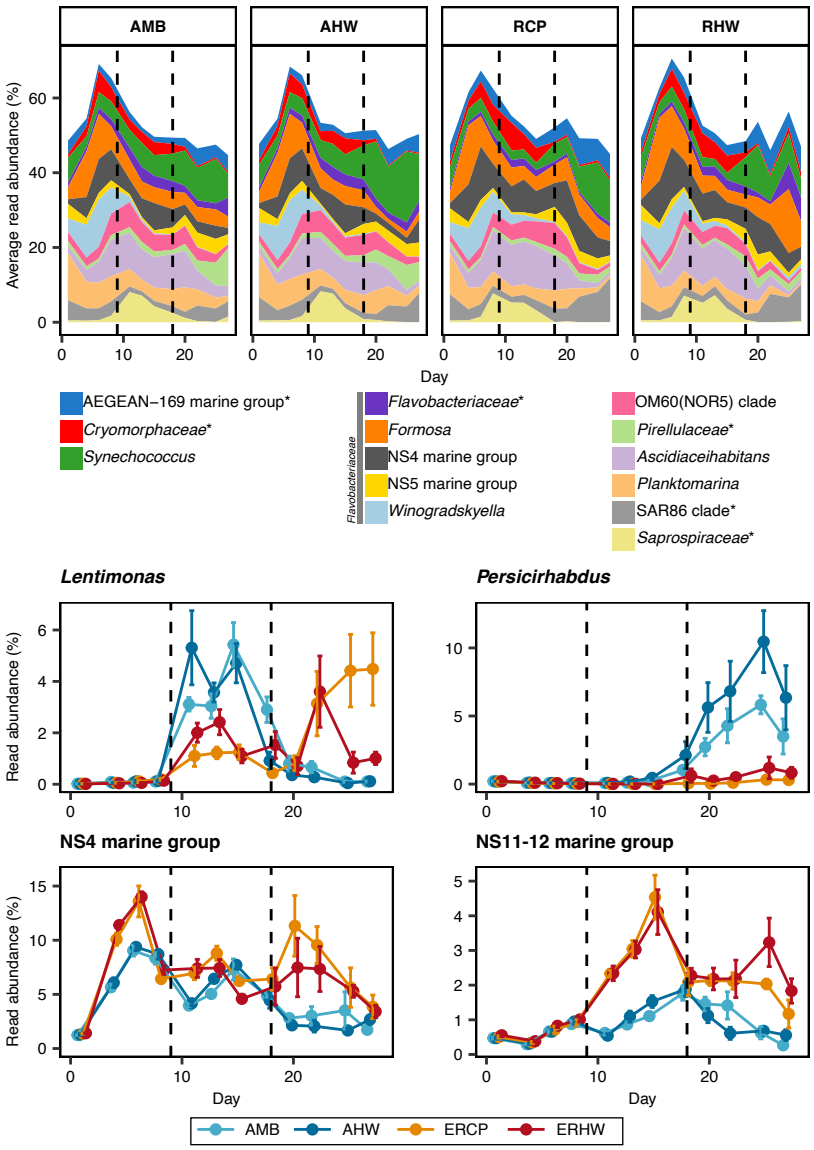

Figure 4.3: Microbial community composition assessed by 16S rRNA sequencing. Top: 14 most abundant genera. Mean of 4 replicates is shown. Bottom: Individual taxa over the sampling campaign. Dots represent mean, with standard deviation (4 replicates). Colours represent experimental condition. Dotted vertical line is beginning and end of heatwave. Asterisk indicate taxonomic groups identified on the family level only.

were unaffected from the heatwaves (GAM, NS11-12: $F(1)=0.759$, $p=0.385$; NS4: $F(1)=0.071$, $p=0.791$) (Fig. 4.3).

4.4.5 No indications of heatwave impact on virus-like particle counts

We next examined the effect of a heatwave on the concentration of virus-like particles (VLP) using fluorescence microscopy. VLP abundances were only assessed in the ambient (AMB + AHW) treatments. Concentrations were more than 10-fold higher than total cell counts (Fig. 4.4). Their fluctuations over the sampling period were less than those of total cell counts, while

the variance between replicates was much greater. VLP concentrations increased from 8.8 $\pm 1.6 \times 10^7$ VLP mL^{-1} to 13.5 $\pm 2.5 \times 10^7$ VLP mL^{-1} after 20 days (Fig. 4.4). This increase was steady for the heatwave replicates, whereas a minor decrease in abundances could be observed in the ambient control treatment. However, no significant influence could be detected between the AMB and AHW treatment (GAM, $F(1)=2.411$, $p=0.123$), suggesting a limited impact of the applied heatwave on virus-induced lysis.

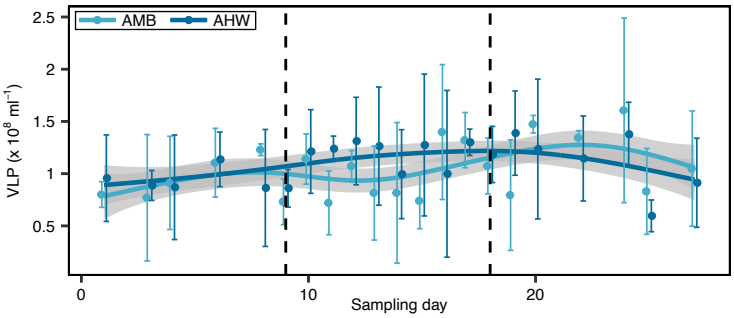

Figure 4.4: Virus-like particle (VLP) concentrations during the mesocosm experiment. Shown are mean and standard deviation across four replicates as dots and error bars, respectively. Colored curves are GAM models with 95% confidence intervals as ribbons. Dashed lines indicate beginning and end of heatwave treatment.

4.4.6 Dilution experiments indicate no treatment-specific influence on cell division or grazing rates

To assess the influence of the applied treatments on taxon-specific cell division and grazing rates, we conducted dilution experiments once a week. Similar to VLP counts, dilution experiments were only conducted on the ambient (AMB + AHW) treatments. First, we assessed cell division and grazing for total cell counts. Over all samples and replicates, cell division rates 0.9 $\pm 0.3\,\mathrm{d}^{-1}$ (mean $\pm$sd) were comparable to grazing rates 0.9 $\pm 0.5\,\mathrm{d}^{-1}$ (Fig. 4.4). We could not detect an influence of the heatwave on cell division rates based on total cell counts (GAM, $F(1)=0.734$, $p=0.40$), while grazing rates were significantly different (GAM, $F(1)=9.38$, $p=0.006$). However, this is most likely attributable to the last data point, when the informative value might be low, as discussed earlier.

Additionally, we investigated taxon-specific cell division and grazing rates. SAR11 cell division rates averaged 0.6 $\pm 0.3\,\mathrm{d}^{-1}$ and were stable over time (Fig. 4.5). We could not detect an effect of the heatwave treatment (GAM, $F(1)=3.214$, $p=0.091$). Similarly, grazing rates were not affected by the heatwave treatment (GAM, $F(1)=0.042$, $p=0.84$). However, grazing decreased from 0.7 $\pm 0.3\,\mathrm{d}^{-1}$ on day 6 to 0.2 $\pm 0.3\,\mathrm{d}^{-1}$ on day 13. Subsequently, grazing rates increased again towards starting conditions. Besides SAR11, we got some first insights into cell division and grazing rates of *Bacteroidota* and *Gammaproteobacteria*, for which only one replicate was

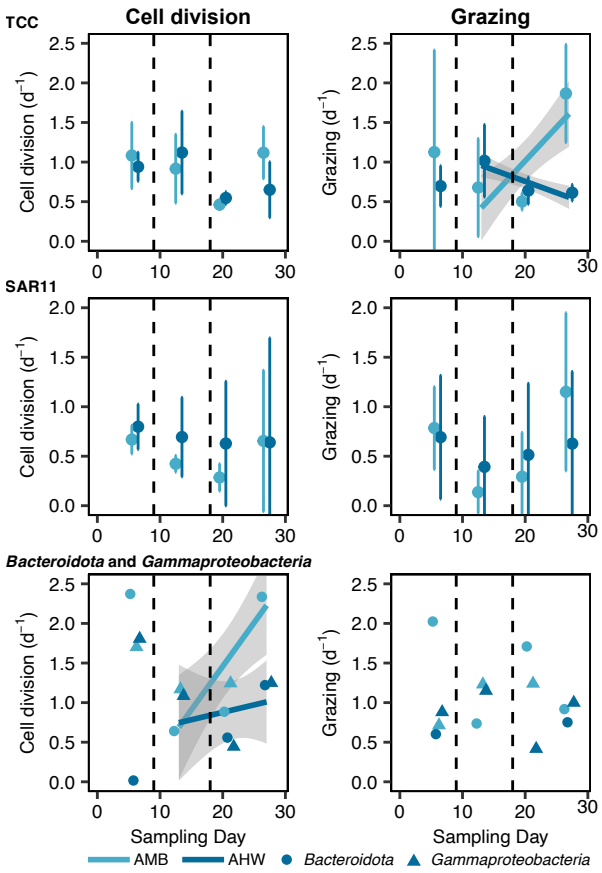

Figure 4.5: Cell division and grazing rates, determined by dilution experiments. Dashed lines indicate beginning and end of the heatwave treatment. Shown are mean and standard deviation across four replicates as dots and error bars, respectively. In case of *Bacteroidota* and *Gammaproteobacteria*, only one replicate was assessed. Colored lines are GAM models with 95% confidence intervals as ribbons, where statistically significant differences between AMB and AHW treatments could be detected.

analyzed. Both, cell division and grazing rates were larger than those of SAR11 and exceeded those derived by total cell counts. Cell division rates were reduced after the heatwave (GAM, $F(1)=32.0$, $p=0.004$) with the same considerations applicable as described above (Fig. 4.5). Grazing rates were not affected by the heatwave (GAM, $F(1)=0.713$, $p=0.405$).

4.4.7 High abundance of filaments during the sampling campaign

During the sample preparation of the total cell counts, we noticed considerable amounts of filamentous microbial cells. Filaments were absent in the beginning of the incubation, increased to $1.0 \pm 0.1 \times 10^5$ filaments mL^{-1} (mean $\pm$sd) and $1.8 \pm 0.1 \times 10^5$ filaments mL^{-1} on day 14 and 12 for the ambient (AMB + AHW) and future Ocean (RCP + RHW) treatments, respectively (Fig. 4.6). Filament occurrence differed significantly between the two treatments (GAM, $F(1)=108.594$, $p<0.001$), but we could not detect an effect of the heatwave treatment (GAM, $F(1)=0.395$, $p=0.53$).

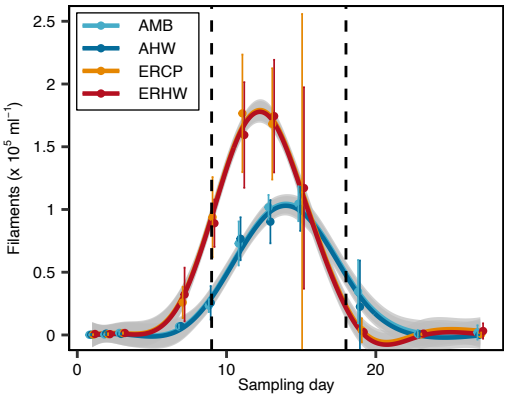

Figure 4.6: Number of filamentous bacteria during sampling period. Dashed lines indicate beginning and end of the heatwave treatment. Shown are mean and standard deviation across four replicates as dots and error bars, respectively. Colored curves are GAM models with 95% confidence intervals as ribbons.

4.5 Discussion

Anthropogenic influences are shaping the future ocean. We assessed the impacts of increased CO_2, temperature, and N:P ratio, as well as the exposure to a heatwave, on the microbial food web. For this study, we used mesocosms of 520 L to avoid bottle effects and best resemble *in situ* conditions. Nevertheless, we observed increasing variances, especially in the total cell counts, after approximately 3 weeks of the incubations. Previous mesocosms studies report similar results (Endres et al. 2014; Hevroni et al. 2023; Hoppe et al. 2008) indicating reduced interpretability post the 3-week mark. Additionally, the emergence of filamentous microorganisms raised questions about potential limitations. They are uncommon in sea-surface waters and are possibly linked to reduced water movement. Filaments are more common in freshwater habitats (Jurgens et al. 1999; Pernthaler et al. 2004) and have been associated with high grazing pressure, as the filamentous bacteria become too large for the predator to be consumed (Jurgens et al. 1999). They have previously been reported from mesocosm experiments (Riemann et al. 2000) and could indicate a common limitation. Interestingly, filament abundance was almost twice as high in the future ocean scenarios, compared to the ambient treatments, which might indicate higher grazing pressure (discussed below). Despite those recognized limitations, mesocosms are valuable for their ability to capture the full breadth of species and genetic diversity, while offering the flexibility for controlled experimental manipulations (Moustaka-Gouni et al. 2016).

On a different note, while the temperature for the simulated marine heatwave was raised over two days to slowly increase the temperature, the conditions for the future ocean treatments were applied as a 'shock'. The temperature was raised by +3 °C within one day, while the pH was lowered by 0.3 and the CO_2 concentration increased by the addition of 1.8 L of CO_2 saturated seawater. The future ocean will change over decades, meaning that the microbiome can adapt to the new conditions slowly. Considering the high abundance and short generation times of microbes, the microbial community is designed to evolve quickly (Hutchins and Fu 2017) and

might cope with the changes different to any laboratory experiment.

4.5.1 Effect of future ocean scenario due to altered bottom-up processes

We tested the effects of a future ocean scenario with an integrated approach of increased temperature, CO_2 concentration, and N:P ratio, as well as a decreased pH. Chlorophyll a concentrations were not affected by the future ocean scenarios and neither was phytoplankton biomass (Meunier et al. in prep). Nevertheless, the exudated organic matter and the resulting carbohydrate composition may be affected (Mühlenbruch et al. 2018), which in turn could influence the microbial community.

Total cell counts were altered by the future ocean scenario, with less fluctuation in the cell abundances and an earlier second bloom in cell abundances. Based on previous research, we did not expect an effect by the increased CO_2 concentrations (Bergen et al. 2016; Hutchins and Fu 2017; Moustaka-Gouni et al. 2016; Tsiola et al. 2023) but a positive effect of the increased temperatures (Bergen et al. 2016; Hutchins and Fu 2017) on the microbial community. However, the effects of temperature may not only be on the microbial community but also on the predators and viruses, which would lead to no observable effect (Tsiola et al. 2023). However, grazer abundances were not altered between the ambient (AMB + AHW) and future ocean scenarios (RCP + RHW; Meunier et al. in prep). While VLP abundances were not assessed in the future ocean scenarios (RCP+RHW), increased temperatures during the heatwave did not affect VLP abundances. The remaining factors, namely increased CO_2 and altered nutrients, are not expected to affect the virus community (Zhang et al. 2021). Overall, the differences observed in total cell counts likely result from changes in bottom-up factors (substrate availability) rather than top-down controls (grazing or virus-induced lysis). It is known that phytoplankton increase their photosynthetic activity in response to elevated temperatures and CO_2 levels (Gattuso et al. 2013). Moreover, the composition of carbohydrates in organic matter derived from phytoplankton is observed to vary during a phytoplankton bloom (Kappelmann et al. 2019; Vidal-Melgosa et al. 2021). Therefore, the observed differences in cell counts can be attributed to variations in the phytoplankton community.

On a taxon-specific level, we could not detect any major differences between the ambient and future ocean scenarios. FISH-based relative abundances were comparable between the experimental conditions for SAR11, *Bacteroidota*, or *Gammaproteobacteria*. Additionally, the assessed 16S data did not reveal any major differences either. However, the 16S data suggests that individual taxa may be affected from the future ocean scenarios. For example, the increased relative abundance of *Lentimonas* (*Verrucomicrobiota*) in the ambient treatments might indicate increased abundances of fucoidan. Fucoidan is a complex sulfated polysaccharide, which *Lentimonas* is one of the few taxa able to digest (Sichert et al. 2020). This provides further evidence for our above-stated suggestion that differences in total cell counts are bottom-up

driven. Another example includes *Persicirhabdus*, which were increased in relative abundance in the ambient treatments. They are typically particle-attached bacteria, previously found to be associated with phytoplankton (Wang et al. 2024). On the other hand, NS11-12 and NS4 marine group (both *Bacteroidota*) benefited from the future ocean scenarios. Both groups are commonly found in the marine habitats and during phytoplankton blooms (Meziti et al. 2015; Xu et al. 2021). In summary, we observed a few minor effects of the future ocean scenario on the microbial community and a more prominent alteration in total cell counts. Observed changes are likely due to altered bottom-up effects. Overall, the diverse microbial community remains functionally resistant to the future ocean but is shaped by the phytoplankton community.

4.5.2 Microbial community resistant to heatwave treatments

The microbial community was resilient to the marine heatwave treatment, exhibiting only minor non-significant differences between the treatments. It is worth noting, however, that Meunier et al. (in prep) identified a significant impact of the heatwave on total cell counts on the same data, using a different statistical approach. While this study employed generalized additive models (GAMs) to accommodate the high fluctuations observed in the parameters throughout of the sampling campaign, Meunier et al. (in prep) opted for generalized linear models (GLM). Our choice of GAMs was driven by their capacity to more accurately capture the complex dynamics of our data, suggesting they are more suitable for modeling the nuanced effects observed during the heatwave.

We could not observe an effect of the heatwave on FISH-based abundances, nor on cell division or grazing rates. Contrary to expectations, the moderate autumn heatwave (+2 °C for 5 days) had limited impacts on cell division and grazing rates. The microbial community is well adapted to warmer waters, which are frequently observed during summer months (Joint and Smale 2017). In fact, we expected increased microbial productivity and cell division rates during the heatwave (Hutchins and Fu 2017), which might in turn be compensated by higher mortality rates (Machado et al. 2020; Moustaka-Gouni et al. 2016). However, the heatwave treatments did not have any noticeable effect on the cell division or grazing rates, with two exceptions, both in the fourth week of the experiment. The high variability and low significance after 3 weeks have been discussed multiple times throughout this paper. Regarding VLP counts, they too appeared largely unaffected by the heatwave, although a positive effect of temperatures was expected. Theoretically, rising temperatures and the potential stress from the heatwave could trigger prophages to enter the lytic cycle, thereby increasing VLP counts (Breitbart 2012). Yet, the slight and statistically insignificant effect does not align with these expectations. Instead, it suggests a robust VLP community, likely in close correlation with the abundances of their host cells, underscoring the complex dynamics within marine microbial ecosystems during environmental perturbations.

To summarize, our study provides a valuable understanding of the resilience and adaptive capabilities of marine microbial communities in the face of anthropogenic-driven changes. While some effects of a future ocean scenario and a marine heatwave were observed, the overall resilience of the microbial community suggests an ecosystem's stability. The study revealed that while the microbial community's composition and dynamics are indirectly influenced by substrate availability, they remain largely resilient to abiotic environmental shifts. However, the study underscores the need for cautious interpretation of mesocosm experiments. They stress the ongoing need for in-depth research to dissect the complex reactions of marine microbial ecosystems to environmental changes, underscoring their crucial role in ecosystem stability.

4.6 Supplementary Information

4.6.1 Supplementary Tables

Table 4.1: FISH probes used in this study. Probes were labelled with horseradish-peroxidase (HRP) at their 5' end. Helper and competitors were unlabelled and are written in *italics*. FA = formamide concentration in the hybridization buffer.

Targeted Taxon	Name	Sequence (5' → 3')	FA (%)	Citation
All bacteria	EUB338-I	GCTGCCTCCCG TAGGAGT	35	Amann et al. 1990
	EUB338-II	GCAGCCACCCG TAGGTGT	35	Daims et al. 1999
	EUB338-III	GCTGCCACCCG TAGGTGT	35	Daims et al. 1999
SAR11	SAR11-152R	ATTAGCACAAG TTTCCYCGTGT	25	Rappé et al. 2002
	SAR11-441R	TACMGTCATTT TCTTCCCCGAC	25	Rappé et al. 2002
	SAR110487mod	CGGACCTTCTT ATTCGGG	25	Rappé et al. 2002
	SAR11-542R	TCCGAACTACG CTAGGTC	25	Rappé et al. 2002
	SAR11-732R	GTCAGTAATGA TCCAGAAAGYT G	25	Rappé et al. 2002
	SAR11-487modh3	*CGGCTGCTGGC ACGAAGTTAGC*	25	Morris et al. 2002
Bacteroidota	CF319a	TGGTCCGTGTC TCAGTAC	35	Manz et al. 1996
Gammaproteobacteria	Gam42a	GCCTTCCCACA TCGTTT	35	Manz et al. 1992
	Bet42a	*GCCTTCCCACTT CGTTT*	35	Manz et al. 1992

Table 4.3: ACME tool settings for automated image analysis. SBR related to signal-to-background-ratio. MGV is mean gray value. Nr_A594_Signals and Nr_A594_Signals correspond to the number of signals in the A488 (16S FISH) and A594 (Autofluorescence) channels.

Dye	Settings	Subsettings
DAPI	Area>18 and Area<250 and SBR>1.5 and length<20	Nr_A594_Signals=0 and Nr_A488_Signals>=1
A488 (16S FISH)	Area>18 and Area<100 and SBR>1.5 and MGV>90	Nr_A594_Signals=0
A594 (Autofluorescence)	Area>18	

References

Amann, R. I., B. J. Binder, R. J. Olson, S. W. Chisholm, R. Devereux, and D. Stahl (1990). "Combination of 16S rRNA-targeted oligonucleotide probes with flow cytometry for analyzing mixed microbial populations". *Applied and Environmental Microbiology* 56.6, pages 1919–1925 (cited on page 106).

Amorim, F. d. L. L. de, K. H. Wiltshire, P. Lemke, K. Carstens, S. Peters, J. Rick, L. Gimenez, and M. Scharfe (2023). "Investigation of marine temperature changes across temporal and spatial gradients: providing a fundament for studies on the effects of warming on marine ecosystem function and biodiversity". *Progress in Oceanography* 216, page 103080 (cited on page 89).

Apprill, A., S. McNally, R. Parsons, and L. Weber (2015). "Minor revision to V4 region SSU rRNA 806R gene primer greatly increases detection of SAR11 bacterioplankton". *Aquatic Microbial Ecology* 75.2, pages 129–137 (cited on pages 93, 97).

Arandia-Gorostidi, N., T. M. Huete-Stauffer, L. Alonso-Sáez, and X. A. G. Morán (2017). "Testing the metabolic theory of ecology with marine bacteria: different temperature sensitivity of major phylogenetic groups during the spring phytoplankton bloom". *Environmental Microbiology* 19.11, pages 4493–4505 (cited on page 90).

Barbosa, A. B., B. A. Mosley, H. M. Galvão, and R. B. Domingues (2023). "Short-Term Effects of Climate Change on Planktonic Heterotrophic Prokaryotes in a Temperate Coastal Lagoon: Temperature Is Good, Ultraviolet Radiation Is Bad, and CO_2 Is Neutral". *Microorganisms* 11.10, page 2559 (cited on page 90).

Bennke, C. M., G. Reintjes, M. Schattenhofer, A. Ellrott, J. Wulf, M. Zeder, and B. M. Fuchs (2016). "Modification of a high-throughput automatic microbial cell enumeration system for shipboard analyses". *Applied and Environmental Microbiology* 82.11, pages 3289–3296 (cited on page 93).

Bergen, B., S. Endres, A. Engel, M. Zark, T. Dittmar, U. Sommer, and K. Jürgens (2016). "Acidification and warming affect prominent bacteria in two seasonal phytoplankton bloom mesocosms". *Environmental Microbiology* 18.12, pages 4579–4595 (cited on pages 90, 103).

Berner, C., M. Bertos-Fortis, J. Pinhassi, and C. Legrand (2018). "Response of microbial communities to changing climate conditions during summer cyanobacterial blooms in the Baltic Sea". *Frontiers in Microbiology* 9, page 1562 (cited on page 90).

Breitbart, M. (2012). "Marine viruses: truth or dare". *Annual Review of Marine Science* 4, pages 425–448 (cited on page 104).

Breitbart, M., C. Bonnain, K. Malki, and N. A. Sawaya (2018). "Phage puppet masters of the marine microbial realm". *Nature Microbiology* 3.7, pages 754–766 (cited on page 90).

Brüwer, J. D., L. H. Orellana, C. Sidhu, H. C. Klip, C. L. Meunier, M. Boersma, K. H. Wiltshire, R. Amann, and B. M. Fuchs (2023). "*In situ* cell division and mortality rates of SAR11, SAR86,

Bacteroidetes, and *Aurantivirga* during phytoplankton blooms reveal differences in population controls". *mSystems*, e01287–22 (cited on page 90).

Buchan, A., G. R. LeCleir, C. A. Gulvik, and J. M. González (2014). "Master recyclers: features and functions of bacteria associated with phytoplankton blooms". *Nature Reviews Microbiology* 12.10, pages 686–698 (cited on page 90).

Callahan, B. J., P. J. McMurdie, M. J. Rosen, A. W. Han, A. J. A. Johnson, and S. P. Holmes (2016). "DADA2: High-resolution sample inference from Illumina amplicon data". *Nature Methods* 13.7, pages 581–583 (cited on page 94).

Cheng, L., K. E. Trenberth, J. Fasullo, T. Boyer, J. Abraham, and J. Zhu (2017). "Improved estimates of ocean heat content from 1960 to 2015". *Science Advances* 3.3, e1601545 (cited on page 89).

Daims, H., A. Brühl, R. Amann, K.-H. Schleifer, and M. Wagner (1999). "The domain-specific probe EUB338 is insufficient for the detection of all Bacteria: development and evaluation of a more comprehensive probe set". *Systematic and Applied Microbiology* 22.3, pages 434–444 (cited on page 106).

Deans, F. S. C. (2022). "The influence of climate change on marine bacterioplankton communities and greenhouse gases in New Zealand waters". Thesis. University of Otago (cited on page 90).

DeVries, T., M. Holzer, and F. Primeau (2017). "Recent increase in oceanic carbon uptake driven by weaker upper-ocean overturning". *Nature* 542.7640, pages 215–218 (cited on page 89).

Dupont, C. L., D. B. Rusch, S. Yooseph, M.-J. Lombardo, R. Alexander Richter, R. Valas, M. Novotny, J. Yee-Greenbaum, J. D. Selengut, and D. H. Haft (2012). "Genomic insights to SAR86, an abundant and uncultivated marine bacterial lineage". *The ISME Journal* 6.6, pages 1186–1199 (cited on page 90).

Endres, S., L. Galgani, U. Riebesell, K.-G. Schulz, and A. Engel (2014). "Stimulated bacterial growth under elevated pCO_2: Results from an off-shore mesocosm study". *PLoS One* 9.6, e99228 (cited on pages 90, 102).

Fadeev, E., M. G. Cardozo-Mino, J. Z. Rapp, C. Bienhold, I. Salter, V. Salman-Carvalho, M. Molari, H. E. Tegetmeyer, P. L. Buttigieg, and A. Boetius (2021). "Comparison of two 16S rRNA primers (V3–V4 and V4–V5) for studies of arctic microbial communities". *Frontiers in Microbiology* 12, page 637526 (cited on page 97).

Fuchs, B. M., J. Pernthaler, and R. Amann (2007). "Single cell identification by fluorescence *in situ* hybridization". *Methods for General and Molecular Microbiology*, pages 886–896 (cited on page 92).

Gao, K., Y. Zhang, and D.-P. Häder (2018). "Individual and interactive effects of ocean acidification, global warming, and UV radiation on phytoplankton". *Journal of Applied Phycology* 30, pages 743–759 (cited on pages 89, 90).

Gattuso, J.-P., A. Magnan, R. Billé, W. W. Cheung, E. L. Howes, F. Joos, D. Allemand, L. Bopp, S. R. Cooley, and C. M. Eakin (2015). "Contrasting futures for ocean and society from different anthropogenic CO_2 emissions scenarios". *Science* 349.6243, aac4722 (cited on page 89).

Gattuso, J.-P., K. J. Mach, and G. Morgan (2013). "Ocean acidification and its impacts: an expert survey". *Climatic Change* 117, pages 725–738 (cited on pages 89, 103).

Giovannoni, S. J. (2017). "SAR11 bacteria: the most abundant plankton in the oceans". *Annual Review of Marine Science* 9, pages 231–255 (cited on page 90).

Hevroni, G., F. Vincent, C. Ku, U. Sheyn, and A. Vardi (2023). "Daily turnover of active giant virus infection during algal blooms revealed by single-cell transcriptomics". *Science Advances* 9.41, eadf7971 (cited on page 102).

Hobday, A. J., L. V. Alexander, S. E. Perkins, D. A. Smale, S. C. Straub, E. C. Oliver, J. A. Benthuysen, M. T. Burrows, M. G. Donat, and M. Feng (2016). "A hierarchical approach to defining marine heatwaves". *Progress in Oceanography* 141, pages 227–238 (cited on page 89).

Hoppe, H.-G., P. Breithaupt, K. Walther, R. Koppe, S. Bleck, U. Sommer, and K. Jürgens (2008). "Climate warming in winter affects the coupling between phytoplankton and bacteria during the spring bloom: a mesocosm study". *Aquatic Microbial Ecology* 51.2, pages 105–115 (cited on page 102).

Hutchins, D. A. and F. Fu (2017). "Microorganisms and ocean global change". *Nature Microbiology* 2.6, pages 1–11 (cited on pages 90, 102–104).

Joint, I. and D. A. Smale (2017). "Marine heatwaves and optimal temperatures for microbial assemblage activity". *FEMS Microbiology Ecology* 93.2, fiw243 (cited on pages 90, 104).

Jurgens, K., J. Pernthaler, S. Schalla, and R. Amann (1999). "Morphological and compositional changes in a planktonic bacterial community in response to enhanced protozoan grazing". *Applied and Environmental Microbiology* 65.3, pages 1241–1250 (cited on page 102).

Kappelmann, L., K. Krüger, J.-H. Hehemann, J. Harder, S. Markert, F. Unfried, D. Becher, N. Shapiro, T. Schweder, and R. I. Amann (2019). "Polysaccharide utilization loci of North Sea *Flavobacteriia* as basis for using SusC/D-protein expression for predicting major phytoplankton glycans". *The ISME Journal* 13.1, pages 76–91 (cited on pages 90, 103).

Landry, M. and R. Hassett (1982). "Estimating the grazing impact of marine micro-zooplankton". *Marine Biology* 67, pages 283–288 (cited on page 94).

Lara, E., J. M. Arrieta, I. Garcia-Zarandona, J. A. Boras, C. M. Duarte, S. Agustí, P. F. Wassmann, and D. Vaqué (2013). "Experimental evaluation of the warming effect on viral, bacterial and protistan communities in two contrasting Arctic systems". *Aquatic Microbial Ecology* 70.1, pages 17–32 (cited on page 90).

Lauro, F. M., D. McDougald, T. Thomas, T. J. Williams, S. Egan, S. Rice, M. Z. DeMaere, L. Ting, H. Ertan, and J. Johnson (2009). "The genomic basis of trophic strategy in marine bacteria". *Proceedings of the National Academy of Sciences* 106.37, pages 15527–15533 (cited on page 90).

Lee, H., K. Calvin, D. Dasgupta, G. Krinner, A. Mukherji, P. Thorne, C. Trisos, J. Romero, P. Aldunce, and K. Barret (2023a). *IPCC, 2023: Climate Change 2023: Synthesis Report, Summary for Policymakers. Contribution of Working Groups I, II and III to the Sixth Assessment Report of the Intergovernmental Panel on Climate Change [Core Writing Team, H. Lee and J. Romero (eds.)]. IPCC, Geneva, Switzerland*. Journal Article. Intergovernmental Panel on Climate Change (IPCC) (cited on page 89).

Lee, H. B., D. H. Jeong, B. C. Cho, and J. S. Park (2023b). "Comparative analyses of eight primer sets commonly used to target the bacterial 16S rRNA gene for marine metabarcoding-based studies". *Frontiers in Marine Science* 10, page 1199116 (cited on page 97).

Machado, K. B., A. M. Antunes, C. P. Targueta, J. G. Fernandes, T. N. Soares, and J. C. Nabout (2020). "DNA metabarcoding reveals the responses of prokaryotes and eukaryotes microbiota to warming: Are the patterns similar between taxonomic and trophic groups?" *Ecological Indicators* 115, page 106452 (cited on page 104).

Manz, W., R. Amann, W. Ludwig, M. Vancanneyt, and K.-H. Schleifer (1996). "Application of a suite of 16S rRNA-specific oligonucleotide probes designed to investigate bacteria of the phylum cytophaga-flavobacter-bacteroides in the natural environment". *Microbiology* 142.5, pages 1097–1106 (cited on page 106).

Manz, W., R. Amann, W. Ludwig, M. Wagner, and K.-H. Schleifer (1992). "Phylogenetic oligodeoxynucleotide probes for the major subclasses of proteobacteria: problems and solutions". *Systematic and Applied Microbiology* 15.4, pages 593–600 (cited on page 106).

Martin, M. (2011). "Cutadapt removes adapter sequences from high-throughput sequencing reads". *EMBnet. journal* 17.1, pages 10–12 (cited on page 94).

Meunier, C. L., J. Schmidt, A. Ahme, A. Balkoni, K. Berg, M. Boersma, J. D. Brüwer, B. M. Fuchs, L. Gimenez, M. Guignard, R. Schulte-Hillen, B. Krock, J. Rick, H. Stibor, M. Stockenreiter, F. Weber, K. H. Wiltshire, S. Wohlrab, and I. V. Kirstein (in prep). "Plankton communities today and tomorrow – impacts of global change and marine heatwaves in a multiple-driver mesocosm experiment" (cited on pages 91, 92, 96, 103, 104).

Meziti, A., K. A. Kormas, M. Moustaka-Gouni, and H. Karayanni (2015). "Spatially uniform but temporally variable bacterioplankton in a semi-enclosed coastal area". *Systematic and Applied Microbiology* 38.5, pages 358–367 (cited on page 104).

Moreno, H. D., M. Köring, J. Di Pane, N. Tremblay, K. H. Wiltshire, M. Boersma, and C. L. Meunier (2022). "An integrated multiple driver mesocosm experiment reveals the effect of global change on planktonic food web structure". *Communications Biology* 5.1, page 179 (cited on page 89).

Morris, R. M., M. S. Rappé, S. A. Connon, K. L. Vergin, W. A. Siebold, C. A. Carlson, and S. J. Giovannoni (2002). "SAR11 clade dominates ocean surface bacterioplankton communities". *Nature* 420.6917, pages 806–810 (cited on page 106).

Moustaka-Gouni, M., K. A. Kormas, M. Scotti, E. Vardaka, and U. Sommer (2016). "Warming and acidification effects on planktonic heterotrophic pico-and nanoflagellates in a mesocosm experiment". *Protist* 167.4, pages 389–410 (cited on pages 102–104).

Mühlenbruch, M., H.-P. Grossart, F. Eigemann, and M. Voss (2018). "Mini-review: Phytoplankton-derived polysaccharides in the marine environment and their interactions with heterotrophic bacteria". *Environmental Microbiology* 20.8, pages 2671–2685 (cited on page 103).

Parada, A. E., D. M. Needham, and J. A. Fuhrman (2016). "Every base matters: assessing small subunit rRNA primers for marine microbiomes with mock communities, time series and global field samples". *Environmental Microbiology* 18.5, pages 1403–1414 (cited on pages 93, 97).

Pernthaler, J., E. Zöllner, F. Warnecke, and K. Jürgens (2004). "Bloom of filamentous bacteria in a mesotrophic lake: identity and potential controlling mechanism". *Applied and Environmental Microbiology* 70.10, pages 6272–6281 (cited on page 102).

Pörtner, H.-O., D. C. Roberts, E. S. Poloczanska, K. Mintenbeck, M. Tignor, A. Alegría, M. Craig, S. Langsdorf, S. Löschke, V. Möller, et al. (2022). *IPCC, 2022: Summary for policymakers*. Cambridge University Pres (cited on page 89).

Rappé, M. S., S. A. Connon, K. L. Vergin, and S. J. Giovannoni (2002). "Cultivation of the ubiquitous SAR11 marine bacterioplankton clade". *Nature* 418.6898, pages 630–633 (cited on page 106).

Riemann, L., G. F. Steward, and F. Azam (2000). "Dynamics of bacterial community composition and activity during a mesocosm diatom bloom". *Applied and Environmental Microbiology* 66.2, pages 578–587 (cited on page 102).

Sarmento, H., J. M. Montoya, E. Vázquez-Domínguez, D. Vaqué, and J. M. Gasol (2010). "Warming effects on marine microbial food web processes: how far can we go when it comes to predictions?" *Philosophical Transactions of the Royal Society B: Biological Sciences* 365.1549, pages 2137–2149 (cited on page 90).

Sichert, A., C. H. Corzett, M. S. Schechter, F. Unfried, S. Markert, D. Becher, A. Fernandez-Guerra, M. Liebeke, T. Schweder, and M. F. Polz (2020). "*Verrucomicrobia* use hundreds of enzymes to digest the algal polysaccharide fucoidan". *Nature Microbiology* 5.8, pages 1026–1039 (cited on page 103).

Tsiola, A., E. Krasakopoulou, D. Daffonchio, C. Frangoulis, T. M. Tsagaraki, S. Fodelianakis, and P. Pitta (2023). "Responses of Free-Living Planktonic Bacterial Communities to Experimental Acidification and Warming". *Microorganisms* 11.2, page 273 (cited on pages 90, 103).

Vidal-Melgosa, S., A. Sichert, T. B. Francis, D. Bartosik, J. Niggemann, A. Wichels, W. G. Willats, B. M. Fuchs, H. Teeling, and D. Becher (2021). "Diatom fucan polysaccharide precipitates carbon during algal blooms". *Nature Communications* 12.1, page 1150 (cited on page 103).

Wang, F.-Q., D. Bartosikt, C. Sidhu, R. Siebers, D.-C. Lu, A. Trautwein-Schult, D. Becher, B. Huettel, J. Rick, I. V. Kirstein, K. H. Wiltshire, T. Schweder, B. M. Fuchs, M. M. Bengts-

son, H. Teeling, and R. I. Amann (2024). “Particle-attached bacteria act as gatekeepers in the decomposition of complex phytoplankton polysaccharides”. *Microbiome* (cited on page 104).

Wickham, H. (2011). *ggplot2*. Volume 3. Wiley Interdisciplinary Reviews: Computational Statistics. Springer-Verlag New York, pages 180–185 (cited on page 94).

Wickham, H., R. François, L. Henry, K. Müller, and D. Vaughan (2023). *dplyr: A Grammar of Data Manipulation*. R package version 1.1.2 (cited on page 94).

Wilke, C. O. (2020). *cowplot: Streamlined Plot Theme and Plot Annotations for 'ggplot2'*. R package version 1.1.1 (cited on page 94).

Wood, S. N. (2011). “Fast stable restricted maximum likelihood and marginal likelihood estimation of semiparametric generalized linear models”. *Journal of the Royal Statistical Society Series B: Statistical Methodology* 73.1, pages 3–36 (cited on page 94).

Xu, S., C. He, S. Song, and C. Li (2021). “Spatiotemporal dynamics of marine microbial communities following a *Phaeocystis* bloom: biogeography and co-occurrence patterns”. *Environmental Microbiology Reports* 13.3, pages 294–308 (cited on page 104).

Zeder, M., A. Ellrott, and R. Amann (2011). “Automated sample area definition for high-throughput microscopy”. *Cytometry Part A* 79.4, pages 306–310 (cited on page 93).

Zhang, R., M. G. Weinbauer, and P. Peduzzi (2021). “Aquatic viruses and climate change”. *Current Issues in Molecular Biology* 41.1, pages 357–380 (cited on page 103).

5

General Discussion

This thesis explores the bacterial life cycle (Fig. 1.2), from cell replication to cell death by phages or grazing, using fluorescence microscopy. In environmental samples, growth is often estimated based on changes in abundance over time. This approach may result in inaccurate observations and conclusions, because it does not account for mortality. To overcome this, I introduced the frequency of dividing cells as a proxy to study cell division rates *in situ*. Combined with net growth rates (i.e., changes in abundance over time), I calculated that ∼90% of bacterial production is recycled within one day during a phytoplankton bloom. I next used direct-geneFISH to target three individual phages and quantified the number of phage-infected SAR11 cells globally and during a phytoplankton bloom. Last, I assessed the influences of future ocean scenarios on the bacterial community, including cell division and grazing rates. These influences have been discussed in Chapter 4 and will not be covered again. However, insights gained into the microbial community dynamics will be included in this discussion.

In this chapter, I will delve into the methodological approaches used in this study to explore the bacterial life cycle, highlighting further applications and their inherent limitations. Subsequently, this discussion will examine how this research, in combination with direct-geneFISH, is part of the beginning of taxon-specific quantitative phage ecology in environmental samples. Next, the discussion will focus on the insights gained regarding the ecology of SAR11. In particular, the ability of SAR11 to increase their cell division rate before the phytoplankton bloom and the effect of phage-lysis on the SAR11 community will be addressed. Last, the discussion will address the intriguing phenomenon of zombie cells and their emergence. Considering the global abundance of zombie cells (ca. 4% of total cell counts), their role in microbial ecology will be discussed. This chapter will be rounded off with an outlook addressing the unresolved questions of this thesis.

5.1 Methodological discussion

In environmental microbiology, visualization techniques remain the gold standard for quantification efforts. They additionally provide unique solutions to study the bacterial life-cycle, as shown in this thesis. Here, I expand the discussion on the frequency of dividing cells and the

advances in taxon-specific quantitative viral ecology. The orthogonal approaches of microscopy based quantifications and diversity assessments via bioinformatic approaches will be elaborated, with references to the discussions in Chapters 2 and 3.

5.1.1 The power of frequency of dividing cells

The concept of the frequency of dividing cells (FDC in this paragraph) is visualized in Figure 5.1 and has been described in Chapter 2. Briefly, for each cell replication, the cell needs to double its genome and separate it into the future daughter cells before the cleavage. The intracellular DNA distribution may, thus, be studied to identify dividing cells. What are the limitations, and what are the advantages of the method?

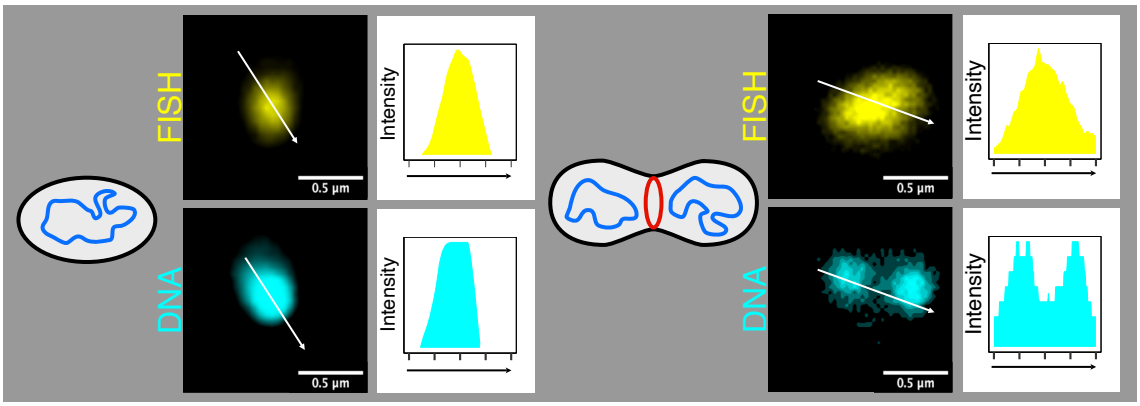

Figure 5.1: Conceptual overview of the frequency of dividing cells. Representative microscopy images of a non-dividing (left) and a dividing (right) SAR11 cell from the phytoplankton bloom in Chapter 2 (April 2, 2020). Histograms represent fluorescence intensity along drawn arrows. Images were recorded on a ZEISS LSM780 and analysed using the ZEN software.

Although the analysis of the FDC has been first introduced in 1979 (Hagström et al. 1979), it is rarely used in marine or aquatic environments. Instead, labelled substrate incubations became the standard to determine bacterial production (Hagström et al. 2017). With advancements in automatic image acquisition and image cytometry, analysis of the FDC is now cost- and time-efficient. In Chapter 2, I demonstrate that the FDC is a valid proxy for the cell division rates in the assessed taxa, which allowed the calculation of taxon-specific cell division rates over an entire phytoplankton bloom. However, the correlations between the FDC and *in situ* cell division rates were taxon-specific and varied between experiments. With the example of SAR11, the higher range of FDC (10% of SAR11 cells) in 2020, represented the baseline during the 2018 phytoplankton spring bloom (Fig. 2.3). The differences likely stem from the effect of staining and imaging conditions. Exposure times were kept coherent within one experimental unit (i.e., sampling year), but they needed to be adjusted between the sampling years (30 vs. 20 ms). This is necessary and inevitable, as the analysis of under or overexposed images is almost

impossible. Hence, while the FDC is a suitable proxy for cell division rates, additional corrections are needed to calculate absolute values of cell division rates. At the current stage, it is unclear whether a general correlation across different taxa and experiments would ever be possible. The use of standards, such as laboratory cultures with a known FDC or fluorescent particles, should be explored to eliminate the differences due to methodological approaches described above. Nevertheless, determining the FDC as proxy for *in situ* cell division rates is recommended, especially in coherent data sets, such as from time series data.

Although multi-cellular aggregates (i.e., filamentous bacteria and chains or other aggregates of cocci) are rare in marine samples and unlikely to impact the conclusion of this study, the pertinent question remains whether the FDC can also be determined for them. The ability to distinguish individual bacterial cells by the image segmentation method is a prerequisite to determine the FDC. While this is straightforward for chains of cocci, filaments may present more complex scenarios, as distinguishing between individual dividing cells is often not possible. Moreover, when it comes to filaments, assessing cellular growth, i.e., the gain in biovolume, might be of greater interest than assessing the FDC. Finally, above described morphologies would contain multiple spatially separated genome copies. In the analyses of this thesis, I removed any cell containing three or more local DNA maxima, which contributed <0.5% of the taxon-specific cell counts.

Microscopy vs. bioinformatic approaches to assess cell division

The FDC is a better proxy for cell division rates than those from bioinformatic approaches, such as the Growth Rate inDex (GRiD; Emiola and Oh 2018). GRiD, based on the peak-to-trough ratio, assesses the differential read coverage of the replication origin and terminus of individual MAGs in the metagenome, and has two main limitations. First, values of GRiD were inconsistent and depended on the choice of mapping algorithm. Second, GRiD values did not agree with microscopy-derived assessments, i.e. FDC, biovolume, and ribosome densities (Chapter 2). Although new bioinformatic approaches emerge (e.g., Larkin et al. 2023), they are based on the same principle and need to be yet verified with experimental data. The current tools are based on short-read metagenomes and there might be improvements in assessing cell division from long-read (e.g., PacBio or Oxford Nanopore) metagenomes in the future. While the sequencing depth of short-read metagenomes is much higher, long-read metagenomes tend to result in contigs of greater lengths (Orellana et al. 2023), which might improve the contig organization for identifying peaks and troughs. A combination of MAGs derived from long-read metagenomes and obtained coverage from short-read metagenomes would be ideal for the approach but is economically not recommendable.

Further applications of the frequency of dividing cells

Following the results from Chapter 2, FDC analyses have been included with different research questions and samples from diverse habitats, providing further evidence of the FDC as a valuable concept and its applicability to other research questions. As cell division rates scale with metabolic processes in bacteria (Kirchman 2018), studying the FDC is suitable to assess the metabolic activity. For example, in the manuscript *Niche differentiation within bacterial key-taxa in stratified surface waters of the Southern Pacific Gyre* (Oggerin et al., submitted to the ISME Journal), the FDC and results from metatranscriptomes agree that two distinct AEGEAN-169 populations thrive in the upper ocean while being rather inactive in deeper water. In a different example, the microbial community in sandy sediment samples was fractionated (i.e., porewater, loosely attached, and firmly attached to sand grains) and their cell division as well as metabolic activity was assessed. Bacteria from the pore-water and loosely attached fraction both showed higher FDC and O_2 consumption rates, compared to firmly attached bacteria (Moncada et al., *in prep*). In conclusion, the additional analyses provide further evidence that the FDC is a valuable tool to asses bacterial activity. It is an easy-to-implement method that could be used with existing or new FISH-based datasets or studies.

The frequency of dividing cells in future projects

Given the broad implications and the ease of calculations, I recommend including the analysis of the FDC for future environmental studies using 16S FISH and automated microscopy. Determining the FDC is a cost-effective and time-efficient method for a deeper ecological insight. The open source software MicrobeJ (plug-in for Fiji/ImageJ; Ducret et al. 2016; Schindelin et al. 2015) is free of charge for scientific purposes and the automated analysis of the FDC takes approximately 2 s to 3 s for each field of view on a standard laptop (MacBook Pro, M1 Max chip, 32 GB memory). Determining the FDC from the MicrobeJ analysis requires an additional data transformation step, currently solved with a custom R script, which could be simplified in the future for a wider audience. Basic coding skills are not required but advantageous. Nevertheless, to further facilitate future projects, the custom R script, a tutorial, as well as a reproducible example data set can be found on GitLab[1].

To conclude, if microscopy images are available, analyzing the FDC is highly recommendable, as it offers an easy-to-implement approach for obtaining novel and significant results. The analysis does not require incubation experiments to study microbial cell division in the environment. However, a calibration with other experimental data, such as dilution experiments, is yet required to calculate absolute rates. Additional data from future research will show whether a general correlation between FDC and cell division rates is applicable.

[1] https://gitlab.mpi-bremen.de/jbruewer/determining-frequency-of-dividing-cells

5.1.2 Quantitative virus ecology

Common methods for quantifying virus[2] abundances include both culture-dependent and independent strategies. Culture-dependent techniques, such as infectivity and plaque assays (Bhatt et al. 2022), necessitate the availability of the viral host, which may not be available (Solden et al. 2016). Culture-independent approaches include (meta)genomic approaches (see below), electron microscopy (Ackermann 2012), fluorescence microscopy (Noble and Fuhrman 1998), and flow cytometry (Brussaard 2004). The latter three methods are used to identify virus-like particles based on a non-specific stain (uranyl acetate for electron microscopy or a nucleic acid stain) and physical or morphological parameters. However, they do not allow for a more detailed taxonomic identification and have thus limited utility for answering the two pertinent parameters in ecology: The identification ("Who is out there") and quantification ("how many") of individual taxonomic groups.

Taxon-specific quantifications in viral ecology is still in its infancy. Although counting virus-like particles using fluorescence microscopy was introduced around the same time as the use of 16S fluorescence *in situ* hybridization for quantifying bacterial cells (Amann et al. 1995; DeLong et al. 1989), the field of quantitave viral ecology has lagged behind its bacterial counterpart. While the bacterial community - diversity and abundances - can be readily explored based on the 16S rRNA, no such universal marker is available for viruses or phages in particular (Pappas et al. 2021). Additionally, the high copy number of 16S rRNAs in each bacterial cell aids in the detection through *in situ* hybridization due to the natural signal amplification. Despite these challenges, the era of taxon-specific quantifications of viruses in environmental samples has started (Baran et al. 2018; Barrero-Canosa et al. 2017), as discussed below.

Taxon-specific quantifications in viral ecology

The further developments and adjustments of direct-geneFISH (Barrero-Canosa et al. 2017) and the polony method (Baran et al. 2018) enable the taxonomic identification and quantification of viruses and their hosts from environmental samples. Direct-geneFISH is a suitable tool to visualize and identify individual virus species. The direct-geneFISH probes need to cover ∼3000 bp (10 probes of 300 bp each), labelled with multiple fluorophores each, to achieve a gene detection efficiency of >90% (Barrero-Canosa et al. 2017; Zeugner et al. 2021). The smaller degenerate primers of the polony method, on the other hand, allow the labelling of conserved genes, such as the major capsid protein of cyanophages, and thus the targeting of larger phylogenetic groups (Baran et al. 2018; Mruwat et al. 2021). The advantages of direct-geneFISH include that it can be combined with 16S FISH, as done in Chapter 3. This combination enabled the identification of zombie cells, because the cell's host cells were lacking a 16S FISH signal. Additionally, study-

[2] As a reminder: Viruses infect all domains of life. Those infecting bacteria are called phages. Those infecting Archaea are called viruses. In this section, I will use the most precise term, wherever possible.

ing the intracellular location of the direct-geneFISH signal in an infected cell, may hint toward the intracellular organization of virus replication, which has previously been demonstrated with other imaging techniques (Banas et al. 2023; Chaikeeratisak et al. 2017). Last, direct-geneFISH allows to estimate the intracellular virus gene density in infected host cells, which could indicate virus burst sizes (i.e., how many new virus particles are produced) and would be a valuable ecological insight. The virus gene density could be assessed similarly to the ribosomal content of bacterial cells (Chapter 2) by measuring the fluorescence intensity of the direct-geneFISH signal, which may be combined with the signal area. Direct-geneFISH not only facilitates taxon-specific quantifications in environmental samples but also paves the way for groundbreaking insights into virus-host interactions and deeper insights into viral ecology.

In this thesis, I have only demonstrated the identification of phage-infected host cells. However, it is possible to visualize different infection states, including the quantification of 'free' phages that are not intracellular. Previous research has visualized an entire infection cycle of a virus infecting *Candidatus* Altiarchaeum in a low-complexity environment (Rahlff et al. 2021; Turzynski et al. 2023). Additionally, the identification of free phages has first been shown with the antibody-based geneFISH approach (Allers et al. 2013). In a similar way, I previously designed direct-geneFISH probes for phage Baltilda (Table S5.1), which infects the gammaproteobacterial host *Psychromonas arctica* (Bartlau 2020). Phages from the phage lysate (i.e., 0.2 µm filtrate) were immobilized on 0.02 µm filters and subsequently hybridized using direct-geneFISH, following the methods in Chapter 3 of this thesis with Baltilda-specific probes (Table S5.1) and UNK probes of unknown function (Barrero-Canosa et al. 2017) as a negative control (Fig. 5.2). A detection efficiency of ∼55% could be achieved (data not shown; quantified using automated microscopy), demonstrating the feasibility of quantifying free phages. While some signals appear larger, as two or more phages aggregated, phage signals in generally appear larger than their physical size, which was also previously shown (Allers et al. 2013). This is partly due to the point spread function, increasing the appearance of objects, which are smaller than Abbe's diffraction limit of light[3].

Direct-geneFISH may be combined with different microscopy techniques and can detect phages in different environments. The above-mentioned visualization of virus infection in *Ca.* Altiarchaeum was later combined with electron microscopy, using the advances of both microscopy methods (Banas et al. 2023). In a different example, correlative imaging of direct-geneFISH and electron microscopy has enabled the observation of virion phagocytosis by a sponge, with the sponge actively altering the phage-to-microbe ratios (Jahn et al. 2021). In future projects, direct-geneFISH could be used to visualize and localize viruses in different environments, which could be an advantage of direct-geneFISH over the polony method. For example, the phage-to-bacteria ratio in cnidarian mucus is enriched compared to the surrounding

[3]Resolution is constrained by Abbe's diffraction limit of light: $d = \frac{\lambda}{2n\ sin\alpha}$, where d is the resolution, λ the excitation wavelength and $n\ sin\alpha$ can be approximated with the numerical aperture of the objective (n is the refractive index of the medium and α the angular aperture of the objective; Abbe 1873). Hence, the resolution is ∼250 nm for DAPI with an excitation maximum at 358 nm and a microscope with a numerical aperture of 1.4.

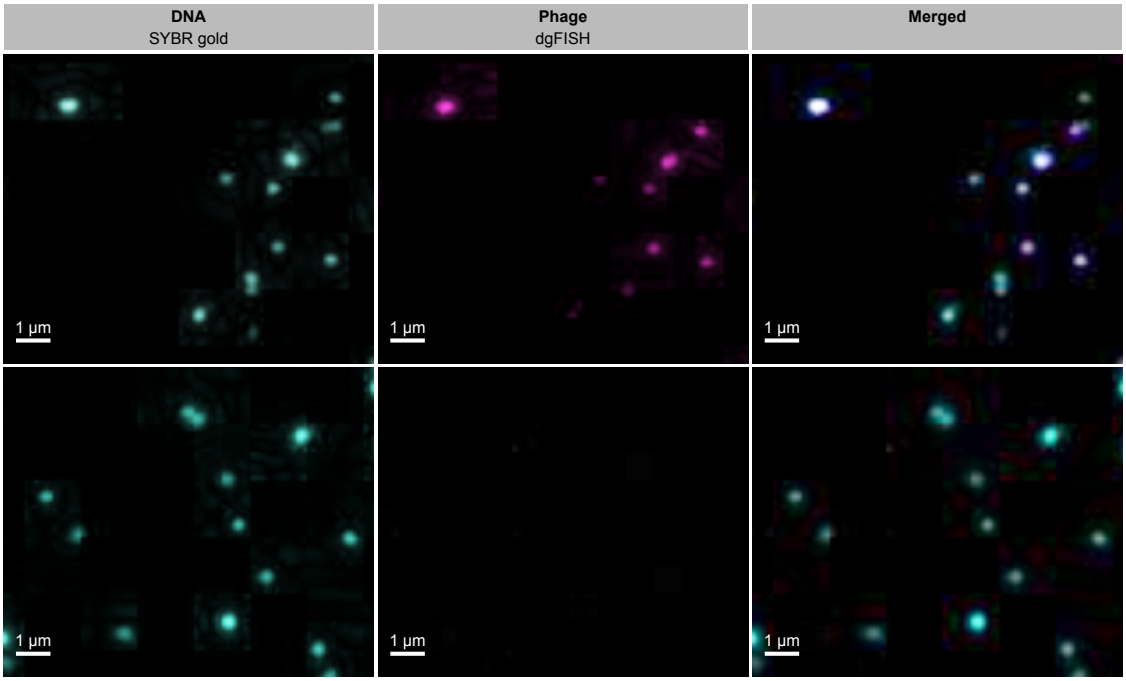

Figure 5.2: Microscopy images of free phages. Automatically recorded microscopy images of phage Baltilda (Bartlau 2020). Phages from a 0.2 µm filtrate were immobilized on 0.02 µm AnoDisc filters. DNA of phages was stained with SYBR gold and hybridized using direct-geneFISH (Alexa594). Top: Hybridization with Baltilda-specific probes. Bottom: Hybridization with UNK probes (Barrero-Canosa et al. 2017) that served as a negative control. Images were recorded on a Zeiss AxioImager.Z2m (further specifications see Chapter 3).

water, as the phages contain Ig-like domains that bind to mucin glycoproteins (Barr et al. 2013). In a similar manner, particles in the water column are enriched in phages and other viruses (Breitbart 2012). Metagenomics suggests that the taxonomic composition of these communities differ significantly from free-living communities (Breitbart 2012; Coutinho et al. 2023; Salazar et al. 2016), which could be tested using direct-geneFISH. Additionally, the rate of infected cells could be determined, if combined with 16S FISH as in Chapter 3. Direct-geneFISH is a versatile and powerful tool, offering unparalleled insights into the spatial and ecological dynamics of viral infections across diverse environments.

Improvement of sequencing technologies and bioinformatic tools

While microscopy methods continue to be the gold standard for quantifying viruses, bioinformatic approaches are required to study the taxonomic and genetic diversity, which in turn enable probe or primer design for *in situ* quantifications. Several newly developed bioinformatic tools allow the identification of viruses in environmental metagenomes and metatranscriptomes, such as VirFinder (Ren et al. 2017), VirSorter (Roux et al. 2015), VIBRANT (Kieft et al. 2020), Phigaro (Starikova et al. 2020), DeepVirFinder (Ren et al. 2020), and COBRA (Chen and Banfield 2024), while others improve the annotation of viral hypothetical proteins (Flamholz et al. 2024;

Terzian et al. 2021). Extensive metagenomic studies have explored the genetic and taxonomic diversity of phages and have discovered hundreds to thousands of unknown viruses (Hurwitz and Sullivan 2013). Additionally, digital PCR (Tadmor et al. 2011), qPCR (Matteson et al. 2013; Rozon and Short 2013), and metagenomic approaches aim to provide quantitative estimates of virus abundances from metagenomes (López-García et al. 2023). However, there are still uncertainties in bioinformatic quantifications and discrepancies to microscopy-derived results (Chapter 3; Roux and Brum 2023). In efforts to close the gap, Roux and Brum (2023) propose using spike-ins during sequencing and more paired microscopy- and sequencing-based studies, as done in Chapter 3. Generally, a combined approach of quantifications derived from microscopy with diversity assessments utilizing sequencing methods is needed to progress taxon-specific viral ecology.

The full virus approach

Methodological advances have enhanced our ability to detect and quantify viruses, including phages, in environmental samples, as discussed above (see also: Turzynski et al. 2021). Following the example of the full ribosomal approach, we have reached the era of the full virus approach (Fig. 5.3). Improvements in sequencing technologies, in conjugation with better bioinformatic tools, allow the identification of putative novel viruses, as well as improved phylogenetic analyses and taxonomies (Turner et al. 2021). Bioinformatic approaches may assess community compositions, while visualization techniques are required for quantifications and localizations (see above). This is the second major step of the full virus approach. Direct-geneFISH probes or (degenerate) primers for the polony method are designed *in silico*, which will improve with expanding databases over time. Free viruses or virus-infected cells can be identified with direct-geneFISH or the polony method. The full virus approach has already been used in a few studies, including this thesis. For example, although *Greip* has been isolated, it was not accessible to us. Nevertheless, I successfully designed direct-geneFISH probes and detected *Greip*-infected cells in the environment. Other examples include the above-mentioned viruses of *Ca.* Altiarchaeum (Banas et al. 2023; Rahlff et al. 2021) and cyanophages (Baran et al. 2018; Mruwat et al. 2021). The complete virus approach contains all aspects of diversity assessment up to the identification and quantification of viruses in environmental samples.

5.1.3 Species-specific grazing by eukaryotes

Grazing by bacterivorous predators is the second main mortality factor for free-living bacteria, besides phage-mediated lysis. As this thesis focuses on taxon-specific growth and mortality processes, I want to briefly review the literature on species-specific grazing by eukaryotes. This is motivated by the results of Chapter 2, indicating that mortality (including grazing) recycles up to 90% of bacterial biomass production each day.

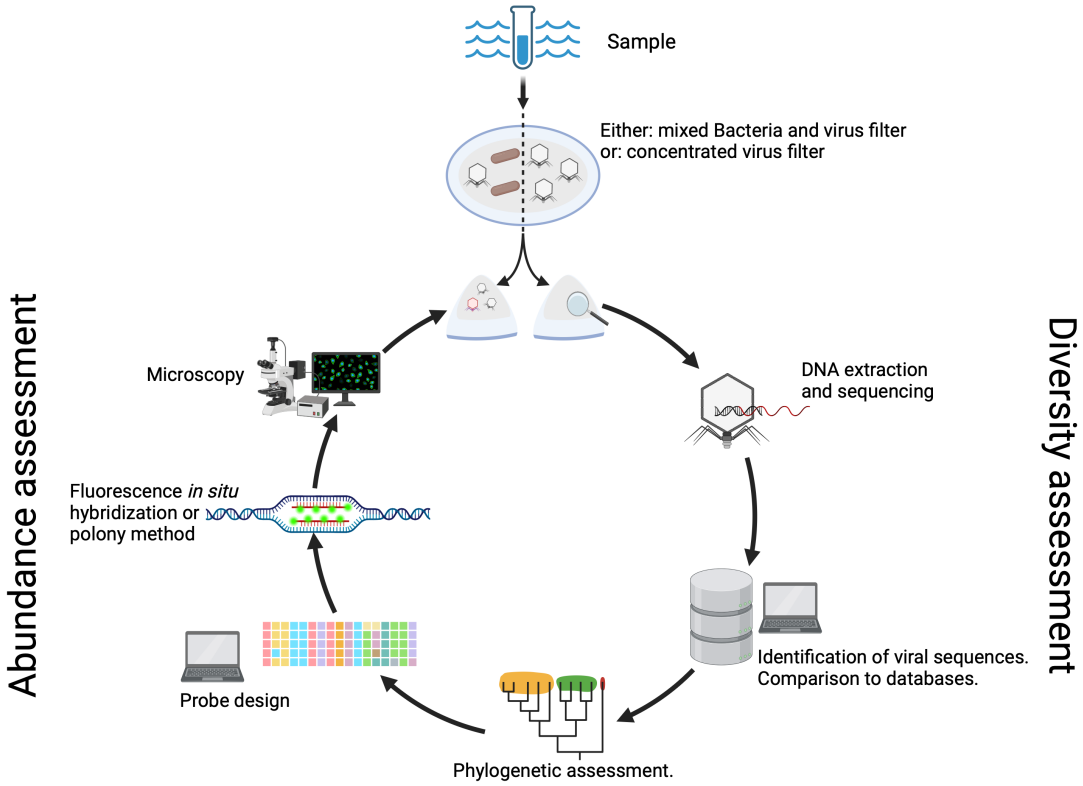

Figure 5.3: The full virus cycle, following the example of the full ribosomal approach. The aim is to identify viruses from sequencing information and quantify and visualize them by molecular techniques. Created with BioRender.com.

Some ciliates have a taxon-specific food preference, which would lead to species-specific mortality. In laboratory experiments, the ciliates *Chilodonella* sp. and *Tetrahymena* sp. had a preference for *Pseudomonas costantinii* over *Serratia plymuthica* (Dopheide et al. 2011). Another laboratory-based study found a food preference for gram-negative bacteria by some protists, demonstrating the impact of cell wall structure on prey selection (Hirakata et al. 2020). Similarly, surface properties of SAR11 have been shown to reduce the clearance by cnidarians (Dadon-Pilosof et al. 2017). To simultaneously identify the flagellate predator and bacterial prey in environmental samples, double CARD-FISH hybridizations may be used (Ballen-Segura et al. 2017; Beisner et al. 2019; Koppelle et al. 2022; Piwosz et al. 2021). For example, Ballen-Segura et al. (2017) used CARD-FISH to identify a preference for archaeal cells by some mixotrophic flagellates in high-mountain lakes, while mixotrophic and heterotrophic flagellates from an oligotrophic Antarctic lake preferred *Alphaproteobacteria* over *Bacteroidota* (Gerea et al. 2013). While these findings emphasize the complex nature of microbial predation, little is known about selective feeding by planktonic marine grazers.

5.2 New insights into SAR11 ecology

Bacteria of the SAR11 clade have long been thought to be slow-growing oligotrophs. Pure cultures of *Ca.* P. ubique grow at 0.5 cell divisions d^{-1} in the laboratory (Carini et al. 2013; Rappé et al. 2002), which can be increased by ∼70% in co-cultures with *Prochloroccucs* (Becker et al. 2019). Slow growth rates (max. 0.7 cell divisions d^{-1}) were further supported by dilution experiments from environmental samples (Teira et al. 2009). In Chapter 2, I report contrasting information and demonstrate cell division rates of up to 1.9 cell divisions d^{-1} for SAR11 before and during a phytoplankton spring bloom. Our findings are in line with other studies reporting fast growth rates (1.5 to 1.8 cell divisions d^{-1}, Ferrera et al. 2011; Sánchez et al. 2020; Sánchez et al. 2017) of SAR11 in environmental samples with altered resource availability and removal of mortality factors. Further support comes from numerous studies finding high metabolic activity of SAR11, when assessed by labeled substrate uptake rates (Laghdass et al. 2012; Malmstrom et al. 2005; Malmstrom et al. 2004; Mary et al. 2006).

SAR11 cell division rates reported in this thesis were comparable to known copiotrophic taxa that respond fast to phytoplanktom blooms, such as *Bacteroidota* and *Aurantivirga*. However, while the copiotrophs had high cell division rates days before the *in situ* cell abundance increased, SAR11 had fast cell division rates during unexpected times: They started to increase their division rates two to three weeks before the phytoplankton bloom (i.e., the increase of chlorophyll a) in both assessed phytoplankton blooms in 2018 and 2020 (Chapter 2). The same phenomenon was observed during the Helgoland phytoplankton spring bloom 2022 (Fig. 5.4, Fuchs et al. *unpublished*). The question is: What enables the early start of high cell division of SAR11?

5.2.1 What enables the early start of high cell division of SAR11?

Phytoplankton spring blooms are enabled by high nutrient concentrations, increasing temperatures, and increasing light availability. During the blooms, phytoplankton release great amounts of organic matter, which fuels a diverse heterotrophic bacterial community. However, SAR11 start to increase their cell division rates well before the phytoplankton bloom, as discussed above, and are the only taxonomic group to do so (Chapter 2). What enables SAR11 to increase their cell division rate? What do they use as a carbon source? I propose that the discrepancy can be explained by three main factors (Fig. 5.5):

1. Increased light availability and proteorhodopsin-dependent ATP synthesis
2. Increasing but generally low production of organic matter by phytoplankton and high-affinity substrate uptake by SAR11, and
3. An internal cycling of organic matter, probably triggered through phage-induced lysis.

SAR11 contain proteorhodopsin and are capable of proteorhodopsin-dependent ATP synthesis (Giovannoni 2017). While lab-based assays suggested that light availability does not support

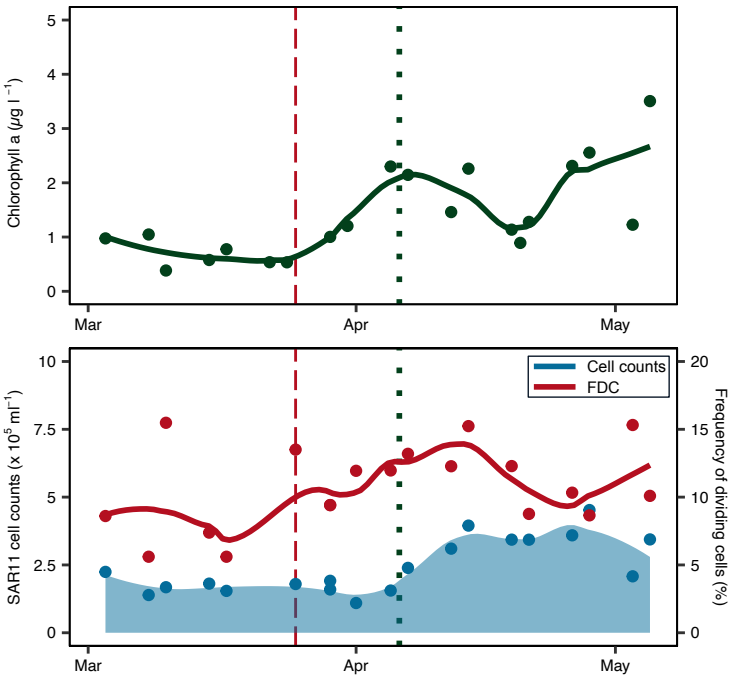

Figure 5.4: The 2022 Helgoland phytoplankton spring bloom. Chlorophyll a concentrations (upper panel), SAR11 cell counts (blue), and SAR11-specific frequency of dividing cells (FDC, red) were determined as described in Chapter 2. Raw values and *loess* smoothing are visualized. Red dashed line represents the start of increased SAR11 FDC, green dotted line represents increased chlorophyll a values. Data courtesy of Fuchs et al. (*unpublished*).

SAR11 growth (Steindler et al. 2011), environmental growth experiments found that light availability had the biggest positive effect on SAR11 cell division rates, compared to other taxa (Sánchez et al. 2020). In fact, this is similar to the observation that only SAR11 had increased cell division rates before the phytoplankton blooms, although many more bacteria have the ability of proteorhodopsin-dependent ATP synthesis (Dupont et al. 2012; Song et al. 2015). Incubation experiments with labeled CO_2 and subsequent Raman profiling of environmental samples revealed rapid uptake and incorporation of ^{13}C by SAR11 (Jing et al. 2022; Jing et al. 2018). SAR11 may be capable of anaplerotic CO_2 fixation and the authors found large parts of the Calvin-Benson cycle in SAR11 MAGs from their experiments. However, the authors could not exclude that labeled CO_2 was fixed by phytoplankton, e.g., *Synechococcus*, and the products metabolized by SAR11 (Jing et al. 2018).

Above a threshold of 25 (Chapter 2) to 35 Einstein $m^{-2}d^{-1}$ (Lami et al. 2009), SAR11 benefits from the increasing light intensities. This is in the same order of magnitude as required to initiate a phytoplankton bloom ($\sim$35 Einstein $m^{-2}d^{-1}$) at the latitude of Helgoland in the North Atlantic (Siegel et al. 2002). In early phases of the bloom, phytoplankton abundances and chlorophyll a levels are low but carbohydrate analysis revealed the production of organic matter at low concentrations (Fig. S5.1, S5.2; Sidhu et al. 2023). Hence, the harvested light energy

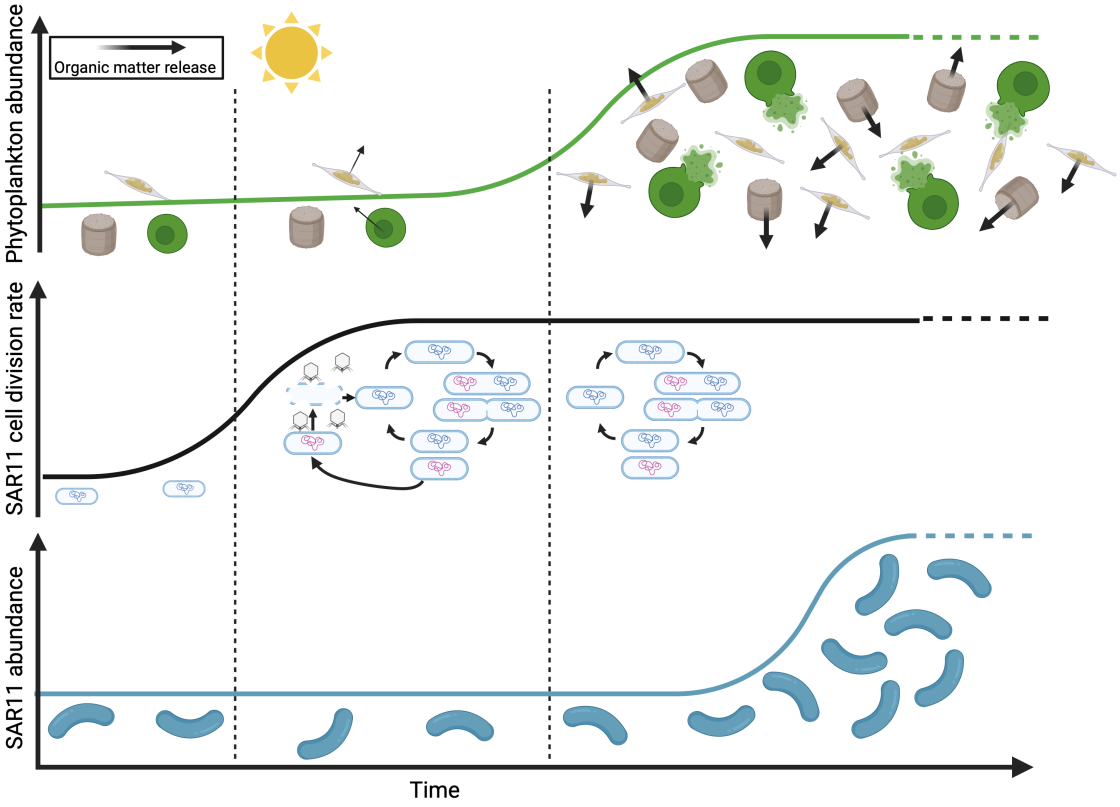

Figure 5.5: Conceptual overview of what fuels the increased SAR11 cell division before the phytoplankton bloom. Y-axis represents time over a phytoplankton spring bloom. The sun pictogram indicates the threshold of increased light availability enabling phytoplankton growth. Top: Phytoplankton abundance. Thick and thin arrows from the phytoplankton cells visualize amount of organic matter produced by phytoplankton. Middle: SAR11 cell division rate. Bottom: SAR11 cell abundance. Dashed lines indicate the beginning of increased SAR11 cell division and increasing phytoplankton abundances, respectively. Created with BioRender.com.

could fuel the import of phytoplankton-derived organic matter at low concentrations. In fact, high expression levels of high-affinity ABC and TRAP transporters within SAR11 have previously been reported during a phytoplankton bloom (Teeling et al. 2012).

In an attempt to find a target molecule facilitating rapid SAR11 cell division rates for this thesis, I queried the carbohydrate abundance data from the 2020 phytoplankton bloom (Sidhu et al. 2023). The data suggests an increase in fucoidan (Supplementary Text), which is most likely no substrate for SAR11, as it requires a whole array of specific enzymes to be digested and metabolized (Orellana et al. 2021; Sichert et al. 2020). Additionally, observed increases of β-1,3-D-glucans (e.g., laminarin) would be a substrate for many bloom responders, although this might be impeded by low concentrations. There are additional trends which only allow vague hypotheses and are not further discussed here (Supplementary Text, Fig. S5.1, S5.2). For better chances to find a target molecule, future studies could assess expression levels of substrate binding proteins, which are known to provide SAR11 with a high probability of using substrates at low concentrations (Bosdriesz et al. 2015; Noell and Giovannoni 2019). Additionally, future

studies could measure glycine, pyruvate, or other low molecular-weight compounds, including one-carbon compounds, as they are known to facilitate SAR11 growth (Sun et al. 2011) and are produced by phytoplankton (Mincer and Aicher 2016).

Next, an internal organic matter cycling could enable fast growth rates before the phytoplankton blooms in SAR11. In Chapter 3, I could show that phage-mediated mortality likely prevents the increase in SAR11 cell abundances. The resulting released organic matter could, thus, fuel other SAR11 cells. This system is not a perpetuum mobile, as light-harvested energy and low concentrations of organic matter (see above) are available.

Supporting evidence comes from carbon flux models based on environmental data from previous Helgoland phytoplankton blooms (Eigemann et al. 2024; Mayerhofer et al. 2021). During phytoplankton blooms, organic matter consumption by bacteria is almost equal to the production by phytoplankton. However, during non-bloom situations, heterotrophic bacteria consume >3-times the organic matter produced by phytoplankton, indicating an internal cycling of organic matter (Eigemann et al. 2024). Additional support was recently brought forward based on metatranscriptomic data (Beidler et al. 2023). Although the focus of the latter study is not SAR11, both studies provide evidence for the internal cycling of organic matter within the microbial loop.

To summarize and conclude, SAR11 increase their growth rates before the assessed phytoplankton spring blooms, which is counterintuitive. Increasing light availability and the proteorhodopsin-based ATP synthesis by SAR11 probably yield the required amount of energy, while low concentrations of phytoplankton-derived organic matter and a phage-mediated internal cycling of organic matter could provide fixed organic carbon (Fig. 5.5).

5.2.2 Are SAR11 defense specialists?

The idea that SAR11 might be resistant to viral lysis (Suttle 2007) has persisted and shaped the narrative of the scientific literature, despite the first isolation of pelagiphages in 2013 (Zhao et al. 2013). More recently, Zhong et al. (2023) found that extracellular 16S rRNA copy numbers were low compared to their intracellular counterparts. The authors offered the possible explanation of below-average phage-induced lysis rates in SAR11. Although it needs to be elucidated whether other phage-host systems also result in zombie cells, the here-introduced phenomenon of zombie cells in SAR11 serves as an alternative explanation to the observation of low extracellular 16S rRNA copy numbers. Zombies are ribosome-deprived cells and will not release 16S rRNA copies into the environment upon lysis.

Recent studies provide further evidence for a high impact of phages on the SAR11 community and found a greater effect of phages on SAR11, than *Roseobacter*, *Gammaproteobacteria*,

or *Bacteroidota* (Ferrera et al. 2011; Sánchez et al. 2020). In this thesis, highest numbers of phage-infected cells were identified when cell division rates of the host cells were the fastest, reminiscent of the 'killing the winner' mechanism (discussed in Chapter 3). It should be noted that other known pelagiphages may behave differently than those tested in this thesis. Last, the here-assessed time series revealed that phage infection patterns during spring blooms may be acute and short-term, as previously suggested by metagenomics (Bartlau et al. 2022). This could indicate that the effect of the pelagiphages on their host might easily be underestimated when samples are taken at the wrong time.

Besides mortality by phages, bacteria are exposed to grazing by eukaryotes, too. A common defense mechanism in sediment or freshwater microbiomes includes forming filaments, which are too large for protists to ingest (Kiørboe 2024). SAR11, on the other hand, was thought to evade grazing by eukaryotes through their small cell sizes. Additionally, it has been shown that the hydrophobicity of the SAR11 cell surface reduces the clearance rate by cnidarians (Dadon-Pilosof et al. 2017), which is in line with SAR11 being defense specialists. However, the above-mentioned studies (Ferrera et al. 2011; Sánchez et al. 2020) show that eukaryotic grazing, besides phage-induced lysis, is an important mortality factor in reducing SAR11 cell abundances. Future research should focus on taxon-specific prey preferences by eukaryotic grazers, as discussed above. To conclude, in this thesis, I provide multiple lines of evidence that SAR11 have cell division rates similar to typical copiotrophic taxa. Additionally, SAR11 *in situ* abundances are substantially shaped by phage infections and potentially eukaryotic grazing. Hence, it can be concluded that they are most likely not general defense specialists.

5.3 Zombie cells

Despite their notable global abundance, discovering zombie cells was a surprise. It required multiple methodological verifications to accept the validity of the discovery confidently. These verifications included the confirmation of high hybridization efficiencies (>90%) with 16S FISH in uninfected controls, the observation of zombie cells in pure cultures (both Fig. 3.1), ruling out the possibility of cross-infection to other taxa than SAR11 (Fig. S3.3), and their global distribution in all analyzed data sets (Fig. 3.4). This rigorous validation process solidified their existence and importance for microbial ecology.

Are zombie cells not simply virocells? A virocell is a virus-infected cell whose purpose is to build new virions instead of two new cells (Forterre 2011; Forterre 2021). Based on the current understanding, zombies are a stage of phage infection with very little to no ribosomes. Thus, virus capsid proteins need to be produced before a cell enters the zombie stage, as zombie cells would not be able to produce them. In a personal communication, Patrick Forterre suggested referring to the zombie cells as 'dead virocells', which I found less indicative than the term zombie cells. The term zombie has been inspired by the zombie apocalypse film genre, with origins tracing back to

the movie *Night of the Living Dead* (1968). When one of the main characters (Karen) died, she became a zombie herself and started killing her loved ones. Thus, zombies are in a state of being 'dead', yet with the ability to kill their peers.

5.3.1 The emergence of zombie cells

Different possibilities for the emergence of zombie cells have thoroughly been discussed in Chapter 3. Here, I briefly outline the most parsimonious explanation, namely the use of RNA as a resource for phage genomes, with an emphasis on the phage replication cycle. The phage attaches to and inserts its genome into the host cell (Fig. 5.6). Early genes are immediately produced, followed by middle genes, including the DNA polymerase. Until this point, there is no difference between textbook knowledge and zombie cells. However, between the middle and late genes, the phages include the transcription of ribonucleotide dehydrogenases and an exonuclease (see Chapter 3). Structural proteins are being produced and putatively in parallel, host ribosomal and other RNA are digested. The nucleotides are converted to deoxyribonucleotides by the dehydrogenases described above (Fig. 5.6). All viruses, including phages, require the host ribosomes for protein synthesis. Hence, the timing of the ribosome degradation is essential. Digestion of ribosomes too early would result in no structural phage proteins being synthesized. In contrast, too late ribosome digestion would be useless, as the valuable resources would be unavailable for phage genome synthesis. Due to the importance of ribosomes for phage propagation, I propose that the use of ribosomal RNA is rather a side-effect of using RNA in general as a resource for phage genome synthesis. As a consequence, not every phage infection results in a zombie cell. Further experiments to test this hypothesis are suggested in the Outlook.

Is the use of RNA necessary? Nucleotides are generally scarce. For example, cyanophages contain photosynthesis genes and thereby increase the photosynthetic activity of their hosts. However, instead of boosting carbon fixation, the excess energy is used for nucleotide synthesis to subsequently produce new cyanophage genomes (Lindell et al. 2004; Puxty et al. 2015; Thompson et al. 2011). The genome size of the cyanobacterial host is approximately double that of SAR11, while their phage genome sizes are comparable to the pelagiphages. Hence, the use of RNA as a resource could be an alternative to the altered photosynthetic machinery in cyanophages and underscored that RNA is a valuable resource for producing phage genomes.

5.3.2 Zombie cells in microbial ecology

"Who is out there and how many" are two fundamental questions in microbial ecology. The general bacterial probe (EUB338 I-III) is frequently used as a positive control in 16S FISH experiments (Amann et al. 1990; Daims et al. 1999). The analyses regularly result in 5 – 30% of DAPI-stained cells without a 16S FISH signal, which I will refer to as the "EUB/DAPI mismatch" in this paragraph. It was argued that the EUB/DAPI mismatch could be the result of: i) Low

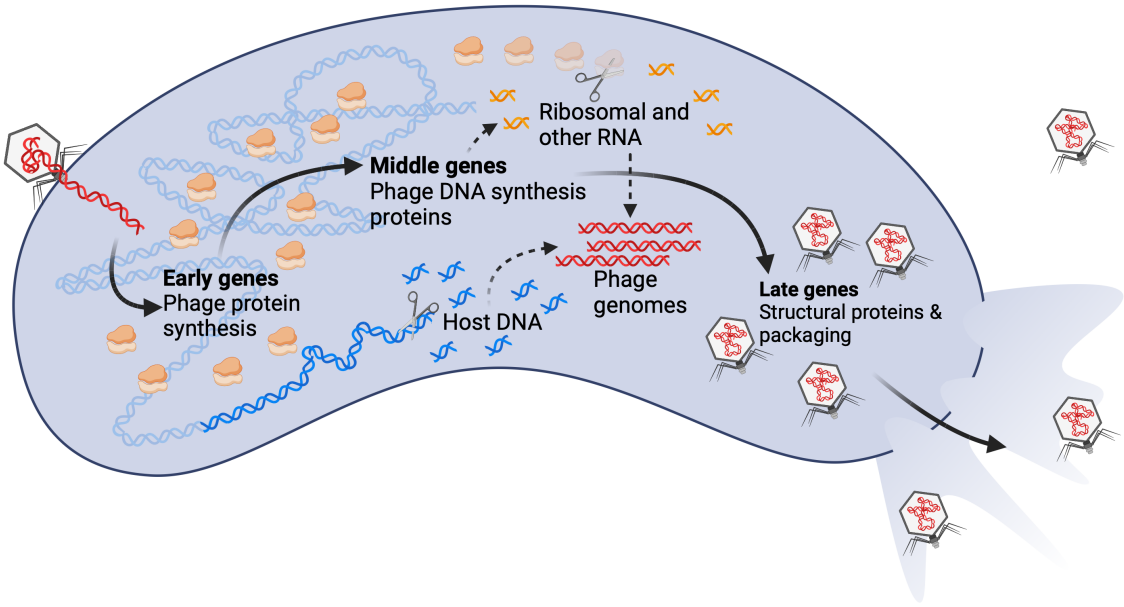

Figure 5.6: Conceptual phage infection in SAR11, which leads to the formation of a zombie cell. The figure should be read as a timeline from left to right. Between middle and late genes, RNA nucleotides are processed to be available for phage genome synthesis. Created with BioRender.com.

hybridization efficiency or low signal intensities of 16S FISH. In other terms, the cells were considered false negatives and not correctly identified. ii) DAPI staining double-stranded DNA from giant viruses, extracellular vesicles, or other residues of lysed cells. iii) 'ghost cells', which lack a nucleoid (condensed DNA; Zweifel and Hagström 1995). The authors argued, the observed DAPI staining could be a false positive result of DAPI binding to reactive bacterial surfaces.

The discovery of zombie cells adds a new explanation for the frequently observed EUB/DAPI mismatch. In the Helgoland 2020 spring bloom analysis, zombie counts reached up to 14% of the total cell counts (4th May, 2020), while the fraction of SAR11-positive cells was extremely low. Across all samples analyzed in Chapter 3, SAR11-derived zombies contributed ∼4% of total cell counts, accounting for a substantial proportion of DAPI-positive total cell counts. During my thesis, I focused on three pelagiphages, two of which were available as a pure culture. Both of these exhibited the phenomenon of zombie cells, while 16S staining patterns of the negative control (HTVC023P) also suggest the occurrence of zombie cells (Table S1 from Chapter 3). Additionally, it is possible that other phages, not infecting SAR11, cause a similar phenomenon within their hosts. For example, a recent study traced an infection of T4 phages within *Escherichia coli* cells using a combination of direct-geneFISH and 16S FISH (Grodner et al. 2023). The authors noticed a decreasing ribosome content in T4-infected cells, which is highly reminiscent of the proposed pathway of zombie cells. The discovery of zombie cells, which is most likely not limited to the three examples assessed in this study, is an additional plausible explanation for the EUB/DAPI mismatch and underscores the unexplored complexities in microbial ecology.

5.4 Concluding remarks

Microorganisms and their viruses have a profound impact on the biogeochemical cycles of the oceans and, thus, the global climate. A thorough understanding of their activity is required to comprehend their impact on the environment. This thesis demonstrates how multiple fluorescence microscopy-based methods can be used to study the bacterial life cycle, as well as microbial and viral activity. The era of taxon-specific viral quantifications in complex environmental samples has begun. Future studies should continue to use the orthogonal approaches of diversity assessments from sequencing data and quantifications with microscopy techniques. The insights from this thesis concerning the dynamics of SAR11 and their phages highlight the significance of considering both cellular and viral components to fully understand microbial ecosystems. In addition, the discovery of 'zombie cells' underscores the hidden complexities in microbial ecology that await discovery by future research.

5.5 Outlook

In this thesis, I discovered zombie cells, which are phage-infected but ribosome-deprived. The possibilities of their origin have been discussed and I propose the following experiments to further elucidate their origin. Briefly, zombie cells are either a result of an abortive infection (i.e., a phage-defense mechanism) or a result of RNA usage for phage genome synthesis. Staining phage-infected and zombie cells with an RNA-specific dye might prove either hypothesis. SYTO RNASelect is the only commercially available RNA-selective stain. As an alternative, Cesaretti et al. (2023) introduced a novel compound with 100x brighter fluorescence when bound to RNA, compared to DNA. If RNA nucleotides are used for phage genome synthesis, the RNA-specific signal would be absent or significantly reduced in zombie cells.

Secondly, electron microscopy images of phage-infected and zombie cells might unravel distinct morphological features, which could hint towards the origin of zombie cells. If zombie cells can be distinguished by their morphology, TEM could reveal, whether phage particles are produced, as this remains a hypothesis at present. Thirdly, more phage-host pairs should be analysed (e.g., using direct-geneFISH) to test whether zombie cells are unique to pelagiphages and their hosts or if they are a common phenomenon.

Independent of zombie cells, there are many more pelagiphages and other phage host pairs to be studied. As the identification of zombie cells demonstrates, many more discoveries are waiting to be made. One (I) could easily open an entire research group, focusing on the quantification of viruses and their microbial hosts in the environment, using the full virus approach. The orthogonal approaches of diversity assessments by sequencying efforts and quantifications via

direct-geneFISH or the polony method will facilitate many exiting results.

As a next step, I would aim to target larger taxonomic groups by direct-geneFISH. Currently, the method is constrained by the number of fluorophores for sufficient detection, which in turn requires many polynucleotides as probes. A signal amplification, for example by a branched hybridization chain reaction (HCR) with non-labeled helper probes, as recently suggested (Grodner et al. 2023), could allow to reduce the number and length of direct-geneFISH probes. With this signal amplification, probes as short as primers could be used to detect greater phylogenetic groups.

Last, phage-infected cells in environmental samples were visualized and quantified using direct-geneFISH in this thesis. In the next step, free phages (i.e., extracellular phages) should be quantified using direct-geneFISH. The possibility of visualizing and counting free phages was exemplified in this discussion. For marine planktonic samples, I suggest to start targeting pelagiphages, as they are predicted to be the most abundant phages in the ocean (Martinez-Hernandez et al. 2019; Zhao et al. 2013). Research questions could address: How many free phages of a certain taxon can be found in the water column? Is the number of free phages correlated to the number of phage-infected cells? If not, what are the factors influencing the absorption and/or penetration of host cells?

5.6 Supplementary Material

5.6.1 Supplementary Text

Monosaccharide and high molecular weight dissolved organic matter (HMWDOM) composition from the 2020 phytoplankton bloom

The monosaccharide analysis is based on acid hydrolysis of HMWDOM and subsequent high-performance anion exchange chromatography with pulsed amperometric detection (HPAEC-PAD). It revealed an increase in fucose, galactose, and mannose (Fig. S5.1). Fucose could indicate an increasing concentration of fucoidan, which is most likely no substrate for SAR11, as it requires a whole array of specific enzymes and bacterial microcompartments to be digested and metabolized (Orellana et al. 2021; Sichert et al. 2020). The HMWDOM analysis is based on carbohydrate microarrays and polysaccharide-specific monoclonal antibodies (Vidal-Melgosa et al. 2021). It found an increase in β-1,3-D-glucans (e.g., laminarin), β-1,4-D(galacto)(gluco)mannan, alginate, and cellulose. An increase in alginate was only detected by the epitope BAM7, which has a known cross-specificity for fucose-containing sulfated polysaccharides (Torode et al. 2016). Other alginate-specific antibodies (BAM6, BAM8, BAM9, BAM10, BAM11, Table 5.2) showed little increase. Further, it would be expected that laminarin would fuel the growth of many other bloom responders, too, although this might be impeded by concentrations that are too low. Next, SAR11 cell division rates decreased during the bloom, which co-varied with signal intensities of epitopes LM21, which bind to glucomannan and galactomannan (Marcus et al. 2010), and CBM3a, which binds to cellulose and xyloglucan (Hernandez-Gomez et al. 2015). All these carbohydrates are commonly detected in diatoms, or green algae, including macroalgae (Baghel et al. 2021; Chiovitti et al. 2005; Mikkelsen et al. 2014). This might indicate an increased abundance of algae, which could not be detected by algal biovolume/abundance estimates (Sidhu et al. 2023). Additionally, the extraction via NaOH denotes that the substrate might not be available to the planktonic community, but bound in particles. Nevertheless, CBM3a detects cellulose, which is a relatively simple substrate of beta-1,4-linked glucose units and is predominantly taken up by SAR11 and other *Alphaproteobacteria* in the North Sea (Alonso and Pernthaler 2006).

5.6.2 Supplementary Tables

Table 5.1: Direct-geneFISH probes for phage Baltilda. Purified lysate samples of phage Baltida (infecting *Psychromonas arctica*) were stained with direct-geneFISH probes.

Probe name	Sequence (5' → 3')
Psy_111_A_1	ATGACAGACGAAAACGTAATTTCAATCACAGCAAACGGTGCTTC AGTTAGAGAAGCCGTTAATAACATCATTACCAACAGCAACTACA CACAAGCGGCTATTGCTCGTGAAACGTCTATTGGTAAAGCGCGTT TATCTCAATTTTTATCTAATAGCTACACAGGCGACAACGGTCCGA TTATTAGCACACTAGCGCAGTGGATTGAGTTGCACAGCAACAAA CAAAATATCATGCCCTCTGCTCCTGATTTTGTTCACACCACTACC GCTAAACAAGTGATCTCAACATTACGTTATGCAC
Psy_111_A_2	AAGCCGTGGCGATGGTATGAGCGTGGTTATGGGTGCGCCTGGTG TAGGTAAAAGCGCAGCGGCTAAATACTACGCCGACAAAATGCCT AACTGTTGGTTGATTGTTGCCTCTCCAAGTATCTCAGGCTTGATC GGTTTCTTTTATGAATTGGCATTAGAACTAGGCATTGAAAATGCT CCTCGCCGTAAAGACTCACTTTGCCATGCTATTCGTCATCGTTTA GCAGGCTCTAATGGCCTTATCGTGATTGATGAAGCAGACCATCTG CAACTGGAAGTCATTGAAGAGTTGCGCGTGA
Psy_111_A_3	AGATGGTGGGAGACTCAAGAAAAGTAGACCTTTCACGTCTTGAA TCTCGCATAGCCAAACGCCTATCAATACCCAAAGTTAAAAAAAG CGATATCACCTCAATTGCCACAGCATGGGGATTAACAAGCGCCC TTGAAATGGCTTTGATTGAAAAGATAGCAGGAAAGCGCGGCCAG TTAAGAAAGCTTAGCCACACACTGCGCCTTGCTTCAATGATTGCG CAAGGCTGTAACGAACGCATGAGCGAGGCCCATATTAGAGACGC ATTTAACGACCTAAAACAAGGAGGAAATGACCATGT
Psy_111_A_4	GGCTTACCCAGTATCACTAAATACACTTAAAGCAAAAATTAACA TCGCCAAAACGCAATTAGGCATGGATGAAGATGTTTACCGTGCA GTCCTAAAAGATGCGACAGGTAAAATTAGCTTGAAAGCAATGAA CCTTGCAGACCACATGATGGTGCTTCATGCAATGGAACAACGCG GGTTCAAAGCAAAAAAGCCAACCGCAAAAAACGGTAAACGGTT ATCAAATCCAAGTAGCCAAACTGCTTTTGCACGTAAACCACAAG ATAAAATAGTCGCAATGTGGATCACCATGAATCGTCA

Probe name	Sequence (5' → 3')
Psy_111_A_5	CGGTTTTGTTGAAGATGGTAGTGAAACAGCTTTAGATAAATTCAT TAATAACCAAACCAAAAGAATGGGCATGTTTGCTGTGACTAGCT TACGTTTTTTAAGCCCGATACAAGCGAGCAAAGTGATTGAAGTG CTTAAAAAGTGGCATATTCGCGAAATGACAAAAGCATTAACACC CTATGAAAAAGTAGCTGTGATGCCTTATCAAGACTTAGTGAATTA CTTTAATAGCGTATTCCCGAGCCTTGACAGCACGCGACACAATA ACCAAGAACAGCAAACAGAGGTTAGCCAAT
Psy_111_A_6	TGCCATTACTAAGCAACTGGCTGCATTGTCAGATGACGATCATCA ATGGTCGGTATTGCGTTGGCCTGAACGTTTGCAAACGCTTTATGC CGTTGTATTGAAGGAACTACAGCATTTGAGTTTTGACGATAACCA TAAACACCGTTTAGCCGTGAATATTATCACCGCTCAGGCGCATTA CTTAGGCGGCCGAGAGTTATACCTACCAACGAATAAAACATTAA AAGAAGCATTACGGGATTTAGATATTTTCAACCGTTTCCACGGGA ATAACATTCCCCAGTTAGCGCGTGAACATAA
Psy_111_A_7	GCTGAACTTGAAAGCGATGAGCGCAAGTTTAACTTAGGTCAACT GCATTCAACCATGCAAAAAGAACTCGCAAGCAATGATCCTTATG TTCGCAGATGGCGACCAACGTTTGGTTACGCTGTTTGTTTGGCAT GGTGCCTGGTCTTTTTTGGGTTGGCCTATGCGATGGTTTTCCATCC TACCGACGCCGCAGAACTGGTTAATAGTGTTGTTGCGCTTACTCC TCTGTTTGGTTTCGCATTAAGTATCTTGGGTATCAGTATTCATAA ACGTTCACTTGATAAACAAGTCATGTCAGGC
Psy_111_A_8	GACTTATTGCCAGATGATGTAAAAAAGCTATTAGATACGTTATTA CGTGATAGCAAGCATTCTCAAAAAGAAATTGTAGAAGCAGTTCA TGCTTATATTGATGAGCAAGGTTATGACGAAAGTATAAAACCCT CGACGTCAGGCGTTAATCGCTATTCTTCAAAAATGGAGAAAGTA GGTAAAAACCTGCGTGAAATGCGTGAAATTTCACAAGTATGGGT TGCCGAGTTGGGCGACAAACCAACGGGTGAAGTCACTAAGTTGG TGCTTGAAATGGGCCGTTCTCAGTTGTTTAAAGCC
Psy_111_A_9	TTTTGATGCGACGGGTAATGGTGGCTATTTAGCGGAACAAGCTTT ACTTAAATACGGCACTGAAATGGTTGATACCGTGATGCTCAATG AAAGATGGTATCGCGAATGGATGCCAAAACTAAAAGCAGAATTT GAAGATGCCAATATTCAATTACCCAAGCACCAAGACAATCTTGA TGATTTACGCCATATCAAAGTGATCAACGGCGTACCAAAAATTG AGAAAGGCAAAAGCAAAGGCGAAGACGGCAAACAGCGTCACGG TGATATGGCTGTTGCCCTCGTCATGGCAATTCGTGC

Probe name	Sequence (5' → 3')
Psy_111_A_10	TAAGTGAAGTGGGTGAATACTTATTAGATATCCACGAACAACGA TTTAAAGATCAAGTGTCGCCAGAGGGAACCCCTTGGAAATCCGT TAGCGCTGAAACCCTTAAAAATAAAACAAGACCTGATCGGATTT TACGTGAAGAAGGTAATCTTGCTGATTTGCTAACTTACCAACTAG GCGACCAACAACTTAGTTTTGGTACTAATTTAGTTTATGGTGCAA CGCATCAATATGGCCGTGCCAGTGCAAATATTGATGCACGTGAA TGGTTAGGCTTAAATGAACAGCAATCACAATCTG
Psy_111_A_11	GAACTATTTAGCGCTTGAACCTTTGCTTGTTGAGAAAATTAAAGC GTTGACTTTGTTTAATGATGTGCTTTCTAGCGAACAACTCAGCAA AATAACCGAAGAAAATCAATCAACACCTTCAGCGCATATTGCGT ACTTGGGCGATGTAATCCAAGACACTAAAGAAGGTGGTTTAGCG AGTAAAGTAAAACAACGTTGGATGGTGGTTATCGCTGTTCAAAC TTTTGATGGTACTGAGACATTGAGCGAAGCAGGTGAATTAATGG GCGCGGTACTTCAACAGTTGCAAGGTTGGGTA

Table 5.2: Full names of epitopes to Fig. S5.1 For further details, please see Additional file 15 in Sidhu et al. (2023).

Epitope	Short name
Partially methyl-esterified/de-esterified HG	JIM5
Non-blockwise partially methyl-esterified HG	LM7
Rhamnogalacturonan I backbone	INRA-RU2
Rhamnogalacturonan I backbone	INRA-RU1
Galactosyl residue(s) on rhamnogalacturonan I	LM16
(1→4)-β-D-galactan	LM5
(1→5)-α-L-arabinan	LM6
(1→5)-α-L-arabinan	LM6-M
Cellulose	CBM3a
(1→3)-β-D-glucan	BS-400-2
(1→3)(1→4)-β-D-glucan	BS-400-3
(1→4)-β-D-(galacto)(gluco)mannan	BS-400-4
(1→4)-β-D-(galacto)(gluco)mannan	LM21
(1→4)-β-D-(galacto)(gluco)mannan	LM22
Xyloglucan (XXXG motif, both galactosylated and non-galactosylated)	LM25
Branched (1,6-Gal) (1→4)-β-D-galactan	LM26
Xylosyl residues	LM23
Alginate - mannuronate-rich epitope	BAM6
Alginate - mannuronate-guluronate	BAM7
Alginate - mannuronate-guluronate	BAM8
Alginate - mannuronate-guluronate	BAM9
Alginate - mannuronate-guluronate	BAM10
Alginate - $\sim$7 guluronate residues	BAM11
Control anti-rat	Rat
Control anti-mouse	Mouse
Control anti-His	His

5.6.3 Supplementary Figures

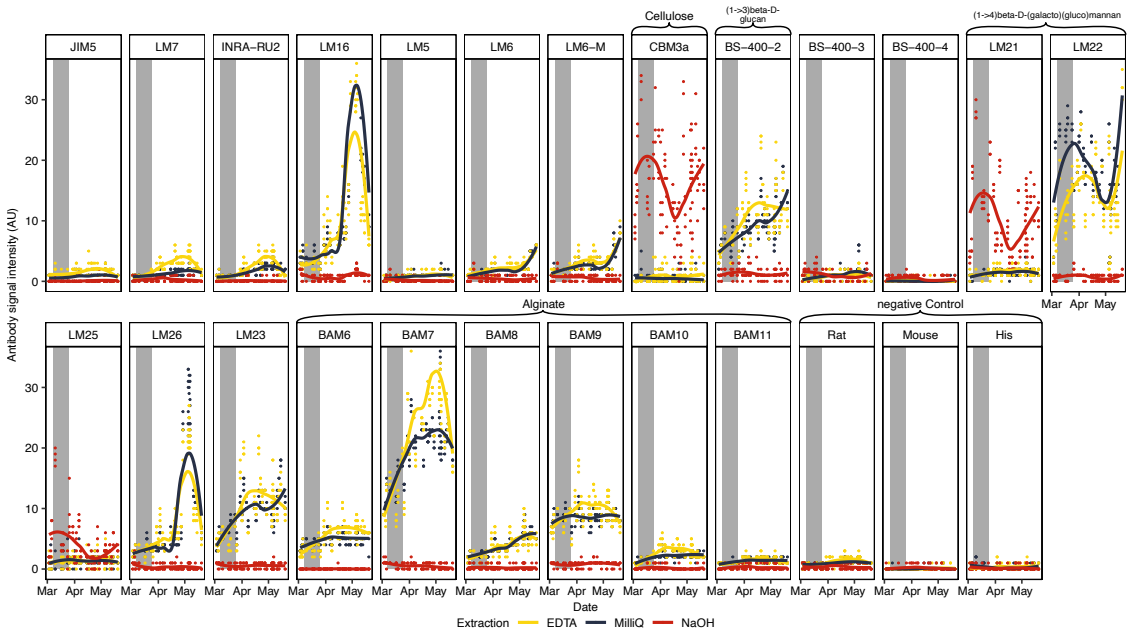

Figure S5.1: High-molecular weight compound concentration during the Helgoland phytoplankton spring bloom 2020. Grey box is the time of high interest between the increase of cell division increase of SAR11 and the beginning of phytoplankton bloom. Samples were taken in triplicates (dots). Loess smoothing was applied over the entire spring bloom. Colors indicate the extraction method. The graph is divided into different epitopes. The full names of epitopes are provided in Table 5.2. Data was published in Sidhu et al. (2023)

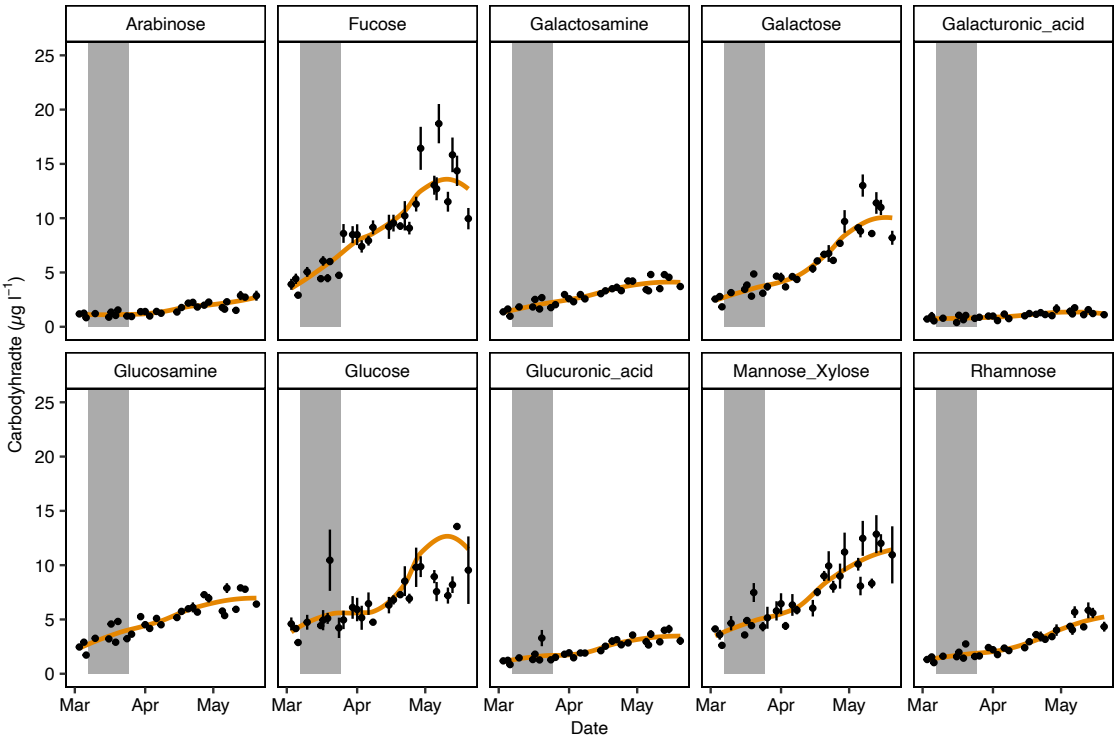

Figure S5.2: Monosaccharide analysis after acid hydrolysis during the Helgoland phytoplankton spring bloom 2020. Grey box is the time of high interest between the increase of cell division increase of SAR11 and the beginning of phytoplankton bloom. Loess smoothing was applied over the entire spring bloom. The graph is divided for different monosacchardides. Data was published in Sidhu et al (2023).

REFERENCES

Abbe, E. (1873). "Beiträge zur Theorie des Mikroskops und der mikroskopischen Wahrnehmung". *Archiv für mikroskopische Anatomie* 9.1, pages 413–468 (cited on page 118).

Ackermann, H.-W. (2012). "Bacteriophage electron microscopy". *Advances in Virus Research* 82, pages 1–32 (cited on page 117).

Affronti, L. F. and H. G. Marshall (1994). "Using frequency of dividing cells in estimating autotrophic picoplankton growth and productivity in the Chesapeake Bay". *Hydrobiologia* 284, pages 193–203 (cited on page 6).

Allers, E., C. Moraru, M. B. Duhaime, E. Beneze, N. Solonenko, J. Barrero-Canosa, R. Amann, and M. B. Sullivan (2013). "Single-cell and population level viral infection dynamics revealed by phage FISH, a method to visualize intracellular and free viruses". *Environmental Microbiology* 15.8, pages 2306–2318 (cited on pages 8, 118).

Alonso, C. and J. Pernthaler (2006). "*Roseobacter* and SAR11 dominate microbial glucose uptake in coastal North Sea waters". *Environmental Microbiology* 8.11, pages 2022–2030 (cited on page 131).

Amann, R. and B. M. Fuchs (2008). "Single-cell identification in microbial communities by improved fluorescence *in situ* hybridization techniques". *Nature Reviews Microbiology* 6.5, pages 339–348 (cited on page 6).

Amann, R. I., B. J. Binder, R. J. Olson, S. W. Chisholm, R. Devereux, and D. Stahl (1990). "Combination of 16S rRNA-targeted oligonucleotide probes with flow cytometry for analyzing mixed microbial populations". *Applied and Environmental Microbiology* 56.6, pages 1919–1925 (cited on pages 6, 127).

Amann, R. I., W. Ludwig, and K.-H. Schleifer (1995). "Phylogenetic identification and *in situ* detection of individual microbial cells without cultivation". *Microbiological Reviews* 59.1, pages 143–169 (cited on pages 6, 117).

Ansorge, R., S. Romano, L. Sayavedra, M. á. G. Porras, A. Kupczok, H. E. Tegetmeyer, N. Dubilier, and J. Petersen (2019). "Functional diversity enables multiple symbiont strains to coexist in deep-sea mussels". *Nature Microbiology* 4.12, pages 2487–2497 (cited on page 8).

Azam, F., T. Fenchel, J. G. Field, J. S. Gray, L. A. Meyer-Reil, and F. Thingstad (2022). "The Ecological Role of Water-Column Microbes in the Sea". *Classic Papers with Commentaries*.

Edited by T. E. Miller and J. Travis. Chicago: University of Chicago Press, pages 384–390 (cited on page 1).

Baghel, R. S., C. Reddy, and R. P. Singh (2021). "Seaweed-based cellulose: Applications, and future perspectives". *Carbohydrate Polymers* 267, page 118241 (cited on page 131).

Ballen-Segura, M., M. Felip, and J. Catalan (2017). "Some mixotrophic flagellate species selectively graze on archaea". *Applied and Environmental Microbiology* 83.2, e02317–16 (cited on pages 4, 121).

Banas, I., S. P. Esser, V. Turzynski, A. Soares, P. Novikova, P. May, C. Moraru, M. Hasenberg, J. Rahlff, and P. Wilmes (2023). "Spatio-functional organization in virocells of small uncultivated archaea from the deep biosphere". *The ISME Journal* 17.10, pages 1789–1792 (cited on pages 8, 118, 120).

Baran, N., S. Goldin, I. Maidanik, and D. Lindell (2018). "Quantification of diverse virus populations in the environment using the polony method". *Nature Microbiology* 3.1, pages 62–72 (cited on pages 117, 120).

Barr, J. J., R. Auro, M. Furlan, K. L. Whiteson, M. L. Erb, J. Pogliano, A. Stotland, R. Wolkowicz, A. S. Cutting, and K. S. Doran (2013). "Bacteriophage adhering to mucus provide a non–host-derived immunity". *Proceedings of the National Academy of Sciences* 110.26, pages 10771–10776 (cited on page 119).

Barrero-Canosa, J., C. Moraru, L. Zeugner, B. M. Fuchs, and R. Amann (2017). "Direct-geneFISH: a simplified protocol for the simultaneous detection and quantification of genes and rRNA in microorganisms". *Environmental Microbiology* 19.1, pages 70–82 (cited on pages 7, 117–119).

Bartlau, N. (2020). "Diversity and function of phages modulating North Sea bacteria". Thesis (cited on pages 118, 119).

Bartlau, N., A. Wichels, G. Krohne, E. M. Adriaenssens, A. Heins, B. M. Fuchs, R. Amann, and C. Moraru (2022). "Highly diverse flavobacterial phages isolated from North Sea spring blooms". *The ISME Journal* 16.2, pages 555–568 (cited on pages 4, 126).

Becker, J. W., S. L. Hogle, K. Rosendo, and S. W. Chisholm (2019). "Co-culture and biogeography of *Prochlorococcus* and SAR11". *The ISME Journal* 13.6, pages 1506–1519 (cited on page 122).

Becker, S., J. Tebben, S. Coffinet, K. Wiltshire, M. H. Iversen, T. Harder, K.-U. Hinrichs, and J.-H. Hehemann (2020). "Laminarin is a major molecule in the marine carbon cycle". *Proceedings of the National Academy of Sciences* 117.12, pages 6599–6607 (cited on page 2).

Beidler, I., N. Steinke, T. Schulze, C. Sidhu, D. Bartosik, J. Krull, T. Dutschei, B. Ferrero-Bordera, J. Rielicke, V. Kale, T. Sura, A. Trautwein-Schult, I. V. Kirstein, K. H. Wiltshire, H. Teeling, D. Becher, M. Bengtsson, J.-H. Hehemann, U. Bornscheuer, R. Amann, and T. Schweder (2023). "Alpha-glucans from bacterial necromass indicate an intra-population loop within the marine carbon cycle". *ResearchSquare* (cited on page 125).

Beisner, B. E., H.-P. Grossart, and J. M. Gasol (2019). “A guide to methods for estimating phagomixotrophy in nanophytoplankton”. *Journal of Plankton Research* 41.2, pages 77–89 (cited on page 121).

Bennke, C. M., G. Reintjes, M. Schattenhofer, A. Ellrott, J. Wulf, M. Zeder, and B. M. Fuchs (2016). “Modification of a high-throughput automatic microbial cell enumeration system for shipboard analyses”. *Applied and Environmental Microbiology* 82.11, pages 3289–3296 (cited on page 6).

Bhatt, M., C. Einstein, Kiran, A. Fayaz, V. Rai, M. Karki, A. Kumar, A. K. Yadav, and K. K. Rajak (2022). “Methods for Quantification of Viruses”. *Protocols for the Diagnosis of Pig Viral Diseases*. Springer, pages 31–47 (cited on page 117).

Bligh, M., N. Nguyen, H. Buck-Wiese, S. Vidal-Melgosa, and J.-H. Hehemann (2022). “Structures and functions of algal glycans shape their capacity to sequester carbon in the ocean”. *Current Opinion in Chemical Biology* 71, page 102204 (cited on page 2).

Bosdriesz, E., S. Magnósdóttir, F. J. Bruggeman, B. Teusink, and D. Molenaar (2015). “Binding proteins enhance specific uptake rate by increasing the substrate–transporter encounter rate”. *The FEBS Journal* 282.12, pages 2394–2407 (cited on pages 5, 124).

Breitbart, M. (2012). “Marine viruses: truth or dare”. *Annual Review of Marine Science* 4, pages 425–448 (cited on page 119).

Breitbart, M., C. Bonnain, K. Malki, and N. A. Sawaya (2018). “Phage puppet masters of the marine microbial realm”. *Nature Microbiology* 3.7, pages 754–766 (cited on pages 2, 4).

Brock, T. D. (1967). “Bacterial growth rate in the sea: direct analysis by thymidine autoradiography”. *Science* 155.3758, pages 81–83 (cited on page 7).

Brussaard, C. P. (2004). “Optimization of procedures for counting viruses by flow cytometry”. *Applied and Environmental Microbiology* 70.3, pages 1506–1513 (cited on page 117).

Buchan, A., G. R. LeCleir, C. A. Gulvik, and J. M. González (2014). “Master recyclers: features and functions of bacteria associated with phytoplankton blooms”. *Nature Reviews Microbiology* 12.10, pages 686–698 (cited on pages 1, 2).

Bunse, C. and J. Pinhassi (2017). “Marine bacterioplankton seasonal succession dynamics”. *Trends in Microbiology* 25.6, pages 494–505 (cited on page 2).

Carini, P., L. Steindler, S. Beszteri, and S. J. Giovannoni (2013). “Nutrient requirements for growth of the extreme oligotroph ‘*Candidatus* Pelagibacter ubique’ HTCC1062 on a defined medium”. *The ISME Journal* 7.3, pages 592–602 (cited on pages 5, 122).

Cesaretti, A., E. Calzoni, N. Montegiove, T. Bianconi, M. Alebardi, M. A. La Serra, G. Consiglio, C. G. Fortuna, F. Elisei, and A. Spalletti (2023). “Lighting-Up the Far-Red Fluorescence of RNA-Selective Dyes by Switching from Ortho to Para Position”. *International Journal of Molecular Sciences* 24.5, page 4812 (cited on page 129).

Chaikeeratisak, V., K. Nguyen, K. Khanna, A. F. Brilot, M. L. Erb, J. K. Coker, A. Vavilina, G. L. Newton, R. Buschauer, and K. Pogliano (2017). "Assembly of a nucleus-like structure during viral replication in bacteria". *Science* 355.6321, pages 194–197 (cited on page 118).

Chen, L. and J. F. Banfield (2024). "COBRA improves the completeness and contiguity of viral genomes assembled from metagenomes". *Nature Microbiology* (cited on page 119).

Chiovitti, A., R. E. Harper, A. Willis, A. Bacic, P. Mulvaney, and R. Wetherbee (2005). "Variations in the substituted 3-linked mannans closely associated with the silicified walls of diatoms". *Journal of Phycology* 41.6, pages 1154–1161 (cited on page 131).

Chow, C.-E. T. and J. A. Fuhrman (2012). "Seasonality and monthly dynamics of marine myovirus communities". *Environmental Microbiology* 14.8, pages 2171–2183 (cited on page 4).

Ciais, P., C. Sabine, G. Bala, L. Bopp, V. Brovkin, J. Canadell, A. Chhabra, R. DeFries, J. Galloway, and M. Heimann (2014). "Carbon and other biogeochemical cycles". *Climate change 2013: the physical science basis. Contribution of Working Group I to the Fifth Assessment Report of the Intergovernmental Panel on Climate Change*. Cambridge University Press, pages 465–570 (cited on page 1).

Coclet, C. and S. Roux (2021). "Global overview and major challenges of host prediction methods for uncultivated phages". *Current Opinion in Virology* 49, pages 117–126 (cited on page 8).

Coutinho, F. H., C. B. Silveira, M. Sebastián, P. Sánchez, C. M. Duarte, D. Vaqué, J. M. Gasol, and S. G. Acinas (2023). "Water mass age structures the auxiliary metabolic gene content of free-living and particle-attached deep ocean viral communities". *Microbiome* 11.1, pages 1–14 (cited on page 119).

Czechowska, K., D. R. Johnson, and J. R. van der Meer (2008). "Use of flow cytometric methods for single-cell analysis in environmental microbiology". *Current opinion in microbiology* 11.3, pages 205–212 (cited on page 6).

Dadon-Pilosof, A., K. R. Conley, Y. Jacobi, M. Haber, F. Lombard, K. R. Sutherland, L. Steindler, Y. Tikochinski, M. Richter, F. O. Glöckner, M. T. Suzuki, N. J. West, A. Genin, and G. Yahel (2017). "Surface properties of SAR11 bacteria facilitate grazing avoidance". *Nature Microbiology* 2.12, pages 1608–1615 (cited on pages 121, 126).

Daims, H., A. Brühl, R. Amann, K.-H. Schleifer, and M. Wagner (1999). "The domain-specific probe EUB338 is insufficient for the detection of all Bacteria: development and evaluation of a more comprehensive probe set". *Systematic and Applied Microbiology* 22.3, pages 434–444 (cited on page 127).

DeLong, E. F., G. S. Wickham, and N. R. Pace (1989). "Phylogenetic stains: ribosomal RNA-based probes for the identification of single cells". *Science* 243.4896, pages 1360–1363 (cited on page 117).

Díez-Vives, C., J. M. Gasol, and S. G. Acinas (2014). "Spatial and temporal variability among marine *Bacteroidetes* populations in the NW Mediterranean Sea". *Systematic and Applied Microbiology* 37.1, pages 68–78 (cited on page 4).

Dopheide, A., G. Lear, R. Stott, and G. Lewis (2011). “Preferential feeding by the ciliates *Chilodonella* and *Tetrahymena* spp. and effects of these protozoa on bacterial biofilm structure and composition”. *Applied and Environmental Microbiology* 77.13, pages 4564–4572 (cited on pages 4, 121).

Ducret, A., E. M. Quardokus, and Y. V. Brun (2016). “MicrobeJ, a tool for high throughput bacterial cell detection and quantitative analysis”. *Nature Microbiology* 1.7, pages 1–7 (cited on page 116).

Dupont, C. L., D. B. Rusch, S. Yooseph, M.-J. Lombardo, R. A. Richter, R. Valas, M. Novotny, J. Yee-Greenbaum, J. D. Selengut, and D. H. Haft (2012). “Genomic insights to SAR86, an abundant and uncultivated marine bacterial lineage”. *ISME Journal* 6.6, pages 1186–1199 (cited on page 123).

Eigemann, F., K. Tait, B. Temperton, and F. L. Hellweger (2024). “Heterotrophic prokaryotes internal carbon recycling compensates mismatches between phytoplankton production and heterotrophic prokaryotic consumption”. *bioRxiv*, page 2024.01. 10.574976 (cited on page 125).

Emiola, A. and J. Oh (2018). “High throughput *in situ* metagenomic measurement of bacterial replication at ultra-low sequencing coverage”. *Nature Communications* 9.1, page 4956 (cited on page 115).

Ferrera, I., J. M. Gasol, M. Sebastián, E. Hojerová, and M. Koblížek (2011). “Comparison of growth rates of aerobic anoxygenic phototrophic bacteria and other bacterioplankton groups in coastal Mediterranean waters”. *Applied and Environmental Microbiology* 77.21, pages 7451–7458 (cited on pages 122, 126).

Field, C. B., M. J. Behrenfeld, J. T. Randerson, and P. Falkowski (1998). “Primary production of the biosphere: integrating terrestrial and oceanic components”. *Science* 281.5374, pages 237–240 (cited on page 1).

Flamholz, Z. N., S. J. Biller, and L. Kelly (2024). “Large language models improve annotation of prokaryotic viral proteins”. *Nature Microbiology* (cited on page 119).

Forterre, P. (2011). “Manipulation of cellular syntheses and the nature of viruses: the virocell concept”. *Comptes Rendus Chimie* 14.4, pages 392–399 (cited on page 126).

Forterre, P. (2021). “The Virocell Concept”. *Encyclopedia of Virology (Fourth Edition)*. Edited by D. H. Bamford and M. Zuckerman. Oxford: Academic Press, pages 23–27 (cited on page 126).

Francis, T. B., D. Bartosik, T. Sura, A. Sichert, J.-H. Hehemann, S. Markert, T. Schweder, B. M. Fuchs, H. Teeling, and R. I. Amann (2021). “Changing expression patterns of TonB-dependent transporters suggest shifts in polysaccharide consumption over the course of a spring phytoplankton bloom”. *The ISME Journal* 15.8, pages 2336–2350 (cited on page 2).

Friedlingstein, P., M. O’sullivan, M. W. Jones, R. M. Andrew, L. Gregor, J. Hauck, C. Le Quéré, I. T. Luijkx, A. Olsen, and G. P. Peters (2022). “Global carbon budget 2022”. *Earth System Science Data Discussions* 2022, pages 1–159 (cited on page 1).

Fuhrman, J. A. and F. Azam (1980). "Bacterioplankton secondary production estimates for coastal waters of British Columbia, Antarctica, and California". *Applied and Environmental Microbiology* 39.6, pages 1085–1095 (cited on page 7).

Fuhrman, J. A., J. A. Cram, and D. M. Needham (2015). "Marine microbial community dynamics and their ecological interpretation". *Nature Reviews Microbiology* 13.3, pages 133–146 (cited on pages 2–4).

Gerdts, G., A. Wichels, H. Döpke, K.-W. Klings, W. Gunkel, and C. Schütt (2004). "40-year long-term study of microbial parameters near Helgoland (German Bight, North Sea): historical view and future perspectives". *Helgoland Marine Research* 58.4, pages 230–242 (cited on page 2).

Gerea, M., C. Queimaliños, M. R. Schiaffino, I. Izaguirre, I. Forn, R. Massana, and F. Unrein (2013). "*In situ* prey selection of mixotrophic and heterotrophic flagellates in Antarctic oligotrophic lakes: an analysis of the digestive vacuole content". *Journal of Plankton Research* 35.1, pages 201–212 (cited on page 121).

Gest, H. (2004). "The discovery of microorganisms by Robert Hooke and Antoni Van Leeuwenhoek, fellows of the Royal Society". *Notes and Records of the Royal Society of London* 58.2, pages 187–201 (cited on page 5).

Giovannoni, S. J. (2017). "SAR11 bacteria: the most abundant plankton in the oceans". *Annual Review of Marine Science* 9, pages 231–255 (cited on pages 4, 5, 122).

Giovannoni, S. J., T. B. Britschgi, C. L. Moyer, and K. G. Field (1990). "Genetic diversity in Sargasso Sea bacterioplankton". *Nature* 345.6270, pages 60–63 (cited on page 6).

Glenwright, A. J., K. R. Pothula, S. P. Bhamidimarri, D. S. Chorev, A. Baslé, S. J. Firbank, H. Zheng, C. V. Robinson, M. Winterhalter, and U. Kleinekathöfer (2017). "Structural basis for nutrient acquisition by dominant members of the human gut microbiota". *Nature* 541.7637, pages 407–411 (cited on page 4).

Gray, D. A., J. B. White, A. O. Oluwole, P. Rath, A. J. Glenwright, A. Mazur, M. Zahn, A. Baslé, C. Morland, and S. L. Evans (2021). "Insights into SusCD-mediated glycan import by a prominent gut symbiont". *Nature Communications* 12.1, page 44 (cited on page 4).

Grodner, B., H. Shi, O. Farchione, A. C. Vill, I. Ntekas, P. J. Diebold, W. R. Zipfel, I. L. Brito, and I. De Vlaminck (2023). "Spatial Mapping of Mobile Genetic Elements and their Cognate Hosts in Complex Microbiomes". *bioRxiv*, page 2023.06. 09.544291 (cited on pages 128, 130).

Hagström, Å., F. Azam, C. Berg, and U. L. Zweifel (2017). "Isolates as models to study bacterial ecophysiology and biogeochemistry". *Aquatic Microbial Ecology* 80.1, pages 15–27 (cited on pages 6, 114).

Hagström, U. Larsson, P. Hörstedt, and S. Normark (1979). "Frequency of dividing cells, a new approach to the determination of bacterial growth rates in aquatic environments". *Applied and Environmental Microbiology* 37.5, pages 805–812 (cited on pages 6, 114).

Hernandez-Gomez, M. C., M. G. Rydahl, A. Rogowski, C. Morland, A. Cartmell, L. Crouch, A. Labourel, C. M. Fontes, W. G. Willats, and H. J. Gilbert (2015). "Recognition of xyloglucan

by the crystalline cellulose-binding site of a family 3a carbohydrate-binding module". *FEBS letters* 589.18, pages 2297–2303 (cited on page 131).

Hirakata, Y., M. Hatamoto, M. Oshiki, T. Watari, N. Araki, and T. Yamaguchi (2020). "Food selectivity of anaerobic protists and direct evidence for methane production using carbon from prey bacteria by endosymbiotic methanogen". *The ISME Journal* 14.7, pages 1873–1885 (cited on pages 4, 121).

Hurwitz, B. L. and M. B. Sullivan (2013). "The Pacific Ocean Virome (POV): a marine viral metagenomic dataset and associated protein clusters for quantitative viral ecology". *PloS One* 8.2, e57355 (cited on page 120).

Jahn, M. T., T. Lachnit, S. M. Markert, C. Stigloher, L. Pita, M. Ribes, B. E. Dutilh, and U. Hentschel (2021). "Lifestyle of sponge symbiont phages by host prediction and correlative microscopy". *The ISME Journal* 15.7, pages 2001–2011 (cited on page 118).

Jing, X., Y. Gong, T. Xu, P. A. Davison, C. MacGregor-Chatwin, C. N. Hunter, L. Xu, Y. Meng, Y. Ji, B. Ma, J. Xu, and W. E. Huang (2022). "Revealing CO_2-Fixing SAR11 Bacteria in the Ocean by Raman-Based Single-Cell Metabolic Profiling and Genomics". *Biodes Res* 2022, page 9782712 (cited on page 123).

Jing, X., H. Gou, Y. Gong, X. Su, L. Xu, Y. Ji, Y. Song, I. P. Thompson, J. Xu, and W. E. Huang (2018). "Raman-activated cell sorting and metagenomic sequencing revealing carbon-fixing bacteria in the ocean". *Environmental Microbiology* 20.6, pages 2241–2255 (cited on page 123).

Kappelmann, L., K. Krüger, J.-H. Hehemann, J. Harder, S. Markert, F. Unfried, D. Becher, N. Shapiro, T. Schweder, and R. I. Amann (2019). "Polysaccharide utilization loci of North Sea *Flavobacteriia* as basis for using SusC/D-protein expression for predicting major phytoplankton glycans". *The ISME Journal* 13.1, pages 76–91 (cited on pages 2, 4).

Kieft, K., Z. Zhou, and K. Anantharaman (2020). "VIBRANT: automated recovery, annotation and curation of microbial viruses, and evaluation of viral community function from genomic sequences". *Microbiome* 8.1, pages 1–23 (cited on page 119).

Kiørboe, T. (2024). "Predation in a microbial world: Mechanisms and trade-offs of flagellate foraging". *Annual Review of Marine Science* 16, pages 361–381 (cited on pages 3, 126).

Kirchman, D. L. (2016). "Growth rates of microbes in the oceans". *Annual Review of Marine Science* 8, pages 285–309 (cited on page 4).

Kirchman, D. L. (2018). *Processes in microbial ecology*. Oxford University Press (cited on pages 6, 7, 116).

Koppelle, S., D. López-Escardó, C. P. Brussaard, J. Huisman, C. J. Philippart, R. Massana, and S. Wilken (2022). "Mixotrophy in the bloom-forming genus *Phaeocystis* and other haptophytes". *Harmful Algae* 117, page 102292 (cited on page 121).

Krüger, K., M. Chafee, T. Ben Francis, T. Glavina del Rio, D. Becher, T. Schweder, R. I. Amann, and H. Teeling (2019). "In marine *Bacteroidetes* the bulk of glycan degradation during algae

blooms is mediated by few clades using a restricted set of genes". *The ISME Journal* 13.11, pages 2800–2816 (cited on page 4).

Laghdass, M., P. Catala, J. Caparros, L. Oriol, P. Lebaron, and I. Obernosterer (2012). "High contribution of SAR11 to microbial activity in the North West Mediterranean Sea". *Microbial Ecology* 63, pages 324–333 (cited on page 122).

Lami, R., M. T. Cottrell, B. J. Campbell, and D. L. Kirchman (2009). "Light-dependent growth and proteorhodopsin expression by *Flavobacteria* and SAR11 in experiments with Delaware coastal waters". *Environmental Microbiology* 11.12, pages 3201–3209 (cited on page 123).

Larkin, A. A., G. I. Hagstrom, M. L. Brock, N. S. Garcia, and A. C. Martiny (2023). "Basin-scale biogeography of *Prochlorococcus* and SAR11 ecotype replication". *The ISME Journal* 17.2, pages 185–194 (cited on page 115).

Legendre, L., R. B. Rivkin, M. G. Weinbauer, L. Guidi, and J. Uitz (2015). "The microbial carbon pump concept: Potential biogeochemical significance in the globally changing ocean". *Progress in Oceanography* 134, pages 432–450 (cited on page 1).

Lindell, D., M. B. Sullivan, Z. I. Johnson, A. C. Tolonen, F. Rohwer, and S. W. Chisholm (2004). "Transfer of photosynthesis genes to and from *Prochlorococcus* viruses". *Proceedings of the National Academy of Sciences* 101.30, pages 11013–11018 (cited on pages 2, 127).

Liu, Y. (2007). "Overview of some theoretical approaches for derivation of the Monod equation". *Applied Microbiology and Biotechnology* 73, pages 1241–1250 (cited on page 4).

Lombard, V., H. Golaconda Ramulu, E. Drula, P. M. Coutinho, and B. Henrissat (2013). "The carbohydrate-active enzymes database (CAZy) in 2013". *Nucleic Acids Research* 42.D1, pages D490–D495 (cited on page 4).

López-García, P., A. Gutiérrez-Preciado, M. Krupovic, M. Ciobanu, P. Deschamps, L. Jardillier, M. López-Pérez, F. Rodríguez-Valera, and D. Moreira (2023). "Metagenome-derived virus-microbe ratios across ecosystems". *The ISME Journal*, pages 1–12 (cited on page 120).

Lyons, A. B. (2000). "Analysing cell division in vivo and in vitro using flow cytometric measurement of CFSE dye dilution". *Journal of Immunological Methods* 243.1-2, pages 147–154 (cited on page 6).

Malmstrom, R. R., M. T. Cottrell, H. Elifantz, and D. L. Kirchman (2005). "Biomass production and assimilation of dissolved organic matter by SAR11 bacteria in the Northwest Atlantic Ocean". *Applied and Environmental Microbiology* 71.6, pages 2979–2986 (cited on page 122).

Malmstrom, R. R., R. P. Kiene, M. T. Cottrell, and D. L. Kirchman (2004). "Contribution of SAR11 bacteria to dissolved dimethylsulfoniopropionate and amino acid uptake in the North Atlantic Ocean". *Applied and Environmental Microbiology* 70.7, pages 4129–4135 (cited on page 122).

Marcus, S. E., A. W. Blake, T. A. Benians, K. J. Lee, C. Poyser, L. Donaldson, O. Leroux, A. Rogowski, H. L. Petersen, and A. Boraston (2010). "Restricted access of proteins to mannan

polysaccharides in intact plant cell walls". *The Plant Journal* 64.2, pages 191–203 (cited on page 131).

Martinez-Hernandez, F., ò. Fornas, M. Lluesma Gomez, I. Garcia-Heredia, L. Maestre-Carballa, M. López-Pérez, J. M. Haro-Moreno, F. Rodriguez-Valera, and M. Martinez-Garcia (2019). "Single-cell genomics uncover Pelagibacter as the putative host of the extremely abundant uncultured 37-F6 viral population in the ocean". *The ISME Journal* 13.1, pages 232–236 (cited on page 130).

Mary, I., J. Heywood, B. Fuchs, R. Amann, G. Tarran, P. Burkill, and M. Zubkov (2006). "SAR11 dominance among metabolically active low nucleic acid bacterioplankton in surface waters along an Atlantic meridional transect". *Aquatic Microbial Ecology* 45.2, pages 107–113 (cited on page 122).

Matteson, A. R., J. M. Rowe, A. J. Ponsero, T. M. Pimentel, P. W. Boyd, and S. W. Wilhelm (2013). "High abundances of cyanomyoviruses in marine ecosystems demonstrate ecological relevance". *FEMS Microbiology Ecology* 84.2, pages 223–234 (cited on page 120).

Mayerhofer, M. M., F. Eigemann, C. Lackner, J. Hoffmann, and F. L. Hellweger (2021). "Dynamic carbon flux network of a diverse marine microbial community". *ISME Communications* 1.1, page 50 (cited on page 125).

Mikkelsen, M. D., J. Harholt, P. Ulvskov, I. E. Johansen, J. U. Fangel, M. S. Doblin, A. Bacic, and W. G. Willats (2014). "Evidence for land plant cell wall biosynthetic mechanisms in charophyte green algae". *Annals of Botany* 114.6, pages 1217–1236 (cited on page 131).

Mincer, T. J. and A. C. Aicher (2016). "Methanol production by a broad phylogenetic array of marine phytoplankton". *PloS One* 11.3, e0150820 (cited on page 125).

Moraru, C., P. Lam, B. M. Fuchs, M. M. Kuypers, and R. Amann (2010). "GeneFISH–an *in situ* technique for linking gene presence and cell identity in environmental microorganisms". *Environmental Microbiology* 12.11, pages 3057–3073 (cited on page 7).

Morris, R. M., M. S. Rappé, S. A. Connon, K. L. Vergin, W. A. Siebold, C. A. Carlson, and S. J. Giovannoni (2002). "SAR11 clade dominates ocean surface bacterioplankton communities". *Nature* 420.6917, pages 806–810 (cited on page 6).

Mruwat, N., M. C. Carlson, S. Goldin, F. Ribalet, S. Kirzner, Y. Hulata, S. J. Beckett, D. Shitrit, J. S. Weitz, and E. V. Armbrust (2021). "A single-cell polony method reveals low levels of infected *Prochlorococcus* in oligotrophic waters despite high cyanophage abundances". *The ISME Journal* 15.1, pages 41–54 (cited on pages 117, 120).

Mühlenbruch, M., H.-P. Grossart, F. Eigemann, and M. Voss (2018). "Mini-review: Phytoplankton-derived polysaccharides in the marine environment and their interactions with heterotrophic bacteria". *Environmental Microbiology* 20.8, pages 2671–2685 (cited on page 2).

Noble, R. T. and J. A. Fuhrman (1998). "Use of SYBR Green I for rapid epifluorescence counts of marine viruses and bacteria". *Aquatic Microbial Ecology* 14.2, pages 113–118 (cited on page 117).

Noell, S. E. and S. J. Giovannoni (2019). "SAR11 bacteria have a high affinity and multifunctional glycine betaine transporter". *Environmental Microbiology* 21.7, pages 2559–2575 (cited on pages 5, 124).

Norris, N., N. M. Levine, V. I. Fernandez, and R. Stocker (2021). "Mechanistic model of nutrient uptake explains dichotomy between marine oligotrophic and copiotrophic bacteria". *PLoS Computational Biology* 17.5, e1009023 (cited on page 5).

Orellana, L. H., T. B. Francis, M. Ferraro, J.-H. Hehemann, B. M. Fuchs, and R. I. Amann (2021). "*Verrucomicrobiota* are specialist consumers of sulfated methyl pentoses during diatom blooms". *The ISME Journal* 16.3, pages 630–641 (cited on pages 2, 3, 124, 131).

Orellana, L. H., K. Krüger, C. Sidhu, and R. Amann (2023). "Comparing genomes recovered from time-series metagenomes using long-and short-read sequencing technologies". *Microbiome* 11.1, page 105 (cited on page 115).

Pappas, N., S. Roux, M. Hölzer, K. Lamkiewicz, F. Mock, M. Marz, and B. E. Dutilh (2021). "Virus Bioinformatics". *Encyclopedia of Virology*, page 124 (cited on page 117).

Pernthaler, J. (2005). "Predation on prokaryotes in the water column and its ecological implications". *Nature Reviews Microbiology* 3.7, pages 537–546 (cited on page 4).

Piwosz, K., I. Mukherjee, M. M. Salcher, V. Grujčić, and K. Šimek (2021). "CARD-FISH in the sequencing era: opening a new universe of protistan ecology". *Frontiers in Microbiology* 12, page 640066 (cited on page 121).

Polimene, L., S. Sailley, D. Clark, A. Mitra, and J. I. Allen (2017). "Biological or microbial carbon pump? The role of phytoplankton stoichiometry in ocean carbon sequestration". *Journal of Plankton Research* 39.2, pages 180–186 (cited on page 1).

Poulsen, L. K., G. Ballard, and D. A. Stahl (1993). "Use of rRNA fluorescence *in situ* hybridization for measuring the activity of single cells in young and established biofilms". *Applied and Environmental Microbiology* 59.5, pages 1354–1360 (cited on page 6).

Puxty, R. J., A. D. Millard, D. J. Evans, and D. J. Scanlan (2015). "Shedding new light on viral photosynthesis". *Photosynthesis Research* 126, pages 71–97 (cited on pages 2, 127).

Rahlff, J., V. Turzynski, S. P. Esser, I. Monsees, T. L. Bornemann, P. A. Figueroa-Gonzalez, F. Schulz, T. Woyke, A. Klingl, and C. Moraru (2021). "Lytic archaeal viruses infect abundant primary producers in Earth's crust". *Nature Communications* 12.1, page 4642 (cited on pages 8, 118, 120).

Rappé, M. S., S. A. Connon, K. L. Vergin, and S. J. Giovannoni (2002). "Cultivation of the ubiquitous SAR11 marine bacterioplankton clade". *Nature* 418.6898, pages 630–633 (cited on pages 5, 6, 122).

Reintjes, G., B. M. Fuchs, M. Scharfe, K. H. Wiltshire, R. Amann, and C. Arnosti (2020). "Short-term changes in polysaccharide utilization mechanisms of marine bacterioplankton during a spring phytoplankton bloom". *Environmental Microbiology* 22.5, pages 1884–1900 (cited on page 3).

Ren, J., N. A. Ahlgren, Y. Y. Lu, J. A. Fuhrman, and F. Sun (2017). "VirFinder: a novel k-mer based tool for identifying viral sequences from assembled metagenomic data". *Microbiome* 5.1, pages 1–20 (cited on page 119).

Ren, J., K. Song, C. Deng, N. A. Ahlgren, J. A. Fuhrman, Y. Li, X. Xie, R. Poplin, and F. Sun (2020). "Identifying viruses from metagenomic data using deep learning". *Quantitative Biology* 8, pages 64–77 (cited on page 119).

Roux, S. and J. R. Brum (2023). "Counting dots or counting reads? Complementary approaches to estimate virus-to-microbe ratios". *The ISME Journal* 17.10, pages 1521–1522 (cited on page 120).

Roux, S., F. Enault, B. L. Hurwitz, and M. B. Sullivan (2015). "VirSorter: mining viral signal from microbial genomic data". *PeerJ* 3, e985 (cited on page 119).

Rozon, R. and S. Short (2013). "Complex seasonality observed amongst diverse phytoplankton viruses in the Bay of Quinte, an embayment of Lake Ontario". *Freshwater Biology* 58.12, pages 2648–2663 (cited on page 120).

Salazar, G., F. M. Cornejo-Castillo, V. Benítez-Barrios, E. Fraile-Nuez, X. A. álvarez-Salgado, C. M. Duarte, J. M. Gasol, and S. G. Acinas (2016). "Global diversity and biogeography of deep-sea pelagic prokaryotes". *The ISME Journal* 10.3, pages 596–608 (cited on page 119).

Sánchez, O., I. Ferrera, I. Mabrito, C. R. Gazulla, M. Sebastián, A. Auladell, C. Marín-Vindas, C. Cardelós, I. Sanz-Sáez, and M. C. Pernice (2020). "Seasonal impact of grazing, viral mortality, resource availability and light on the group-specific growth rates of coastal Mediterranean bacterioplankton". *Scientific Reports* 10.1, page 19773 (cited on pages 122, 123, 126).

Sánchez, O., M. Koblížek, J. M. Gasol, and I. Ferrera (2017). "Effects of grazing, phosphorus and light on the growth rates of major bacterioplankton taxa in the coastal NW Mediterranean". *Environmental Microbiology Reports* 9.3, pages 300–309 (cited on page 122).

Schattenhofer, M., B. M. Fuchs, R. Amann, M. V. Zubkov, G. A. Tarran, and J. Pernthaler (2009). "Latitudinal distribution of prokaryotic picoplankton populations in the Atlantic Ocean". *Environmental Microbiology* 11.8, pages 2078–2093 (cited on page 6).

Schindelin, J., C. T. Rueden, M. C. Hiner, and K. W. Eliceiri (2015). "The ImageJ ecosystem: An open platform for biomedical image analysis". *Molecular Reproduction and Development* 82.7-8, pages 518–529 (cited on page 116).

Sekar, R., B. M. Fuchs, R. Amann, and J. Pernthaler (2004). "Flow sorting of marine bacterioplankton after fluorescence In Situ hybridization". *Applied and Environmental Microbiology* 70.10, pages 6210–6219 (cited on page 6).

Sichert, A., C. H. Corzett, M. S. Schechter, F. Unfried, S. Markert, D. Becher, A. Fernandez-Guerra, M. Liebeke, T. Schweder, and M. F. Polz (2020). "*Verrucomicrobia* use hundreds of enzymes to digest the algal polysaccharide fucoidan". *Nature Microbiology* 5.8, pages 1026–1039 (cited on pages 3, 124, 131).

Sidhu, C., I. V. Kirstein, C. L. Meunier, J. Rick, V. Fofonova, K. H. Wiltshire, N. Steinke, S. Vidal-Melgosa, J.-H. Hehemann, and B. Huettel (2023). "Dissolved storage glycans shaped the community composition of abundant bacterioplankton clades during a North Sea spring phytoplankton bloom". *Microbiome* 11.1, pages 1–18 (cited on pages 123, 124, 131, 135, 136).

Siegel, D., S. Doney, and J. Yoder (2002). "The North Atlantic spring phytoplankton bloom and Sverdrup's critical depth hypothesis". *science* 296.5568, pages 730–733 (cited on page 123).

Sison-Mangus, M. P., S. Jiang, R. M. Kudela, and S. Mehic (2016). "Phytoplankton-associated bacterial community composition and succession during toxic diatom bloom and non-bloom events". *Frontiers in Microbiology* 7, page 1433 (cited on page 2).

Solden, L., K. Lloyd, and K. Wrighton (2016). "The bright side of microbial dark matter: lessons learned from the uncultivated majority". *Current Opinion in Microbiology* 31, pages 217–226 (cited on page 117).

Song, J., A. Choi, M. Im, Y. Joung, S. Yoshizawa, J.-C. Cho, and K. Kogure (2015). "*Aurantivirga profunda* gen. nov., sp. nov., isolated from deep-seawater, a novel member of the family *Flavobacteriaceae*". *International Journal of Systematic and Evolutionary Microbiology* 65.12, pages 4850–4856 (cited on page 123).

Sowell, S. M., A. D. Norbeck, M. S. Lipton, C. D. Nicora, S. J. Callister, R. D. Smith, D. F. Barofsky, and S. J. Giovannoni (2008). "Proteomic analysis of stationary phase in the marine bacterium "*Candidatus* Pelagibacter ubique"". *Applied and Environmental Microbiology* 74.13, pages 4091–4100 (cited on page 5).

Sperling, M., J. Piontek, A. Engel, K. H. Wiltshire, J. Niggemann, G. Gerdts, and A. Wichels (2017). "Combined carbohydrates support rich communities of particle-associated marine bacterioplankton". *Frontiers in Microbiology* 8, page 65 (cited on pages 2, 3).

Starikova, E. V., P. O. Tikhonova, N. A. Prianichnikov, C. M. Rands, E. M. Zdobnov, E. N. Ilina, and V. M. Govorun (2020). "Phigaro: high-throughput prophage sequence annotation". *Bioinformatics* 36.12, pages 3882–3884 (cited on page 119).

Steindler, L., M. S. Schwalbach, D. P. Smith, F. Chan, and S. J. Giovannoni (2011). "Energy starved *Candidatus* Pelagibacter ubique substitutes light-mediated ATP production for endogenous carbon respiration". *PloS One* 6.5, e19725 (cited on page 123).

Sullivan, M. B., J. S. Weitz, and S. Wilhelm (2017). "Viral ecology comes of age". *Environmental Microbiology Reports* 9.1, pages 33–35 (cited on page 2).

Sun, J., L. Steindler, J. C. Thrash, K. H. Halsey, D. P. Smith, A. E. Carter, Z. C. Landry, and S. J. Giovannoni (2011). "One carbon metabolism in SAR11 pelagic marine bacteria". *PloS One* 6.8, e23973 (cited on pages 5, 125).

Suttle, C. A. (2005). "Viruses in the sea". *Nature* 437.7057, pages 356–361 (cited on page 2).

Suttle, C. A. (2007). "Marine viruses—major players in the global ecosystem". *Nature Reviews Microbiology* 5.10, pages 801–812 (cited on pages 5, 125).

Tada, Y., A. Taniguchi, I. Nagao, T. Miki, M. Uematsu, A. Tsuda, and K. Hamasaki (2011). "Differing Growth Responses of Major Phylogenetic Groups of Marine Bacteria to Natural Phytoplankton Blooms in the Western North Pacific Ocean". *Applied and Environmental Microbiology* 77.12, pages 4055–4065 (cited on page 6).

Tadmor, A. D., E. A. Ottesen, J. R. Leadbetter, and R. Phillips (2011). "Probing individual environmental bacteria for viruses by using microfluidic digital PCR". *Science* 333.6038, pages 58–62 (cited on page 120).

Tang, B.-L., J. Yang, X.-L. Chen, P. Wang, H.-L. Zhao, H.-N. Su, C.-Y. Li, Y. Yu, S. Zhong, and L. Wang (2020). "A predator-prey interaction between a marine *Pseudoalteromonas* sp. and Gram-positive bacteria". *Nature Communications* 11.1, page 285 (cited on page 3).

Teeling, H., B. M. Fuchs, D. Becher, C. Klockow, A. Gardebrecht, C. M. Bennke, M. Kassabgy, S. Huang, A. J. Mann, and J. Waldmann (2012). "Substrate-controlled succession of marine bacterioplankton populations induced by a phytoplankton bloom". *Science* 336.6081, pages 608–611 (cited on pages 3–5, 124).

Teeling, H., B. M. Fuchs, C. M. Bennke, K. Krüger, M. Chafee, L. Kappelmann, G. Reintjes, J. Waldmann, C. Quast, and F. O. Glöckner (2016). "Recurring patterns in bacterioplankton dynamics during coastal spring algae blooms". *eLife* 5, e11888 (cited on pages 2, 5).

Teira, E., S. Martínez-García, C. Lønborg, and X. A. álvarez-Salgado (2009). "Growth rates of different phylogenetic bacterioplankton groups in a coastal upwelling system". *Environmental Microbiology Reports* 1.6, pages 545–554 (cited on page 122).

Terzian, P., E. Olo Ndela, C. Galiez, J. Lossouarn, R. E. Pérez Bucio, R. Mom, A. Toussaint, M.-A. Petit, and F. Enault (2021). "PHROG: families of prokaryotic virus proteins clustered using remote homology". *NAR Genomics and Bioinformatics* 3.3, lqab067 (cited on page 120).

Thompson, L. R., Q. Zeng, L. Kelly, K. H. Huang, A. U. Singer, J. Stubbe, and S. W. Chisholm (2011). "Phage auxiliary metabolic genes and the redirection of cyanobacterial host carbon metabolism". *Proceedings of the National Academy of Sciences* 108.39, E757–E764 (cited on pages 2, 127).

Torode, T. A., A. Siméon, S. E. Marcus, M. Jam, M.-A. Le Moigne, D. Duffieux, J. P. Knox, and C. Hervé (2016). "Dynamics of cell wall assembly during early embryogenesis in the brown alga Fucus". *Journal of Experimental Botany* 67.21, pages 6089–6100 (cited on page 131).

Tripp, H. J. (2013). "The unique metabolism of SAR11 aquatic bacteria". *Journal of Microbiology* 51, pages 147–153 (cited on page 5).

Turner, D., A. M. Kropinski, and E. M. Adriaenssens (2021). "A roadmap for genome-based phage taxonomy". *Viruses* 13.3, page 506 (cited on page 120).

Turzynski, V., L. Griesdorn, C. Moraru, A. R. Soares, S. A. Simon, T. L. Stach, J. Rahlff, S. P. Esser, and A. J. Probst (2023). "Virus-host dynamics in archaeal groundwater biofilms and the associated bacterial community composition". *Viruses* 15.4, page 910 (cited on page 118).

Turzynski, V., I. Monsees, C. Moraru, and A. J. Probst (2021). “Imaging techniques for detecting prokaryotic viruses in environmental samples”. *Viruses* 13.11, page 2126 (cited on page 120).

Vidal-Melgosa, S., A. Sichert, T. B. Francis, D. Bartosik, J. Niggemann, A. Wichels, W. G. Willats, B. M. Fuchs, H. Teeling, and D. Becher (2021). “Diatom fucan polysaccharide precipitates carbon during algal blooms”. *Nature Communications* 12.1, page 1150 (cited on pages 2, 131).

Wang, Y., S. Ferrinho, H. Connaris, and R. J. Goss (2023). “The impact of viral infection on the chemistries of the earth’s most abundant photosynthesizes: metabolically talented aquatic cyanobacteria”. *Biomolecules* 13.8, page 1218 (cited on page 2).

Weinbauer, M. G., S. Suominen, J. Jezbera, M.-E. Kerros, S. Marro, and J. R. Dolan (2019). “Shifts in cell size and community composition of bacterioplankton due to grazing by heterotrophic flagellates: evidence from a marine system”. *Aquatic Microbial Ecology* 83.3, pages 295–308 (cited on page 4).

Whitman, W. B., D. C. Coleman, and W. J. Wiebe (1998). “Prokaryotes: the unseen majority”. *Proceedings of the National Academy of Sciences* 95.12, pages 6578–6583 (cited on page 1).

Wigington, C. H., D. Sonderegger, C. P. Brussaard, A. Buchan, J. F. Finke, J. A. Fuhrman, J. T. Lennon, M. Middelboe, C. A. Suttle, and C. Stock (2016). “Re-examination of the relationship between marine virus and microbial cell abundances”. *Nature Microbiology* 1.3, pages 1–9 (cited on page 2).

Wilhelm, S. W. and C. A. Suttle (1999). “Viruses and nutrient cycles in the sea: viruses play critical roles in the structure and function of aquatic food webs”. *Bioscience* 49.10, pages 781–788 (cited on page 2).

Williams, H. N., D. S. Lymperopoulou, R. Athar, A. Chauhan, T. L. Dickerson, H. Chen, E. Laws, T.-K. Berhane, A. R. Flowers, and N. Bradley (2016). “*Halobacteriovorax*, an underestimated predator on bacteria: potential impact relative to viruses on bacterial mortality”. *The ISME Journal* 10.2, pages 491–499 (cited on page 3).

Woese, C. R. and G. E. Fox (1977). “Phylogenetic structure of the prokaryotic domain: the primary kingdoms”. *Proceedings of the National Academy of Sciences* 74.11, pages 5088–5090 (cited on page 6).

Yang, L., J. A. Haagensen, L. Jelsbak, H. K. Johansen, C. Sternberg, N. Høiby, and S. Molin (2008). *In situ growth rates and biofilm development of Pseudomonas aeruginosa populations in chronic lung infections* (cited on page 6).

Yokokawa, T., T. Nagata, M. T. Cottrell, and D. L. Kirchman (2004). “Growth rate of the major phylogenetic bacterial groups in the Delaware estuary”. *Limnology and Oceanography* 49.5, pages 1620–1629 (cited on page 4).

Zeder, M., A. Ellrott, and R. Amann (2011). “Automated sample area definition for high-throughput microscopy”. *Cytometry Part A* 79.4, pages 306–310 (cited on page 6).

Zeugner, L. E., K. Krüger, J. Barrero-Canosa, R. I. Amann, and B. M. Fuchs (2021). “In situ visualization of glycoside hydrolase family 92 genes in marine flavobacteria”. *ISME Communications* 1.1, page 81 (cited on pages 8, 117).

Zhao, Y., B. Temperton, J. C. Thrash, M. S. Schwalbach, K. L. Vergin, Z. C. Landry, M. Ellisman, T. Deerinck, M. B. Sullivan, and S. J. Giovannoni (2013). “Abundant SAR11 viruses in the ocean”. *Nature* 494.7437, pages 357–360 (cited on pages 125, 130).

Zhong, K. X., J. F. Wirth, A. M. Chan, and C. A. Suttle (2023). “Mortality by ribosomal sequencing (MoRS) provides a window into taxon-specific cell lysis”. *The ISME Journal* 17.1, pages 105–116 (cited on page 125).

Zweifel, U. L. and Å. Hagström (1995). “Total counts of marine bacteria include a large fraction of non-nucleoid-containing bacteria (ghosts)”. *Applied and Environmental Microbiology* 61.6, pages 2180–2185 (cited on page 128).

ACKNOWLEDGEMENTS

In the Versicherung an Eides Statt, I specifically affirm that this dissertation is my own work. And it is nothing but the truth. And I am proud of it. Nevertheless, this work would not have been possible without the support and advice of many people.

My deepest gratitude is dedicated to **PD Dr. Bernhard Fuchs** and **Prof. Dr. Rudolf Amann**. I spent many hours in your office and had many exciting scientific discussions.
I would like to thank the reviewers of this study, **Dr. Cristina Moraru** and **Prof. Dr. Stephen Giovannoni**, who both fuelled my enthusiasm before finishing this thesis. I would further like to thank **Isabella Wilkie** and **Julia Pamphile dos Santos** for being on the examination committee.

Prof. Dr. Jakob Pernthaler, **Dr. Nikolaus Leisch**, **Dr. Antje Wichels**, **Dr. Yanlin Zhao**, **Dr. Nina Bartlau** were all part of my thesis committee meetings and helped me to improve my studies. Additionally, **Niko** and **Dr. Benedikt Geier** were passionate about my research and (crazy) ideas at the beginning of my work for this thesis. If it were not for you, I would not have used the automatic microscope as much. Thank you!

I would further like to thank all collaborators of my manuscripts. Without the positive controls, provided by **Dr. Yanlin Zhao**, I would have given up on the pelagiphage story. Thank you very much!
I received excellent technical assistance from **Kathrin Büttner**, **Andreas Ellrott**, **Jörg Wulf**, **Mirja Meiners**, **Anja Greiser**, and **Dr. Peter Rücknagel**. Thanks for always looking after me and having my back!
Special thanks to the **automated microscope** and the computer. I could count on you whenever needed!

Kathi, **Seba**, **Cedric**, **Sabine**, **Laura**, **Taylor**, **Nina**, **Anni**, **Greta** (and others): Thank you for sharing offices, labs, and good jokes! Thanks to the entire Molecular Ecology department and anyone whom I might have missed in this acknowledgment.
Thank you, **Jörg** for your suggestion of the term 'zombie'.

I would like to thank **Shobhit Agrawal** and **Andreas Eich** for everything. The actual list would be too long to be included here.
Andreas & **Vanessa Schick**, **Jan Popp**, **Dominik Hölzen**, **Anton Misfeld** und alle weiteren Hübenbecker: Danke für die vielen Lagerfeuer, guten Geschichten und die gemeinsame Zeit.

Danke **Mami** und **Papi**! Ohne euer Vertrauen wäre es sicherlich nie zu dieser Arbeit gekommen. Danke auch an **Jonas** & **Anne** mit **Albrecht**, **Berenike** und **Nathanael**, sowie **Jule** & **Janco** mit **Jonna** und **Jelle**. Ich bin stolz einer von euch zu sein.
Aber jetzt würde ich auch gerne mal auf dem Klingelschild stehen …

Der letzte Dank geht an meine liebe Ehefrau **Franzi** und unsere Tochter **Frida**. Es ist nicht in Worte zu fassen was ich empfinde oder wie dankbar ich euch beiden bin. Ein Lächeln von Frida genügt um den Alltagsstress verfliegen zu lassen. Ohne euer ständiges Verständnis für meine Situation wäre ich womöglich kaputt gegangen.

Universität Bremen

Universität Bremen | Fachbereich 02 | Postfach 33 04 40, 28334 Bremen

Universität Bremen
Fachbereich 2
Prüfungsamt Chemie
z. Hd. Frau Frauke Ernst
Leobener Straße

28359 Bremen
Deutschland

Prüfungsamt
Chemie

Frauke Ernst
Geschäftsstelle
Fachbereich 02
Leobener Str. / NW2
D-28359 Bremen

Verwaltungspavillon 06
Tel. 0421 218-62802
Fax 0421 218-9862802
frauke.ernst@uni-bremen.de
www.fb2.uni-bremen.de

Versicherung an Eides Statt

Name, Vorname	Brüwer, Jan David
Matrikel-Nr.	4007015
Straße	Celsiusstr. 1
Ort, PLZ	Bremen, 28359

Ich, Jan David Brüwer,

versichere an Eides Statt durch meine Unterschrift, dass ich die vorstehende Arbeit selbständig und ohne fremde Hilfe angefertigt und alle Stellen, die ich wörtlich dem Sinne nach aus Veröffentlichungen entnommen habe, als solche kenntlich gemacht habe, mich auch keiner anderen als der angegebenen Literatur oder sonstiger Hilfsmittel bedient habe.
Ich versichere an Eides Statt, dass ich die vorgenannten Angaben nach bestem Wissen und Gewissen gemacht habe und dass die Angaben der Wahrheit entsprechen und ich nichts verschwiegen habe.
Die Strafbarkeit einer falschen eidesstattlichen Versicherung ist mir bekannt, namentlich die Strafandrohung gemäß § 156 StGB bis zu drei Jahren Freiheitsstrafe oder Geldstrafe bei vorsätzlicher Begehung der Tat bzw. gemäß § 161 Abs. 1 StGB bis zu einem Jahr Freiheitsstrafe oder Geldstrafe bei fahrlässiger Begehung.

Ort, Datum / Unterschrift